UNIVERSITY OF VALENCIA

FACULTY OF CHEMISTRY

DEPARTMENT OF ANALYTICAL CHEMISTRY

NOVEL MONOLITHIC MATERIALS FOR MINIATURIZED SEPARATION TECHNIQUES

Thesis presented to obtain the degree of doctor of philosophy in chemistry under the program of "Experimental Techniques in Chemistry"

Enrique Javier Carrasco Correa

Supervisors:

Prof. Guillermo Ramis-Ramos

Prof. José Manuel Herrero-Martínez

VNIVERSITAT DE VALÈNCIA Facultat de Química

Departament de Química Analítica

D. Guillermo Ramis Ramos y D. José Manuel Herrero Martínez, Catedrático y Profesor Titular del Departamento de Química Analítica de la Universidad de Valencia,

Certifican

Que la presente memoria, que lleva por título "*Novel monolithic materials for miniaturized separation techniques*" constituye la Tesis Doctoral de D. Enrique Javier Carrasco Correa.

Asimismo, certifican haber dirigido y supervisado tanto los distintos aspectos del trabajo como su redacción.

Y para que así conste a los efectos oportunos y a petición del interesado, firmamos la presente en Burjassot, a 18 de Mayo de 2015.

Guillermo Ramis Ramos

José Manuel Herrero Martínez

VNIVERSITAT DE VALÈNCIA

Department of Analytical Chemistry

Faculty of Chemistry

Prof. Dr. Guillermo Ramis Ramos and Dr. José Manuel Herrero-Martínez from the Departament of Analytical Chemistry of the University of Valencia,

This is to certify that the present work entitled "*Novel monolithic materials for miniaturized separation techniques*" constitutes the PhD thesis of Mr. Enrique Javier Carrasco Correa.

The undersigned also certify that they have supervised all the aspects of the present work, including its writing.

In witness thereof, we signed the present document in Burjassot, 18th May 2015.

Guillermo Ramis Ramos

José Manuel Herrero Martínez

Preface

This Thesis is presented as "a compendium of publications", as it is regulated by the University of Valencia (Reglamento 29/11/2011, ACGUV 266/2011). Accordingly, the first part of the thesis contains a general introduction where all the articles are presented, with justification of the subject and also explaining the original contribution of the PhD candidate. The PhD student has contributed substantially in all stages of development of all the articles, from the development of the idea, literature search, experimental realization, analysis and interpretation of data, drafting and preparation of the manuscript, and monitoring and final correction thereof according to the recommendations of the referees. Then the published articles are included. These correspond entirely to indexed journals. The most recently submitted articles are also included. All articles have been written by Enrique Javier Carrasco-Correa (identified as first author), with corrections and final review by the supervisors of this Thesis. According to the regulation quoted above, the last part of the thesis contains a comprehensive summary of results, discussion and conclusions.

Esta Tesis se acoge a la modalidad "compendio de publicaciones", contemplada en el Reglamento de la Universidad de Valencia de 29/11/2011 (ACGUV 266/2011). De acuerdo con dicha normativa, la primera parte de la Tesis contiene una introducción general, donde se presentan los trabajos compendiados, justificando su temática y explicando la aportación original del doctorando. El doctorando ha contribuido sustancialmente en todas las etapas de desarrollo de todos los artículos, desde la elaboración de la idea, búsqueda bibliográfica, realización experimental, análisis e interpretación de los datos, redacción y preparación del manuscrito, y seguimiento y corrección final del mismo de acuerdo con las recomendaciones de los evaluadores. A continuación se incluyen los artículos ya publicados, los cuales corresponden en su totalidad a revistas indexadas, más los artículos recientemente enviados. Todos los artículos han sido escritos por Enrique Javier Carrasco Correa (identificado como primer autor), con correcciones y revisión final por parte de los supervisores de esta Tesis. De acuerdo con la normativa citada, la última parte de la Tesis contiene un resumen global de resultados, discusión y conclusiones.

Science knows no country, because knowledge belongs to humanity, and is the torch which illuminates the world.

La ciencia no conoce país, porque el conocimiento pertenece a la humanidad, y es la antorcha que ilumina el mundo.

Louis Pasteur

A mi familia

AGRADECIMIENTOS

ACKNOWLEDGEMENTS

La realización de esta Tesis Doctoral no habría sido posible sin la ayuda y el apoyo de un gran número de personas:

En primer lugar, quisiera agradecer a mis Directores, El Dr. Guillermo Ramis Ramos y al Dr. José Manuel Herrero Martínez, por su ayuda, dedicación y todos los conocimientos que me han transmitido. Su confianza, apoyo y paciencia han sido fundamentales para poder llevar a cabo este proyecto. Tampoco hay que olvidarse de los buenos momentos que hemos disfrutado juntos.

Además, quisiera dar las gracias al Dr. Ernesto F. Simó Alfonso, por su contribución al desarrollo de mi trabajo y por haber estado dispuesto a ayudarme cuando lo he necesitado.

I also thanks everyone from Tübingen laboratory in Germany for made my stay so easy, especially to Dr. Michael Lämmerhofer for all his help and patience, danke schön.

Por otro lado, agradecer a mis compañeros del Laboratorio 10, con los que he compartido tantas cosas… cosas buenas, otras no tan buenas, agobios, preocupaciones, trabajo y momentos de diversión: A Aarón por transmitir esa tranquilidad intrínseca y estar dispuesto siempre a ayudar a los demás, a Isabel por su sabiduría y sensatez que le dan un poco de cordura al laboratorio, a María Navarro por todos los momentos locos y divertidos del laboratorio así como por los viernes de Bar que son un anti estresante natural y María Vergara… que pese a todo nuestros desacuerdos y desencuentros, tengo que decir que sin alguien con quien discutir todo habría sido un poco más aburrido. Tampoco me olvido de todos los que han pasado por el laboratorio: Agustín, Ceci, José, Juan, Laura, Marta, Óscar, Rocío y muchos otros.

No me puedo olvidar de dos de mis mentoras del laboratorio 10, las Dras. Miriam Beneito y María Jesús Lerma que tan buenos momentos hemos pasado y tanto me han enseñado en todos estos años. Además agradezco a todos mis compañeros de otros laboratorios (3, 4, 11 y el edificio de investigación) del Departamento por todos los momentos juntos que hemos pasado. Mención especial a Marina y a Diego por todos los momentos que hemos compartido. No me puedo olvidar de Casandra por su apoyo y por todos los viajes juntos a congresos que hemos hecho, que no hubiesen sido lo mismo sin ella. También agradecer a todos los profesores y personal del Departamento, con los que ha sido una verdadera satisfacción relacionarme y trabajar.

I also thanks Dra. Federica for her friendship and making the stay much easier. Best regards Pomodorina.

No me voy a permitir olvidarme de mis amigos del "Time's up": a Alba por estar siempre ahí, en los buenos y malos momentos, a Asun por su alegría contagiosa, a Alaina por todos esos ratos juntos, a Isuha por la amistad que hemos forjado estos años y estar siempre ahí, a JuanLu que aunque nos llevamos soportando más de 10 años, aún seguimos ahí, aguantando todo y manteniendo la amistad, a Lau que pese a la distancia siempre ha estado ahí para todo lo que he necesitado, y por tener una paciencia infinita conmigo, a Merce por estar siempre presente cuando la he necesitado y a Rosa por ser la mini y aguantar todo lo que me he metido con ella.

No me iba a olvidar tampoco de mis amigos del fútbol, todos los jueves han sido sagrados y nos hemos juntado para "echarnos una pachanga" y liberar las tensiones del trabajo. Además, mencionar ese gran grupo de whatsapp que tenemos en el que las risas que nos echamos no tienen precio. Tampoco me puedo olvidar de mis amigos de Xirivella (aunque algunos sean de Valencia), Aitor, Ángel, Carlos, Fernando, Jaime, José Manuel, Laura, Luis C., Luis S. Manolo, Manu y Víctor que pase el tiempo que pase siempre seremos amigos.

Gracias también al Ministerio de Ciencia e Innovación por la beca predoctoral que me concedieron y la ayuda extra en la estancia.

Y como no, agradecer también a mi familia: mis abuelos, tías, tíos y primas, por demostrar siempre tanto interés en mi trabajo y por estar ahí, en especial a mi Abuelo, que pese a que ya no está con nosotros, sé que estaría orgulloso de mí por haber llegado hasta aquí, Gracias.

No me puedo olvidar, especialmente de mis padres, quienes siempre han estado a mi lado y me han apoyado en todas mis decisiones además de su ayuda incondicional en todos los aspectos.

A todos vosotros, y a los que aunque no haya nombrado, pero que han sido partícipes de que todo haya llegado a buen fin, GRACIAS.

Abbreviations

1,4-BuOH	1,4-Butanediol
1-PrOH	1-Propanol
ACN	Acetonitrile
AGE	Allyl glycidyl ether
AIBN	Azobisisobutyronitrile
AIC	Allyl isocyanate
AMPS	2-Acrylamido-2-methyl-1-propanesulfonic acid
BGE	Background electrolyte
BHT	Butylated hydroxytoluene
BMA	Butylmethacrylate
BPB	Butylparaben
BSA	Bovine serum albumin
BSE	Backscattered electron
CE	Capillary electrophoresis
CEC	Capillary electrochromatography
CGE	Capillary gel electrophoresis
cHPLC	Capillary high performance liquid chromatography
COD	Codeine
CR	Congo red
CS	Chiral selector
CYC	Cyclohexanol
CZE	Capillary zone electrophoresis
DBC	Dynamic binding capacity
DBS	Dulbecco’s phosphate-buffered saline

DEA	Diethylamine
DLLME	Dispersive liquid-liquid microextraction
DMFA	Dimethylformamide
DMSO	Dimethyl sulfoxide
DNA	Deoxyribonucleic acid
DNB-Leu	(R,S)-N-3,5-dinitrobenzoyl-leucine
DOD	1-Dodecanol
DP	Declustering potential
DPDS	2,2’-Dipiridyl disulfide
DVB	Divinyl benzene
EDAX	Energy dispersive X-ray
EDMA	Ethylene dimethacrylate
EIC	Extracted ion chromatogram
EMPV	Electromagnetic proportional valve
EO	Essential oil
EP	Entrance potential
EPB	Ethylparaben
ESA	European Space Agency
ESI	Electrospray ionization
EtOH	Ethanol
FA	Formic acid
FID	Flame ionization detector
GA	Glutaraldehyde
GC	Gas chromatography
GMA	Glycidyl methacrylate
GNP	Gold nanoparticle

HAcO	Acetic acid
HDT	1,6-Hexanedithiol
HIC	Hydrophobic interaction chromatography
HILIC	Hydrophilic interaction chromatography
HMD	Hexamethylene-1,6-diamine
HMT	1-Hexanethiol
IPA	Isopropanol
LOD	Limit of detection
MEKC	Micellar electrokinetic chromatography
MeOH	Methanol
META	(Methacryloyloxy)ethyl trimethylammonium chloride
MNP	Magnetic nanoparticle
MPB	Methylparaben
MRM	Multiple reaction monitoring
MS	Mass spectrometry
MTBE	Methyl-*t*-butylether
NAC	N-Acetyl-cysteine
NACME	N-Acetyl-L-cysteine methyl ester
NaSH	Sodium hydrogen sulfide
NECEEM	Non equilibrium capillary electrophoresis of equilibrium mixtures
NH_4HF_2	Ammonium blifluoride
nHPLC	Nano high performance liquid chromatography
NMR	Nuclear magnetic resonance
NP	Nanoparticle
OP	Organophosphorous pesticide

PC	L-α-phosphatidylcholine
P_C	Peak capacity
PEG	Poly(ethylene glycol)
PMI	Polymethacrylimide
PMPMS	Poly-3-mercaptopropyl methylsiloxane
PPB	Propylparaben
PVA	Poly (vinylalcohol)
PVP	Polyvinylpyrrolidone
R_C	Critical pair resolution
R_G	Global resolution
RP	Reversed-phase
SCBH	Sodium cyanoborohydride
SEC	Size exclusion chromatography
SEM	Scanning electronic microscopy
SNP	Silver nanoparticle
SoyPC	Soy bean L-α-phosphatidylcholine
STY	Styrene
SWNT	Single-walled carbon nanotube
T	Mixing point
t-BuCQN	O-9-*tert*-butylcarbamoyl-quinine
TCM	Trichloromethane
TD	Thermal desorption
TEA	Triethylamine
TEM	Transmission electronic microscopy
TGA	Thermogravimetric analysis
THF	Tetrahydrofuran

TIC	Total ion chromatogram
Tris	Tris(hydroxymethyl)aminomethane
UPLC	Ultra-high pressure liquid chromatography
VMNP	Vinylized magnetic nanoparticle
VOC	Volatile organic compound
WAX	Weak anion-exchange
γ-MPS	3-(Trimethoxysilyl)propyl methacrylate

INDEX

ABSTRACT

In this PhD Thesis novel porous polymer materials and their potential application in miniaturized separation techniques are mainly described. The first section (Chapters 1-3), contains a general introduction, where the impact of monolithic materials (Chapter 2) on chromatography is widely discussed. In Chapter 3, an introduction to the characterization of some polymers and essential oils is presented. Chapters 1-3 were written in compliance with the aforementioned regulation of the University of Valencia, thus constituting the required general introduction.

The second part of this PhD Thesis focuses on the preparation, characterization of application of novel monolithic materials to be used in capillary/nano liquid chromatography (c/nano-LC) and in capillary electrochromatography (CEC) as separation media. In these miniaturized LC systems, low flow rates (μL min^{-1}) are used, which implies accurate control of the dead time and delay volumes (which is particularly critical for gradient elution). With this aim, a practical procedure to implement synchronized gradient elution in commercial cLC systems was developed (Chapter 4). The benefits of synchronization on efficiency and time saving were demonstrated. Taking into account this synchronization approach, a method for the determination of parabens in biological fluids was developed. In this method, methacrylate monoliths and nano-LC coupled to mass spectrometry (MS) were used (Chapter 5).

The wide variety of easily available chemistries is one of the advantages of polymeric monolithic columns. To obtain monoliths with the desired chromatographic properties, the chemical modification of reactive monoliths is one of the strategies most commonly adopted. Consequently, it is important to know both the number of reactive sites available for functionalization and the functionalization yield. In Chapter 6, a simple gas chromatography – flame ionization detector (GC-FID) method capable of providing this information is described.

In the following chapters, different monolithic materials were prepared by chemical modification of its pore surface, in order to achieve stationary phases with enlarged areas and enhanced properties. For this purpose, several ligands as epinephrine (Chapter 7), phosphatidylcholine (Chapter 8), polythiol (Chapter 9), a codeine derivative (Chapter 10), and silver nanoparticles (Chapter 11), among others, have been attached onto the pore surface. In some cases, the enhancement of pore surface coverage with these ligands has provided the highest values published until now. These materials have been successfully applied in the separation of different types of target analytes (alkyl benzenes, aromatic hydrocarbonds, chiral compounds, proteins, etc.). Also, in this second part, the synthesis and applications of hybrid porous polymeric materials using magnetic nanoparticles (Chapter 12) have been described. An enhancement of

the surface area of these monoliths with respect to the parent monolith, giving rise to excellent separations of organophosphorous pesticides, has been demonstrated.

Finally, in the third part of this PhD Thesis, the characterization of different raw materials by electromigration and chromatographic techniques is described. Within these materials, water soluble polymers such as polyvinyl alcohol (Chapter 13) (used as additive in laundry products) and a rigid polymeric foam (Rohacell®, Chapter 14) which is used in aeronautical and space applications were studied. Also, a method for the analysis of the alcoholic constituents present in essential oils (Chapter 15), of importance in cosmetic and personal care products, was developed.

SECTION I. INTRODUCTION

Chapter 1. Miniaturization in separation techniques

1.1. Introduction

Miniaturization, an emerging trend in Analytical Chemistry along the last third of the last century, is still today an important issue. As Richard Feynman said in 1959, "there's plenty of room at the bottom". Electrophoresis and other electromigration techniques were successfully miniaturized to the capillary scale along the 1980-1990 decade, and further miniaturization, including microchip technologies, followed. Capillary electrophoresis (CE) and capillary electrochromatography (CEC) are today widely used. More recently, commercial instruments for capillary- and nano-scale high-performance liquid chromatography (cHPLC and nHPLC) have become increasingly popular. Advantages over non-miniaturized techniques are the capability of handling small samples, low consumption of reagents and reduced waste volumes [1]. This is well within the current trends and objectives of a Green Analytical Chemistry [1]. Also, as a result of the reduced flow rate, cHPLC and nHPLC systems are more adequate than conventional HPLC for coupling with mass spectrometry (MS).

On the other hand, along with miniaturization, a number of technical problems related to the control of operation times, injection systems, connectors, accuracy of volumes and reduction of sample carryover, have emerged. Fortunately, several manufacturers are continuously marketing new instruments with increasingly improved characteristics. Great efforts have been made to improve miniaturized HPLC instrumentation and applications entailing theoretical, technological and methodological studies. As a result, miniaturized separation techniques have become complementary with respect to conventional HPLC [2], as well as strongly competitive in a wide number of applications, particularly within the bioanalytical and life sciences fields, and especially in proteomics and other “omics” [3].

1.2. Capillary and nano liquid chromatography systems

So far, definitions for cHPLC and nHPLC, establishing frontiers between them and with respect to larger scale conventional HPLC have not been widely accepted. However, it has been suggested [4-5] that nHPLC should be applied to chromatographic separations performed in capillary columns of internal diameters in the 10 to 100 μm range, whereas cHPLC should be reserved for separations performed using columns within the 100 to 500 μm range.

In use today, there are basically two different designs of cHPLC and nHPLC systems, namely split and splitless pumped. The former are based on the splitting of a primary flow to provide the very small secondary flow required at the injection device and analytical column. This design is depictured in Fig. 1.1. Alternative designs make use of pump modules which directly produce the low flow rates without flow splitting [6].

Aside from the system design, miniaturized columns should be used. These are usually made of either fused silica or stainless steel. As in conventional HPLC, both the packed-bed and monolith approaches are used to construct the stationary phases in cHPLC and nHPLC. Due to the many and outstanding advances achieved along the last decades in packed-column technology, excellent narrow columns for low scale HPLC are today available. Advances concerns to the purity of the silica support, spherical regularity of particles, narrow size range, controlled pore diameter and pore deepness, and packing compactness and homogeneity. Improvements in efficiency and resolution, even at large flow rates have been achieved. Thus, reduced analysis time without sacrificing separation performance, has been made possible. In addition, a variety of well-defined surface chemistries with extended pH-stability, providing different selectivity, has become available.

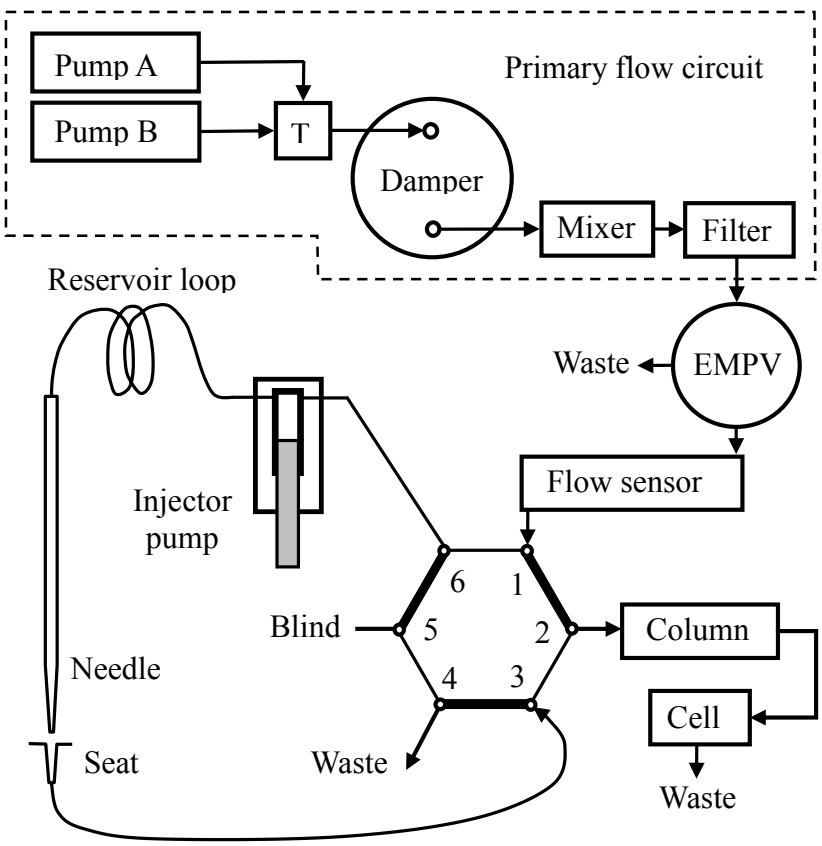

Fig. 1.1. Scheme of a cHPLC system which relies on the splitting of a primary flow (T, mixing point; EMPV, electromagnetic proportional valve).

As in conventional HPLC, packings containing particles with diameters such as 2.7, 3 or 5 μm, are rather usual. Sub-2 μm particles, going down even to 1.5 μm, are also used; however, chromatographs and fittings especially design to withstand pressures as high as 60 or even 100 MPa are required (ultra-performance or UPLC systems). Concerning to monoliths for operating low scale HPLC, a perspective is provided in the next chapter.

As recommended in conventional HPLC, a precolumn should be also used in low scale HPLC. In addition to a faster column degradation, capillaries are easily blocked at the inlet, particularly when real samples are injected.

Preconcentration on auxiliary columns can be also performed when the system allows some automation flexibility, including, for instance, column switching. Techniques for sample clean-up or on-column focusing can be implemented.

1.3. Capillary electromigration techniques

Electrophoresis is a physical phenomenon that involves the transport of charge in an electric field. Using a background electrolyte (BGE), and in the presence of the field, ions with more charge density move faster than ions with less charge density, allowing separation. In modern CE, the usual support is by far a polyimide coated silica capillary. The electric field can be also used for a second purpose: to transport the whole content of the capillary in two ways, i.e. forward with respect to either the inlet or the outlet ends, and also with respect to the detector location. This is achieved thanks to the interfacial phenomenon known as electro-osmotic flow (EOF).

Usually, electrophoresis is used to transport ions and thereby to achieve separation by the different electrical charge density at the surface of them. When the analytes are charged, the separation mechanism is purely electrophoretic: the ions move with a constant speed, which is proportional to its charge and inversely proportional to friction with the surrounding medium. In contrast, in CEC and micellar electrokinetic chromatography (MEKC), electrophoresis could be present, but there are always other forces at play. In CEC, the electric field is used to pump the mobile phase through a particle-packed or monolithic stationary phase. Since pumping should be achieved by EOF, the surface of the stationary phase should have a net electrical charge. Nonionic analytes are separated by true chromatographic distribution between the mobile and stationary phases. In principle, the electric field is used in CEC only to drive the mobile phase along the separation system; however, it can be also simultaneously used to separate charged analytes. Thus, in CEC, charged analytes are separated by a mixed mechanism, in which both chromatographic

retention on the stationary phase and electrophoresis are significant. The same happens in MEKC in relation to nonionic and ionic analytes; however, with the difference that micelles are used as a pseudo-stationary phase. The electric field drives the continuous and pseudo-stationary phases at different speeds, even in opposite directions, and the analytes distribute between them.

CE, CEC, MEKC and other techniques (such as capillary electro-focusing) can be grouped under the common name of capillary electromigrations. In them, a potential drop between 5 and 30 kV is used to create an intense electric field along the capillary. Tubes of internal diameter between 25 and 100 μm are used. The small section of the capillary limits the current intensity and helps in dissipating the generated heat. CEC is similar to cHPLC and nHPLC, with the difference that the mobile phase is pumped internally, by means of the EOF, plus the presence of the additional electrophoretic separation mechanism for ionic analytes. Electro-osmotic pumping provides an almost flat profile for the mobile phase axial linear velocity. This largely reduces A-term of the Van Deemter model, thus improving efficiency. Capillary electromigrationss are rapid (5-15 min) and usually highly efficient (from 100.000 up to few millions theoretical plates). Other important features are the ability to handle micro samples (1 to 50 nL are injected), minimal reagent consumption and high flexibility, since it is easy to modify the selectivity by adding reagents to the BGE.

The scope of capillary electromigrationss extends to all types of organic and inorganic ions, from small to very large molecular masses (proteins, deoxyribonucleic acid (DNA) fragments and synthetic polymers). Chemical species without net electric charge (uncharged and double ions) cannot be separated by CE; however, a charged additive which associates to the analyte in the solution (e.g. an ionic surfactant, even below its critical micellar concentration) could promote separation, and CEC or MEKC can also be alternatively used. The only limitation is solubility of the sample in a minimally conducting medium. This medium can be water or polar organic solvents (such

as methanol or acetonitrile). Only totally apolar media (such as hydrocarbons and its halogenated homologs) are excluded.

Chapter 2. Monoliths: historical perspective, synthesis and analytical applications

2.1. Monoliths: historical perspective

Monoliths for chromatography, catalysis and other applications directly derive from disperse macroporous polymers. These materials, developed around 1950, are obtained by suspension polymerization. An organic mixture containing the monomer or monomers (usually a vinyl derivative), a crosslinker (such as a divinyl derivative), an initiator and a porogenic solvent is dispersed upon stirring in a suspending medium, usually an aqueous phase. Solvating or non-solvating solvents, or soluble linear polymers, are used as porogens. Thermally induced decomposition of the initiator causes polymerization to start within the dispersed droplets, ultimately leading to the production of spherical polymer particles. After polymerization, the porogen is washed away, revealing the typical macroporous morphology. Macroporous polymers are characterized by fixed porous structures that persist regardless of the solvent employed, and even in the dry state. Their internal structure consists of an interconnected array of polymer microglobules separated by pores, and their structural rigidity is secured through extensive crosslinking. They are widely used as ion-exchangers to purify water and industrial effluents, but also in other applications including adsorbents, supports for solid phase synthesis, reagent immobilization, chromatographic packed-beds, etc.

Soon in the 50s of the 20th century emerged the idea of constructing macroporous polymers within a mold, thus constituting a single piece rather than a disperse material. However, the adequate technology to achieve high-performance single-rod monoliths was not developed until the 90s of the century [7-8]. The first successful high-performance separations associated with rigid macroporous polymers prepared by bulk polymerization in a closed mold were achieved by Hjertén *et al.* in the late 80s and early 90s [7, 9]. Original demonstrations of sufficiently rigid materials in analytical column format are due to Svec and Fréchet, which described a macroporous rod based on a methacrylate copolymer [7, 10]. Afterwards, a poly(styrene-*co*-divinylbenzene) [poly(STY-*co*-DVB)] monolith was developed by Wang *et al.*

[11]. These monoliths were suitable for the separation of proteins under reversed-phase (RP) gradient conditions.

The expression "monolithic" was also introduced by Svec *et al.* [12]. This term became rapidily popular, since it is an easy-to-use single word with an ancient etymology and a very long history. This Greek word, "monolithos", meaning a single stone, often with a pillar shape, is applied to ancient monuments, as the stones of the Stonehenge circle in England, or many Egyptian monoliths, including single stone obelisks (like those standing in the middle of Saint Pierre Square at the Vatican and in the Place de la Concorde, Paris) and the *Colossi of Memmon* (Fig. 2.1). In the late 90s, Tanaka's group at Kyoto (Japan) introduced the inorganic silica-based analogs of polymeric monoliths. As macroporous polymers, silica-based monoliths also have a hierarchical pore structure [13-14].

Fig. 2.1. Colossi of Memmon, Tebas, Egypt.

Unlike the dispersed materials, monolithic media are produced by unstirred polymerization within the confines of a mold, and without adding any suspending phase. This produces a single continuous macroporous material with interconnected channels, capable of supporting flow at reduced pressures. It is characterized by a bimodal pore size distribution consisting of both large

micrometer-sized channels and much smaller pores in the 10 nm size range. This unique porosity profile and the lack of any observed wall effect (opened channels along the walls of the mold due to volume shrinkage) result from the absence of both the interfacial tension between aqueous and organic phases, as well as the lack of dynamic forces typical of stirred dispersions.

At first, many practitioners did not believe that materials such as monoliths might attract the attention of the chromatographic community or, even less, be useful. However, the considerable effort of enthusiastic scientists, despite hostile reactions, invoked the interest of their colleagues on monolithic stationary phases. Its popularity is now supported by trade names of commercial processes and products that in one way or another include the word monolith. As observed in Fig. 2.2, the number of publications concerning monoliths, which increased largely within the 2000-2006 period, has still not decayed.

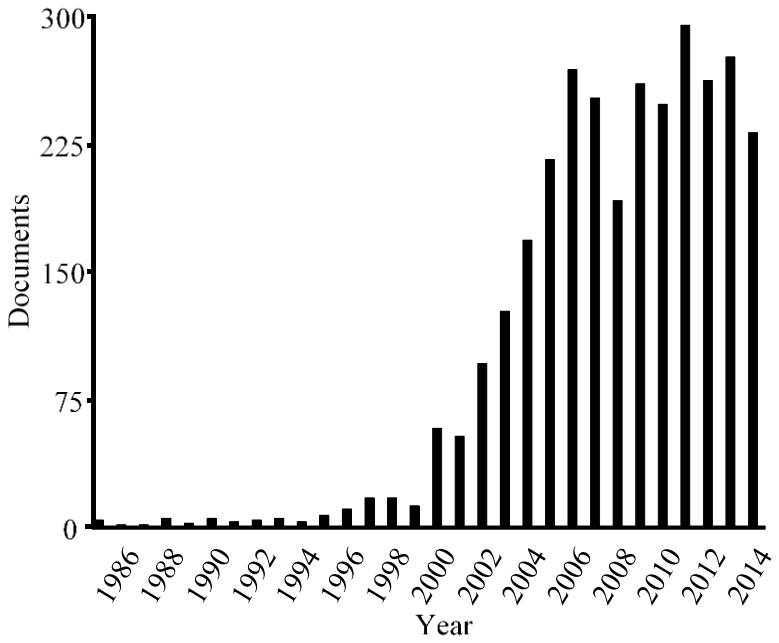

Fig. 2.2. Publication profile for monolithic columns

In comparison to packed-bed columns, monolithic stationary phases have some advantages. Thus, due to their continuous structure, retaining frits are not necessary. Also, packing techniques are complex, whereas monoliths are easily constructed *in-situ* almost independently from the shape and nature of the confining support (frequently a silica capillary tube, but also a variety of other materials and shapes). This is a great advantage to fill up micro-fluidic devices with a stationary phase, particularly when the mold has a complex geometry. In addition, the variety of synthesis procedures and the different materials that can be employed provides large flexibility of the surface chemistries, and allows the use in a wide range of separation methodologies. Among this, adaptability to the requirements of modern HPLC-MS is today highly appreciated. Polymeric monoliths have the necessary versatility to be easily adapted when small volumes of biological samples containing valuable analytes of a wide range of molecular masses and polarities, should be handled.

2.2.Preparation of polymeric monoliths

Monolithic stationary phases can be subdivided into two main categories, *i.e.* silica-based and polymer-based. Silica monoliths are prepared by using sol-gel technology [15-16]. This involves sequential hydrolysis, condensation reactions, and subsequent polycondensation of the silica alkoxide precursor. On the other side, organic polymer-based monolithic materials are commonly synthetized by free radical polymerization. This thesis is exclusively focused on organic polymeric monoliths, also including hybrid monoliths with a polymeric structural mainframe. The preparation, properties and applications of a wide variety of polymeric monoliths have been the subject of numerous excellent reviews. The text which follows has been mainly extracted from a selection of these reviews [17-34]. Other relevant articles that are not reviews have been also used to write this chapter [35-37].

As commented above for the disperse macroporous polymers, monoliths are also prepared from a polymerization mixture containing a monomer or a mixture of monomers, a crosslinker (a bifunctional monomer), an initiator (an ion or molecule which generates a radical) and a porogenic solvent or a mixture of porogenic solvents (which are inert respecting to polymerization). Although three steps of polymerization progress are usually distinguished (Fig. 2.3), namely initiation, propagation and termination, a polymeric monolith is generally constructed in a single operation. During initiation, active centers are created from which polymer chains are generated. At first, one or two radicals are created from the initiating molecules. Then, the radicals are transferred from the initiator to the surrounding monomers. Several choices are available for these initiators. Thus, initiation can be started by thermal decomposition, photolysis, redox reactions (e.g. with a persulfate), ionizing radiation, electrochemically, with a plasma or by sonication [38]. Propagation takes most of the polymerization time. During propagation, the chain length of the polymers increases. A chain begins when a free radical uses a π-electron to form a stable bond with a carbon atom. This turns the whole new molecule into another radical, which attacks another monomer in the surroundings. Once a chain has been initiated, it propagates until there is no more available monomer (living polymerization) or until termination by deactivation of the radical [39].

According to the mold shape, monoliths with different formats are obtained. The first pioneering approaches mimicked formats typical of packed columns. Analytical size columns with inner diameters ranging from 4 to 10 mm were the first to be used mostly for the separation of proteins [40-41]. However, rapid development of areas such as genomics and proteomics, typically handling only very small samples, required columns with much narrower bore, which ultimately led to the introduction of capillaries filled with monoliths [42-45]. Other formats are monolithic disks [46], cylinders [47] and fillings of microfluidic channels [48].

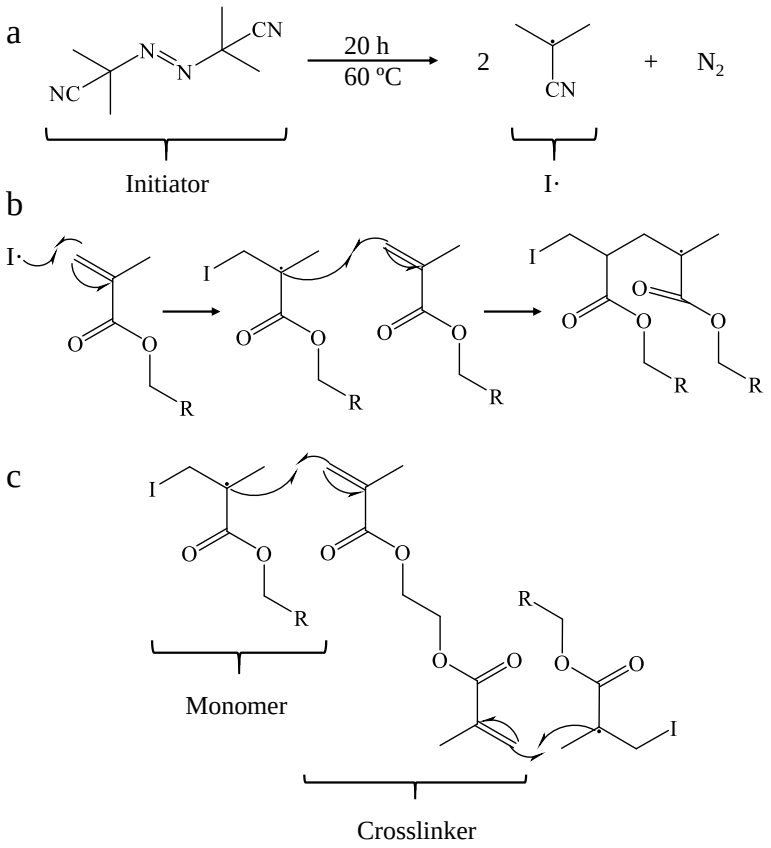

Fig. 2.3. Polymerization mechanism. (a) decomposition of the initiator; (b) radical monomer initiation and polymeric chain growth; (c) radical polymerization between monomer and crosslinker.

2.3. Influence of polymerization variables on polymeric monoliths

Most of the publications dealing with the development of monolithic columns are focused on the optimization of the composition of the polymerization mixture. Factors such as the composition and concentration of porogens, degree of crosslinker, type of monomer and the type of initiation are evaluated. These variables have shown to have influence on the porous properties of monoliths and consequently their chromatographic performance, and would be briefly discussed in the following sections.

2.3.1. Selection of the porogens

A single solvent or a mixture of them can be used as porogen in the polymerization mixture. Changing the porogen affects the solvation of the polymer chains during the early stages of the polymerization [49-50]. As a result, larger pores are generally obtained if poorer solvents are used because of an earlier onset of polymer phase separation [52].

An example of the influence of the porogen concentration is showed in Fig. 2.4. DOD is a macroporogen (stimulates the formation of large pores) because as solvating agent it is a poor solvent. When the DOD concentration increases over 30 wt%, the pore diameter (mode value) increases critically. However, the choice of porogens for the preparation of porous polymer monoliths remains an art rather than science. This is why not that many porogens have been used, and most often proven porogen mixtures are exclusively employed. For example, the mixture of cyclohexanol (CYC) and DOD formerly used to prepare porous poly(GMA-*co*-EDMA) beads was later adopted to prepare this and other molded monoliths [52]. Yet, these porogens have been used over and over again [53-56]. Similarly, a mixture of toluene with higher alcohols stills remains popular for the preparation of monoliths from STY and DVB [12]. In contrast, Huber's group used a mixture of decanol and THF as a porogen while focusing on the preparation of poly(STY-*co*-DVB) monoliths [57-59]. Their capillary columns separated well oligo- and polynucleotides and nucleic acids [60]. The same mixture of porogens was also used for the preparation of poly(GMA-*co*-DVB) columns [61]. Santora *et al.* carried out experiments with single solvent porogens including tetrahydrofuran (THF), acetonitrile (ACN), toluene, chlorobenzene, hexane, methanol (MeOH), dimethylformamide (DMFA), and methyl-*t*-butyl ether (MTBE); these solvents were used to prepare series of poly(DVB), poly(STY-*co*-DVB), poly(EDMA), and poly(methyl methacrylate-*co*-EDMA) monoliths [62]. Although some of these solvents afforded polymers with a surface area as large as 820 m^2 g^{-1}, it is unlikely that they would be permeable to flow since the pores were rather

small. Zhu *et al.* used another set of single porogens comprising CYC, 1-propanol (1-PrOH), DOD, dimethylsulfoxide (DMSO), and 1,4-butanediol (1,4-BuOH) for the preparation of monolithic poly(GMA-*co*-EDMA) columns [63]. Once again, none of these porogens enabled formation of monolith with the desired porous properties. In contrast, use of a binary porogens such as a mixture of 1,4-BuOH and dimethyl sulfoxide (DMSO) led to monolithic capillaries with excellent permeability.

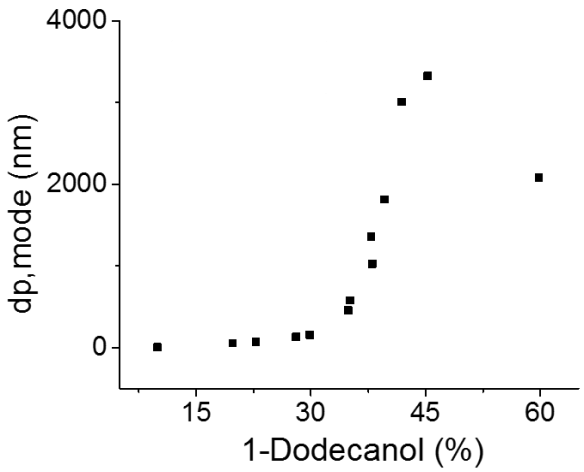

Fig. 2.4. Influence of the 1-dodecanol (DOD) concentration (porogen) in the mode of the pore size distribution (dp, mode, nm) for poly(glycidyl methacrylate-*co*-ethylenedimethacrylate) [poly(GMA-*co*-EDMA)] monolith prepared from different mixtures at a polymerization temperature of 70 ºC.

A new challenge arrived in the arena of porogens with the "reinvention" of CEC in the late 1990s [64]. The monolith had to contain both hydrophobic moieties providing the RP retention and ionizable functionalities required to sustain the EOF. In addition, the polymerization mixture had to be homogeneous to facilitate handling. Svec *et al.* have designed a unique porogenic system comprising water, 1,4-BuOH, and 1-PrOH that dissolved hydrophobic alkyl methacrylate monomer, EDMA (crosslinker), highly hydrophilic 2-acrylamido-2-methyl-1-propanesulfonic acid (AMPS), and

azobisisobutyronitrile (AIBN) (initiator) [65-67]. Monoliths with the desired porous structure and with an anionic surface were obtained with this mixture. Once again, this mixture has become quite popular [68-69].

Another family of porogens is represented by solutions of polymer in a solvent. In a very thorough study, the effects of poly(ethylene glycol) (PEG) dissolved in 2-methoxyethanol on the porous properties of poly(GMA-*co*-trimethylolpropane trimethacrylate-*co*-triethylene glycol dimethacrylate) monoliths were considered [70]. Thus, Irgum's group found that at larger molecular weight of PEG, the pores were larger. They also monitored the effect of numerous solvents used as a co-porogen on the porous properties. Novotny's group used a solution of poly(ethylene oxide) in N-methylformamide to prepare an homogeneous polymerization mixture consisting of acrylamide, methylene-bisacrylamide, acrylic acid, and alkyl acrylates [71]. An aqueous solution of PEG was later used as porogen for the preparation of monoliths from poly(ethylene glycol diacrylates) [72]. Li *et al.* described monolithic poly(ethylene glycol methyl ether acrylate-co-polyethylene glycol diacrylate) capillary columns prepared using poly(propylene glycol)-block-poly(ethylene glycol)-block-poly(propylene glycol) triblock copolymer with diethyl ether as porogen. These columns were tested for size exclusion chromatography [73]. A combination of high molecular mass polystyrene and chlorobenzene was used for the preparation of poly(glycerol dimethacrylate) monoliths with the interesting morphology, which is depicted in Fig 2.5 [74]. This monolith contained certain amount of mesopores and was used for the separation of small molecules with an efficiency of up to 34000 plates/m. Sinitsyna *et al.* tested a series of porogens including solutions of polystyrene in a toluene–DOD mixture and poly(dimethylsiloxane) in a hexane-DOD mixture for the preparation of poly(GMA-*co*-EDMA) monolithic layers. They found that these monoliths prepared in the presence of polystyrene were best suited for the immobilization of antibodies and suitable for the fabrication of protein microarrays [75].

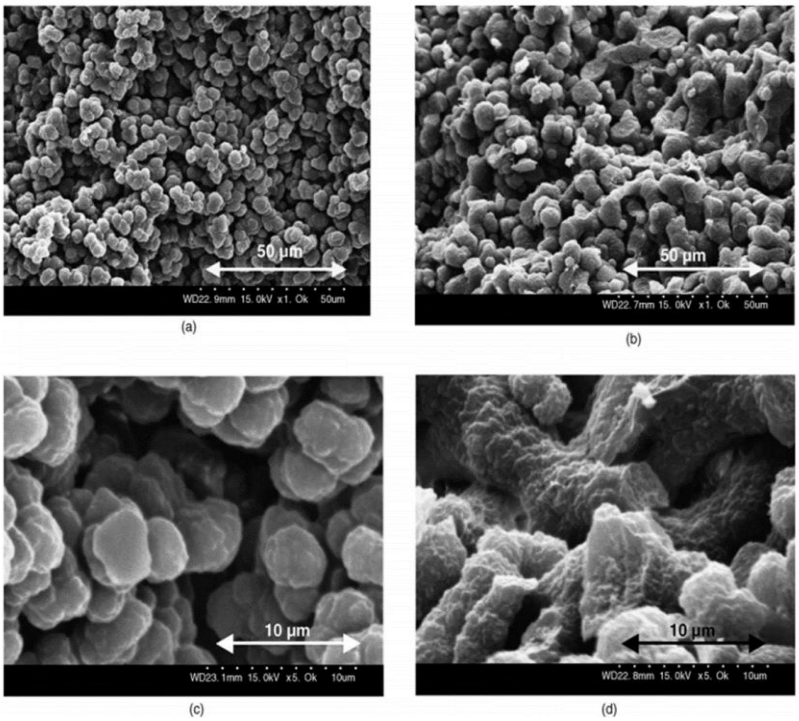

Fig. 2.5. Effect of the molecular mass (M_w) of poly(styrene) on the morphology of poly(GMA-*co*-EDMA) monoliths. (a) M_w = 50,000, ×1000. (b) M_w = 3,840,000, ×1000. (c) M_w = 50,000, ×5000. (d) M_w = 3,840,000, ×5000. Polymerized at 60 ◦C for 24 h with AIBN as initiator (10 mg mL^{-1}); GMA/poly(styrene) solution in chlorobenzene = 35/65, v/v [75].

2.3.2. Selection of the crosslinker

The effect of the crosslinker is in some way opposite to that of the porogens. Thus, increasing the percentage of the crosslinker decreases the average pore diameter of the resulting monolith due to the formation of highly crosslinked, less swellable polymer nuclei during the early stages of the polymerization. Similar to the situation with porogens, the number of most often used crosslinkers is limited (Fig 2.6). One of the reasons is commercial availability of these compounds. Ethylene dimethacrylate is most often used in the acrylate/methacrylate family of monoliths, methylenebisacrylamide is

preferred for aqueous systems whereas DVB is typically used with styrenic monomers [76].

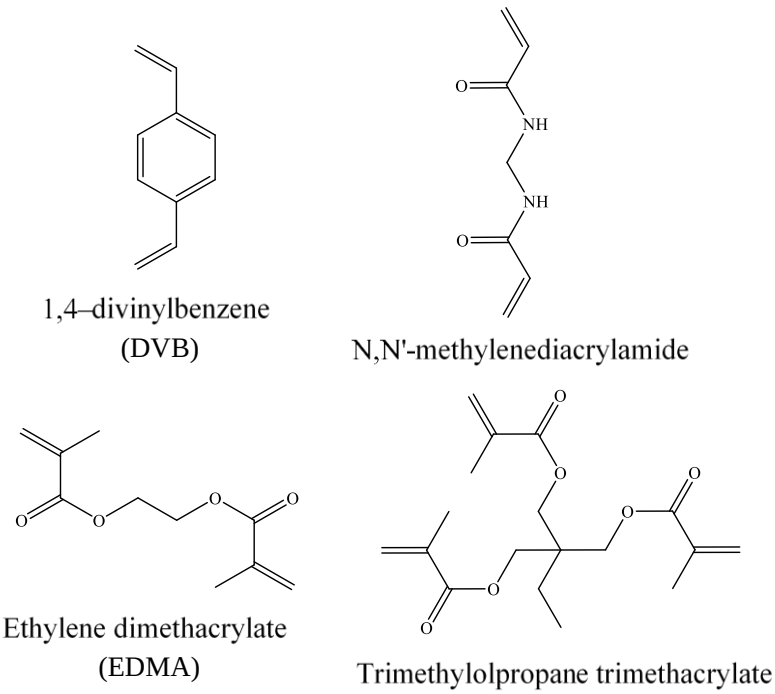

Fig. 2.6. Examples of crosslinkers used for the preparation of porous polymeric monoliths.

This does not mean that other crosslinkers can be used. For example, El Rassi's group introduced pentaerythritol diacrylate monostearate, that combines both crosslinking and hydrophobic functionalities, in the preparation of monoliths for CEC, affinity chromatography and HPLC [77-78]. This monomer was later used by others [79]. Trimethylolpropane trimethacrylate is another crosslinker often used for the preparation of monoliths [80-81].

2.4.3. Selection of the monomer and its influence over the surface chemistry

The surface chemistry of macroporous polymer monoliths can be easily modified providing virtually infinite possibilities. The surface chemistry should be selected according to the desired application. For example, hydrophobic moieties are required for RP chromatography, ionizable groups must be present for the separation in ion-exchange mode, groups with a specific reactivity are necessary for affinity modes, and enantioselective separations cannot be achieved without chiral functionalities. Further, monoliths with vastly different and finely tuned polarities may be obtained by direct copolymerization of different monomers. For instance, monoliths with controlled levels of hydrophilic, hydrophobic and charged functionalities can be obtained. In addition to the selection of monomers, the desired surface chemistry can be obtained either by incorporating additives to the polymerization mixture (e.g. nanoparticles, NPs) or by modifying the surface of the monolith after polymerization. These two strategies, namely pre- and post-functionalization, can be combined since they are not mutually exclusive.

First, a great number of surface functionalities can readily be obtained by the direct polymerization of the selected functional monomers. A few examples of monomers that have been used for the preparation of porous rigid monoliths are shown in Fig. 2.7. Almost any monomer, including water-soluble hydrophilic monomers, which are not suitable for standard polymerization in aqueous suspensions, may be used to form a monolith. This greatly increases the variety of surface chemistries that can be obtained directly, without requiring further monolith modification.

A variety of organic polymer-based monoliths based on polyacrylamide [82-83], polystyrene [12, 84-85], polyacrylate, [86-87] and polymethacrylate [12, 88-89] monomers has been extensively investigated. The advantages of organic-based monoliths over others as silica-based monoliths are a simpler and

faster preparation, wide variety of functional monomers, wider pH stability, and better biocompability. All these reactive pendant groups may further be transformed to afford functionalities for which no monomer precursor is readily available. Furthermore, ionizable monoliths, useful for CEC and for cation and anion exchange retention can be achieved using AMPS, (methacryloyloxy)ethyl trimethylammonium chloride (META), respectively. Zwitterionic functionalities and chiral monomers have been also used [51, 90-92].

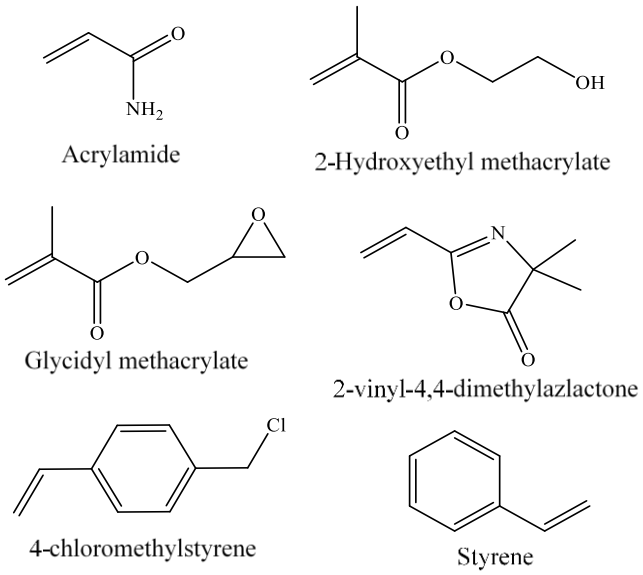

Fig. 2.7. Example of monomers used for the preparation of porous monoliths.

The first monolithic capillary column for hydrophobic interaction chromatography of proteins, introduced by Hjertén in 1991, was based on an acrylamide derivative [93]. Shortly afterwards, the same group introduced an important advance by bonding the monolith to the walls of the supporting tube. Thus, prior to polymerization, the fused silica capillary was treated with 3-(trimethoxysilyl)propyl methacrylate (γ-MPS) to afford polymerizable double bonds attached to the wall. The authors this time opted for a weak cation exchange column. The capillary filled with the polymerization mixture consisting of piperazine diacrylamide, methacrylamide, acrylic acid,

ammonium sulfate (co-porogen), water and the redox initiation system, was polymerized for 5 h. The methacryloyl functionalities covalently attached to the wall also participated in the polymerization. Since acrylamide-based monolithic capillary columns are highly polar, the range of separation mechanisms using these columns has been extended to normal phase [94].

In addition to acrylamide, STY has been also extensively used. This type of monolithic capillaries was commercialized by LC Packings (Sunnyvale, CA, USA). Horvath *et al.* reported the preparation of porous rigid monolithic capillary columns for HPLC by polymerizing 2:1 mixtures of STY and DVB initiated by AIBN in the presence of various porogenic solvents such as MeOH, ethanol (EtOH), water, and toluene [95]. Premstaller *et al.* prepared poly(STY-*co*-DVB) monolithic columns in 0.2 mm ID capillaries using THF/decanol as porogenic solvents [96]. These columns were tested for the rapid and highly efficient HPLC separation of protein digests followed by electrospray ionization (ESI)-MS detection enabling protein identification [97]. A significant improvement in the separation ability of the monolithic columns for peptides was demonstrated by Ivanov *et al.* [98]. They explored the use of poly(STY-*co*-DVB) monolithic capillary columns for the LC-ESI-MS analysis of peptide mixtures of tryptic digests. Both polymerization conditions and mobile-phase composition were optimized for chromatographic performance leading to efficiencies over 100,000 plates m^{-1}. The limits of detection were also very low.

Poly(STY-*co*-DVB) monolithic capillary columns developed by Huber's and Henion's groups and connected to a mass spectrometer were used for the separation of proteins [99-100]. Excellent separations requiring 10–15 min in a shallow gradient mode were demonstrated with capillaries comprising both poly(STY-*co*-DVB) monolith and their alkylated counterparts. For the separation in the RP mode, monolithic poly(STY-*co*-DVB) columns were prepared in silica capillaries using a mixture of THF and decanol as porogen. With gradients of ACN in 0.1 mol L^{-1} triethylammonium acetate, these

monolithic columns allowed the rapid and highly efficient separation of single-stranded oligodeoxynucleotides and double-stranded DNA fragments by ion-pair RP-HPLC [96].

Metha- or acrylate-based monoliths comprise the largest and most examined class of polymer separation materials. One of the most popular functional methacrylate monomers is GMA [70, 101]. Merhar *et al.* [102] investigated the effect of monomer, including GMA and other nine (hydroxypropyl methacrylate, dimethylaminoethyl methacrylate and different alkyl methacrylates). The monomer was copolymerized with EDMA and it was established that the pore radius decreased significantly with increasing hydrophobicity of the side group of the monomer with regard to GMA. In the case of acrylates, PEG-acrylates and PEG-diacrylates containing three or more moieties in the PEG chains have been used to synthesize monoliths with improved biocompatibility. For example, both monomers were copolymerized to afford a porous monolith that resists adsorption of both acidic and basic proteins when using an aqueous buffer without any organic solvent additives [103].

Another class of reactive monoliths is that based on nornornene monomers. Buchmeiser *et al.* developed an atypical approach to monolithic columns [104-105]. They used ring-opening metathesis copolymerization of norborn-2-ene and 1,4,4a,5,8,8a-hexahydro-1,4-exo,endo-5,8-dimethano naphthalene within a capillary in the presence of porogenic solvents such as toluene, methylene chloride, MeOH and 2-propanol (isopropanol, IPA). A ruthenium catalyst was used to prepare monolithic separation media with typical macroporous morphology. By variation of the polymerization conditions such as the ratio of monomers, the porogenic solvents and the temperature, the pore size was varied within a broad range affording materials with specific surface areas in a range of 60 – 210 m^2 g^{-1}. The living character of the ring opening metathesis polymerization enabled a simple preparation of these functionalized norbornene-based monoliths. Adding one more

derivatization step that involves functional norborn-2-ene and 7-oxanorborn-2-ene monomers that react with the surface-bound initiator, the pores can be provided with a number of typical functional groups such as carboxylic acid, tertiary amine, or even cyclodextrin [104, 106].

However, the polymerization conditions optimized for one system cannot be transferred immediately to another without further experimentation. The use of new monomer mixtures always requires optimization of polymerization conditions in order to achieve sufficient permeability of the resulting monolith [108]. This could result in a tedious experimental process [35, 108]. Another possible limitation related to this is that not all the functional monomers added will be exposed to the polymer surface since both the functional monomers and the crosslinker (which is present in a large proportion) are also part of the surface and not only of the monolithic scaffold [109].

2.3.4. Initiating systems in polymeric monolithic columns

As mentioned above, the polymeric monolithic columns are usually prepared via free-radical polymerization. The polymerization mixture, consisting in monomers, porogens and an initiator, is usually initiated by high temperature, or by UV irradiation with AIBN [110-112]. However, other less common approaches to initiate the polymerization are the use of γ-radiation [113] or a chemical agent [114].

In contrast to changes in the composition of the polymerization mixture, temperature is an especially effective means of control, allowing the production of macroporous materials with different pore size distributions from a single polymerization mixture [12, 49]. In an example reported by Svec *et al.* [35], a monolith prepared at 70 °C showed a sharp maximum close to 1000 nm. Instead of this, the same polymerization mixture, but polymerized at 130 ºC gave rise to a monolith with a very broad pore size distribution, spanning from 10 to 1000

nm with no distinct maximum. These shifts in pore size distribution as a result of changes in polymerization temperature can readily be explained in terms of the nucleation rates [12, 49].

The temperature affects mostly the specific surface area that is typically related to the small pores. If the polymerization temperature is low, the reaction rate is slow and transfer of a substantial part of monomers from solution to the nuclei occurs. Polymerization at the nuclei surface is kinetically preferred rather than the forming of new nuclei. The polymer molecules that are formed in the solution after the original nucleation grows. These are captured by the growing nuclei and form larger clusters with less individualized texture. This results in a low surface area. At higher temperature, the polymerization reaction is very fast and more growing chains are transformed into new nuclei and eventually into new individual globules rather than being captured by the primary nuclei. These globules are small and, therefore, their surface is large [49].

The accurate control of polymerization temperature during the preparation of large size monoliths is far more problematic than within capillaries. The unstirred nature of the polymerization within the confines of a mold hampers the dissipation of the considerable heat produced by the exothermic polymerization reaction. In addition to an overall deviation from the desired polymerization temperature, the magnitude of the exotherm has been shown to vary radially across the contents of the mold, leading to monoliths with heterogeneous pore structures [115]. Such inhomogeneities could severely limit the effectiveness of monoliths in larger scale applications such as catalysis or preparative chromatography. Therefore, specific techniques have been developed to obtain even larger diameter monoliths with homogeneous pore structures. These include the continuous gradual addition of the polymerization mixture to a heated reaction vessel [115], or a batch polymerization under “living” free radical conditions.

As an alternative to thermal initiation, photoinitiation emerged in the arena of monoliths in 1997 [51]. A systematic study of the preparation of monoliths from GMA and trimethylolpropane trimethacrylate clearly demonstrated the potential of photopolymerization that was found significantly faster than the thermally initiated process. This new technique did not initially find too much resonance, since the thermally initiated polymerization was the standard choice. Further, thermal initiation was well suited for the preparation of monolithic structures that completely filled the entire volume of a hermetically closed mold such as a column for HPLC. However, completely filled devices might not always be desired. For example, the preparation of monoliths in microfluidic chips requires their formation in a specific location while other parts must remain open. Therefore, a photolight initiated polymerization process is very well suited to achieve monolith formation within a specified space. Using a mask, the polymerization may be restricted to the irradiated areas beneath the open parts of the mask, while monomers do not convert to polymer in those areas that are not irradiated. The same technology is widely used for microelectronic patterning.

In addition, compared to thermally initiated polymerization, photopolymerization is significantly faster even at room temperature and can be completed in minutes rather than in hours. Since it runs at room temperature, a number of less common porogens including those with low boiling point such a methanol, ethanol, chloroform, ethyl acetate, and hexane can also be used [111]. The only limitations of this technique are in the use of UV transparent molds with a small size in one dimension and UV transparent monomers. The former is readily achieved using polytetrafluoroethylene (PTFE) coated capillaries and glass chips. The latter excludes aromatic monomers such as STY and DVB but leaves available a plethora of other monomers and crosslinkers. The latter excludes aromatic monomers such as STY and DVB but leaves available a plethora of other monomers and crosslinkers. Using this irradiation system, a large number of acrylates and methacrylates such as GMA, butyl

acrylate and BMA, sulfobetaines, butanediol diacrylate, and EDMA are included. For example, Daley and Oleshuk developed monolithic columns from the fluorinated aliphatic monomers 1H,1H-heptafluorobutyl acrylate and 2,2,3,3-tetrafluoro-1,4-butyl diacrylate and used them for the separations of fluorous tagged molecules using aqueous ACN as the mobile phase [116]. Lee's group copolymerized AMPS, 2-(diethylamino)ethyl methacrylate and 2-(acryloyloxy)ethyl trimethylammonium chloride with triethylene glycol diacrylate as the crosslinker [45]. The latter impaired the monoliths with enhanced hydrophilicity and reduced undesired hydrophobic interaction of proteins with the monolith during the ion-exchange chromatography. More recently, the introduction of arrays of light emitting diodes represents a new twist in the field of photopolymerized monoliths [117-118].

Using photopolymerization, the photoinitiator constitutes a very important component of the polymerization mixture. The quite popular AIBN decomposes under UV irradiation to afford free radicals [111, 119-120]. Since this initiator can also be used for the thermally initiated polymerization, comparative studies of both these approaches have been carried out [111, 122]. Only minor differences in the chromatographic performance of both types of columns have been found. However, the thermal monoliths exhibited higher back pressures than photopolymerized, thus indicating a difference in the porous structure. Other initiators, specifically designed for photopolymerization, are aromatic ketones such as 2-methoxy-2-phenylacetophenone (benzoin methyl ether) [51, 90, 122] and 2,2-dimethyl-2-phenylacetophenone [45, 123-126] that work at different wavelengths.

The use of ammonium peroxodisulfate and tetramethylenediamine has been described as a chemical initiating system for the preparation of butyl methacrylate (BMA), butyl acrylate and hexyl methacrylate-based monolithic columns for CEC [121, 86]. Monoliths obtained with this initiation system showed important differences in morphology compared with those prepared with AIBN as thermal initiator. In addition, the redox initiating system based

on persulfate provided some advantages such as better permeability of the resulting monoliths, and a fine control of the pore size over the porogens ratio, which made these columns highly suitable for separation methods. However, the redox systems requires a high content of water, at least a 20 wt% in the porogenic solvent, for the complete solubilization of the salt in the polymerization mixture, consequently, it cannot be employed when slightly water soluble monomers are used [112]. However, the use of peroxide derivatives (lauryl and benzoyl peroxides) has demonstrated to be an efficient alternative and to extend this initiating system to the preparation of polymeric monoliths in non-aqueous media [112].

2.4. Chemical modification of the surface chemistry

A low surface area is a drawback for chromatographic applications, since both retention and sample load capacity decreased. Low surface area also limits other applications which also rely on interactions with surface active sites, such as catalysis and adsorption. Several approaches have been reported that further increase the ability to balance the hydrodynamic and surface properties of these materials [127-128]. For example, monolithic materials with high specific surface areas of 300 $m^2 g^{-1}$ and completely novel porosity profiles have been produced by polymerization at substantially elevated temperatures using 2,2,6,6-tetramethyl-1-pyperio-dinyloxy- mediated “living” free radical process [127]. However, it is complicated to develop new monoliths with high surface area by exclusively manipulating the composition of the polymerization mixture, without further derivatization of the resulting polymer. Consequently, other approaches to increase the surface area of monoliths involve surface hybridization with other compounds, including polymers and NPs. It should be noted that these two approaches do not exclude each other.

The preparation of a monolith with reactive functionalities and its subsequent modification increases the number of available chemistries to afford

stationary phases for a variety of separation modes. Since the functional monomer constitutes both the bulk and the active surface of the monolith, a substantial percentage of the functional units remains buried within the highly crosslinked polymer matrix and is inaccessible for the desired interactions. Then, a better utilization of a rare functional monomer might involve its grafting polymerization on the pore surface of a "generic" monolith. As commented above, GMA monoliths constitute the typical all-purpose platform to modify the surface chemistry of the monoliths once polymerization has been completed [129-130]; however, in addition to GMA, other reactive monomers including 4-(chloromethyl)styrene [85] and 2-vinyl-4,4-dimethylazlactone [35] have been also used to achieve reactive monoliths.

Typically, to modify the surface of a reactive monolith, pores are filled with the derivatization reagent and allowed to react. This can be made either in static (filling the capillary, sealing the ends and allowing it to react for a fixed time and temperature) and in dynamic conditions (with recirculation of the derivatization solution). Dynamic derivation could be more effective due to the presence of a constant (not decreasing) concentration of the reagent. Once the reaction is completed, the monolith is flushed with a solvent to remove all unreacted components and it gets ready for application. For example, Fig. 2.8 shows the reaction of GMA-based monolith with diethylamine (DEA), which leads to a widely used anion exchanger [132]. The reaction of poly(chloromethylstyrene-co-DVB) with ethylenediamine and then with γ-gluconolactone completely switches the surface polarity from hydrophobic to hydrophilic [133]. The major benefit of this modification is simplicity of the single step polymerization process that was previously optimized.

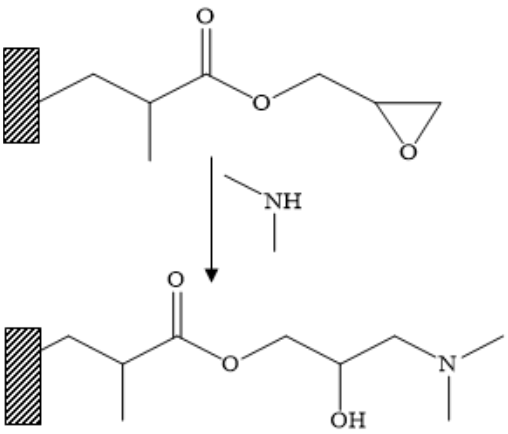

Fig. 2.8. Reaction scheme for the functionalization of poly(GMA-co-EDMA) monoliths with DEA.

The typical *in situ* polymerization approach used for monolithic media yields a single interactive site for every incorporated and accessible monomer unit. However, the conversion yield could be low, particularly if there is steric hindrance (e.g. with large and rigid ligands), or if unwanted side reactions take place. The development of methods for the evaluation of monolith surface modification, that is, to establish the conversion yield, constitutes a largely ignored area, where few advances have been reported. In this thesis, a universal method for the evaluation of grafting of ligands of any kind on GMA-based monoliths is described (see Chapter 6).

On the other hand, the attachment of reactive polymer chains to the internal surface of the pores leading to "hairy" pores can increase dramatically the density of accessible reactive groups [35]. This approach can be performed via chemical reaction [131, 134] or by UV-initiated polymerization [135-136]. While the former can be used for the functionalization of monoliths inside normal bore columns, UV-initiated grafting is more commonly used for the modification of monoliths prepared within narrow capillaries and microfluidic devices. Müller has demonstrated that the Ce(IV) initiated grafting of polymer chains onto the internal surface of porous beads afforded excellent separation media for biopolymers [137]. Svec *et al.* have used a similar reaction to graft

poly(2-acrylamido-2-methyl-1-propanesulfonic acid) onto the internal surface of hydrolyzed poly(GMA-*co*-EDMA) monoliths [138]. In this thesis, the grafting of a polythiol on a GMA-based monolith, providing a still reactive platform for further surface modification is described (see Chapter 9). In addition to the increase of the ligand density of the column (and therefore its analyte retention and sample loading capacities), grafting of polymers can be also used to increase the hydrophilicity of the polymer surface in order to reduce the non-specific interactions between analytes and the monolith scaffold [139-140].

According to other functionalization, photografting has been employed largely in the last years due to its wide applicability. Technically speaking, photografting is the covalent incorporation of functional additives to a polymer matrix or polymer surface using a light-induced mechanism. Thus, a "finished" polymer can be still "grown up" after light stimulation followed by the incorporation of monomers to the new reactive sites. Rånby *et al.* [141] have described the photografting onto polymer films applying aromatic ketones such as benzophenone as photoactive component. Photografting also enables control of porous properties of the monolith independently from management of its surface chemistry. In other words, photografting can be used first to improve the porous structure of a "generic" monolith, which can be followed by further photografting surface functionalization. An example is, the sequential two-step photografting of Fig 2.9 [142]. In the first step, initiator moieties are formed at the pore surface by UV irradiation of a polymer monolith that is in contact with a benzophenone solution. The second step of graft polymerization is then carried out with a solution containing only monomer. UV irradiation liberates the immobilized latent free radicals located on the polymer that then initiate graft polymerization from the surface. The photoinitiated process also enables the simultaneous grafting of more than a single monomer. Eeltink *et al.* co-grafted (2-methacryloyloxy)ethyltrimethylamonium chloride and butyl acrylate to control EOF in CEC columns [143]. The downturn of photografting is the

need of UV transparent "molds" and monomers. Thus, typical polyimide coated capillaries and aromatic monomers such as styrene cannot be used. Also, due to UV adsorption of the polymer matrix itself, the photografting is effective only for monoliths in which one dimension is short.

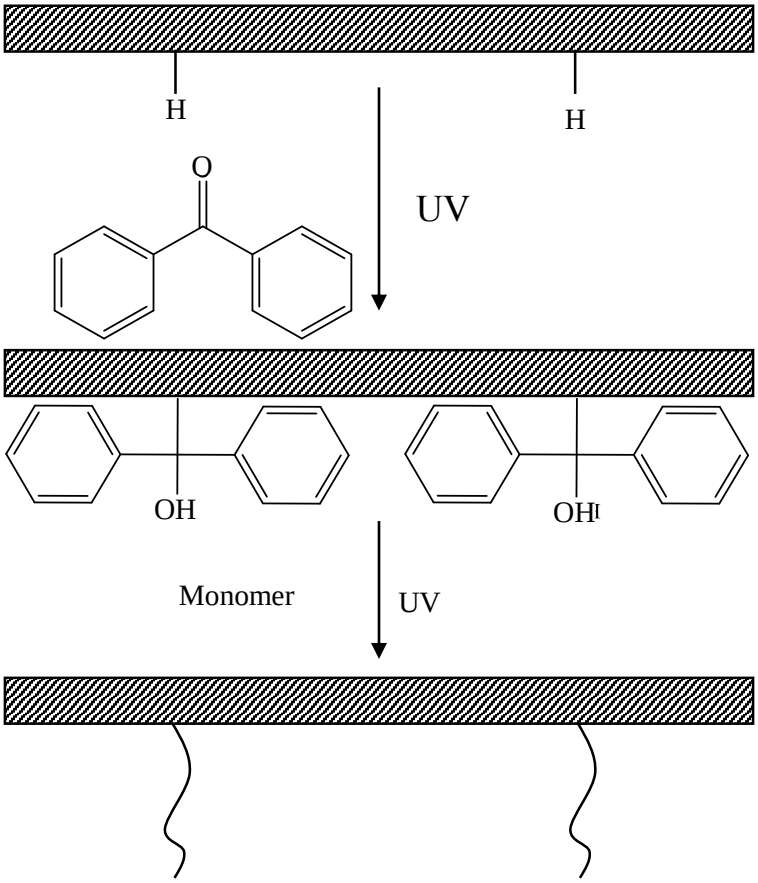

Fig. 2.9. Sequential two-step photografting scheme.

2.5. Introduction of nanoparticles to the monolith surface

Functionalization with NPs is the latest technique providing the possibility of tailoring the surface characteristics of monoliths [144-145]. NPs can offer numerous advantages; for example, their large surface-to-volume ratio can potentially facilitate mass transfer and enhance separation efficiency [146].

Further, the larger surface should result in enhanced retention and increased sample loading capacity.

The NPs can be introduced into the monolith by simple entrapment during polymerization [147-149]. Entrapment of NPs in the porous polymer matrix is technically feasible and straightforward; however, most of them would be buried within the monolithic matrix and not be available at the pore surface for the desired interactions [144]. Also, there might be some limitations regarding the amount of NPs that can be added (and therefore the extent of functionality reached) due to the incompatibility in the polarity of the nanoparticles and the polymerization mixture. Another approach is based on the previous derivatization of the NPs with a desirable functionality capable of copolymerizing with the functional monomers [149]. In this thesis we described the incorporation to a monolith of iron oxide NPs via vinylization and copolymerization (see Chapter 12). Alternatively, NPs can be used to decorate pore surfaces after preparation of a generic monolith [145, 150-152]. Indeed, using NPs contributes to the complexity of the nano- and micro-structured monolith. New parameters are added to both column preparation and post-polymerization steps. Optimization of these parameters could result in improved performance characteristics and other benefits.

A few decades ago, Dionex introduced very successful column packings for ion chromatography that consisted of non-porous micrometer sized poly(STY-*co*-DVB) beads sulfonated on their outer surface that were covered with anionic latex nanoparticles. Inspired by this approach, Svec *et al.* prepared a monolith by copolymerization of BMA, EDMA, and AMPS [145]. Then, a dispersion of 60 nm latex particles bearing quaternary amine functionalities was pumped through the capillary. SEM micrographs clearly revealed NPs attached to the pore surface. This monolith then enabled a fast separation of carbohydrates. Simultaneously, Haddad's group used a similar process that afforded latex-coated polymer monolith and used it for the separation of anions in CEC and cHPLC, respectively [153-154]. Although both these approaches

afforded the desired separations, the surface coating with latex particles was not complete thus limiting the loading capacity. This problem was solved by Hilder *et al.*, who optimized the surface modification conditions and achieved a homogeneous coverage of the pore surfaces with latex particles [156].

Another early example is that tested by Horvath's group in 2005, in which single-walled carbon nanotubes (SWNTs) were incorporated into the porous structure of poly(vinyl benzyl chloride-*co*-EDMA) [147]. This approach worked by simply adding the modified NPs to the polymerization mixture. The nanotubes were physically entrapped by the polymer, probably with part of them close to the pore surface or protruding from it. The authors report on improvements in the performance of the materials for liquid phase separations and observable changes in retention and selectivity. Navarro-Pascual-Ahuir *et al.* [157] have prepared BMA-based monoliths with embedded carboxy-SWNTs for CEC separations. These materials showed an enhanced resolution of neutral solutes and even a remarkable capability to separate enantiomers. On the other hand, Nischang *et al.* copolymerized just 1 wt% of a C60 fullerene bearing methacrylate monomer together with the typical polymerization mixtures for the preparation of poly(GMA-*co*-EDMA) monoliths or poly(BMA-*co*-EDMA) monoliths [149]. The authors claim an unprecedented efficiency, however the origin of the improved performance stays largely unexplained. It was suggested that the C60 chemistry, or the altered morphology of the monolith, or both contributed to the improved performance [156]. More recently, the incorporation of graphene oxide nanosheets into porous polymer monoliths has also been explored, and these columns have been used for CEC of small sized solutes [158].

Thayer *et al.* used a commercial ProSwift™ SCX-1S (4.6 mm × 50 mm) monolith column for surface modification [150]. A dilute aqueous solution of pellicular anion exchange NPs (DNAPac PA200) was pumped through the column until breakthrough was observed. The nanoparticle-coated monolith exhibited a further increase in sample load capacity and enhanced mass transfer

along with the chromatographic behavior typical of pellicular phases. The nanoparticle coating improved the selectivity and helped control tailing and band broadening associated with hydrophobic interactions compared to porous bead phases. In addition, the monolith showed separation of derivatized oligonucleotides from their unlabeled parents, and the ability to resolve several isobaric ribonucleic acid (RNA) linkage isomers, as well as phosphorothioate diastereoisomers in deoxyribonucleic acid (DNA) and RNA.

Lee *et al.* [159] reported the synthesis of monoliths composites containing embedded gold nanoparticles (GNPs). Functional groups were also bonded on the polymer surface to perform as bio-specific interaction sites. The detection of low molecular weight and biological analytes on the surface of these monoliths was demonstrated using surface enhanced Raman scattering spectroscopy and fluorescence microscopy. Under optimized conditions, and fortunately, the majority of the GNPs segregated to the surface of pores and hence, they were not "hidden" in the bulk of the polymer material. The NPs were strongly attached to the polymer surface, due to their partial embedding in the polymer matrix.

Svec *et al.* have immobilized GNPs on the pore surface of polymer monoliths [160]. First, epoxy groups of poly(GMA-*co*-EDMA) monolith reacted with cysteamine to afford thiol functionalities that are known to be well suited for the interaction with GNPs. Then, the NPs were formed in situ via reaction of chloroauric acid with trisodium citrate at elevated temperature. Alternatively, a preformed dispersion of GNPs was pumped through the functionalized monolith. The GNPs were held firmly onto the surface of the monolith by stable multivalent linkages that prevented them from being washed out from the column, even when the eluent contained competing thiols. The GNPs have shown to contribute significantly to the separation performance. For example, no separation of peptides could be observed using the poly(GMA-*co*-EDMA) monolith, and only a poor separation was achieved with its cysteamine modified counterpart. In contrast, a good separation of peptides was obtained

with the column containing the GNPs. This column was also used for the selective "fishing out" of peptides containing thiol group.

In an extension of this surface modification, the dynamic nature of the bond between gold and thiol groups has been exploited to tailor the surface chemistry through the binding of a variety of "exchangeable" thiol-containing moieties (see Fig. 2.10) [161]. This approach implied the introduction of a new concept, that of monoliths with exchangeable chemistries. First, surface modification of the monolith was conducted by pumping a cysteamine solution through the capillary column, thus affording a monolith with thiol groups. Two approaches were examined for the subsequent incorporation of GNPs: (1) in situ preparation via reduction of chloroauric acid using sodium citrate, which resulted in 15.37 % of GNPs with 40–50 nm in size; and (2) modification via pumping a solution (1.4×10^{12} particles mL^{-1}) of commercially available preformed NPs (15 nm) onto the thiol rich pore surface of the modified monolith. Although slower than the in situ formation of GNPs, this later approach was simpler, and provided a much higher content of GNPs. Capillary columns with RP and ion exchange (IEX) functionalities were then obtained by flushing the GNP-containing monoliths with 1-octadecanethiol and sodium-2-mercaptoethanesulfonate, respectively. The modified columns were examined for the rapid separation of a standard protein mixture. In this thesis, we described the development of monolithic columns with a high coverage of silver nanoparticles (SNPs) by means of self-assembly process and its application for the nano-LC separation of small molecules and proteins (Chapter 11).

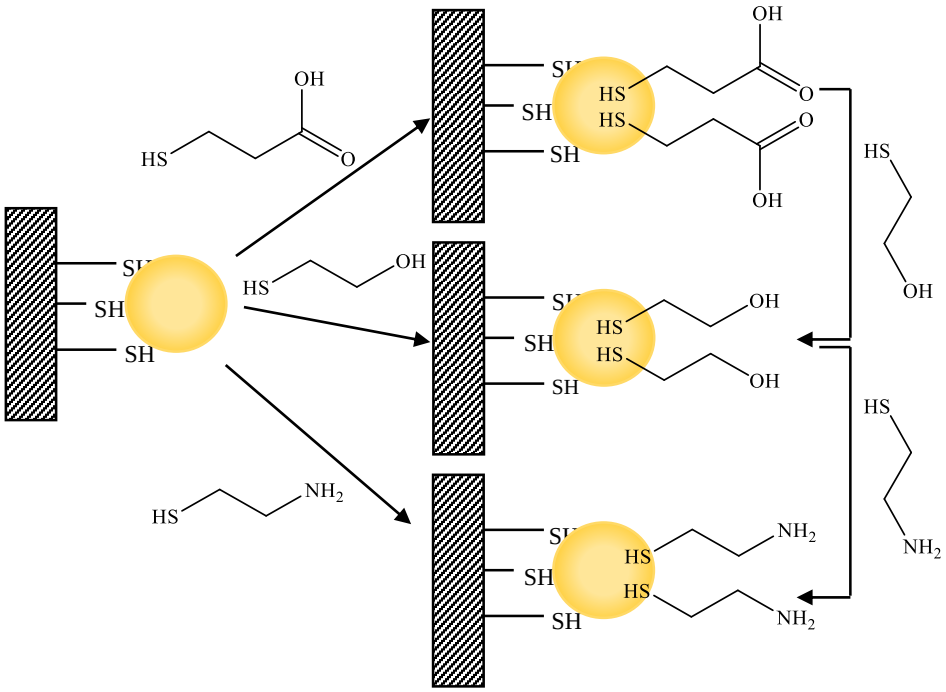

Fig. 2.10. Scheme of surface modification of a poly(GMA-*co*-EDMA) monolith reacted with cysteamine and posterior attachment with GNPs. The column is treated directly or by successive reactions with 3-thiopropionic acid, mercaptoethanol and cysteamine [161].

Other NPs including hydroxyapatite [148], iron oxide [162] and silver [151, 157] have been used to incorporate nanostructure features into monolithic materials. The nanoparticles of hydroxyapatite, $Ca_{10}(PO_4)_6(OH)_2$, possess both positive and negative charges stemming from calcium and phosphate ions, respectively. These active groups potentially enable a combination of retention mechanisms including cation- and anion-exchange, as well as calcium ion affinity [148]. Commercially available hydroxyapatite nanoparticles (50 nm) were therefore dispersed in the polymerization mixture consisting of HEMA, EDMA, CYC and DOD. Thermally initiated polymerization was conducted at 60 °C for 20 h. Previous experiments with GNPs showed that modification via surface coating can afford monoliths with more accessible NPs and higher coverage of pore surface than physical entrapment; however, in the case of the hydroxyapatite NPs, rapid clogging of the column hindered post-

polymerization modification of the monolith. Clogging occurred because of the presence of both positive and negative charges on the surface of the NPs, which favors particle agglomeration. In order to optimize the polymerization mixture, a constant amount of NPs was admixed to the polymerization mixtures containing different proportions of monomers. Although column permeability decreased by increasing the proportion of the NPs, the columns with the highest NP to monomer ratio showed the best performance for the separation of proteins in IEX mode, possibly because more NPs were buried inside the monolith with a higher content of monomers becoming inaccessible for separation.

2.6. Application of monoliths in the context of the separation science

2.6.1. Monoliths for CEC

CEC is a "hybrid" separation method in which uncharged molecules are separated in a fused-silica capillary, typically packed with C18-modified silica beads as in RP-HPLC, but where the mobile phase is driven through the capillary by an EOF [163]. In theory, extremely high efficiencies can be obtained for CEC separations due to the rather flat plug flow profile of the mobile phase, which allows reduced zone broadening. Although CEC was invented in the early 1970s [164], and its potential for packed capillary columns was demonstrated in the 1980s [165], serious technical problems slowed the development of this promising separation technique [166]. These problems include the difficult fabrication of frits within a capillary, the packing of beads into a tube with a very small diameter, the limited stability of packed columns, and the formation of bubbles capables of cutting off the current within the capillary during runs.

The development of monolithic columns has provided a very good solution to overcome these technical problems. Also, in contrast to the soft gels, rigid monoliths are not compressible and do not change their size substantially on swelling. In addition, various monomers can be polymerized directly, providing columns with both well-controlled porous properties [167] and a high number of surface chemistries [168-171]. Fig. 2.11 shows a representative high-efficiency example of the application as separation media for CEC.

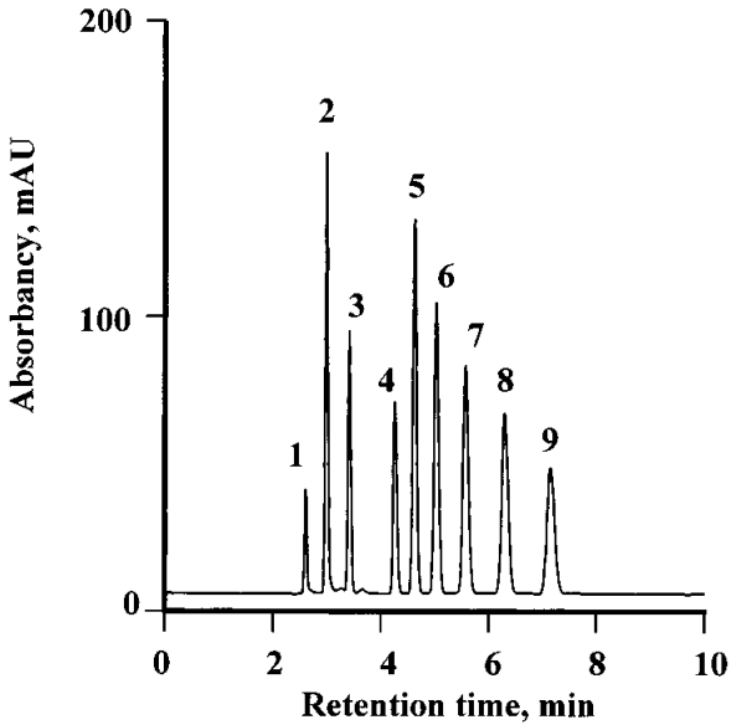

Fig. 2.11. Electrochromatographic separation of benzene derivatives on a monolithic capillary column of poly(GMA-*co*-EDMA). Mobile phase, 80:20 (v/v) mixture of ACN and 5 mmol/L phosphate buffer of pH 7. Peak identification, 1, thiourea; 2, benzyl alcohol; 3, benzaldehyde; 4, toluene, 5, ethylbenzene; 6, propylbenzene; 7, butylbenzene and 8, pentylbenzene [66].

2.6.2. Monoliths for RP chromatography

Separations of large molecules in the RP mode continue to be an active area of research for those working with polymer monoliths. Thus, a large percentage of applications for RP organic polymer monolith columns are in the field of proteomics [109]. A number of reviews have highlighted progression of monolithic column technology for this area [172]. One advantage frequently cited for employing polymer monoliths as chromatographic stationary phases is the ease of preparation in a wide range of column dimensions. Extending the use of polymer monoliths to separations of substantially more complex mixtures of large proteins, Huber *et al.* [173] demonstrated a "top-down" approach to LC–MS analysis of photosynthetic membrane proteins from various plant species using capillary poly(STY-*co*-DVB) monolithic columns and ESI-MS detection (Fig. 2.12). A number of intact proteins could be identified by comparing the measured intact mass with the theoretical molecular mass values. It is interesting to note that a relatively high column temperature (78°C) was employed to improve the resolution between the largest membrane proteins (M_w 40– 50 kDa).

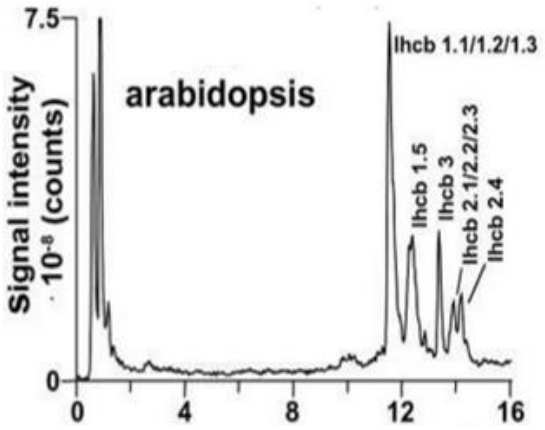

Fig. 2.12. RPLC separation with MS detection of photosystem II antenna from *Arabidopsis*. Column, PS-DVB-monolith [173]. Column: 60x0.20 mm i.d.; mobile phase: A) 0.05% TFA in water and B) ACN, linear gradient from 37.8 to 48.5% B in 20 min. Flow rate: 2 µL min^{-1}. Detection by ESI-MS with quadrupole ion trap.

2.6.3. Monoliths for HILIC

Monomers containing ionizable groups can also be used as stationary phases for hydrophilic interaction chromatography (HILIC). Thus, Chen *et al.* [174] reported the preparation of poly(methacrylic acid-*co*-EDMA) monoliths using mixtures of DMSO and PEG of different molecular masses as porogen. These hydrophilic monoliths were applied to the separation of a tryptic digest of bovine serum albumin (BSA) using HILIC-ESI- MS.

2.6.4. Monoliths for ion-exchange chromatography

IEX is a highly selective chromatographic mode for analyzing biomacromolecules, being able to resolve, for example, proteins which differ by only a single charged group [109, 175]. IEX can be conducted at near physiological conditions, and due to the mild chromatographic interactions involved it also causes less conformational changes or structural rearrangements compared to RP-HPLC. On the other hand, while eluent pH has a negligible effect on the ionization of strong ion-exchangers, it affects the extent of ionization of weak IEX functionalities, thus providing more opportunities to control selectivity and separation efficiency [109]. Minimizing non-specific interactions is also important to avoid slow adsorption–desorption kinetics that lead to band broadening and peak asymmetry [176]. Biocompatibility of the material is therefore an important feature that should be taken into account when designing a stationary phase for the separation of biomolecules [177]. This concept, along with a classification of biocompatible polymers and monoliths, was well-defined in a review published by Li and Lee [176].

Post-polymerization modification is another approach to obtain functional monoliths for IEX. Among others, GMA-based monoliths have been widely used for incorporating different functionalities through the epoxy group, which

readily reacts with various reagents containing, for example, amine [161, 178] or thiol groups [179]. While there are several reports (see, e.g. [180]) on the synthesis of weak anion-exchange columns via reaction of surface epoxy groups with amines like DEA, less effort has been made to prepare its strong counterpart. In one report, quaternary amine functionalities were incorporated in poly(GMA-*co*-DVB) monolith in a two-step reaction involving the ring-opening of the epoxy group with ethylenediamine followed by the alkylation of the resultant tertiary amine with diethyl sulfate [181].

A systematic study on the parameters affecting the modification reaction of poly(GMA-*co*-EDMA) monolith with DEA and triethylamine (TEA) was conducted by Bruchet *et al.* [182]. Their results indicated that while 96% of the epoxy groups were converted to tertiary amine functionality after an 8 h reaction in pure DEA at 65 °C, conversion efficiency did not exceed more than 68% even at 85 °C for the reaction with pure TEA. Subsequently, a significant improvement in reaction efficiency was obtained by the addition of a protic solvent to the reaction. Over 90% transformation to quaternary amine was finally achieved using TEA dissolved in 50% (v/v) aqueous EtOH after 4 h reaction at 85 °C. Increasing the reaction time from 4 to 8 h and the amine concentration in aqueous EtOH from 10 to 50% (v/v) no further enhancement in the reaction yield was achieved.

Post-polymerization modification also enables tailoring the hydrophilicity of materials. For example, a fairly good transformation of surface chemistry from highly hydrophobic into hydrophilic in styrene-based materials such as poly(4-vinylbenzyl chloride-*co*-DVB) was successfully performed through a two-step modification process comprising reaction with ethylenediamine followed by γ-gluconolactone [85]. The modified column exhibited hydrophilicity that was comparable to poly(GMA-*co*-EDMA) after complete hydrolysis of the epoxy groups to diols. To increase hydrophilicity, Ott *et al.* [140] modified the surface of a GMA-based monolith with a hydrophilic PEG diamine (2 kDa) via a multi-step approach. The remaining epoxy groups of the

generic monolith were first acid-hydrolyzed to hydroxyl groups prior to the reaction with 3-glycidyloxypropyltrimethoxysilane. The silanization reaction was conducted for 1 h at room temperature. The column was then filled with the polymer and incubated at 55 °C overnight in order to afford a hydrophilic coating.

2.6.5. Monoliths for hydrophobic interaction chromatography

Compared to other chromatographic modes, hydrophobic interaction chromatography (HIC) using monolithic columns has not been widely studied. This mild separation technique involves the use of an eluent containing a high salt concentration to enhance the hydrophobic interactions between biomolecules present in the eluent and the hydrophobic ligands in the stationary phase. Decreasing the salt content in the mobile phase then causes the biomolecules to elute according to their hydrophobicity. Generally, the stationary phases used in this chromatographic mode are characterized by a hydrophilic matrix containing a low density of a hydrophobic ligand on the surface [43]. Like IEX, the selection of a proper "biocompatible" polymeric matrix is also important in HIC in order to prevent the irreversible adsorption of biomolecules on the polymeric surface. The introduction of hydrophobic ligands into the stationary phase can be performed using monomers bearing both hydrophobic and hydrophilic functional groups. As has been mentioned previously, another way to introduce hydrophobic ligands on the polymer surface is by surface modification reactions.

2.6.6. Monoliths for size-based separations

Size exclusion chromatography (SEC) is a chromatographic mode used for the separation of high molecular mass compounds according to their hydrodynamic sizes. An ideal SEC column should be "inert", that is, it should

not have secondary interactions with the analytes, and also should present a significant percentage of meso- and micro-pores. The last requisite is the most difficult to achieve in polymeric monoliths, since these materials generally present primarily large through pores (macropores). In order to prepare monolithic columns with these characteristics, poly(BMA-*co*-EDMA) monoliths were prepared by systematically changing the polymerization conditions [183]. However, the resulting columns prepared showed a limited selectivity in the separation of poly(STY) standards compared to that obtained using particle-packed microcolumns [184].

Li *et al.* [73] used porogen surfactants (block-copolymers of poly(propylene oxide) and-poly(ethylene oxide)) of different molecular masses to confer mesoporosity to poly(ethylene glycol methyl ether acrylate-*co*-PEG diacrylate) monolithic columns. The authors synthesized a series of monoliths under different polymerization conditions and tested these columns for the SEC separation of proteins and peptides. They also synthesized poly(PEG methacryalte-co-PEG diacrylate) monoliths, but in this case using a ternary porogenic mixture consisting of DOD, hexane and a non-ionic polyoxyethylene surfactant (Brij 58P) [185]. Although the introduction of a surfactant of the Brij series as co-porogen increased the mesoporosity of the materials obtained, the peak capacity achieved with these columns was still limited. Finally, monolithic columns were used as stationary phases in hydrodynamic chromatography for the separation of synthetic polymers (poly(STY) and poly(methylmethacrylate) [186].

In contrast to SEC, hydrodynamic chromatography separations are based on partitioning within a non-uniform flow profile in which large molecules experience a greater mean velocity than smaller molecules which can approach to the wall more closely [187]. Edam *et al.* prepared poly(STY-*co*-DVB) monoliths within wide-bore stainless steel columns [186]. A set of polymers with different pore sizes were prepared by changing the porogen composition. The results showed how the porous structure of the monoliths can determine

the selectivity window obtained for each column. While polymers with pore sizes around 260 nm showed a good selectivity and good peak symmetry, polymers with larger macropores showed a combined SEC-hydrodynamic chromatography retention mechanism.

2.7. Future of monolith technology

For years, much of the focus in the development of polymer monoliths was on improving their performance for the separation of small molecules [188]; however, the performance and range of applications for large molecules is also an important area. Work in this area is driven more strongly by specific applications such as proteomics and protein and DNA purification. It can reasonably be expected that this will continue to be the case, for what is now a mature technology with a number of commercial products already available. Polymer monoliths also offer advantages for the separation or purification of other large particular matter such as cells [189], and it is likely that there will be significant future developments in this area. If this technology is to realize its full potential, then it is vital that the benefits continue to be demonstrated for a range of real applications, rather than for standard separations.

At the same time, it is clear that for a number of applications polymer monoliths do not yet offer separation performance that matches that of particle-packed columns. This may be viewed as both a limitation but also an opportunity. The recent significant developments in polymeric monolithic columns for the separation of small molecules has shown that by using new approaches such as hyper-crosslinking [190] or the incorporation of NPs [191], there can be significant performance benefits. It can reasonably be expected that similar or other approaches can be used to improve the morphology of polymer monoliths designed for the separation of large molecules. As well as improvements in the synthesis and thus morphology of these materials, as demonstrated by Nischang, considerable performance benefits can be realized

simply through the choice of the most appropriate operating conditions. This is well demonstrated for the example of small molecule separations and it is likely that such approaches will offer similar improvements for separations of large molecules, in particular where it is desirable to minimize diffusion-driven transport. The benefits of such approaches will continue to be limited by the extent of knowledge concerning the morphology and general porous properties of monolithic materials. The suite of techniques available for characterization of polymer monoliths and for the evaluation of surface modifications has improved, but it is clear that these are still areas where much further development is needed, in particular for the analysis of these materials under typical operating conditions rather than in the dry state. Finally, another unexplored area is the development of techniques for the 3D evaluation of the distribution of pores and defects in monoliths, as well as adequate models for their description.

Chapter 3. Identification and characterization of raw materials

3.1. Introduction

Raw materials are either directly extracted from nature or are subsequently used in the manufacturing of products or goods. The term “raw material” is used also to denote materials which are still in an unprocessed or minimally processed state. Raw materials are a critical part of any industry; therefore, it is of utmost importance to identify and characterize them. In addition, quality control is a must during the manufacturing process, and ensuring the quality of incoming raw materials can greatly improve operational performance, decrease economical budgets, enhance high-quality products and detect future problems in the final products. Quality control of raw materials is also essential to maintain the characteristics of the final product, which is utmost relevance to also maintain the customer fidelity. Therefore, laboratory controls are an integral part of Good Manufacturing Practice and the requirements thereof are regulated. Quality controls for raw materials comprise identity, purity and content testing. Frequently, they are carried out following legal regulations or according to the customer’s own preferences or instructions.

The term raw material is a very broad category, thus thousands of materials are included. For example, crude oil is a raw material which could provide finished materials such as fuel, plastics and other products. However, at the same time these finished products could be raw materials for other processes. In addition, any raw material could exhibit a range of drastically different properties, particularly if it contains a complex mixture of compounds. For this reason, different methods for characterization are frequently required to characterize raw materials. In addition, the same raw material could be used with different purposes and the necessary quality control methods could be different.

In all circumstances, the best technique and optimal method is that provides the quality parameters required by a costumer. Within this concern, speed, accuracy and low operational costs are highly appreciated. Although, the raw materials is an immense category, only two families namely, synthetic polymers and essential oils, will be considered in this thesis.

3.2. Synthetic polymers as raw materials

Synthetic polymers are rarely homogeneous chemical species. Rather, they feature multiple distributions in molecular mass, chemical composition, chain architecture, functionality, and so on [192]. Polymeric materials are characterized by long chains of repeated units known as monomers. The nature by which the chains intertwine determine the polymer macroscopic properties. The polymer chain orientations are random or can take an order. Polymers are used in many industry fields due to its wide variety and easy dedicated synthesis. Polymers are found in many products from cleaners to medicine and building blocks and structural parts of all kind of devices.

Depending on the industry, the quality control of polymers is focused in different characteristics. For example, in cleaning products, the purity, average and molecular mass and oligomer distributions are important [193], whereas in spatial applications an important aspect is adsorption and outgassing of unwanted compounds [194-196]. Also, in medicine, biocompatibility is an important issue [197].

3.3. Separation and characterization of polymers

Polymers are structurally characterized by many techniques including nuclear magnetic resonance (NMR), UV-visible, fluorescence, X-ray spectroscopy [198], surface analysis with scanning electron microscopy, infrared with attenuated total reflectance, atomic force microscopy [199] and thermal analysis [200] among others.

Although, several non separation methodologies are usually employed for characterizing polymers, separation methods are frequently necessary for industrial process monitoring and quality control. Depending on the separation mechanism, different information about the polymer is usually retrieved.

Separation methodology as SEC, often in combination with viscosity, light scattering and/or refractive index detection, is the most commonly applied technique for characterizing the molecular size of synthetic polymers [201-202]. In SEC, a column packed with porous particles and a ‘strong’ solvent as eluent are used for separating compounds based on their hydrodynamic molecular volume. Large

polymers are excluded from the pores of the particles to a greater extent and hence elute earlier from the column than smaller compounds. MS is mainly used for the analysis of low molecular weight polymers; however, it is of great value in the characterization of polycharged molecules, including proteins and other biopolymers [203]. When a polymer molecule has many charges or is easily ionizable, MS can provide accurate information on its chemical structure, specifically on its molar mass, number of charged sites, and implicitly on its chemical composition and functionality. However, even with a simple homopolymer sample, rather complex MS spectra can be obtained because of the presence of isotopes, salt adducts and fragments of the main polymer. The information retrieved largely depends on the interface and ionization technique, as well as on the type of mass analyzer.

Free solution CE or capillary zone electrophoresis (CZE), is a robust method for polymer separation. CZE differs from the commonly known capillary gel electrophoresis (CGE) since the capillary does not contain any stationary phase: it is just filled with the BGE and a large electrical fields is created by applying high voltage to the ends of the capillary. CZE does not require tedious sample preparation. It has several advantages over traditional separation for the characterization of synthetic polymers. In addition to CZE, other nonaqueous and aqueous CE techniques for the characterization of synthetic polymers, including CGE and capillary isoelectric focusing have been described [204-205]. Using CE techniques, information about size, shape, surface charge and formation of intramolecular associates can be gained [206]. MEKC has been used for the characterization of heparins (highly charged polysaccharides) and polyacrylic acids (Fig. 3.1) [207]. However, the characterization of non-charged polymers using CE has been scarcely investigated. In this way, polyethylene glycols have been analyzed by CZE previous derivatization with an anhydride, which provides chromophore groups and electrical charges at both polymer ends [208-209].

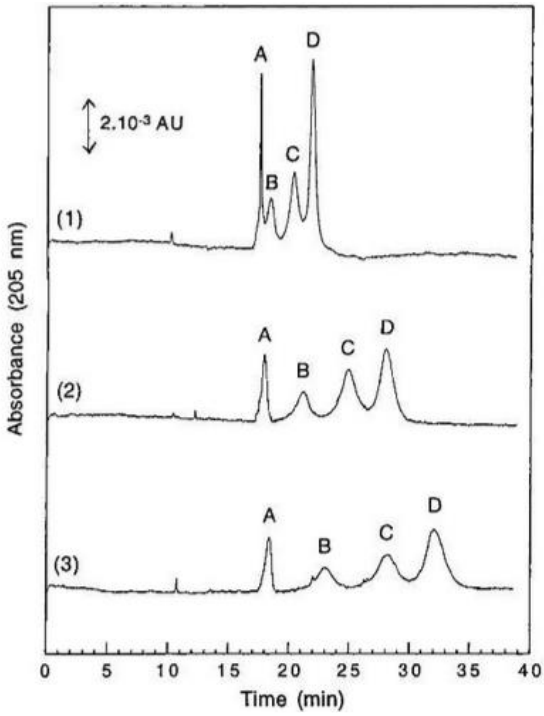

Fig. 3.1. CE separation of polyacrylic acids in the absence of EOF with PEG-coated capillary. BGE: 10 mM borax pH 9.2, containing (1) 3 mM, (2) 5 mM and (3) 10 mM of N-dodecyl-N,N-dimethyl-3-ammonium-1-propanesulfonate. Peak identification: (A) precursor, (B) 1% C12, (C) 3% C12 and (D) 7% C12 [207].

Non-equilibrium CE of equilibrium mixtures (NECEEM) is an important technique capable of providing information about proteins and DNA fragments using fluorescent markers [210-212]. Although this methodology is also important to obtain information about polymers. Using the NECEEM methodology, poly(vinylpyrrolidone) (PVP) was characterized [213]; for this purpose, the azo-dye Congo Red (CR), which forms a charged and colored PVP–CR complex was employed. In addition, similar methodology was followed in this thesis to develop a method able to predict the molecular mass and the tacticity (stereoregularity) of polyvinyl alcohol (PVA, Chapter 13).

3.4. Essential oils

Essential oils (EOs) are very interesting natural plant products which also possess biological activity. The term "biological" comprises all activities exhibited by these mixtures of hundreds or even thousands of volatile compounds, including the strong sensorial impact (mainly coming from mono- and sesquiterpenoids, benzenoids, phenylpropanoids, etc.) exerted on humans, animals and other plants. EOs, obtained from plant parts by steam distillation, have a wide variety of applications, mainly in cosmetics, personal care products and in natural medicine [214]. Apart from its wide use in the flavor and cosmetic industries, several pharmacological (antimicrobial, antifungal, insecticidal, anthelmintic, antioxidant) properties have been reported [215-217]. Quick and reliable characterization methods for essential oils in order to control industry manufacturing applications, its influence on human health and the defense of the consumer rights detecting adulterations are required.

3.5. Characterization of essential oils

In the course of the last half century, a great number of techniques have been developed and applied to the analysis of essential oils. Part of them has been replaced nowadays by either more effective or easier-to-handle techniques, while other methods have maintained their significance and have been permanently improved. Before going into detail, the analytical facilities in the sixties of the last century should be considered briefly. The methods available for the analysis of essential oils were at that time thin-layer chromatography, various types of LC, and gas liquid chromatography (GC). In addition, several spectroscopic techniques such as UV and IR spectroscopy, MS, and ^{1}H-NMR spectroscopy were available [218].

In the decades that followed, several additional techniques were developed and applied to essential oils analysis, including: GC-MS, HPLC, different kinds of countercurrent chromatography, supercritical fluid chromatography (including multidimensional coupling techniques), ^{13}C-NMR, near infrared, and Raman spectroscopy [219]. A multitude of the so-called hyphenated techniques, which means online couplings of chromatographic separation devices to spectrometers, yielding

valuable structural information of the individual separated components, made their identification more feasible.

However, the separation capability of GC exceeded all the other separation techniques, even when only packed columns were used. The evolution of this technique in the past can be impressively demonstrated, for instance, with examples of the GC separation of essential oils [219]. Thus, the essential oil of rue (*Ruta graveolens*) was separated by Bruno in 1961 [220] into eight constituents, which represented one of the first GC analyses of EOs. Only a few years later in 1964, the separation of the same oil improved using a Perkin Elmer GC equipped with a 2 m packed column and a thermal conductivity detector operated under isothermal conditions yielding 20 constituents. A further improvement of the separation of the rue oil was obtained after the introduction of temperature programming of the column oven, yielding approximately 80 constituents [221]. The last significant improvements were a result of the development of high-resolution capillary columns and the sensitive flame ionization detector (FID). By means of a 50 m glass capillary with 0.25 mm I.D., the rue oil could be separated into approximately 150 constituents, in 1981 [222].

The advantage online coupling of a chromatographic device to a spectrometer is that complex mixtures can be analyzed in detail by spectral interpretation of the separated individual components. The coupling of a GC with MS is the most often used and well established technique for the analysis of essential oils, due to the easy-to-handle powerful systems concerning sensitivity, data acquisition and processing, and above all their relatively low cost. The very first application of a GC-MS coupling for the identification of EO constituents using a capillary column was published by Buttery *et al.* (1963) [223]. Since then, many technical advances, including computerized data acquisition and treatment, have been incorporated to the GC-MS instruments.

The great majority of today's GC-MS applications utilize one-dimensional capillary GC with quadrupole MS detection and electron ionization. An example is shown in Fig. 3.2. Nevertheless, there are substantial numbers of applications using different types of mass spectrometers and ionization techniques. The proliferation of

GC-MS applications is also a result of commercially available easy-to-handle dedicated mass spectral libraries (e.g., NIST/EPA/NIH 2005; WILEY Registry 2006; MassFinder 2007; and diverse printed versions such as Jennings and Shibamoto, 1980; Joulain and König, 1998; and Adams, 1989, 1995, 2007 inclusive of retention indices) providing identification of the separated compounds. However, this type of identification has the potential of producing some unreliable results, if no additional information is used. This is because some compounds, for example, the sesquiterpene hydrocarbons a-cuprenene and b-himachalene, exhibit identical fragmentation pattern and only very small differences of their retention index values. This example demonstrates impressively that even a good library match and the additional use of retention data may lead in some cases to questionable results, and therefore require additional analytical data, for example, from NMR measurements, are required for disambiguation.

Owing to the volatility and low UV absorptivity of most of their components, essential oils have been scarcely analyzed by HPLC [224-227]. HPLC reports dealing with essential oils have focused on the detection of the non-volatile fraction of citrus oils [228-231], and with sample cleaning or fractionation previous to GC [232]. However, HPLC has been also used to detect specific terpenoids [233-234]. Recently, Turek and Stintzing [235] have reported an HPLC-UV-MS^2 method to fingerprint essential oils. The essential oils were characterized by their respective UV peak patterns, which were mainly due to the absorbent components.

On the other hand, traditional strategies for the development of robust GC and HPLC methods to separate the components of complex samples, as EOs samples, require considerable skill and patience of the chromatographer. This labor-intensive and time-consuming process is shortened and greatly facilitated by using a computer-assisted HPLC method development software [236]. Further, the chances of finding a true absolute optimum, rather than a secondary relative optimum, largely increase. Both, the advances in instrumentation technologies and the optimization software have made it easy the analysis of complex mixtures including essential oils. In this thesis, using computer-assisted method development, we describe an HPLC-UV

method to determine the main alcohols present in essential oils (Chapter 15) and its comparison with GC-FID and GC-MS techniques.

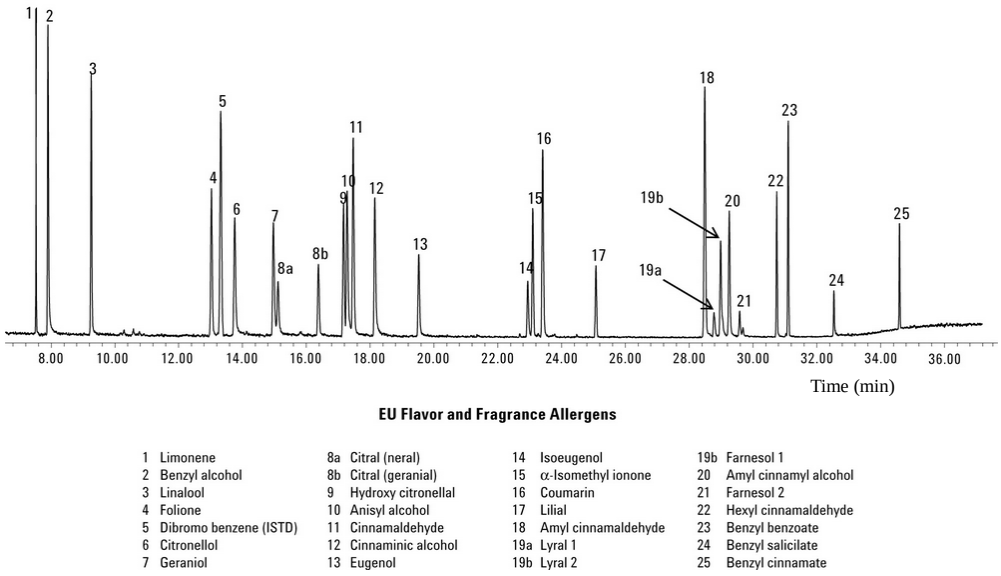

Fig. 3.2. TIC of an Ylang ylang (*Cananga odorata*) essential oil sample diluted 1:20 in ACN and analyzed by GC-MS [236].

References

[1] J. Hernández-Borges, Z. Artuki, A. Rocco, S. Fanali, J. Sep. Sci., 30 (2007) 1589.

[2] K.E. Karlsson, M. Novotny, Anal. Chem., 60 (1988) 1662.

[3] Y. Ishihama, J. Chromatogr. A, 1067 (2005) 73.

[4] J.P.C. Vissers, M. Ursem, J.P. Salzmann, Anal. Chem., 68 (1996) 1507.

[5] Y. Saito, K. Jinno, T.J. Greibrokk, J. Sep. Sci., 27 (2004) 1379.

[6] E. Rapp, U. Tallarek, J. Sep. Sci., 26 (2003) 453.

[7] F. Svec, J.M.J. Fréchet, Anal. Chem., 64 (1992) 820.

[8] F. Svec, J.M.J. Fréchet, Chem. Mater., 7 (1995) 707.

[9] S. Hjerten, J.L. Liao, R. Zhang, J. Chromatogr. A, 473 (1989) 273.

[10] J.M.J. Fréchet, F. Svec, US patent (1994) 5334310.

[11] Q.C. Wang, F. Svec, J.M.J. Fréchet, Anal. Chem., 65 (1993) 2243.

[12] C. Viklund, F. Svec, J.M.J. Fréchet, K. Irgum, Chem. Mater., 8 (1996) 744.

[13] H. Minakuchi, K. Nakanishi, N. Soga, N. Ishizuka, N. Tanaka, Anal. Chem., 68 (1996) 3498.

[14] K. Nakanishi, H. Minakuchi, N. Soga, N. Tanaka, J. Sol-Gel Sci. Technol., 8 (1997) 547.

[15] M. Kato, K. Sakai-Kato, N. Matsumoto, T. Toyo'oka, Anal. Chem., 74 (2002) 1915.

[16] D. Allen, Z. El Rassi, Electrophoresis, 24 (2003) 3962.

[17] S. Hjertén, Ind. Eng. Chem. Res., 38 (1999) 1205.

[18] F.E. Regnier, HRC-J., 23 (2000) 19.

[19] F. Svec, E.C. Peters, D. Sýkora, J.M.J. Fréchet, J. Chromatogr. A, 887 (2000) 3.

[20] D. Josic, A. Buchacher, A. Jungbauer, J. Chromatogr. B, 752 (2001) 191.

[21] M.R. Buchmeiser, J. Chromatogr. A, 918 (2001) 233.

[22] N. Tanaka, H. Kobayashi, K. Nakanishi, H. Minakuchi, N. Ishizuka, Anal. Chem., 73 (2001) 420A.

[23] N. Tanaka, H. Knobayashi, N. Ishizuka, H. Minakuchi, K. Nakanishi, K. Hosoya, T. Ikegami, J. Chromatogr. A, 965 (2002) 35.

[24] K. Cabrera, J. Sep. Sci., 27 (2004) 843.

[25] K. Miyabe, G. Guiochon, J. Sep. Sci., 27 (2004) 853.

[26] F. Svec, J. Sep. Sci., 27 (2004) 1419.

[27] F. Svec, C.G. Huber, Anal. Chem., 78 (2006) 2100.

[28] D. Schaller, E.F. Hilder, P.R. Haddad, J. Sep. Sci., 29 (2006) 1705.

[29] F. Svec, J. Chromatogr. B, 841 (2006) 52.

[30] G. Guiochon, J. Chromatogr. A, 1168 (2007) 101.

[31] S.D. Chambers, K.M. Glenn, C.A. Lucy, J. Sep. Sci., 30 (2007) 101.

[32] R. Wu, L. Hu. F. Wang, M. Ye, H. Zou, J. Chromatogr. A, 1184 (2008) 62.

[33] F. Svec, A.A. Kurganoc, J. Chromatogr. A, 1184 (2008) 281.

[34] F. Svec, T.B. Tennikova, Z. Deyl, Monolithic Materials: Preparation, Properties, and Applications, Elsevier, Amsterdam (2003).

[35] F. Svec, J. Chromatogr. A, 1217 (2010) 902.

[36] F. Svec, J. Chromatogr. A, 1228 (2012) 250.

[37] I. Nischang, I. Teasdale, O. Brüggemann, J. Chromatogr. A, 1217 (2010) 7514.

[38] G. Odian, Principles of Polymerization (4th ed.) New York, Wiley-Interscience (2004).

[39] Polymer Synthesis, Case Wester Reserve University 2010.

[40] S. Hjertén, J.L. Liao, R. Zhang, J. Chromatogr., 473 (1989) 273.

[41] F. Watanabe, T. Kubo, K. Jaya, K. Hosoya, J. Chromatogr. A, 1216 (2009) 7402.

[42] F. Svec, J. Sep. Sci., 27 (2004) 1419.

[43] Y.Y. Li, H.D. Tolley, M.L. Lee, J. Chromatogr. A, 1217 (2010) 4934.

[44] H.W. Zhong, Z. El Rassi, J. Sep. Sci., 32 (2009) 10.

[45] Y. Li, B.H. Gu, H.T. Dennis, M.L. Lee, J. Chromatogr. A, 1216 (2009) 5525.

[46] I. Kalashnikova, N. Ivanova, T. Tennikova, Anal. Chem., 80 (2008) 2188.

[47] K. Branovic, G. Lattner, M. Barut, A. Strancar, D. Josic, A. Buchacher, J. Immunol. Methods, 271 (2002) 47.

[48] J.A. Deverell, T Rodemann, J.A. Smith, A.J. Canty, R.M. Gujit, Sens. Actuators B, 155 (2011) 388.

[49] F. Svec, J.M.J. Fréchet, Macromolecules, 28 (1195) 7580.

[50] E.C. Peters, F. Svec, J.M.J. Fréchet, C. Viklund, K. Irgum, Macromolecules, 32 (1999) 6377.

[51] C. Viklund, E. Pontén, B. Glad, K. Irgum, P. Hördstedt, F. Svec, Chem. Matter., 9 (1997) 463.

[52] F. Svec, J. Hradil, J. Coupek, J. Kálal, Angew. Macromo. Chem., 48 (1975) 135.

[53] Y. Huo, P.J. Schoenmakers, W.T. Kok, J. Chromatogr. A, 1175 (2007) 81.

[54] S. Eeltink, E.F. Hilder, L. Geiser, F. Svec, J.M.J. Fréchet, G.P. Rozing, P.J. Schoenmakers, W.T. Kok, J. Sep. Sci., 30 (2007) 407.

[55] F.M. Okanda, Z. El Rassi, Electrophoresis, 27 (2006) 1020.

[56] S. Le Gac, J. Charlier, J.C. Camart, C. Cren-Olive, C. Rolando, J. Chromatogr. B, 808 (2004) 3.

[57] A. Premstaller, J. Oberacher, C.G. Huber, Anal. Chem., 72 (2000) 4386.

[58] W. Walcher, H. Oberacher, S. Troiani, G. Holzl, P.J. Oefner, L. Zolla, C.G. Huber, J. Chromatogr. B, 782 (2002) 111.

[59] H. Oberacher, C.G. Huber, Trends Anal. Chem., 21 (2002) 166.

[60] A. Throley, H. Toll, C.G. Huber, Anal. Chem., 77 (2005) 4618.

[61] C.P. Bisjak, R. Bakry, C.W. Huck, G.K. Bonn, Chromatographia, 62 (2005) 31.

[62] B.P. Santora, M.R. Gagne, K.G. Moloy, N.S. Radu, Macromolecules, 34 (2001) 658.

[63] G. Zhu, C. Yang, L. Zhang, Z. Liang, W. Zhang, Y. Zhang, Talanta, 70 (2006) 2.

[64] F. Svec, Capillary Electrochromatography. Elsevier, Amsterdam (2001), p. 183.

[65] E.C. Peters, M. Petro, F. Svec, J.M.J. Fréchet, Anal. Chem., 69 (1997) 3646.

[66] E.C. Peters, M. Petro, F. Svec, J.M.J. Fréchet, Anal. Chem., 70 (1998) 2288.

[67] E.C. Peters, M. Petro, F. Svec, J.M.J. Fréchet, Anal. Chem., 70 (1998) 2296.

[68] D. Moravcová, P. Jandera, J. Urban, J. Planeta, J. Sep. Sci., 26 (2003) 1005.

[69] A. Cantó-Mirapeix, J.M. Herrero-Martínez, C. Mongay-Fernández, E.F. Simó-Alfonso, Electrophoresis, 29 (2008) 4399.

[70] J. Courtois, E. Bystrom, K. Irgum, Polymer, 47 (2006) 2603.

[71] A. Plam, M.V. Novotny, Anal. Chem., 69 (1997) 4499.

[72] T. Kubo, N. Nikamura, K. Hosoya, K. Kaya, J. Polym. Sci. Polym. Chem., 45 (2007) 3811.

[73] Y. Li, H.D. Tolley, M.L. Lee, Anal. Chem. 81 (2009) 4406.

[74] H. Aoki, T. Kubo, T. Ikegami, N. Tanaka, K. Hosoya, D. Tokuda, N. Ishizuka, J. Chromatogr. A, 1119 (2006) 66.

[75] E.S. Sinitsyna, Y. Sergeeva, E.G. Vlakh, N.N. Saprikina, T.B. Tennikova, React. Funct. Polym., 69 (2009), 385.

[76] F. Svec, T.B. Tennikova, Z. Deyl, Monolithic Materials: Preparation, Properties, and Applications, Elsevier, Amsterdam (2003).

[77] F.M. Okanda, Z. El Rassi, Electrophoresis, 27 (2006) 2518.

[78] M. Bedair, Z. El Rassi, J. Chromatogr. A, 1079 (2005) 236.

[79] Z. Jiang, N. W. Smith, P.D. Ferguson, M.R. Taylor, J. Sep. Sci., 31 (2009) 2774.

[80] Q. Zhao, X.F. Li, X.C. Le, Anal. Chem., 80 (2008) 3915.

[81] K. Liu, P. Aggarwal, J.S. Lawson, H.D. Tolley, M.L. Lee, J. Sep. Sci., 36 (2013) 2767.

[82] J. Dong, R. Ou, X. Dong, R. Wu, M. Ye, H. Zou, J. Sep. Sci., 30 (2007) 2896.

[83] S.F. Xie, F. Svec, J.M.J. Fréchet, J. Polym. Sci., Polym. Chem., 35 (1997) 1013.

[84] M. Petro, F. Svec, J.M.J. Fréchet, J. Chromatogr. A, 752 (1996) 59.

[85] Q.C. Wang, F. Svec, J.M.J. Fréchet, Anal. Chem. 67 (1995) 670.

[86] A. Cantó-Mirapeix, J.M. Herrero-Martínez, C. Mongay-Fernández, E.F. Simó-Alfonso, Electrophoresis, 29 (2008) 3858.

[87] A. Cantó-Mirapeix, J.M. Herrero-Martínez, C. Mongay-Fernández, E.F. Simó-Alfonso, Electrophoresis, 599 (2009) 30.

[88] V. Bernabé-Zafón, A. Cantó-Mirapeix, E.F. Simó-Alfonso, G. Ramis-Ramos, J.M. Herrero-Martínez, Electrophoresis, 1929 (2009) 30.

[89] A. Cantó-Mirapeix, J.M. Herrero-Martínez, C. Mongay-Fernández, E.F. Simó-Alfonso, Electrophoresis, 607 (2009) 30.

[90] C. Viklund, K. Irgum, Macromolecules, 33 (2000) 2539.

[91] E.C. Peters, K. Lewandowski, M. Petro, F. Svec, J.M.J. Fréchet, Anal. Chommun, 35 (1998) 83.

[92] M. Lämmerhofer, E.C. Peters, C. Yu, F. Svec, J.M.J. Fréchet, W. Lindner, Anal. Chem., 72 (2000) 4614.

[93] J.L. Liao, R. Zhang, S. Hjertén, J. Chromatogr., 586 (1991) 21.

[94] A. Maruska, C. Ericson, A. Vegvari, S. Hjertén, Anal. Biochem., 241 (1996) 195.

[95] I. Gusev, X. Huang, C. Horváth, J. Chromatogr., 855 (1999) 273.

[96] A. Premstaller, H. Oberacher, C.G. Huber, Anal. Chem., 72 (2000) 4386.

[97] A. Premstaller, H. Oberacher, W. Walcher, A.M. Timperio, L. Zolla, J.P. Chervet, N. Cavusoglu, A. Van Dorsselaer, C.G. Huber, Anal. Chem., 73 (2001) 2390.

[98] A.R. Ivanov, L. Zang, B.L. Karger, Anal. Chem., 75 (2003) 5306.

[99] W. Walcher, H. Oberacher, S. Troiani, G. Holzl, P.J. Oefner, L. Zolla, C.G. Huber, J. Chromatogr. B, 782 (2002) 111.

[100] X. Huang, S. Zhang, G.A. Schultz, J.D. Henion, Anal. Chem., 74 (2002) 2336.

[101] T.B. Tennikova, M. Bleha, F. Svec, T.V. Almazova, B.G. Belenkii, J. Chromatogr., 555 (1991) 97.

[102] M. Merhar, A. Podgornik, M. Barut, M. Zigon, A. Strancar, J. Sep. Sci., 26 (2003) 322.

[103] B. Gu, J.M. Arment, M.L. Lee, J. Chromatogr. A, 1079 (2005) 382.

[104] F. Sinner, M.R. Buchmeiser, Macromolecules, 33 (2000) 5777.

[105] B. Mayr, G. Hoelzl, K. Eder, M.R. Buchmeiser, C.G. Huber, Anal. Chem., 74 (2002) 6080.

[106] F.M. Sinner, M.R. Buchmeiser, Angew. Chem., 39 (2000) 1433.

[107] Q. Wang, F. Svec, J.M.J. Fréchet, J. Chromatogr. A, 669 (1994) 230.

[108] A. Nordborg, E.F. Hilder, Anal. Bioanal. Chem., 394 (2009) 71.

[109] R.D. Arrua, M. Talebi, T.J. Causon, E.F. Hilder, Anal. Chim. Acta, 738 (2012) 1.

[110] L. Geiser, S. Eeltink, F. Svec, J.M.J. Fréchet, J. Chromatogr. A, 1140 (2007) 140.

[111] C. Yu, M. Xu, F. Svec, J.M.J. Fréchet, J. Polym. Sci. A: Polym. Chem., 40 (2002) 755.

[112] A. Cantó-Mirapeix, J.M. Herrero-Martínez, C. Mongay-Fernández, E.F. Simó-Alfonso, Electrophoresis, 29 (2008) 4399.

[113] M. Grasselli, E. Smolko, P. Hargittai, A. Sáfránu, Nucl. Instr. Meth. Phys. Res. B, 185 (2001) 254.

[114] P. Joldsvendová, P. Coulfal, J. Suchánková, E. Tesaøová, Z. Bosáková, J. Sep. Sci., 26 (2003) 1623.

[115] E.C. Peters, F. Svec, J.M.J. Fréchet, Chem. Mater., 9 (1997) 1898.

[116] A.B. Daley, R.D. Oleschuk, J. Polym. Sci., Polym. Chem., 40 (2002) 755.

[117] S. Abele, F.Q. Nie, F. Foret, B. Paull, M. Macka, Analyst, 133 (2008) 864.

[118] Z. Walsj, S. Abele, B. Lawless, D. Heger, P. Klan, M.C. Breadmore, B. Paull, M. Macka, Chem. Commun. (2008) 6504.

[119] D.J. Throckmorton, T.J. Shepodd, A.K. Singh, Anal. Chem., 74 (2002) 784.

[120] V. Augustin, A. Jardy, P. Gareil, M.C. Hennion, J. Sep. Sci., 30 (2007) 2858.

[121] A. Cantó-Mirapeix, J.M. Herrero-Martínez, C. Mongay-Fernández, E.F. Simó-Alfonso, Electrophoresis, 4 (2008) 910.

[122] D. Bandilla, C.D. Skinner, J. Chromatogr. A, 1004 (2003) 167.

[123] B. Gu, Y. Li, M.L. Lee, Anal. Chem., 79 (2007) 5848.

[124] J. Liu, C.F. Chen, C.W. Tsao, C.C. Chang, C.C. Chu, D.L. DeVoe, Anal. Chem., 81 (2009) 2545.

[125] X. Sun, W. Yang, T. Pan, A.T. Woolley, Anal. Chem., 80 (2008) 5126.

[126] B. Gu, Z. Chen, C.D. Thulin, M.L. Lee, Anal. Chem., 78 (2006) 5126.

[127] E.C. Peters, C. Viklund, K. Irgum, F. Svec, J.M.J. Fréchet, Chem. Mater., 8 (1996) 744.

[128] S.F. Xie, F. Svec, J.M.J. Fréchet, Chem. Mater., 10 (1998) 4072.

[129] S.F. Xie, R.W. Allington, F. Svec, J.M.J. Fréchet, F. Svec, Adv. Biochem. Eng. Biotechnol., 76 (2002) 88.

[130] E. Calleri, C. Temporini, F. Gasparrini, P. Simone, C. Villani, A. Ciogli, G. Massolini, J. Chromatogr. A, 1218 (2011) 8937.

[131] V. Frankovic, A. Podgornik, N.L. Kranjc, F. Smrekar, P. Krajnc, A. Strancar, J. Chromatogr. A, 1207 (2008) 84.

[132] F. Svec, J.M.J. Fréchet. Anal. Chem., 54 (1992) 820.

[133] Q. Wang, F. Svec, J.M.J. Fréchet, Anal. Chem., 67 (1995) 670.

[134] N.P. Dinh, Q.M. Cam, A.M. Nguyen, A. Shchukarev, K. Irgum, J. Sep. Sci., 32 (2009) 2556.

[135] T. Rohr, E.F. Hilder, J.J. Donovan, F. Svec, J.M.J. Fréchet, Macromolecules, 36 (2003) 1677.

[136] D. Connolly, B. Paull, J. Sep. Sci., 32 (2009) 2653.

[137] W. Müller, J. Chromatogr., 510 (1990) 133.

[138] C. Viklund, F. Svec, J.M.J. Fréchet, K. Irgum, Biotechnol. Prog., 13 (1997) 597.

[139] J. Krenkova, N.A. Lacher, F. Svec, Anal. Chem., 81 (2009) 2004.

[140] S. Ott, R. Niessner, M. Seidel, J. Sep. Sci., 34 (2011) 2181.

[141] B. Ranby, W.T. Yang, O. Tretinnikov, Nucl. Instrum. Meth. Phys. Res., Sect. B: Beam Interact. Mater. Atoms, 151 (1999) 301.

[142] J. Krenkova, A. Gargano, N.A. Lacher, J.M. Schneiderheinze, F. Svec, J. Chromatogr. A, 1216 (2009) 6824.

[143] S. Eeltink, E.F. Hilder, L. Geiser, F. Svec, J.M.J. Fréchet, G.P. Rozing, P.J. Schoenmakers, W.T. Kok, J. Sep. Sci., 30 (2007) 407.

[144] Y. Xu, Q. Cao, F. Svec, J.M.J. Fréchet, Anal. Chem., 82 (2010) 3352.

[145] E.F. Hilder, F. Svec, J.M.J. Fréchet, J. Chromatogr. A, 1053 (2004) 101.

[146] C. Nilsson, S. Birnbaum, S. Nilsson, J. Chromatogr. A, 1168 (2007) 212.

[147] Y. Li, Y. Chen, R. Xiang, D. Ciuparu, L.D. Pfefferle, C. Horvath, J.A. Wilkins, Anal. Chem., 77 (2005) 1398.

[148] J. Krenkova, N.A. Lacher, F. Svec, Anal. Chem., 82 (2010) 8335.

[149] S.D. Chambers, T.W. Holcombe, F. Svec, J.M.J. Fréchet, Anal. Chem., 83 (2011) 9478.

[150] J.R. Thayer, K.J. Flook, A. Woodruff, S. Rao, C.A. Pohl, J. Chromatogr. B, 878 (2010) 933.

[151] J. Liu, I. White, D.L. DeVoe, Anal. Chem., 83 (2011) 2119.

[152] D. Connolly, B. Twamley, B. Paull, Chem. Commun., 46 (2010) 2109.

[153] J.P. Hutchinson, P. Zakaria. A.R. Bowie, M. Macka, N. Avdalovic, P.R. Haddad, Anal. Chem., 77 (2005) 407.

[154] P. Zakaria, J.P. Hutchinson, N. Avdalovic, Y. Liu, P.R. Haddad, Anal. Chem., 77 (2005) 417.

[155] P.R. Haddad, E.F. Hilder, C. Evenhuis, D. Schaller, C. Pohl, K.J. Flook, Abstr. Papers, American Chemical Society, 2009, ANYL 236.

[156] V. Davankov, M. Tsyurupa, M. Ilyn, L. Pavlova, J. Chromatogr. A, 965 (2002) 65.

[157] M. Navarro-Pascual-Ahuir, M.J. Lerma-García, G. Ramis-Ramos, E.F. Simó-Alfonso, J.M. Herrero-Martínez, Electrophoresis, 34 (2013) 925.

[158] M.M. Wang, X.-P. Yan, Anal. Chem., 84 (2012) 39.

[159] A. Lee, S. Dubinsky, E. Tumarkin, M. Moulin, A.A. Beharry, E. Kumacheva, Adv. Funct. Mater., 21 (2011) 1959.

[160] F. Svec, Electrophoresis, 30 (2009) S68.

[161] Q. Cao, Y. Xu, F. Liu, F. Svec, J.M.J. Fréchet, Anal. Chem., 82 (2010) 7416.

[162] J. Krenkova, F. Foret, J. Sep. Sci., 34 (2011) 2106.

[163] M. Dittmann, K. Wlenand, F. Bek, G.P. Rozing, LC-GC, 13 (1995) 800.

[164] V. Pretorius, B.J. Hopkins, J. Schieke, J. Chromatogr., 99 (1974) 23.

[165] J.W. Jorgenson, K.D. Lukacs, J. Chromatogr., 218 (1981) 209.

[166] B. Boughtflowers, T. Underwood, C.J. Paterson, Chromatographia, 40 (1995) 329.

[167] M.N. Dittman, G.P. Rozing, J. Chromatogr. A, 767 (1997) 33.

[168] C. Fujimoto, Anal. Chem., 67 (1995) 2050.

[169] S. Hjertén, D. Eaker, K. Elenbring, C. Ericson, K. Kubo, J.-L. Liao, C.-M. Zeng, P.-A. Lindström, C. Lindh, A. Palm, T. Srichlayo, L. Valtcheva, R. Zhang, Jpn. J. Electrophor., 39 (1195) 105.

[170] M.N. Dittman, G.P. Rozing, J. Microcolumn Sep., 9 (1997) 399.

[171] T.M. Zimina, R.M., Smith, P.J., Myers, J. Chromatogr. A, 758 (1997) 191.

[172] J. Rozenbrand, B.W.P. Van, J. Sep. Sci., 34 (2011) 1934.

[173] C.G. Huber, W. Walcher, A.M. Timperio, S. Troiani, A. Proceddu, L. Zolla, Proteomics, 4 (2004) 3909.

[174] M.L. Chen, L.M. Li, B.F. Yuan, Q. Ma, Y.Q. Feng, J. Chromatogr. A, 1228 (2012) 54.

[175] Ion-Exchange Chromatography: Principles and Methods, Amersham Biosciences, Uppsala, Sweden (1999).

[176] Y. Li, M.L. Lee, J. Sep. Sci., 32 (2009) 3369.

[177] X. Chen, H.D. Tolley, M.L. Lee, J. Chromatogr. A, 1218 (2011) 4322.

[178] A. Bruchet, V. Dugas, C. Mariet, F. Goutelard, J. Randon, J. Sep. Sci., 34 (2011) 2063.

[179] B. Preinerstorfer, W. Lindner, M. Lämmerhofer, Electrophoresis, 26 (2005) 2005.

[180] F. Svec, J.M.J. Fréchet, J. Chromatogr. A, 705 (1995) 89.

[181] W. Wieder, C.P. Bisjak, C.W. Huck, R. Bakry, G.K. Bonn, J. Sep. Sci., 29 (2006) 2478.

[182] A. Bruchet, V. Duglas, I. Laszak, C. Mariet, F. Goutelard, J. Randon, J. Biomed. Nanotechnol., 7 (2011) 415.

[183] J. Urban, P. Jandera, P. Schoenmakers, J. Chromatogr. A, 1150 (2007) 279.

[184] H.J. Cortes, C.D. Pfeiffer, Anal. Chem., 65 (1993) 1476.

[185] Y. Li, H.D. Tolley, M.L. Lee, J. Chroamtogr. A, 1217 (2010) 8181.

[186] R. Edam, S. Eeltink, D.J. Vanhoutte, W.T. Kok, P.J. Schoenmakers, J. Chromatogr. A, 1218 (2011) 8638.

[187] G. Stegeman, R. Oostervink, J.C. Kraak, H. Poppe, K.K. Unger, J. Chromatogr. A, 506 (1990) 547.

[188] I. Nischang, I. Teasdale, O. Brüggemann, Anal. Bioanal. Chem., 400 (2011) 2289.

[189] A. Kumar, A. Srivastava, Nat. Protoc., 5 (2010) 1737.

[190] J. Urban, F. Svec, J.M.J. Fréchet, Anal. Chem., 82 (2010) 1621.

[191] I. Nischang, J. Chromatogr. A, 1287 (2013) 39.

[192] T. Chang, Adv. Polym. Sci., 163 (2003) 1.

[193] J. Borisch, O. Grosche, U. Wendler, W. Jaeger, H. Engelhardt, Macromol. Chem. Phys., 201 (2000) 447.

[194] ESA-ESTEC, Requirements and Standards Division, Noordwijk, The Netherlands (2008) ECSS-Q-ST-70-01C. Space product-assurance. Cleanliness and contamination control.

[195] ESA-ESTEC, Requirements and Standards Division, Noordwijk, The Netherlands (2008) ECSS-Q-ST-70-02C. Space product assurance. Thermal vacuum outgassing test for the screening of space materials.

[196] ESA-ESTEC, Requirements and Standards Division, Noordwijk, The Netherlands (2011) ECSS-Q-TM-70-52A. Space product assurance. Kinetic outgassing of materials for space.

[197] U. Müller, Med. Device Technol. 19 (2008) 32.

[198] J.L. Koenig, Spectroscopy of polymers, Elsevier, Amsterdam (2008).

[199] K. Merret, R.M. Cornelius, J. Biomater. Sci. Polymer Edn.,13 (2002) 593.

[200] J.D. Menczel, R.B. Prime, Thermal analysis of polymers fundamentals and applications, Wiley, USA (2009).

[201] C. Wu, Handbook of size exclusion chromatography, Marcel-Dekker Inc., New York (1995)

[202] H.G. Barth, B.E. Boyes, C. Jackson, Anal. Chem., 70 (1998) 251.

[203] P.J. Schoenmakers, C.G. de Koster, LG·GC Europe – Recent applications in LC-MS, Novermber 2002.

[204] H.P. Clos, H. Engelhardt, J. Chromatogr. A, 802 (1998) 149.

[205] H. Cottet, C. Simó, W. Vayaboury, A. Cifuentes, J. Chromatogr. A, 1068 (2005) 59.

[206] H. Engelhardt, M. Martin, Adv. Polym. Sci., 165 (2004) 211.

[207] J. Collet, C. Tribet, P. Gareil, Electrophoresis, 17 (1996) 1202

[208] R.A. Wallingford, Anal. Chem., 68 (1996) 2541.

[209] J. P. Barry, D.R. Radtke, W.J. Carton, R.T. Anselmo, J.V. Evans, J. Chromatogr. A, 800 (1998) 13.

[210] M. Berezovski, S.N. Krylov, J. Am. Chem. Soc., 124 (2002) 13674.

[211] A.P. Drabovich, M. Berezovski, V. Okhoninm, S.N. Krylov, Anal. Chem., 78 (2006) 3171.

[212] S.N. Krylov, Electrophoresis, 28 (2007) 69.

[213] M. Beneito-Cambra, J.M. Herrero-Martínez, G. Ramis-Ramos, J. Chromatogr. A, 1216 (2009) 9014.

[214] M. Lis-Balchin, J. Royal Soc. Health, 117 (1997) 324.

[215] S. Burt, Int. J. Food Microbiol., 94 (2004) 223.

[216] F. Bakkali, S. Averbeck, D. Averbeck, M. Idaomar, Food Chem. Toxicol., 46 (2008) 446.

[217] H.M.A. Cavanagh, Nat. Prod. Commun., 2 (2007) 1297.

[218] K. H. Can Vaser, G. Buchbauer, Handbook of essential oils, Taylor and Francis Group, Boca Raton, USA (2010).

[219] K.H. Kubeczka, Application of HPLC for the separation of flavor compounds, Berlin, New Yoir, Walter de Gruyter and Co (1981)

[220] S. Bruno, Farmaco, 16 (1961) 481.

[221] K.H. Kubeczka, Studies on complex mixtures, C. Bicchi and C. Frattini (Eds). Firenze, Italy (1989).

[222] K.H. Kubeczka, Standarization and analysis of essential oils, S. Jain (ed.) New Delhi, India (1981).

[223] R.G. Buttery, W.H. McFadden, R. Teranishi, M.P. Kealy, T.R. Mon, Nature, 200 (1963) 435.

[224] G.B. Lockwood, J. Chromatogr. A., 936 (2001) 23.

[225] M.S.F. Ross, J. Chromatogr., 118 (1976) 273.

[226] V. Solinas, C. Gessa, J. Chromatogr., 219 (1981) 332.

[227] C. Turek, F.C. Stintzing, Anal. Bioanal. Chem., 400 (2011) 3109.

[228] G.B. Lockwood, J. Chromatogr. A., 936 (2001) 23.

[229] P. Dugo, L. Mondello, L. Dugo, R. Stancanelli, G. Dugo, L. Pharm. Biomed. Anal., 24 (2000) 147.

[230] E. Frerot, E. Decorzant, J. Agric. Food Chem., 52 (2004) 6879.

[231] G. Dugo, P.Q. Tranchida, A. Cotroneo, P. Dugo, I. Bonaccorsi, P. Marriott, R. Shellie, L. Mondello, Flavour Fragr. J., 20 (2005) 249.

[232] L. Mondello, P. Dugo, G. Dugo, A.C. Lewis, K.D. Bartle, J. Chromatogr. A., 842 (1999) 373.

[233] V. Solinas, C. Gessa, J. Chromatogr., 219 (1981) 332.

[234] C. Villa, R. Gambaro, E. Mariani, S. Dorato, J. Pharm. Biomed. Anal., 44 (2007) 755.

[235] J.C. Berridge, Techniques for the Automated Optimization of HPLC Separation, Wiley, New York, 1985.

[236] K. Lynam, Sep. Sci., 545 (2015) 1.

SECTION II. DEVELOPMENT AND APPLICATION OF MONOLITHIC STATIONARY PHASES

Chapter 4. Synchronized gradient elution in capillary liquid chromatography

Journal of Chromatography A, 1318 (2013) 142–148

Contents lists available at ScienceDirect

Journal of Chromatography A

journal homepage: www.elsevier.com/locate/chroma

Synchronized gradient elution in capillary liquid chromatography☆

Enrique Javier Carrasco-Correa[a], Agustín Acquaviva[b], José Manuel Herrero-Martínez[a], Guillermo Ramis-Ramos[a,*]

[a] Departament de Química Analítica, Universitat de València, Dr. Moliner 50, 46100 Burjassot, Valencia, Spain
[b] Facultad de Ciencias Exactas, Universidad Nacional de La Plata, Campus Bosque Oeste, La Plata, Argentina

The synchronization of injection valve operation and gradient elution in capillary liquid chromatography (cHPLC) is studied. Focus is placed on the cHPLC systems which rely on the splitting of a primary flow to provide the much smaller secondary flow required at the injection device and analytical column. Owing to the tiny secondary flow rates, synchronization is necessary to achieve proper optimization of gradient elution methods. Otherwise, there is a risk of having the analytes totally or partially eluted in the initial isocratic conditions, and there is no control on the actual gradient profile reaching the column. Synchronization is first achieved by switching back the valve to bypass after injection. This is important to save time, and to avoid the gradient slope to be reduced by mixing within the internal volume of the injector (a 47% of slope reduction in the conditions used in this work). Valve switching to bypass should be produced immediately after the arrival of the end of the sample plug to the valve (t_V). Fine system synchronization is further achieved by starting the gradient at the match time (t_M), which is the time required to match the arrival of both the gradient front and the end of the sample plug to the valve, and therefore also to the column inlet. Synchronization of these two events requires starting the gradient either before or even after the injection, thus to prevent a late or an early arrival of the gradient front to the injection valve, respectively. Owing to their dependence with the backpressure, both t_V and t_M should be measured in the presence of the column at the initial gradient conditions. Simple experiments designed to measure t_V and t_M are described. With synchronization according to the techniques described in this work, control on the real gradient

elution conditions at the column location is maintained. The effects of synchronization on the chromatograms are illustrated by injecting a mixture of alkylbenzenes. At 1 μL min^{-1}, valve switching to bypass reduced analysis time from ca. 36 to 12 min (butylbenzene), and improved peak symmetry (from 2.00 to 0.94 for methylbenzene) and efficiency (the average apparent plate count increased in a ca. 60%). Synchronization according to the match time further improved efficiency (up to ca. 120%).

Keywords: capillary liquid chromatography; injection valve switching; match time in liquid chromatography; synchronized gradient elution.

4.1. Introduction

In HPLC, the dwell time, t_{dw}, is the time required by the solvent mixture to move from the mixing point of the pump module to the column inlet [1-6]. On the other hand, the delay time, t_{de}, is sometimes defined as the time required for the mobile phase to move from the mixing point to the detector cell in the absence of column [5]. According to these definitions, the delay time is the dwell time plus the time required by the mobile phase to move from the column location to the detector cell in the absence of column. This difference is negligible in conventional HPLC, where dwell and delay times are generally used as interchangeable terms; however, owing to the very low flow rates, the difference between delay time and dwell time can be significant in cHPLC and nHPLC. In these techniques, to distinguish between t_{dw} and t_{de} is also pertinent because the injection of a non-retained compound or marker in the absence of column gives a measure of t_{de}, whereas t_{dw} should be indirectly established from other measurements. Therefore, dwell and delay times will be distinguished in this work. As further discussed in this work, there are several contributions to the dwell and delay times, including their dependence from the backpressure, never considered in conventional HPLC, which should be taken into account in cHPLC and nHPLC to achieve proper control of system operation. In this work, focus is put on cHPLC; however, the techniques here developed to control gradient elution through system synchronization can be extended to nHPLC.

Dwell and delay times, which are not an issue in isocratic conditions, have a significant impact on retention and resolution of gradient elution methods [4,6]. In conventional HPLC, the dwell time is particularly important for weakly retained analytes, as well as to transfer methods from one instrument to another [4]. Thus, with a large dwell time the gradient front arrives too late to the column, which could result in the partial or total elution of weakly retained analytes in the initial isocratic conditions. Also, large dwell times complicate the assessment of analyte retentivity/hydrophobicity, and hamper gradient optimization during method development [6]. Finally, for economic reasons,

large dwell times are undesirable when MS detectors of high cost per hour are used [6]. According to Dolan *et al.* [4], to deal with dwell time differences in the transfer of HPLC methods, three approaches can be followed: first, to develop a method with enough resolution among all the peak pairs to tolerate dwell time changes; second, to supplement the method with a sufficiently long initial isocratic period, thus to make possible to subtract the dwell time of the instrument from that period; and third, to set the dwell time to zero by starting the gradient before the injection. However, in cHPLC, owing to the low flow rates at the injection device and column location, the dwell time is always large in comparison to both the gradient time and the global time of the chromatogram. Therefore, in cHPLC, to supplement the method with an extra initial isocratic period is not convenient. It is more advisable to reduce the dwell time as much as possible, and in most cases, to start the gradient before the injection is the only acceptable option.

As shown in this work, system synchronization, involving injection valve switching to bypass immediately after the entrance of the whole sample plug into the column channel, is necessary to achieve proper method development in cHPLC. This prevents the entrance of the gradient front into the internal path of the autosampler. Otherwise, the dwell time will be very large, the gradient will be preceded by a large unwanted isocratic period, and in addition, dilution of the mobile phase by mixing within the large internal volume of the autosampler will largely reduce the gradient slope. This also reduces control on the real gradient profile reaching the column, which becomes a function of the operating conditions, including flow rates, backpressure and sample volume. Lack of control on the elution conditions seriously hampers method development, also having a negative impact on retention, efficiency and resolution. A remarkable improvement is achieved by switching the valve to bypass immediately after the arrival of the end of the sample plug to the valve, at a time which in this work will be called the valve time, t_V. Valve switching to bypass at t_V saves much analysis time, also providing accurate control on the

gradient profile actually arriving to the column. Further, synchronization of valve switching to bypass with the start of the gradient at the pump module is also required to fully exploit the potential of cHPLC instruments. This can be implemented through the match time, t_M, which we have defined as the time required to match the arrival of both the gradient front and the end of the sample plug to the injection valve. Synchronization of these two events will require starting the gradient either before or even after the injection, thus to prevent a late or an early arrival of the gradient front to the injection valve, respectively.

In this work, the discussion is focused on cHPLC systems which rely on the splitting of a primary flow to provide the very small secondary flow required at the injection device and analytical column. Many cHPLC and nHPLC instruments in use today rely on this design. Alternative designs make use of pump modules which directly produce the low flow rates without flow splitting [7]. However, the synchronization procedures described in this work can be also useful for cHPLC systems based on alternative designs. Synchronization is achieved by measuring both t_V and t_M, and by programming the sample injection, the injection valve switching and the gradient start times accordingly. Two simple experiments designed to measure t_V and t_M are described. The benefits of system synchronization, carried out according to the techniques described in this work, are illustrated by separating a test mixture of alkylbenzenes on a laboratory made monolithic polymeric column.

4.2. Experimental

4.2.1. Reagents and materials

To construct the monolithic polymeric column, BMA, EDMA, 1,4-BuOH and γ-MPS from Aldrich (Milwaukee, WI, USA), and 1-PrOH, were used. AIBN from Fluka (Buchs, Switzerland) was used as chemical initiator. The column was constructed inside an uncoated fused-silica capillary of 25 cm of total length and 375 µm O.D. x 250 µm I.D (Polymicro Technologies, Phoenix,

AZ, USA). HPLC-grade ACN, MeOH, acetone and acetic acid (HAcO) from Scharlab (Barcelona, Spain), were also employed. Deionized water was obtained with a Barnstead deionizer (Sybron, Boston, MA, USA). A test mixture containing alkybenzenes (methyl, ethyl, n-propyl and n-butyl, Sigma-Aldrich, Steinheim, Germany) was prepared in ACN (1000 µg mL^{-1} each). This solution was diluted with water (100 µg mL^{-1} of each solute) and injected. Uracil (Sigma-Aldrich) was also used.

4.2.2. Preparation of the monolithic column

First, in order to ensure covalent attachment of the monolith to the inner wall of the fused-silica capillaries, surface modification with γ-MPS was performed as described [8,9]. The monolith was prepared from a polymerization mixture obtained by weighing BMA (24 wt%), EDMA (16 wt%), and a ternary pore-forming solvent constituted by 1,4-BuOH (18 wt%), 1-PrOH (28 wt%) and water (5 wt%). AIBN (1 wt% with respect to the monomers) was added [10]. After mixing and to obtain a clear solution, sonication for 10 min followed by purging with nitrogen for 10 more min was applied. The preconditioned capillary was filled with the mixture up to ca. 18 cm. After thermal polymerization (20 h, 60 ºC), the column was cut to 15 cm of bed length, and an HPLC pump was used to flush the column for 30 min with MeOH to remove the pore-forming solvents and possible unreacted monomers.

4.2.3. Instrument and working conditions

A cHPLC system from Agilent (1200 series, Waldbronn, Germany), constituted by a degasser (Agilent part G1379B), a capillary pump (G1376A) providing a primary flow which was split by an electromagnetic proportional valve (EMPV, G1361-60000), a capillary-flow sensor (maximal flow rate, 20 µL min^{-1}), a micro-well plate autosampler (G1377A, 1260 Infinity series) with

a micro metering device which provides injection volumes from 0.01 - 8 µL with the installed standard loop capillary, and a DAD (G1315C) with an 80 nL quartz cell (6 mm path length cell), was used.

The flow rate at the injection system and column location (secondary flow) was 1 µL min^{-1}, and 0.1 µL injections were made. Gradient elution was implemented by mixing an aqueous 0.1% acetic acid (HAcO) solution (mixture A) with ACN containing 0.1% HAcO (mixture B). Elution was made isocratically with mixture A for a variable time, followed by a linear increase of the percentage of mixture B during a gradient time of 8 min. Experiments addressed to measure the delay time and other system parameters were made with 0.1% of either acetone or uracil added to mixture B [1]. Detection wavelength was 265 nm for acetone and uracil, and 214 nm for alkylbenzenes.

4.3. Results and discussion

4.3.1. Introductory remarks

A scheme of the primary and secondary flow circuits, from the pump mixing point (T) to the detector cell, is shown in Fig. 4.1. The thick lines in the injection valve indicate the ports which are communicated by pairs when the valve is in bypass (e.g., when the sample is being aspirated or waiting for injection), whereas the thin lines indicate how are linked the ports with the valve in mainpass (e.g., immediately after injection). The time intervals in HPLC are due to the displacement of the mobile phase within the primary circuit (before the EMPV) at the primary flow rate, F_1, or to the displacement of the mobile phase or the sample plug within the secondary circuit (after the EMPV) at the secondary flow rate, F_2. Thus, volumes rather than time intervals are the actual building blocks in HPLC operation. However, time intervals rather than volumes are of prime concern during method optimization. For this reason, the discussion that follows will be conducted on a time basis rather than

on a volume basis. Also, whenever possible, the time intervals will be expressed with reference to the moment of the sample injection as the origin of time ($t = 0$). Thus, for clarity, all the time intervals that cannot be referred to the injection time as its origin will be preceded by a capital delta; for instance, the gradient time, which can be started at any moment after the injection (e.g., before the injection or after an initial isocratic period), will be expressed as Δt_G, whereas the delay time, which begins at $t = 0$, will be expressed as t_{de}.

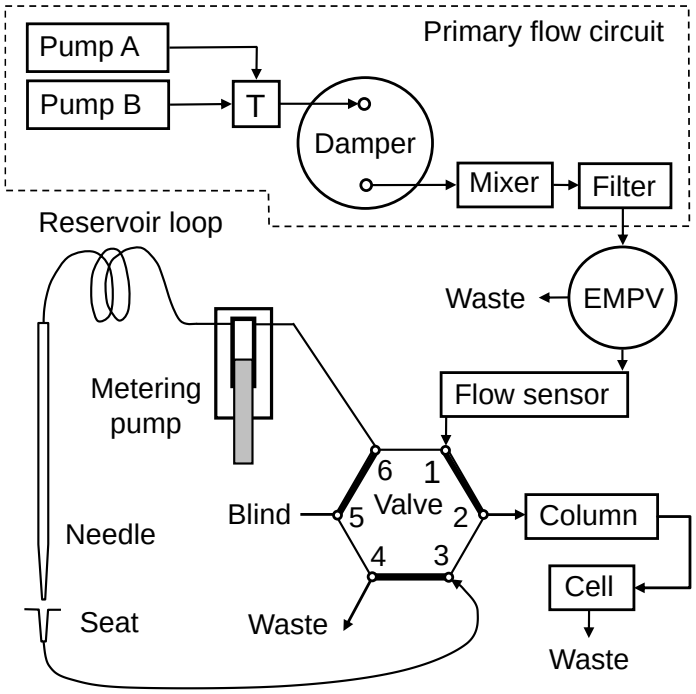

Fig. 4.1. Scheme of a cHPLC system which relies on the splitting of a primary flow (T, mixing point; EMPV, electromagnetic proportional valve).

As indicated in Fig. 4.1, essential elements of the injector are the metering pump which aspirates the sample, the needle and reservoir loop which holds the sample after aspiration, the needle seat where the needle tip closes the high pressure circuit when the valve is in mainpass, and the injection valve. In HPLC autosamplers, the internal volume of the injection loop is always particularly large, to prevent damage to the metering pump which could result from the entrance of sample into it. For instance, the standard capillary loop (used in this

work) and the extended loop of the Agilent cHPLC system provide injection volumes up to 8 and 40 µL, respectively. When the valve is in bypass, all the internal volumes of the injector system are replaced by the negligible volume of the valve internal path between ports 1 and 2. Thus, owing to the relatively large internal volume of the injection system in cHPLC, the delay time measured with the valve in bypass is much lower than the value obtained with the valve in mainpass. Further, with the valve in bypass, reduction of the gradient slope by dilution within the injection system is also avoided. Thus, in this work we will exclusively make use of delay time measurements performed with the valve in bypass, thus avoiding the secondary flow to go through the internal path of the injector. For this purpose, the valve should be switched back to bypass after the injection. Before the arrival of the gradient front to the valve, there is no difference in the composition of the mobile phase filling the bypass and the mainpass circuits. For this reason, the valve can be switched to bypass at any time between the injection and the arrival of the gradient front to the valve. Switching the valve within this time interval will yield exactly the same delay time value, t_{de}. If a column is present, any non-retained compound or marker will arrive to the detector cell after the delay time plus the dead time of the column, Δt_C. Thus, in the presence of a column, the apparent delay time, also measured with the valve in bypass, will be:

$$t'_{de} = t_{de} + \Delta t_C \qquad (4.1)$$

A relevant feature of the systems that rely on the splitting of a primary flow is the dependence of F_1 from the backpressure, P. When the backpressure increases, F_1 is automatically increased by the instrument control software, thus to make possible for the EMPV to maintain the secondary flow rate, F_2, at a fixed selected value (1 µL min^{-1} in this work). For this reason, the primary flow rate can only be programmed by ranges, and these are established by the instrument manufacturer. For the cHPLC system used in this work, three ranges were allowed, i.e. 0.2 - 0.5, 0.5 - 0.8 and 0.8 - 1.3 mL min^{-1}. The highest range was used in this work. The actual values of F_1 are not given by the Agilent

software, but they can be measured by collecting and weighing the mobile phase poured through the EMPV waste during a given time. Using water as mobile phase, and by increasing F_2 to increase the backpressure, we have observed that F_1 increases linearly as P increases. This should make the delay time to decrease linearly as P increases; however, we have also observed that, in fact, the delay time is a complex non-linear function of P (unpublished results). Further, it has been shown that Δt_C is also a function of P [11,12]. Therefore, in order to synchronize the system, the apparent delay time, t'_{de}, instead of the delay time in the absence of the column should be measured. Further, t'_{de} should be established in the same conditions to be found before starting the gradient, that is at the same selected range of F_1, same value of F_2 and same mobile phase and column temperature (thus to not modify the mobile phase viscosity). Further, using a constant value of F_2, we have also observed that the time at which the end of the sample plug reaches the injection valve, t_V, also increases when P increases. Thus, t_V should be also established in the presence of the column, and in the elution conditions to be used before starting the gradient. In this work, the parameters which are required to synchronize the system, namely t_V and t_M, and experiments addressed to measure them, are described.

4.3.2. Gradient profiles obtained by switching the valve to bypass at increasing times

First, the advantages of switching back the valve to bypass after the injection and before the arrival of the gradient front to the valve, instead of maintaining the valve in mainpass, will be further discussed. As indicated above, the latter has two negative consequences which are negligible in conventional HPLC but relevant in cHPLC: a longer delay time and, due to dilution of the mobile phase, a gradient slope lower than programmed. This is shown in Fig. 4.2, where a series of typical experiments addressed to establish

the delay time in the absence of column are given. To obtain the traces, a "zero volume" sample was injected. Since an initial isocratic period was not programmed, the gradient started at the injection time. In trace A, the valve was switched back to bypass 0.1 min after injection, before the arrival of the gradient front to the valve. In trace B, the valve was switched back to bypass at a time slightly longer than that required for the gradient front to arrive to the valve. As observed, owing to the partial entrance of the gradient in the injection loop before valve switching, the first part of the gradient was lost, giving rise to an abrupt step.

The initial step was larger for traces C to D, which were obtained by switching the valve at increasing times. However, the initial step was not present any longer when the valve was switched to bypass at much longer times, specifically after the arrival of the end of the gradient to the valve though the internal path of the injector, or when it was not switch back at all (Fig. 4.2, trace F). However, as also observed in Fig. 4.2, trace F, and as a consequence of the dilution of the mobile phase by mixing inside the large internal volume of the injector, a less steeped gradient and a gradient time much larger than that actually programmed were obtained. Thus, the actual gradient time for Fig. 4.2, trace F, was 11.8 min instead of the programmed 8 min (a 47% increase). Then, to reduce the delay time to a minimum, as well as to avoid the undesirable lengthening of the gradient time, the valve should be switched back to bypass at any time after the arrival of the end of the sample plug to port 2 and before the entrance of the gradient front into the injection loop. In principle, the time to switch back the valve seems not to be critical; however, to switch the valve to bypass immediately after the sample plug end has arrived to the valve is the only way of synchronizing this event with the gradient front. Otherwise, any delay in switching the valve will result in an additional isocratic period preceding the arrival of the gradient front to the valve, and therefore also to the column inlet.

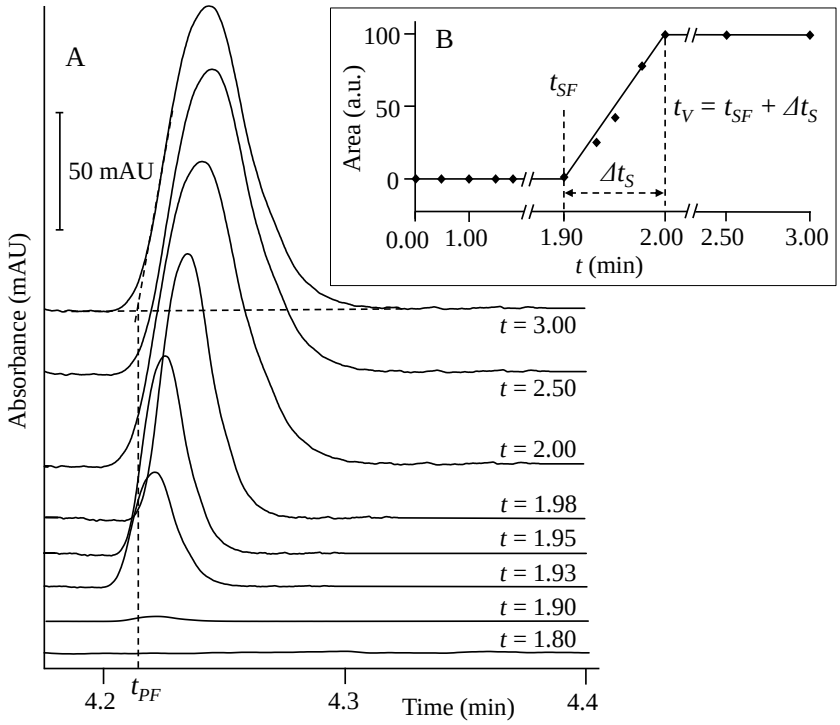

Fig. 4.2. Experiments addressed to measure t_V. Part A: chromatograms obtained by injecting a uracil in the presence of the column while switching the valve to bypass at increasing times, *t*, after the injection. Part B: area of the resulting peak (in arbitrary units) plotted against *t*. For the meaning of the symbols, see the text.

4.3.3. Valve switch time to bypass

As indicated, the injection valve should be switched back to bypass immediately after the arrival of the end of the sample plug to the valve. After aspiration of a sample volume, V_S, injection is produced by switching the valve to mainpass. With the valve in mainpass, the time required for the end of the sample plug to reach the valve is given by the time spent by the sample front to reach the valve port 2, t_{SF}, plus the time necessary for the whole sample plug to exit through port 2, Δt_S:

$$t_V = t_{SF} + \Delta t_S \qquad (4.2)$$

where the subscripts *SF* and *S* stand for sample front and sample, respectively. As discussed above, t_V should be measured in the presence of the column, and using injections of an unretained marker, such as uracil. Also, it should be noted that t_{SF} cannot be deduced from the first perturbation of the baseline produced by the peak of an unretained marker. The arrival of a marker peak to the detector cell is actually produced after the time required for the sample front to arrive to port 2, t_{SF}, plus the time spent from port 2 to the detector cell through the column. A simple experiment addressed to accurately measure t_V is next proposed.

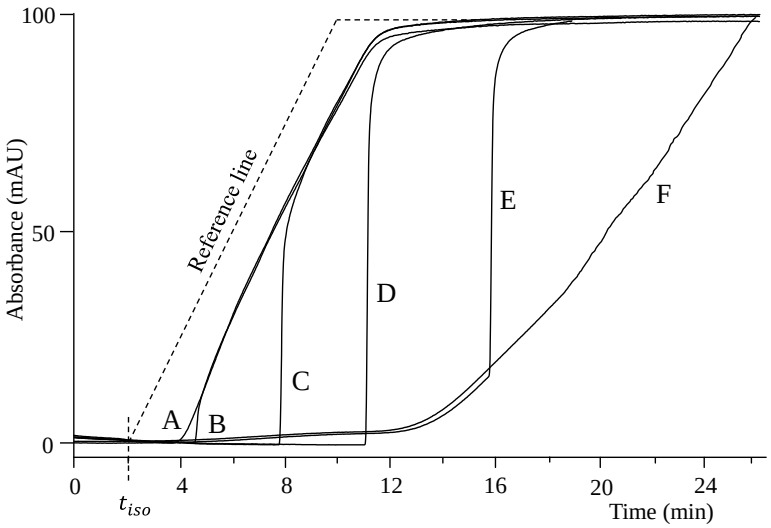

Fig 4.3. Traces obtained in the absence of column by mixing phase A (water containing 0.1% HAcO) with phase B (ACN containing 0.1% HAcO and 0.1% acetone). The 0.8 – 1.3 mL min^{-1} range of the primary flow rate was selected. After an isocratic period of 2 min, a gradient from phase A to phase B in 8 min was programmed in all cases. From trace A to trace F, the valve was switched to bypass at the following increasing times after the injection: 2, 2.5, 4, 8, 12 and 30 min.

For this purpose, the marker was injected and isocratically eluted in the conditions to be found at the beginning of the gradient. In a series of injections, the valve was switched to bypass at increasing time values, t, from zero up to obtain a constant area of the marker peak. As observed in Fig. 4.3A, when the

valve was switched to bypass before the arrival of the sample front to port 2 ($t < t_{SF}$), no peak was obtained. When the valve was switched to bypass after the arrival of the sample front to port 2, but before the arrival of the sample end, a peak smaller than expected was obtained. When the whole sample plug surpassed port 2, an additional increase of t did not produce any further increase of the peak area. In Fig. 4.3B, the peak areas were plotted against *t*. On this plot, the start of the sloping part of the trace, where the points begin to rise, indicates the arrival time of the sample front to the valve port 2, t_{SF}. The point where the slope of the resulting trace changes again to give a plateau is t_V, and the difference between the two points where the slope changes is Δt_S. In principle, to measure Δt_S is not necessary, since it can be calculated as the sample volume, V_S, divided by F_2. Nevertheless, to experimentally establish Δt_S by using an experiment as that shown in Fig. 4.3 has the advantage of revealing any bias between the nominal and the actual values of F_2. Indeed, we have observed that F_2 is not maintained at its nominal value at high values of P. A bias can be also produced as a result of the inaccurate calibration of the flow sensor (see Fig. 4.1).

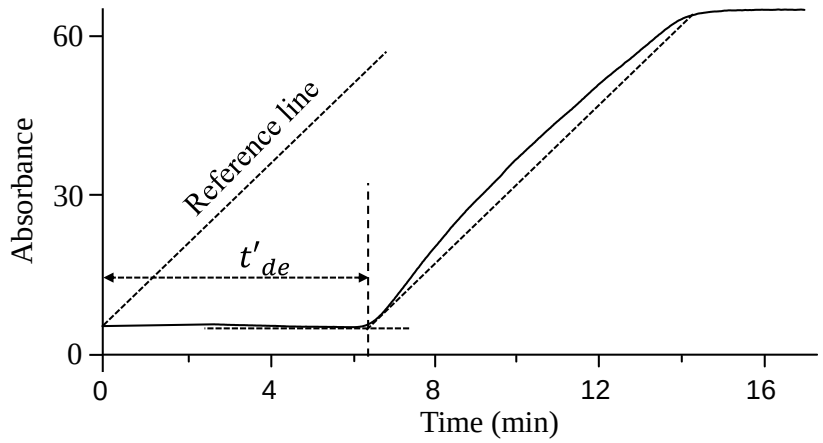

Fig. 4.4. Evaluation of the apparent delay time, t'_{de}, made in the presence of the column by mixing phase A with phase B containing uracil; other details as in Fig. 4.2. The 0.8 – 1.3 mL min^{-1} range of the primary flow rate was selected. The valve was switched to bypass 0.1 min after injection.

4.3.4. The match time

Synchronization of the arrival of both the gradient front and the end of the sample plug to the column inlet should be procured before the column, namely, at the valve port 2. This can only be achieved by switching the injection valve back to bypass immediately after the arrival of the end of the sample plug to port 2. At the same time, the gradient should have been started a given time before or after the injection, just to allow the gradient front to arrive to port 1 simultaneously with the arrival of the end of the sample plug to port 2. A case to be considered is the optional inclusion in the method of an initial isocratic period. This should be also programmed under system synchronization conditions, by further delaying the arrival of the gradient front to port 1 of the valve.

As discussed above, in a given working conditions, the time required by the mobile phase to move from the pump mixing point T to the valve should be supplemented by a match time, t_M, to be subtracted or added to the gradient starting time. Accordingly, the gradient will start either before or after the injection, respectively. Next, a simple procedure to establish t_M is given. First, we will establish the sign criterion as t_M to be negative when the time required by the gradient front to arrive to the valve will be larger than the time required for the valve to switch to bypass according to Eq. (4.1). Then, a negative match time means that the gradient should be started before the injection, which is the most frequent case. Accordingly, the match time will be given by:

$$t_M = t_V - t_{BV} \tag{4.3}$$

where t_{BV} is the time required by the mobile phase to arrive to the valve (the subscript *BV* stands for before the valve). The move of the mobile phase from the mixing point of the pump module to the valve is partially produced at F_1 (before the EMPV) and partially at F_2 (from the EMPV to the valve). Then, it cannot be easily calculated nor directly measured. As next deduced, a simple way of obtaining t_{BV} is to make use of two data which can be easily measured:

the apparent delay time which is obtained in the presence of the column, t'_{de}, and the time required in the same conditions for an unretained compound (e.g. uracil) to arrive to the detector cell. The apparent delay time, t'_{de}, is the sum of two terms: t_{BV} and the time required by the mobile phase to move from the valve to the detector cell, though the column:

$$t'_{de} = t_{BV} + \Delta t_{AV} \tag{4.4}$$

where the subscript *AV* stands for "after the valve". The time spent by the mobile phase before the column, inside the column (the dead time of the column) and after the column until arriving to the detector cell are included in Δt_{AV}. However, to distinguish between these three time intervals is not necessary to calculate the match time. On the other hand, the front part of the peak or band of an unretained compound is given by:

$$t_{PF} = t_{SF} + \Delta t_{AV} \tag{4.5}$$

where the subscript *PF* stands for "peak front". By reorganizing Eqs. (4.2) and (4), and substituting the resulting values of t_{SF} and Δt_{AV} in Eq. (4.5), we have:

$$t_{PV} = t_V - \Delta t_S + t'_{de} - t_{BV} \tag{4.6}$$

According to Eq. (4.3), the match time is the difference between t_V and t_{BV}. Therefore, by substituting and reorganizing, we have:

$$t_M = t_{PF} + \Delta t_S - t'_{de} \tag{4.7}$$

Therefore, the match time can be calculated as the time required from an unretained peak to arrive to the detector cell, plus the time required for the sample volume to exit through the valve port, minus the apparent delay time, all these three parameters being measured with the column and in the conditions to be found at the beginning of the gradient. The former, t_{PF}, can be obtained from the same experiments performed to calculate t_V (Fig. 4.2, part A) if an unretained marker is used. According to Eq. (4.7), the match time increases linearly with Δt_S, then it also increases proportionally to the sample volume,

V_S. On the other hand, both t_{PF} and Δt_S decrease at increasing F_2 values, but t'_{de} decreases with both F_1 and F_2. Therefore, the match time varies non-linearly with the primary and secondary flow rates, and as discussed above it also depends on the backpressure. Thus, the relationship among the match time and F_1 and F_2 exceeds the scope of this work. According to the criterion adopted in Eq. (4.3), most frequently the match time will be negative, indicating how much time in advance the gradient should be started with the respect to the injection. However, at large injection volumes and high primary flow rates (which will reduce t'_{de}), the match time could be positive, which means that in this case the gradient should be started after an isocratic elution period equal to t_M.

4.3.5. Chromatograms of a test mixture obtained without and with synchronization

As deduced from Eq. (4.7), to calculate the match time, t_{PF}, Δt_S and t'_{de} should be established in the conditions to be used in the separation of the test mixture. The two former, established in the experiments shown in Fig. 4.3, were 4.23 and 0.10 min, respectively. To establish the latter, experiments similar to that shown in Fig. 4.2, trace A, but performed in the presence of the column and substituting acetone by uracil, were performed. To prevent the gradient front to enter the internal path of the injector, the valve was switched back to bypass 0.1 min after injection. In Fig. 4.4, the dashed line at the left is the reference or theoretical line to be obtained for a zero delay time and an 8 min gradient time. Thus, the start of the sloping segment of this dotted line coincides with the start of the gradient at the pump module. The continuous line is the actual curve obtained as the gradient progressed. Along the gradient time, the trace did not rise straight; instead it showed a slightly curved shape. This can be partially attributed to the automatic variation of the primary flow rate as a consequence of the variation of viscosity of the ACN-mixtures. Usually, the

delay time is established as the difference between the reference line and the actual trace at mid-rise. However, for synchronization purposes, we are interested in establishing the delay time at the beginning of the gradient, not at mid-rise. For this reason, the beginning of the sloping part of the traces was established at the intersection of the extrapolated baseline with a straight-line tangent to the lower part of the curves, drawn with the same slope as the reference line. Then, t'_{de} was calculated as indicated in Fig. 4.4, as the difference between the beginning of the sloping segments of the experimental curves, and the start of the sloping segment of the reference line. From the resulting value, 6.30 min, according to Eq. (4.7), a match time of –1.97 min was calculated.

Synchronization of the sample injection with the valve and pump operation as proposed above was implemented as indicated in Table 4.1, scheme A. The main problem with the Agilent software used in this work was how to program the start of the gradient at a given time before the injection. This option is not included in the instrument software. Fortunately, the injection valve can be operated at any moment and independently from the injection. Then, the solution adopted in Table 4.1, scheme A, was to inject the sample and to start the gradient simultaneously, but to stop the advance of the sample plug towards the valve after an arbitrary small time period. This was accomplished by switching the valve to bypass after 0.1 min immediately after the injection. According to the experiments given in Fig. 4.3, t_{SF} > 0.1 min, then this time was short enough to prevent the sample front to reach the valve. Then, the valve was maintained in bypass during the calculated match time. This was equivalent to start the gradient the match time period before the injection. Then, the valve was switched again to mainpass to resume the advance of the sample plug towards the valve. The valve was eventually switched again to bypass at t_V, coinciding with the arrival of both the gradient front and the sample end to the valve ports 1 and 2, respectively.

Table 4.1

Synchronized (A), unsynchronized with valve switching to bypass (B) and conventional with valve in mainpass (C) operation schemes in cHPLC; the time values are measured from the injection.

Scheme	Time, min	Valve	Pump operation	Events
A	< 0	Bypass	Isocratic	Start: the sample is aspirated
	0	Mainpass	Gradient	The sample is injected and the gradient starts; the time frame for the sample front to reach port 2 is $t_{SF} = t_V - \Delta t_S$ (in the cHPLC system and conditions used in this work t_{SF} = 1.90 min at F_2 = 1 µL min^{-1})
	0.1	Bypass	Gradient	The sample plug is stopped before the arrival of the sample front to the valve; the gradient front has not arrived to the valve yet (t_{BV} > 0.1 min)
	t_M	Mainpass	Gradient (until Δt_G has been completed)	The sample plug resumes moving; the end of the plug and the gradient front arrives to the valve at the same time
	t_V	Bypass	Gradient (if still required)	The gradient front comes out of the valve immediately after the end of the sample plug
B	< 0	Bypass	Isocratic	Start: the sample is aspirated
	0	Mainpass	Gradient	The sample is injected and the gradient starts
	t_V	Bypass	Gradient	The end of the sample plug reaches the valve; the gradient has still not reached the valve
	$t_V + t_M$	Bypass	Gradient (until Δt_G has been completed)	The gradient front reaches the valve; the less retained analytes could have been totally or partially already eluted in the initial isocratic conditions
C	< 0	Bypass	Isocratic	Start: the sample is aspirated
	0	Mainpass	Gradient	The sample is injected and the gradient starts
	t_V	Mainpass	Gradient (until Δt_G has been completed)	The end of the sample plug reaches the valve; the gradient front could have not reached the valve or could have entered into the injector internal path
	$t >>$	Mainpass	Gradient (if still required)	The gradient front reaches the valve though the injector internal path, largely delayed and diluted; when it will arrive to the column, the

The scheme B of Table 4.1 was used to implement a partially synchronized mode, in which the valve was switched to bypass at t_V, but the gradient was started simultaneously with the injection. This procedure has the advantage of simplicity, since to calculate the match time is not necessary, and it can be implemented by simply adding an order of valve operation to the conventional elution mode. Finally, in scheme C, the chromatogram was obtained by leaving the valve in mainpass after the injection (conventional elution mode). These three operation schemes were applied to a mixture of alkylbenzenes. The chromatograms and the programming of the operations indicated on Table 4.1 according to the Agilent software are given in Fig. 4.5. The retention times, efficiencies (as apparent plate count) and peak symmetries obtained for the operation schemes A, B and C are compared in Table 4.2.

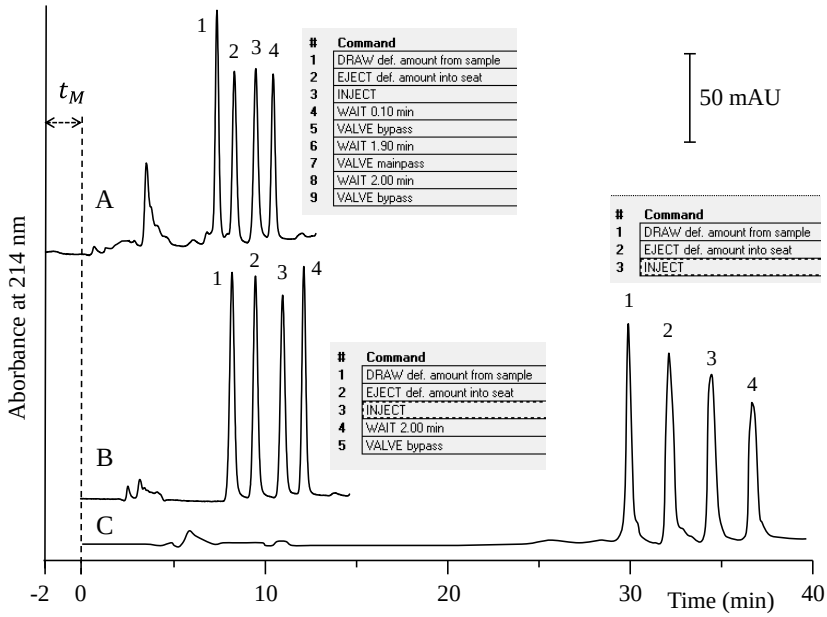

Fig. 4.5. Chromatograms obtained by injecting 0.1 mL of a test mixture containing four alkyl benzenes. The A, B and C chromatograms were obtained by applying the operation schemes A, B and C of Table 4.1, respectively; the inserts show the programming of the operations according to the Agilent software.

Table 4.2

Retention times, efficiencies and peak symmetries of alkyl benzenes for the A (unsynchronized), B (unsynchronized with valve switching to bypass) and C (synchronized) operation schemes of Table 1 (averages of three injections)

	Retention time, min			Apparent plate count per meter, N/L			Peak symmetries		
Peak	A	B	C	A	B	C	A	B	C
1	29.40	8.20	7.29	28400	32100	76200	2.00	0.94	0.92
2	31.80	9.96	8.23	26900	44600	62400	1.58	0.88	0.87
3	34.10	10.94	9.39	38300	55500	67400	1.32	0.93	0.91
4	36.30	12.09	10.33	43400	99200	103200	1.25	0.90	0.89

The chromatograms obtained for the fully synchronized and partially synchronized operation according to schemes A and B, are shown in Fig. 4.5, traces A and B, respectively. The chromatogram of Fig. 4.5, trace C, was obtained by following the conventional elution scheme C. With scheme A, the last peak eluted at ca. 10 min, whereas ca. 12 and 36 min were required in schemes B and C, respectively. Thus, with schemes A and B, the analytes were eluted with a remarkable saving of time with respect to scheme C. By comparing schemes A and B, the last peak also appeared earlier in A, but the time saved was the approximately the same as that spent during the match time (before injection in this work). As deduced from Table 4.2, the average apparent plate count was ca. 120% and ca. 60% higher in schemes A and B with respect to scheme C, respectively. The symmetry factors were similar for schemes A and B, but two-fold larger for scheme C.

4.4. Conclusions

In cHPLC, the entrance of the gradient into the internal path of the injector system largely delays the arrival of the gradient front to the column, also reducing the gradient slope by mixing. Further, the delay time with the injection valve in mainpass is a complex function of the primary and secondary flow rates, also varying with the backpressure. Thus, if the injection valve is maintained in mainpass during elution, control on the elution conditions is lost, which precludes proper method optimization and transfer. This is avoided by switching the injection valve back to bypass after the injection. This should be made both before the arrival of the gradient front to the valve and after the valve time, t_V, that is, when the whole sample plug has exit the valve. Further, synchronization of these two events is achieved through the match time, t_M, which is the time before or after the injection at which the gradient should be started.

To implement synchronized gradient elution, four parameters, i.e. t_{SF}, Δt_{SP}, t_{PF} and t'_{de}, should be measured in the presence of the column, and with the mobile phase composition and flow rates to be found at the beginning of the gradient. The three former are jointly established by successively injecting an unretained marker, and by increasing the time at which the valve is switched to bypass after injection. The last one, t'_{de}, is measured by doping solvent mixture B with the unretained marker. These parameters are used to calculate the valve time, t_V, and the macth time, t_M, according to Eqs. (4.2) and (4.7). The benefits obtained by either switching the valve to bypass immediately after t_V, or by proper use of both t_V and t_M to synchronize the system, have been demonstrated. With the software of the instrument used in this work, a positive match time was easily programmed (as an initial isocratic period). However, programming of a negative match time, which requires starting the gradient before injection, was only possible by stopping the mainpass flow before the arrival of the sample front to the valve, and by resuming it after completing the match time. Thus, to facilitate programming of synchronized elution, the option of starting the gradient before injection should be included in the control software of chromatographs. Software to automatically measure t_{SF}, Δt_{SP} and t_{PF} by successively injecting a marker while switching the valve to bypass at increasing time values would be also of interest.

Acknowledgements

Project CTQ 2010-15335 (MINECO of SPAIN and FEDER); E.J. C-C. thanks the MINECO for an FPI grant for PhD studies and A. A. thanks the ANPCYT (Argentina) for a grant. Thanks are also due to M.C. Garcia-Alvarez-Coque who advised us about the convenience of further investigating the underlying reasons of our troubles in cHPLC.

References

[1] C. F. Poole. The essence of Chromatography, Elservier, Amsterdam, 2003, pp. 380-390.

[2] J. W. Dolan and L. R. Snyder, Liquid Chromatography in Chapter 12, p. 282 Elsevier, Amsterdam 2013.

[3] S. Fanali, P. Haddad, C. Poole, P. Schoenmakers, D. K. Lloyd. Liquid Chromatography: Fundamentals and Instrumentation. Chapters 12 and 13. Elsevier, Amsterdam, 2013.

[4] J. W. Dolan, LCGC 24 (2006) 458.

[5] K. Broeckhoven, D. Cabooter, F. Lynen, P. Sandra, G. Desmet, J. Chromatogr. A, 1217 (2010) 2787.

[6] E. Rogatsky, G. Cruikshank, D. T. Stein, J. Sep. Sci., 32 (2009) 321.

[7] E. Rapp, U. Tallarek, J. Sep. Sci., 26 (2003) 453.

[8] E. C. Peters, M. Petro, F. Svec, J. M. J. Fréchet, Anal. Chem., 70 (1998) 2288.

[9] E. C. Peters, M. Petro, F. Svec, J. M. J. Fréchet, J.M., Anal. Chem., 69 (1997) 3646.

[10] R. A. Serway, J. S. Faughn, College Physics, 6 th Edition Chapter 13, Saunders, Philadelphia, USA, 2004.

[11] S. Pous-Torres, J. R. Torres-Lapasió, J. R., Ruiz-Ángel, M.C. García-Álvarez-Coque, J. Chromatogr. A, 1217 (2010) 5440.

[12] S. Pous-Torres, J. R. Torres-Lapasió, J. R., Ruiz-Ángel, M.C. García-Álvarez-Coque, J. Sep. Sci., 34 (2011) 931.

Chapter 5. Sensitive determination of parabens in human urine and serum using methacrylate monoliths and reversed-phase capillary liquid chromatography-mass spectrometry

Journal of Chromatography A, 1379 (2015) 65–73

Contents lists available at ScienceDirect

Journal of Chromatography A

journal homepage: www.elsevier.com/locate/chroma

Sensitive determination of parabens in human urine and serum using methacrylate monoliths and reversed-phase capillary liquid chromatography–mass spectrometry

Enrique Javier Carrasco-Correa[a], Fernando Vela-Soria[b], Oscar Ballesteros[b], Guillermo Ramis-Ramos[a], José Manuel Herrero-Martínez[a,*]

[a] Department of Analytical Chemistry, University of Valencia, Dr. Moliner 50, 46100 Burjassot, Valencia, Spain
[b] Department of Analytical Chemistry, University of Granada, 18071 Granada, Spain

A method for the determination of parabens in human urine and serum by cLC with UV-Vis and MS detection using butyl methacrylate ester-based monolithic columns has been developed. The influence of composition of polymerization mixture of was studied. The optimum monolith was obtained with butyl methacrylate monomer at 60/40% (wt/wt) BMA/EDMA ratio and 50 wt% porogens (composed of 36 wt% of 1,4-BuOH, 54 wt% 1-PrOH and 10 wt% water). Baseline resolution of analytes was achieved through a mobile phase of acetonitrile/water in gradient elution mode. Additionally, dispersive liquid-liquid microextraction (DLLME) was combined with both cLC-UV-Vis and cLC-MS to achieve the determination of parabens in human urine and serum samples with very low limits of detection. Satisfactory intra- and inter-day repeatabilities were obtained in UV-Vis and MS detection, although the latter provided lower detection limits (up to 300-fold) than the UV-Vis detection. Recoveries for the target analytes from spiked biological samples ranged from 95.2 to 106.7%. The proposed methodology for the ultra-low determination of parabens in human urine and serum samples is simple and fast, the consumption of reagents is very low, and very small samples can be analyzed.

Keywords: Parabens; Methacrylate monolithic columns; Capillary-LC-MS; Human serum; Human urine; DLLME

5.1. Introduction

Parabens are alkyl esters of 4-hydroxybenzoic acid, which constitute a class of antimicrobial agents, widespread used as preservatives in cosmetics, pharmaceuticals, foods and beverages, due to their physicochemical properties such as stability over the pH range and sufficient water solubility to produce the effective concentration in aqueous phase [1-3]. The antimicrobial and antifungal activity of these compounds increases with increasing the alkyl chain length; however, this reduces the solubility of these compounds in water, being the short chain parabens mostly used [4]. There is a limit to the maximum amount of alkyl parabens that can be introduced into foods, cosmetics and medicines [1, 5], although rigorous evidences of possible side effects have been not demonstrated [4]. However, hypersensitivity reactions have been described with the use of hydroxybenzoates and it has also been reported that parabens possess estrogenic activity [4, 6].

The range of products (foods, cosmetics and pharmaceutical formulations) containing parabens is continually growing with the likely consequence of an increase in the levels of human exposure. In the last years, some research groups have designed methods to analyze parabens in pharmaceuticals and cosmetics products by using LC [7-10], GC [8, 11], capillary electrophoretic migration methods [12, 13] and CEC [14-16]. These studies have showed the ubiquitous occurrence of parabens in these products. However, accurate methodologies of parabens determination in biological samples are required to assess the human exposure. In this way, several analytical procedures to determine parabens in human samples as placental tissue [17], breast tumors [18, 19] and biological fluids [20-22] have been described.

cLC as other miniaturized separation techniques (CEC, nano-LC) are in the focus of modern analytical methods and in particular, in the field of bioanalytics and life sciences. The most important advantages of these systems over classical techniques are the reduction of solvent consumption, the reduced environmental impact, the small sample volumes, and the improved suitability

for screening and for coupling with mass spectrometry detection [23]. Within these techniques, a crucial point is the choice of the capillary column used with regard to column stability and lifetime as well as ease of fabrication. Thus, particulate packed columns were first used in CEC and nano-LC. However, the numerous practical drawbacks associated with packing and retaining beads in such narrow bore capillaries have progressively encouraged the development of alternative stationary phases, called monolithic columns, containing *in situ* synthesized stationary phases. Due to their unique chromatographic properties and the easy and flexible preparation, these stationary phases have attracted considerable attention in the last decade and have gained a wide acceptance. Within organic polymer-based monoliths, methacrylate-based material has been widely applied as separation media, due to its unique advantages such as excellent stability under extreme pH conditions and simple preparation [24, 25]. Although parabens have been employed as test solutes in cLC [26, 27], to our knowledge there is no published literature on paraben determination by cLC with UV-Vis and MS detection in biological matrices using polymeric monolithic columns as chromatographic supports.

In order to determine the parabens in different samples, an extraction or pre-concentration step is often required prior to analysis. Solvent phase microextraction, based on a traditional liquid-liquid extraction technique, is a less known method that uses only a few microliters of organic solvent as the extracting phase [28, 29]. Assadi and his co-workers [30] have recently developed a new microextraction technique named DLLME as a high-performance, rapid and inexpensive technique. Its basic principle is the dispersion of an extraction solvent (immiscible in water) assisted with a disperser solvent (miscible in both water and extraction solvents) within an aqueous solution. This generates a very high contact area between the aqueous phase and the extraction solvent. From a commercial, economic and environmental point of view, the advantages of DLLME over conventional solvent extraction methods are simplicity of operation, rapidity, low cost, easy

manipulation, low amounts of organic extraction solvents, high recoveries and enrichment factors, and easier linkage to analytical techniques [31]. However, DLLME has been scarcely applied to the analysis of parabens in human samples [22, 32-35]. Therefore, the combination of DLLME with cLC is undoubtedly a good alternative to develop simple and fast procedures that provide enough sensitivity to detect very low analyte quantities in biological samples.

The aim of this work was to develop an analytical method by cLC for the determination of four parabens (methyl-, ethyl-, *n*-propyl- and *n*-butylparaben) in human urine and serum samples with very low limits of detection (LODs). For this purpose, DLLME preconcentration followed by cLC separation on methacrylate ester-based monolithic columns was performed. In order to optimize the cLC separation, a series of butyl methacrylate monoliths was firstly prepared under several polymerization conditions (porogenic solvent content, monomers/porogens and monomer/crosslinker ratios). The influence of gradient elution conditions on the separation was also examined. Detection by both UV-Vis and MS was studied. The feasibility of these fruitful combinations was investigated, and analytical figures of merit were established. The developed methodologies could be classified among the alternatives proposed by the recent trends of green analytical chemistry, particularly if capillary/nano-LC systems providing a splitless flow of mobile phase are used. Both a split cLC-UV-Vis and a splitless cLC-MS systems were used in this work, achieving with this latter a very small consumption of organic solvent per analysis.

5.2. Materials and methods

5.2.1. Chemicals and reagents

BMA, EDMA, 1,4-BuOH and γ-MPS were from Aldrich (Milwaukee, WI, USA). Methylparaben (MPB), ethylparaben (EPB), propylparaben (PPB) and butylparaben (BPB) were supplied by Alfa Aesar (Massachusetts, MA, USA). 1-PrOH, HPLC-grade ACN and MeOH were from Scharlau (Barcelona, Spain). AIBN was from Fluka (Buchs, Switzerland). Ammonium acetate, hydrochloric acid (37%) and glacial acetic acid were supplied by Panreac (Barcelona). Acetone was purchased from Merck (Darmstadt, Germany). Trichloromethane (TCM) was supplied by Sigma-Aldrich (Madrid, Spain). Unless otherwise stated, other chemicals used were of analytical grade. Deionized water was obtained with a Barnstead deionizer (Sybron, Boston, MA, USA). Uncoated fused-silica capillaries of 150 mm total capillary length and 250 μm I.D. (Polymicro Technologies, Phoenix, AZ, USA) were used. Stock solutions of parabens (100 mg L^{-1}) were prepared in ACN and kept at 4ºC until their use.

Helix pomatia (H1) 4-methylumbelliferyl glucuronide, 4-methylumbelliferyl sulfate and β-glucuronidase/sulfatase were purchased from Sigma-Aldrich. $^{13}C_4$-4-methylumbelliferone was obtained from Cambridge Isotope Laboratories Inc. (Andover, MA, USA). A mixture of $^{13}C_4$-4-methylumbelliferone, 4-methyl-umbelliferyl sulfate, and 4-methylumbelliferyl glucuronide was prepared in water and stored at 4ºC until use. The enzyme solution was prepared daily for each run by dissolving 6 mg of β–glucuronidase/sulfatase (3 10^6 U g $solid^{-1}$) in 1 mL of 1 M ammonium acetate buffer (pH 5.0) (enzymatic solution A, for serum samples treatment), or 10 mg of β–glucuronidase/sulfatase (3 10^6 U g $solid^{-1}$) in 1.5 mL of 1 M ammonium acetate buffer (pH 5.0) (enzymatic solution B, for urine samples treatment). Fetal Bovine serum was purchased from Ibian Technologies (Zaragoza, Spain). Urea, KCl, creatinine, Na_2SO_4, hippuric acid, NH_4Cl, citric acid, $MgSO_4$, $NaH_2PO_4 \cdot H_2O$, $CaCl_2 \cdot 2H_2O$, oxalic acid, lactic acid, glucose, $Na_2SiO_3 \cdot 9H_2O$ and pepsin were purchased from Sigma-Aldrich.

5.2.2. Instrumentation and working conditions

A cLC system from Agilent (1200 series, Waldbronn, Germany), constituted by a degasser (Agilent part G1379B), a capillary pump (G1376A) providing a primary flow which was split by an electromagnetic proportional valve (EMPV, G1361-60000), a capillary-flow sensor (maximal flow rate, 20 µL min^{-1}), a micro-well plate autosampler (G1377A, 1260 Infinity series) with a micrometering device which provides injection volumes from 0.01 to 8 µL with the installed standard loop capillary, and a DAD (G1315C) with an 80 nL quartz cell (6 mm path length cell), was used. Synchronization of the sample injection with the valve and pump operation was implemented as described elsewhere (See Chapter 4, [36]).

Gradient elution was accomplished by mixing an aqueous 0.1% HAcO solution (mixture A) with ACN also containing 0.1% HAcO (mixture B). The primary flow was set at 0.8-1.3 mL min^{-1}, whereas the flow rate at the injection system and column location (secondary flow) was 2 µL min^{-1}. Unless otherwise stated, injection volume was 0.05 µL and detection was set at 254 nm.

Analysis by cLC–MS/MS was performed on an Eksigent nanoLC-2D plus system (Dublin, CA, USA) coupled to a triple-quadrupole tandem mass spectrometer (AB SCIEX QTRAP 5500, Applied Biosystems, USA) via an ESI interface (San Jose, CA, USA). Unless otherwise stated, the injection volume was 50 nL. The flow rate was 1 µL min^{-1}, and the mobile phase consisted of (A) water containing 0.04% ammonium acetate, and (B) ACN containing 0.04% ammonium acetate. The percentage of B was increased from 30 to 100% in 9.7 min.The necessary parameters to synchronize injection with gradient starting and injection valve operation were measured as described elsewhere [36].

The mass spectrometer was operated in electrospray negative ionization

using multiple reaction monitoring (MRM) mode. The MS detection conditions were optimized for each compound by direct infusion of standard solutions (5 ng mL^{-1}). The following MS parameters were used: curtain gas, 138 kPa (20 psi); ion source temperature, 150ºC, ion spray voltage, -2500 V; ion source gas 1, 138 kPa; ion source gas 2, 138 kPa; collision gas, 69 kPa. Nitrogen (99.995%) was used as curtain gas and ion source gas, and helium (99.998%) was used as collision gas. Other adjustments such as declustering potential (DP) and entrance potential (EP) were optimized for each analyte. Optimized parameters for each compound and the mass transitions are given in Table 5.1.

Table 5.1

Selected MRM transitions and optimized potentials.

Compounds	Transitions	DP (V)	EP (V)
MPB	151.1 → 92.0[a]	-55	-20
	151.1 → 135.9[b]	-55	-30
EPB	164.9 → 92.0[a]	-50	-20
	164.9 → 135.9[b]	-50	-20
PPB	179.0 → 92.0[a]	-50	-30
	179.0 → 135.9[b]	-50	-30
BPB	193.0 → 92.0[a]	-50	-20
	193.0 → 135.9[b]	-50	-30

DP, declustering potential; EP, entrance potential

[a]Selected reaction monitoring (SRM) transition used for quantitation

[b]SRM transition for confirmation

Chromatographic permeability (K, m^2) of columns was calculated according to Darcy's law by the following equation:

$$K = (\eta L u)/\Delta P \quad (5.1)$$

where u (m/s) is the linear velocity of mobile phase, η is the viscosity of the

mobile phase (Pa·s), L is the length of the monolithic column (m) and ΔP is the pressure drop across the monolithic column (Pa).

The peak capacity (P_c), was experimentally determined using the Eq. (5.2) [37]:

$$P_C = 1 + \frac{t_G}{1.679 \cdot w_{1/2}} \quad (5.2)$$

where t_G (min) is the total gradient time of the chromatogram and $w_{1/2}$ is average peak width at half height (min) of different solutes across the elution window. The global resolution (R_G) was also measured as the geometric mean of the resolution between the consecutive peak pairs.

The dynamic binding capacity (DBC) was estimated by frontal elution of BPB as model solute. Briefly, monolithic columns were first equilibrated with 30% ACN containing 0.1% HAcO. Then, a BPB solution (2.5 μmol mL^{-1} dissolved in the same solvent) was pumped through the column at 2 μL min^{-1}, followed by UV-Vis monitoring at 254 nm. DBC, expressed in μmol mL^{-1} of column volume, was calculated at 50% of the final absorbance value of the breakthrough curve by using the Eq. (5.3):

$$DBC = C_0 (V - V_0) / V_c \quad (5.3)$$

where C_0 is the analyte concentration (μmol mL^{-1}), V is the volume of the analyte solution pumped through the column at the 50% breakthrough point (mL), V_0 is the dead volume of the cLC system (mL), and V_c is total column volume (mL).

Conditioning steps of the monolithic columns were achieved with an HPLC pump (1100 series, Agilent technologies). SEM micrographs were taken with a scanning electron microscope (S-4100, Hitachi, Ibaraki, Japan) provided with a field emission gun and an EMIP 3.0 image data acquisition system (Rontec, Normanton, UK). Samples for SEM analysis were previously sputter-coated with Au/Pd for 2 min to avoid charging problems; this treatment was

necessary since these materials were not electrically conducting. The SEM images of the monolithic columns in this work were obtained at a magnification of 9000 × using an acceleration voltage of 10 kV and 10-mm working distance.

All pH measurements were made with a Crison (Crison Instruments S.A, Barcelona, Spain) combined glass-Ag/AgCl (KCl 3 M) electrode using a previously calibrated Crison 2000 digital pH-meter. A thermo shaker (model MS–100, Optimum Ivymen System, Cornecta, Spain) was used for enzymatic treatment.

5.2.3. Preparation of polymeric monolithic columns

Prior to the preparation of the columns, and in order to ensure covalent attachment of the monolith to the inner wall of the fused-silica capillaries, surface modification with γ-MPS was performed [38, 39]. Monoliths were prepared from polymerization mixtures containing a bulk monomer (BMA), a cross-linker (EDMA), and a ternary pore-forming solvent (1,4-BuOH/1-PrOH/water). AIBN (1 wt% with respect to the monomers) was also added as polymerization thermal initiator. After mixing, and to obtain a clear solution, sonication for 10 min followed by purging with nitrogen for 10 more min was applied. The preconditioned capillary was filled with the mixture up to a length of 15 cm. To initiate the thermal polymerization, columns were placed in an oven for 20 h at 70°C. After thermal polymerization, an HPLC pump was used to flush the columns for 30 min with MeOH to remove the pore-forming solvents and possible unreacted monomers.

5.2.4. Sample treatment

5.2.4.1. Sample collection and storage

Human serum and urine samples were collected from 10 volunteers at the Management Clinical Laboratory Unit of the *San Agustín* Hospital (Linares, Jaén, Spain). Samples were frozen at –86ºC and stored confidentially and anonymously until analysis. All volunteers signed their informed consent to participate in the study.

5.2.4.2. Enzymatic treatment

The enzymatic treatment was carried out according to a previously published method [22]. Briefly, to evaluate the total amount of parabens in serum and urine, each sample was treated with β–glucuronidase/sulfatase to break the conjugated forms of parabens (formed in the metabolic pathway) into its free forms for a subsequent detection and quantification. For analysis in serum, 1 mL of sample was poured into a centrifuge glass tube, and 50 µL of enzyme solution A was added. Regarding to urine samples, 5 mL of each one was mixed with 100 µL of enzyme solution B. After mixing, the sample was incubated at 37ºC for 24 h.

5.2.4.3. DLLME procedure

Prior to DLLME, serum protein content had to be removed. Acetone (1.0 mL) was added to 1.0 mL of human serum. The mixed solution was shaken for 30 s in a vortex and centrifuged at 3000 rpm (1460 × *g*) for 10 min. The supernatant was transferred to the test tube and diluted with 5% NaCl aqueous solution (w/v) to 10.0 mL. The pH was adjusted to 2.0 with HCl 0.1 M. The protein removal in human urine was not necessary. Thus, 5.0 mL of urine sample was diluted to 10.0 mL with 10% NaCl aqueous solution (w/v) and adjusted at pH 2.0. These solutions were placed in 15 mL screw-cap glass test

tubes.

The DLLME was carried out according to a previously published method [22]. Prior to DLLME, an aliquot of urine or serum (5 mL) was diluted to 10.0 mL with 10% NaCl aqueous solution (w/v). The pH was adjusted to 2.0 with 0.1 M HCl. This solution was placed in a 15 mL screw-cap glass test tube. Then, a mixture of 0.5 mL of acetone (disperser solvent) and 750 µL of TCM (extraction solvent) were mixed and injected rapidly into the aqueous sample (10 mL) with a syringe. The mixture was gently shaken for 10 s and centrifuged at 4000 rpm (2600 × *g*) for 20 min. The TCM phase, sedimented at the bottom of the centrifuge tube, was transferred to a clean glass vial using a 1.0 mL micropipette. The organic phase was evaporated under a nitrogen stream. The residue was dissolved in 100 µL mobile phase and injected into the cLC system.

5.3. Results and discussion

5.3.1. Preparation of poly(BMA-co-EDMA) monolithic columns and separation performance evaluation

Several studies have shown that the composition of the polymerization mixture and reaction conditions strongly affects both the morphology and chromatographic performance of monolithic columns [24, 25, 38-40]. In this study, a series of BMA-based monolithic stationary phases were systematically prepared by variation of several parameters (such as percentages of 1,4-BuOH and 1-PrOH in the porogenic solvent, monomers/porogens and BMA/EDMA ratios) in the polymerization mixture (Table 5.2). Monoliths prepared with 27 wt% 1,4-BuOH in the porogenic solvent (column A1) were clearly unsuitable for any flow-through applications probably due to their small pore sizes (Fig. 5.1A). At 33 wt% 1,4-BuOH, the monolith prepared (column A2) also showed a relatively dense polymeric bed with a low permeability (Table 5.2), showing a tendency to get blocked when it was employed. By increasing the

concentration of 1,4-BuOH (36 and 40 wt%), an increase in the flow-through pores and globule sizes was observed (see Fig. 5.1B as representative example), with a concomitant rise in permeability values (Table 5.2).

Table 5.2

Column	Monomers/Porogens (% wt/wt)	BMA/EDMA (% wt/wt)	1,4-BuOH/ 1-PrOH/H_2O (% wt/wt/wt)	K (10^{-14} m^2)
A1	40:60	60:40	27:63:10	-
A2	40:60	60:40	33:57:10	1.42
A3	40:60	60:40	36:54:10	4.08
A4	40:60	60:40	40:50:10	5.54
A5	30:70	60:40	36:54:10	4.97
A6	50:50	60:40	36:54:10	3.32
A7	50:50	50:50	36:54:10	2.71
A8	50:50	70:30	36:54:10	3.97

Composition of the polymerization mixtures used for the preparation of BMA-based monolithic columns and their permeability[a].

[a]Measured with a mobile phase composed of 30:70 (v/v) ACN-H_2O at a flow rate of 1 µL min^{-1}.

Figure 5.2A-B shows the effect of modifying the 1,4-BuOH content in the porogenic solvent mixture on the separation of parabens. The flow rate was 1 µL min^{-1} and the initial gradient elution conditions for parabens were as follows: an initial isocratic step with 10% ACN for 2 min followed by a linear gradient up to 100% ACN in 9 min. As can be seen, column A3 gave a slightly higher retention for parabens than column A4, which can be explained by the smaller globule structure of column A3 when compared to column A4 (data not shown). Column A3 provided narrower peaks than column A4; however, peak fronting was observed in the chromatograms obtained with these two columns (Figs. 5.2A-B). Peak fronting could be due to inhomogeneities in the monolith

structure, for instance to a lower density of the monolith close to the capillary wall as compared to its center region [41-42]. In order to detect possible structural inhomogeneity in the monoliths, SEM micrographs of the capillary wall and center regions of columns A3 and A4 were taken (Fig. S5.1, traces A-B). However, after careful observation, neither inhomogeneity in the structure of the monoliths or the presence of cracks were detected. Fronting could be still due to a low surface area of the monoliths resulting in a rather reduced binding capacity. The reduction of the injection volume (20-30 nL) did not reduce fronting. To further clarify this point, DBC values were obtained using BPB as a test analyte. The DBC ranged from 1.80 to 2.40 μmol mL^{-1} for monoliths A4 and A3, respectively, which could explain the peak shape observed in chromatograms (Fig. 5.2A-B). At the sight of these experiments, a content of 36 wt% 1,4-BuOH in the porogenic solvent mixture was selected for further experiments. The influence of the ratio of monomers/porogens on the porous and chromatographic properties was next studied (Table 5.2, columns A3, A5 and A6). When the content of the porogenic solvent in the polymerization mixture was reduced (from 30:70 to 50:50 ratio of monomers/porogens), a slight increase in retention was observed. This trend was consistent with the SEM pictures of these monoliths (see Figs. 5.1C, 1B and 1D for columns A5, A3 and A6, respectively), where a reduction of the porogenic solvent content resulted in a reduction of the globule size. Additionally, columns A5 and A6 were examined using SEM. As commented above for columns A3 and A4, no structural inhomogeneities were found (Fig. S5.1, traces C-D). A reduction in the content of porogens (40 wt%) led to monoliths with small macropores and globule sizes, and therefore with a high resistance to flow. Then, a 50:50 (wt/wt) monomers/porogens ratio was selected for the following studies. Column A6 (prepared at this ratio) exhibited the highest DBC (6.2 μmol mL^{-1}) compared to column A5 (1.4 μmol mL^{-1}) and to columns A3 and A4 (see above). As shown in Fig. 5.2, peak fronting was rather reduced for column A6 (trace D). This column also provided the best separation performance when compared to the other columns used in this work (see below).

Next, the EDMA content in the monomer mixture was also studied (Table 5.2, columns A6, A7 and A8). When the weight content of porogenic solvent (36:54:10 wt/wt/wt 1,4-BuOH/1-PrOH/H_2O) was kept constant at 50 wt% and the weight content of EDMA in the monomer mixture was increased from 40 (column A6) to 50 wt% (column A7), the permeability was slightly reduced (Table 5.2); however, non-significant improvement in the quality of separation was evidenced. At 30 wt% of EDMA (column A8), a partial loss of resolution between the analytes was obtained (data not shown). At sight of these results, the column A6 provided the best compromise in terms of resolution, permeability and analysis time.

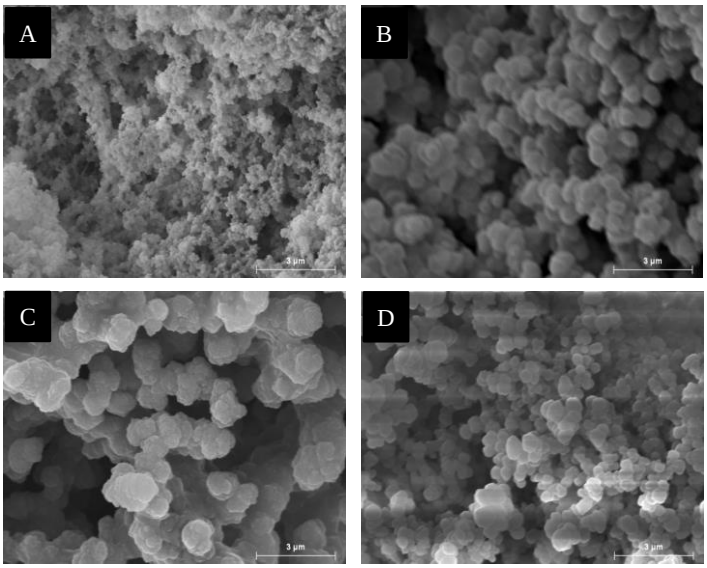

Fig. 5.1. SEM micrographs of BMA-based monoliths prepared at several ratios of 1,4-BuOH/1-PrOH/H_2O (wt/wt/wt): (A) 27:63:10 (column A1), (B) 36:54:10 (column A3). Parts (C) and (D) show monoliths prepared with several monomers/porogens ratios: (C) 30:70 (column A5) and (D) 50:50 (column A6). Other details about the composition of columns are given in Table 5.2.

Next, the elution of parabens using the column A6 with different flow rates and elution gradients was studied. First, the influence of flow rate on the chromatographic performance was examined. Thus, peak capacity (P_C) and

global resolution (R_G) were measured at several flow rates ranging from 1 (0.32 mm s^{-1}) up to 4 µL min^{-1} (1.29 mm s^{-1}). The best P_C and R_G values (24 and 1.2, respectively) were obtained at 2 µL min^{-1} (Fig. 5.3A, 0.64 mm s^{-1}). Then, gradient elution conditions were modified in order to obtain a satisfactory resolution in a reasonable retention time. Both the length of the initial isocratic step and the elution strength at the beginning of the gradient were adjusted. Baseline resolution between all the analyte pairs was achieved (P_C = 22 and R_G = 2.3) within 12 min (Fig. 5.3B). However, in order to analyze complex samples such as urine and serum and to avoid interferences with endogenous substances (which can be particularly important using UV-Vis detection), a further enhancement of resolution is advisable. For this purpose, multisegmented gradients were tried. As observed in Fig. 5.3C, in the selected elution conditions (given in the figure caption), portions of baseline larger than the peak base widths were obtained for all the peak pairs. It should be noted that peak efficiency slightly decreased compared to Fig. 5.3B, but it was still acceptable whereas the resolution achieved was satisfactory to properly address the analysis of biological matrices.

The performance of column A6 was compared to that of previously reported for packed and other monolithic columns. The efficiencies obtained in this work (P_C ranging from 20 to 24) can be favorably compared to those reported for conventional microparticulate columns packed with 5-µm silica particles (P_C = 21 for 12.5-min gradient and 23 for 10 min-gradient time) [43, 44]. However, the efficiencies found were lower than those obtained for packed columns of 3.5 µm and sub-2 µm particles operating at ultra-high pressure liquid chromatography (UHPLC), where the P_C values (at similar gradient run times, 10-15 min) for small molecules (alkyl phenones and parabens) ranged between 100-125 and 115-160, respectively [45, 46]. On the other hand, Lee's group [26, 27] have reported for highly cross-linked monoliths (obtained from single crosslinking monomers), efficiencies given in terms of peak widths (at half peak height) of 3.7-8.2 s, and P_C values ranging

from 50 to 60 for alkyl benzenes (data of alkyl parabens were not given).

An advantage of the method proposed in this work over other reported HPLC methods is lower solvent consumption. Using cLC systems without flow splitting (*e.g.* Eksigent), only 30 µL of mobile phase per analysis within a short analysis time was used. Additionally, the cost of a polymeric monolithic column is less than that of the conventional C18 columns, and the need of specialized ultra-high pressure systems for sub-2 µm particles is not required.

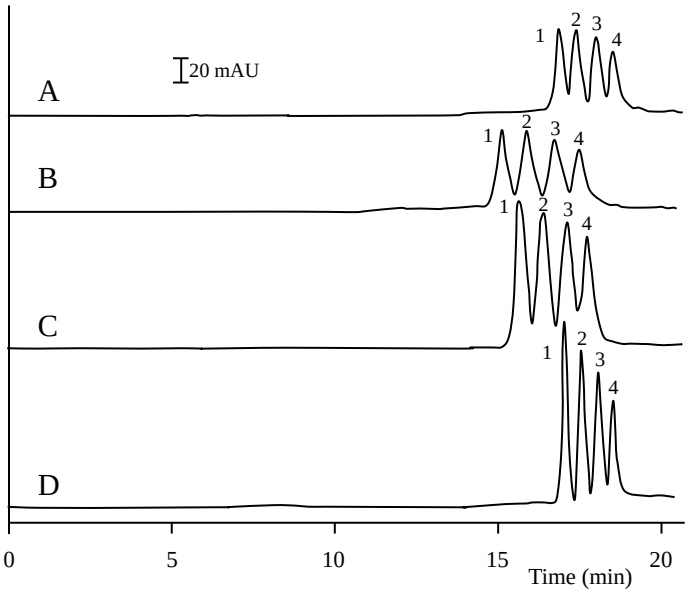

Fig. 5.2. Separations of parabens using BMA-based monolithic columns: (A) column A3, (B) column A4, (C) column A5 and (D) column A6. Conditions: 0 to 2 min isocratic step at 10% ACN and linear gradient from 2 to 9 min up to 100%; flow rate, 1 µL min^{-1}. Peak identification: 1, MPB; 2, EPB; 3, PPB; 4, BPB. Other details about the composition of columns are given in Table 5.2.

Next, the monolithic capillary column was connected to a cLC system coupled with an ESI-MS nanospray in order to reduce the LODs and increase selectivity, as generally required to analyze biological matrices. The MS and MS/MS behavior of parabens under negative ion ESI was investigated using

direct infusion of standard solutions into the mass spectrometer. Thus, the MS response of parabens increased after replacing acetic acid by ammonium acetate in the mobile phase; however, at contents higher than 0.04% NH_4AcO, a weak inhibition of the MS response was observed. Then, a mobile phase containing 0.04% NH_4AcO was selected for both MS/MS optimization and cLC separation. For each compound, the MS parameters were optimized with the aim of getting two characteristic MRM transitions with the highest signal intensity as possible. Thus, the MRM transition with the best MS response was selected for quantification and the second one transition for confirmation of the parabens (see Table 5.1). The MS separation of parabens was tested with the gradient employed in Fig. 5.3B at 1 µL min^{-1} (the maximum flow rate allowed by the Eksigent cLC-MS instrument). These conditions associated to gradient elution synchronization [36], led to longer cLC-MS analysis times (20 min) than those used for cLC-UV-Vis (Fig. 5.3B).

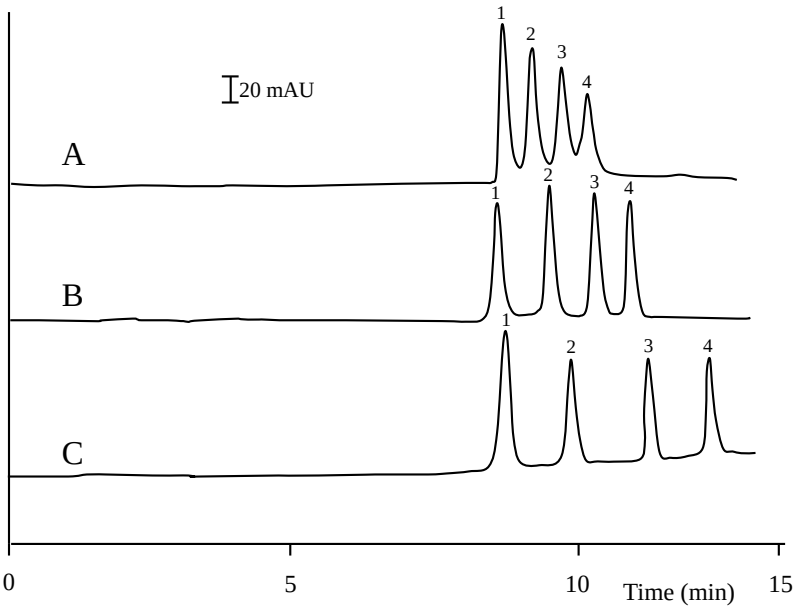

Fig. 5.3. Separations of parabens using column A6 (Table 5.2) under different gradient elution conditions: (A) 0 to 2 min isocratic step at 10% ACN and linear

gradient from 2 to 9 min up to 100%; (B) 0 to 4 min isocratic step at 30% ACN and linear gradient from 2 to 9 min up to 100%; (C) 0 to 4.5 min isocratic step at 30% ACN followed by linear gradient from 4.5 to 5 min up to 45%, from 5 to 8 min up to 55%, from 8 to 9.5 min up to 75%, and from 9.5 to 11.5 min up to 100%. In all cases, the flow rate was 2 µL min^{-1}. Peak identification as in Fig. 5.2.

5.3.2. Quantitation studies and application to urine and serum samples

The cLC-UV-Vis and -MS systems were compared by analyzing a standard mixture of solutes (1 µg mL^{-1} and 5 ng mL^{-1} of each paraben for UV-Vis and MS, respectively). The intra- and inter-day repeatability of retention times and peak areas was measured (Table 5.3). The mixture was injected three times per day during three consecutive days. As shown in Table 5.3, the retention times with RSD values within the 0.22-3.32 and 0.93-4.02% ranges for UV-Vis and MS detection, respectively, were obtained. The RSDs of the peak areas were below 4% and within the 5-5.5% range for UV-Vis and MS detection, respectively. Taking into account the very low LODs which can be reached and the large variability usually affecting the analysis of biological samples at low concentrations, the RSD values found for the peak areas using MS detection are quite adequate (see below).

To estimate the repeatability of preparation monolithic columns, the column-to-column (three columns made from the same polymerization mixture) and batch-to-batch (three batches of three columns each) was established. Both the retention times and peak areas gave RSD values ranging from 4.7 to 5.6% for column-to-column, and from 6.2 to 7.8% for batch-to-batch. More than 100 injections of the standard mixture and 200 injections of real samples were performed without the need of replacing the column; therefore, the stability of the column was satisfactory.

Due to a lack of human urine and serum samples free of parabens, synthetic urine and fetal bovine serum were used for calibration purposes. These strategies have been employed by several authors in literature. Thus,

synthetic urine has been used in the determination of different endocrine disrupting compounds in human urine [47, 48], whereas calf serum or horse serum has been used in the evaluation of endocrine disrupting compounds in human serum [49, 50]. In order to estimate the presence/absence of matrix effects, calibration curves were obtained using standards spiked in deionized water, synthetic urine and fetal bovine serum. The Student's *t* test showed significant differences (at $p = 0.05$ level) among the slopes of the calibration curves when water was compared to the biological matrices, consequently, the standard addition method was used for quantitation.

The calibration curves (at six concentration levels), made in synthetic urine and fetal bovine serum samples, showed adequate linearity up to 25 and 0.5 μg mL^{-1} for UV-Vis and MS detection, respectively. All analytes showed correlations coefficients better than $r = 0.995$ for both detection techniques. The LODs and LOQs of each analyte in these matrices (after DLLME preconcentration) were calculated at signal-to-noise ratios (S/N) equal to 3 and 10, respectively (Table 5.3). The LODs for UV-Vis detection ranged from 7 to 11 ng mL^{-1}, and the LOQs were in the range 23-36 ng mL^{-1}. These values were lower than those found by other authors working with conventional LC using RP-C18 columns (0.2 μg mL^{-1}) [9] or commercial monolithic columns (0.1-0.3 μg mL^{-1}) [10] with DAD detection. However, these LODs were higher than previously reported for the determination of these analytes in serum by LC-MS (0.1-0.2 ng mL^{-1}) [22]. Using cLC-MS, ultra-low LODs (0.01-0.02 ng mL^{-1}) and LOQs (0.04-0.07 ng mL^{-1}) were found. The LODs were 10-fold lower than those previously reported using LC-MS/MS [22].

To evaluate the efficiency and applicability of the proposed extraction methodology (DLLME), a recovery study was also carried out. For this purpose, the analytes at three different concentrations ranging from 0.4 to 15 μg mL^{-1} were added to synthetic urine and fetal bovine serum samples, followed by cLC-UV-Vis analysis. Repeatability (expressed as RSD) was evaluated by performing three replicates at each concentration level. As shown in Table 5.4,

satisfactory recoveries in the range 95.2-106.7 % were found.

Table 5.3

Repeatibility and LODs for parabens standard solutions.

Compounds	Intra-day RSD (%, n = 10)			
	t_R		Peak area	
	cLC-UV	cLC-MS	cLC-UV	cLC-MS
MPB	0.23	1.11	1.61	2.27
EPB	0.22	0.93	1.65	2.14
PPB	0.25	1.03	1.66	2.22
BPB	0.22	0.97	1.71	2.25

Compounds	Intra-day RSD (%, n = 10)			
	t_R		Peak area	
	cLC-UV	cLC-MS	cLC-UV	cLC-MS
MPB	0.23	1.11	1.61	2.27
EPB	0.22	0.93	1.65	2.14
PPB	0.25	1.03	1.66	2.22
BPB	0.22	0.97	1.71	2.25

Compounds	LOD[a] (µg mL^{-1})	LOD[a] (ng mL^{-1})
	cLC-UV	cLC-MS
MPB	0.007; 0.008	0.011; 0.011
EPB	0.007; 0.010	0.012; 0.012
PPB	0.008; 0.011	0.021; 0.021
BPB	0.009; 0.010	0.021; 0.022

[a]For synthetic urine (left) and fetal bovine serum (right) using DLLME preconcentration followed by either cLC-UV or cLC-MS.

The optimized method was applied to the analysis of the target analytes in urine and serum samples collected from different donors. Peak identification in UV-Vis detection was performed by comparing the retention times and absorption spectra with those of the standards, and when necessary, by spiking the sample extracts with the standards. The concentrations found by cLC-UV-Vis and cLC-MS in are given in Table 5.5. The data obtained using both detection techniques were compared. No significant differences were found after application of the statistical test for paired data ($p = 0.05$). However, the paraben levels could not be measured by cLC-UV-Vis in certain biological samples. Consequently, cLC-MS should be preferred due to the much lower LODs that can be reached. Fig. 5.4 shows an example of cLC-UV-Vis and cLC-MRM chromatograms corresponding to samples of the two biological matrices analyzed. As observed in Table 15.5, MPB was quantified using both UV-Vis and MS detection in all urine samples, the concentrations found ranging from 0.050 to 0.342 μg mL^{-1}.

Table 5.4

Recoveries found for the determination of parabens in synthetic urine and fetal bovine serum samples.

Compounds	Synthetic urine RSD (%, n = 3)		
	Low (0.4 μg mL^{-1})	Medium (5 μg mL^{-1})	High (15 μg mL^{-1})
MPB	98.8 ± 13.0	99.8 ± 6.2	106.7 ± 7.7
EPB	95.4 ± 14.1	97.9 ± 6.9	104.9 ± 7.8
PPB	95.2 ± 9.6	98.4 ± 5.1	103.1 ± 4.7
BPB	96.0 ± 10.3	104.9 ± 7.2	100.4 ± 6.3
Compounds	Fetal bovine serum RSD (%, n = 3)		
	Low (0.4 μg mL^{-1})	Low (0.4 μg mL^{-1})	Low (0.4 μg mL^{-1})
MPB	97.7 ± 12.4	97.7 ± 12.4	97.7 ± 12.4
EPB	101.5 ± 13.6	101.5 ± 13.6	101.5 ± 13.6
PPB	95.2 ± 13.0	95.2 ± 13.0	95.2 ± 13.0
BPB	102.8 ± 12.2	102.8 ± 12.2	102.8 ± 12.2

On the contrary, quantitation of the other parabens was possible only in some urine samples. Thus, EPB was quantified using MS detection in 60% of the samples (only in 20% of the samples using UV-Vis), the concentrations ranging from 0.009 to 0.139 μg mL^{-1}; PPB was also ubiquitous, with a concentration range from 0.022 to 0.872 μg mL^{-1}, and BPB was not detected in any urine sample. In the case of serum samples, MPB was quantified using MS detection in 80% of the samples, with concentrations ranging from 0.012 to 0.102 μg mL^{-1}, and EPB was detected only in one serum sample. PPB was also determined in 60% of the samples, with a concentration range from 0.019 to 0.056 μg mL^{-1}, whereas BPB was quantified in 30% of the samples. The presence of each type of paraben in the samples reveals exposure to these compounds, the concentration depending on both exposure level and metabolism. From results given in Table 5.5, it was concluded that at least one of the parabens was present in all the analyzed human samples at detectable concentrations using the DLLME/cLC-MS method.

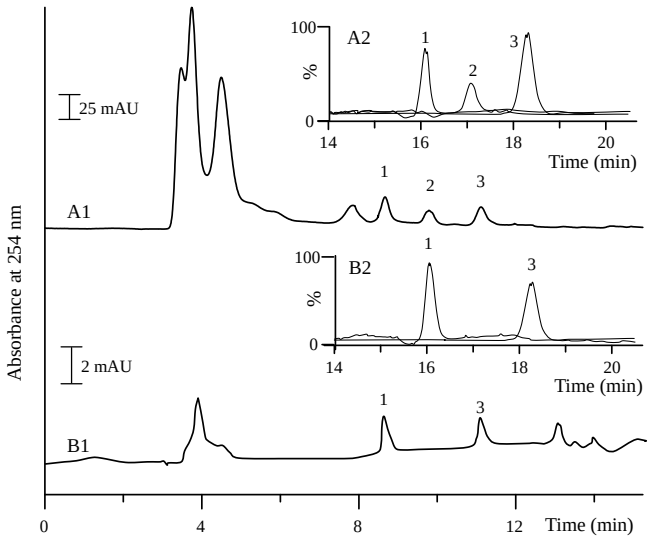

Fig. 5.4. Representative UV-Vis-chromatograms of human (A1) urine (sample U02, Table 5.5) and (B1) serum (sample S01, Table 5.5). Insets are representative MRM chromatograms for MPB (1), EPB (2) and PPB (3) in human urine (A2) and serum (B2). The MRM transitions are given in Table 5.1. Experimental conditions as in Fig. 5.3C. Peak identification as in Fig. 5.2.

Table 5.5
Contents (mean ± SD, n = 3) of free parabens found in human urine and serum samples.

Sample	Concentration (μg mL^{-1})							
	MPB		EPB		PPB		BPB	
	cLC-UV	cLC-MS	cLC-UV	cLC-MS	cLC-UV	cLC-MS	cLC-UV	cLC-MS
Urine								
U01	0.236 ± 0.013	0.232 ± 0.021	0.136 ± 0.008	0.139 ± 0.012	D	0.022 ± 0.001	ND	ND
U02	0.334 ± 0.003	0.341 ± 0.011	0.108 ± 0.006	0.112 ± 0.013	0.346 ± 0.005	0.348 ± 0.009	ND	ND
U03	0.147 ± 0.017	0.151 ± 0.022	ND	ND	0.867 ± 0.021	0.862 ± 0.026	ND	ND
U04	0.196 ± 0.009	0.201 ± 0.013	ND	ND	0.038 ± 0.003	0.035 ± 0.006	ND	ND
U05	0.205 ± 0.011	0.203 ± 0.015	ND	ND	D	0.028 ± 0.014	ND	ND
U06	0.336 ± 0.027	0.342 ± 0.031	D	0.012 ± 0.004	0.034 ± 0.008	0.035 ± 0.007	ND	ND
U07	0.093 ± 0.014	0.097 ± 0.017	D	0.013 ± 0.006	D	0.027 ± 0.002	ND	ND
U08	0.053 ± 0.021	0.050 ± 0.026	ND	ND	0.049 ± 0.008	0.051 ± 0.013	ND	ND
U09	0.096 ± 0.011	0.100 ± 0.015	D	0.009 ± 0.003	D	0.028 ± 0.004	ND	D
U10	0.068 ± 0.024	0.072 ± 0.030	D	0.018 ± 0.005	D	0.022 ± 0.007	ND	ND
Serum								
S01	D	0.027 ± 0.004	ND	ND	D	0.019 ± 0.003	ND	ND
S02	0.099 ± 0.006	0.102 ± 0.009	0.082 ± 0.008	0.085 ± 0.011	0.050 ± 0.013	0.052 ± 0.021	0.060 ± 0.010	0.062 ± 0.013
S03	ND	ND	ND	ND	0.039 ± 0.007	0.036 ± 0.010	D	0.023 ± 0.002
S04	ND	ND	ND	ND	ND	ND	ND	ND
S05	D	0.012 ± 0.003	ND	ND	ND	ND	ND	ND
S06	0.028 ± 0.001	0.031 ± 0.003	ND	ND	ND	ND	D	0.015 ± 0.006
S07	D	0.017 ± 0.003	ND	ND	0.032 ± 0.001	0.033 ± 0.003	ND	ND

5.4. Conclusions

A method based on cLC with UV-Vis and MS detection, using methacrylate ester-based capillary monolithic columns, has been developed for the determination of parabens in biological fluids. The preparation conditions of the monolithic stationary phase and the working conditions for cLC separation using either UV-Vis or MS detection were investigated. The best chromatographic performance was achieved with a BMA-based column prepared at 60:40 (wt/wt) BMA/EDMA and 50% porogens (composed of 36 wt% 1,4-BuOH, 54 wt% 1-PrOH and 10 wt% water), and using gradient elution with an ACN/H_2O as mobile phase. A simple and highly effective clean-up and preconcentration step prior to chromatographic separation was implemented using DLLME. This technique has the advantages of simplicity of operation, rapidity, low-cost and high-recovery rates. The proposed cLC with either UV-Vis or MS detection provided satisfactory separation efficiency and ultra-low LODs (for MS detection) in complex biological samples and within short analysis times (15-20 min). The peak capacity of the proposed method was not as high as reported values for sub-5 µm particle columns and highly cross-linked monoliths; however, all the paraben pairs were very well resolved, with wide-baseline segments in between. Using cLC with splitless flow, the consumption of solvents is very small (20-30 µL of mobile phase per run). Additionally, the developed methodology is enough for detecting parabens with extremely low detection limits in complicated samples. Thus, the proposed DLLME-cLC-MS method could be classified as a "green approach" for the fast, cheaper and simple sensitive analysis of parabens. This methodology might be suitable to be used in routine analysis for clinical purposes, and can be also useful to evaluate possible adverse effects resulting from paraben exposure. The proposed strategy is a green analytical chromatography, which might be useful for other applications.

Acknowledgements

Study supported by Project CTQ2014-52765-R (MINECO of Spain and FEDER funds) and Project of Excellence P09-CTS-4470 (Regional Government of Andalusia). E.J.C-C. thanks the MINECO for an FPI grant for PhD studies and F. V-S. thanks the University of Granada for a PhD fellowship. The authors also thank Dr. Luz Valero-Rustarazo of the Facility for Proteomics of the SCSIE (University of Valencia) for her assistance in cLC-MS/MS.

References

[1] M.G. Soni, G.A. Burdock, S.L. Taylor, N.A. Greenberg, Food Chem. Toxicol., 39 (2001) 513.

[2] U.S. Food and Drug Administration (2009) URL: http://www.fda.gov/cosmetics/productsingredients/ingredients/ucm128042.htm (accessed November 2014).

[3] A. Panusia, L. Gagliardi, J. Pharm. Biomed. Anal., 47 (2008) 786.

[4] A. De Rossi, C. Desiderio, Electrophoresis, 23 (2002) 3410.

[5] European Economic Community (ECC) instruction No. 93/95, Off. J. Eur. Comm., Brussels 1993, Lf: 32-37.

[6] E.J. Routledge, J. Parker, J. Odum, J. Ashby, J. P. Sumpter, Toxicol. Appl. Pharmacol., 153 (1998) 12.

[7] Q. Zhang, M. Lian, L. Liu, H. Cui, Anal. Chim. Acta, 537 (2005) 31.

[8] H.-Y. Shen, H.-L. Jiang, H.-L. Mao, G. Pan, L. Zhou, Y.-F. Cao, J. Sep. Sci., 30 (2007) 48.

[9] W. Gao, C. Legido-Quigley, J. Chromatogr. A, 1218 (2011) 4307.

[10] A. Zotou, I. Sakla, P. D. Tzanavaras, J. Pharm. Biomed. Anal., 53 (2010) 785.

[11] M.A. Farajzadeh, E.M. Khosrowshahi, P. Khorram, J. Sep. Sci., 36 (2013) 3571.

[12] U.D. Uysal, T. Güray, J. Anal. Chem., 63 (2008) 982.

[13] F. Hang, Y.-Z. He, C.-Z. Yu, Talanta, 74 (2008) 1371.

[14] A. De Rossi, C. Desiderio, Electrophoresis, 23 (2002) 3410.

[15] H.-Y. Huang, C. W. Chiu, I.-Y. Huang, J. M. Yeh, Electrophoresis, 25 (2004) 3237.

[16] H.-Y. Huang, I.-Y. Huang, H.Y. Lin, J. Sep. Sci., 29 (2006) 2038.

[17] I. Jiménez-Díaz, F. Vela-Soria, A. Zafra-Gómez, A. Navalón, O. Ballesteros, N. Navea, M.F. Fernández, N. Olea, J.L. Vílchez, Talanta, 84 (2011) 702.

[18] P.D. Darbre, A. Alijarrah, W.R. Miller, N.G. Coldham, M.J. Sauer, G.S. PopeJ. Appl. Toxicol., 24 (2004) 5.

[19] L. Barr, G. Metaxas, C.A.J. Harbach, L.A. Savoy, P.D. Darbre, J. Appl. Toxicol., 32 (2012) 219.

[20] X. Ye, Z. Kuklenyik, A.M. Bishop, L.L. Needham, A.M. Calafat, J. Chromatogr. B, 844 (2006) 53.

[21] X. Ye, A.M. Bishop, L.L. Needham, A.M. Calafat, Anal. Chim. Acta, 622 (2008) 150.

[22] F. Vela-Soria, O. Ballesteros, I. Rodríguez, A. Zafra-Gómez, L. Ballesteros, R. Cela, A. Navalón, Anal. Bioanal. Chem., 405 (2013) 7259.

[23] J. Hernández-Borges, Z. Aturki, A. Rocco, S. Fanali, J. Sep. Sci., 30 (2007) 1589.

[24] F. Svec, J. Chromatogr. A, 1217 (2010) 902.

[25] V. Bernabé-Zafón, A. Cantó-Mirapeix, E.F. Simó-Alfonso, G. Ramis-Ramos, J.M. Herrero-Martínez, Electrophoresis, 30 (2009) 1929.

[26] Y. Li, H.D. Tolley, M.L. Lee, J. Chromatogr. A, 1218 (2011) 1399.

[27] K. Liu, H.D. Tolley, M.L. Lee, J. Chromatogr. A, 1227 (2012) 96.

[28] Y. He, H.K. Lee, Anal. Chem., 69 (1997) 4634.

[29] E. Psillakis, N. Kalogerakis, Trends Anal. Chem., 22 (2003) 565.

[30] M. Rezaee, Y. Assadi, M.R.M. Hosseini, E. Aghaee, F. Ahmadi, S. Berijani, J. Chromatogr., A 1116 (2006) 1.

[31] M.A. Farajzadeh, M. Bahram, J.Å. Jönsson, Anal. Chim. Acta, 591 (2007) 69.

[32] S.C. Cunha, J. O. Fernandes, Talanta, 83 (2010) 117.

[33] M. Vosough, N.R. Mojdehi, A. Salemi, J. Sep. Sci., 35 (2012) 3575.

[34] I. Tarazona, A. Chisvert, A. Salvador, Talanta, 116 (2013) 388.

[35] F. Vela-Soria, O. Ballesteros, A. Zafra-Gómez, I. Ballesteros, A. Navalón, Talanta, 121 (2014) 97.

[36] E.J. Carrasco-Correa, A. Acquaviva, J.M. Herrero-Martínez, G. Ramis-Ramos, J. Chromatogr. A, 1318 (2013) 142.

[37] J.W. Dolan, L.R. Snyder, N.M. Djordjevic, D.W. Hill, T.J. Waeghe, J. Chromatogr. A, 857 (1999) 1.

[38] E.C. Peters, M. Petro, F. Svec, J.M.J. Fréchet, Anal. Chem., 69 (1997) 3646.

[39] E.C. Peters, M. Petro, F. Svec, J.M.J. Fréchet, Anal. Chem., 70 (1998) 2288.

[40] S. Eeltink, J.M. Herrero-Martinez, G.P. Rozing, P.J. Schoenmakers, W. Th. Kok, Anal. Chem., 77 (2005) 7342.

[41] M.T. Dulay, H.N. Choi, R.N. Zare, J. Sep. Sci., 30 (2007) 2979.

[42] A-M.K. Weed, J. Dvornik, J.J. Stefancin, A.A. Gyapong, F. Svec, Z. Zajickova, J. Sep. Sci., 36 (2013) 270.

[43] M.R. Lee, C.Y. Lin, Z.G. Li, T.F. Tsai, J. Chromatogr. A, 1120 (2006) 244.

[44] A.A. Gaona-Galdos, P. López-García, M.S. Aurora-Prado, M.I.R. Miritello-Santoro, E.R.M. Kedor-Harcmann, Talanta, 77 (2008) 673.

[45] Y. Guo, S. Srinivasan, S. Gaiki, Chromatographia, 70 (2009) 1045.

[46] D.T.-T. Nguyen, D. Guillarme, S. Heinisch, M.-P. Barrioulet, J.-L. Rocca, S. Rudaz, J.-L. Veuthey, J. Chromatogr. A 1167 (2007) 76.

[47] S.-Y. Lee, E. Son, J.-Y. Kang, H.S. Lee, M.-K. Shin, H.-S. Nam, S.-Y. Kim, Y.-M. Jang, G.-S. Rhee, Bull. Korean Chem. Soc., 34 (2013) 1131.

[48] M.S. Nahar, S.S. Soliman, J.A. Colacino, A.M. Calafat, K. Battige, A. Hablas, I.A. Seifeldin, D. C. Dolinoy, L. S. Rozek, Environ. Health, 11 (2012) 1-8.

[49] X. Ye, L.J. Tao, L.L. Needham, A.M. Calafat, Talanta, 76 (2008) 865.

[50] A.C. Dirtu, L. Roosens, T. Geens, A. Gheorghe, H. Neels, A. Covaci, Anal. Bioanal. Chem., 391 (2008) 1175.

Supplementary Material

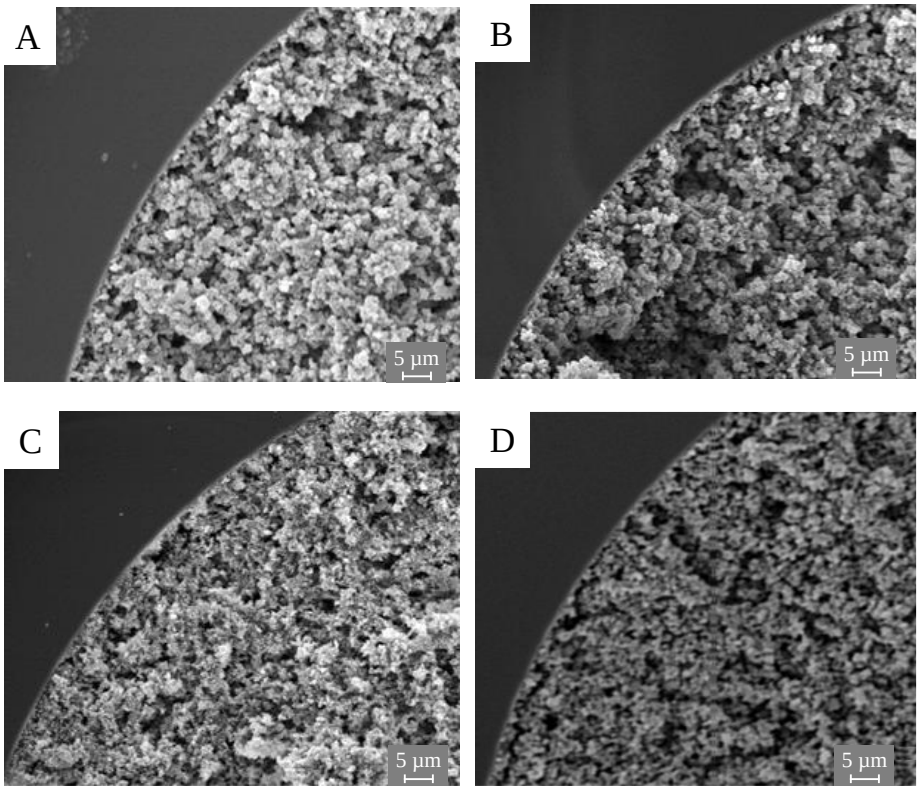

Fig. S5.1. SEM micrographs of BMA-based monoliths in the wall zone, prepared at several ratios of 1,4-BuOH/1-PrOH/H_2O (wt/wt/wt): (A) 27:63:10 (column A1), (B) 36:54:10 (column A3). Parts (C) and (D) show monoliths prepared with several monomers/porogens ratios: (C) 30:70 (column A5) and (D) 50:50 (column A6). Other details about the composition of columns are given in Table 15.2.

Chapter 6. Evaluation of 2,3-epoxypropyl groups and functionalization yield in glycidyl methacrylate monoliths using gas chromatography

Journal of Chromatography A, 1379 (2015) 100–105

Contents lists available at ScienceDirect

Journal of Chromatography A

journal homepage: www.elsevier.com/locate/chroma

Evaluation of 2,3-epoxypropyl groups and functionalization yield in glycidyl methacrylate monoliths using gas chromatography

Enrique Javier Carrasco-Correa*, Guillermo Ramis-Ramos, José Manuel Herrero-Martínez*

Department of Analytical Chemistry, University of Valencia, Dr. Moliner 50, 46100 Burjassot, Valencia, Spain

Poly(GMA-*co*-EDMA) is most frequently used as parent monolith to obtain stationary phases with a variety of surface chemistries for liquid chromatography and capillary electrochromatography. Functionalization is performed by opening the accessible 2,3-epoxypropyl groups of the monolith with a suitable reagent. The number of 2,3-epoxypropyl groups which are accessible before and after the functionalization reaction, and the grafting yield, are important parameters, required both to optimize functionalization and to interpret the chromatographic performance of functionalized monoliths. In this work, a method capable of providing this information for parent and functionalized poly(GMA-*co*-EDMA) monoliths prepared both in silica capillaries and in other supports is proposed. First, sulfuric acid and lithium aluminium hydride are sequentially used to release the 2,3-epoxypropyl groups as glycerol, which is subsequently determined by GC. About 6.0 mmol of 2,3-epoxypropyl groups per gram of monolith was found in this work for the parent monoliths prepared in silica capillaries using UV-initiation. The monoliths were also functionalized using NH_3, DEA and epinephrine, and the amount of residual 2,3-epoxypropyl groups, and hence the functionalization yield, were established by also measuring the GC peak of glycerol. The amounts of 2,3-epoxypropyl groups and the derivatization yields were established with RSDs of 1.7 and 3.4 %, respectively. The proposed method was also applied to the characterization of poly(GMA-*co*-EDMA) monoliths prepared in glass vials.

Significant differences with respect to those prepared in 100 µm I.D. silica capillaries were evidenced.

Keywords: GMA-based monolithic columns; monolith functionalization; reactive monoliths; determination of glycidyl groups; evaluation of derivatization yield; gas chromatography

6.1. Introduction

Organic monolithic stationary phases, which emerged in the early 90s of the past century, are still attracting much interest. Their easy in situ preparation, high permeability and biocompatibility, stability along wide pH-ranges, and readily modifiable surface chemistries make these materials to be a competitive alternative to the conventional particle-based stationary phases [1-3]. In contrast to the single-step copolymerization approaches, the functionalization of the monolith after polymerization is easily performed, offering a much wider range of possibilities. Surface functionalization allows the independent tuning of both surface chemistry and the mechanical and flow-through porous properties of the parent monolith. Also, functionalization provides an excellent way of sequentially using reagents that could be incompatible with polymerization mixtures for solubility or redox reasons. In particular, functionalization at the 2,3-epoxypropyl groups of poly(GMA-*co*-EDMA) by ring opening is the most frequently used methodology for monolith surface modification [5-23]. A wide variety of chromatographic properties (ion-exchange, hydrophobic/hydrophilic, chiral, etc.) can be achieved and finely tuned. Thus, poly(GMA-co-EDMA) based monoliths have been modified by using amines [5,7-9], amino acids [10,11], polymers [9,12], sodium sulfite [13], sodium hydrogen sulfide [9,14], sulfuric acid [15,16], a variety of chiral ligands [9,17-22] and nanoparticles [11, 23].

An important aspect of monolith functionalization is the evaluation of the initial number of 2,3-epoxypropyl groups, and after functionalization, the evaluation of the derivatization yield. During functionalization, part of the 2,3-epoxypropyl groups could remained unreacted, particularly if the functionalization reagent exhibits steric hindrance to access some of them. In addition, part of the 2,3-epoxypropyl groups may have been hydrolyzed to yield 2,3-dihydroxypropyl groups, particularly under harsh functionalization conditions. Then, the functionalization yield should be established by evaluating the joint concentration of both the 2,3-epoxypropyl and 2,3-

dihydroxypropyl groups that are still present after functionalization. Hence, quantitative information about the amount of ligand actually bonded to the monolith can be indirectly derived. This information is relevant both to optimize functionalization procedures and to interpret the chromatographic performance of the functionalized monoliths. However, a literature survey reveals that this relevant information is rarely available. To our knowledge, procedures to determine the functionalization yield of the monolith have been provided and applied in a few reports [8,14,15,22]. Further, the functionalization yield has been generally established in monoliths prepared as bulk probes (as in glass vials), and only rarely inside the capillary columns which have been prepared for LC or capillary electrochromatography CEC separations [8,14]. The material of the bulk probes is generally analyzed by a number of techniques, including FTIR and Raman spectroscopies, differential scanning calorimetry and elemental analysis. These techniques provide useful information about the monolith structure and composition, but the information related to the surface functionalization is frequently missed. Also, when the amount of grafted groups is a minor mass fraction of the monolith, methods addressed to determine the groups by analyzing the whole material are susceptible to be affected by large systematic and random errors. Therefore, the development of a universal procedure which could be employed to determine the amounts of 2,3-epoxypropyl groups and the functionalization yield, independently from the functionalization procedure and grafted reagents, in monoliths prepared in any format, including capillaries, is nowadays a demanding requirement. On the other hand, monoliths prepared as bulk materials may significantly differ from those obtained in capillary format. However, as far as we know, the possible structural and functional differences between monoliths obtained in these largely different formats have not been investigated. A procedure capable of measuring the amount of accessible reactive group with the required accuracy in both capillary monoliths and bulk materials would be also useful to investigate differences between them.

In this work, a method based on two quick reactions, addressed to release the 2,3-epoxypropyl and 2,3-dihydroxypropyl groups as glycerol, followed by its determination by GC-FID, is proposed. The method was applied both to monoliths prepared in capillaries and glass vials, in both cases before and after opening of the epoxy rings with NH_3, DEA and epinephrine. The amount of these ligands that were grafted on the monoliths was first established from the difference between the amount of glycerol found before and after functionalization. Hence, the functionalization yield was calculated as the ratio between the amount of grafted ligands and that of the reactive groups found in the parent monoliths. The results obtained using capillary columns were compared with those obtained using bulk monoliths prepared in glass vials, which provided evidence about their differences.

6.2. Materials and methods

6.2.1. Reagents and other materials

GMA, EDMA, γ-MPS, DEA, NH_3, glycerol, 1-amino-2,3-propanediol, 3-(dimethylamino)-1,2-propanediol, ethylene glycol, diethylene glycol and $LiAlH_4$ were from Aldrich (Milwaukee, WI, USA). MeOH, HPLC-grade diethyl ether (Et_2O) and hexane were from Scharlab (Barcelona, Spain). AIBN was from Fluka (Buchs, Switzerland). Uncoated fused-silica capillaries of 10 cm total length and 375 µm O.D. × 100 µm I.D. with UV-transparent external coating (Polymicro Technologies, Phoenix, AZ, USA) were used.

6.2.2. Instrumentation

To introduce the functionalizing reagents into the monolithic capillary columns, a syringe pump (Model 100, KD Scientific, New Hope, PA, USA) was employed. The washing steps used for monoliths in capillaries were

performed with an HPLC pump (1100 Series, Agilent Technologies, Waldbronn, Germany). A 7890A GC system, equipped with a G4513A autosampler and a FID (Agilent Technologies), and provided with a Zebron ZB-WAX plus column (30 m × 0.25 mm I.D. × 0.25 µm film thickness) from Phenomenex (Aschaffenburg, Germany), was employed. Nitrogen was used as carrier.

6.2.3. Preparation of poly(GMA-co-EDMA) monoliths

For the preparation of monoliths in capillary format, and prior to polymerization, the inner wall of the fused-silica capillaries was modified to provide covalent attachment of the monolith. For this purpose, wall modification with γ-MPS was performed as described [24,25]. The polymerization mixtures were prepared by weighing GMA (20 wt%), EDMA (5 wt%), and a binary pore-forming solvent constituted by CYC (70 wt%) and DOD (5 wt%). AIBN (1 wt% with respect to the monomers) was added as initiator [8,9]. To obtain a clear solution, sonication for 10 min followed by purging with nitrogen for 10 more min was applied. The preconditioned capillary was filled with the polymerization mixture up to a length of 10 cm. Photopolymerization was accomplished by irradiation of the capillaries within an UV chamber at 0.9 J cm^{-2} for 30 min. Then, an HPLC pump was used to flush the columns for 30 min with MeOH to remove the pore-forming solvents and remaining unreacted monomers.

Bulk monoliths were also prepared in 1.5 cm I.D. glass vials by using 0.5 mL of polymerization mixture. The vials were located opened inside the UV chamber to be irradiated in the same conditions as those used for the capillaries, although silanization of their inner was not performed. After polymerization, the vials were broken and the bulk material was separated from the glass pieces. This material was repeatedly washed with MeOH on a Büchner funnel to remove the pore-forming solvents and unreacted monomers and dried at 80 ºC

for 6 h. The bulk polymer was ground into a very fine powder with mortar and pestle.

6.2.4. Functionalization of poly(GMA-co-EDMA) monoliths with amine compounds

The reaction schemes for the functionalization of poly(GMA-*co*-EDMA) monoliths with amine compounds are illustrated in Fig. 6.1. First, the capillary columns were flushed with MeOH, followed by flushing with an aqueous solution of either NH_3, DEA or epinephrine. For NH_3 and DEA, 4.5 M aqueous solutions at 60 ºC were passed for 2 h at 60 µL h^{-1} [9]. For epinephrine, a 10 mM solution in 100 mM aqueous sodium tetraborate of pH 8.0 at 60 ºC was passed for 2 h at 240 µL h^{-1} [8]. Then, the capillaries were washed with MeOH until reaching pH 7 at the outlet.

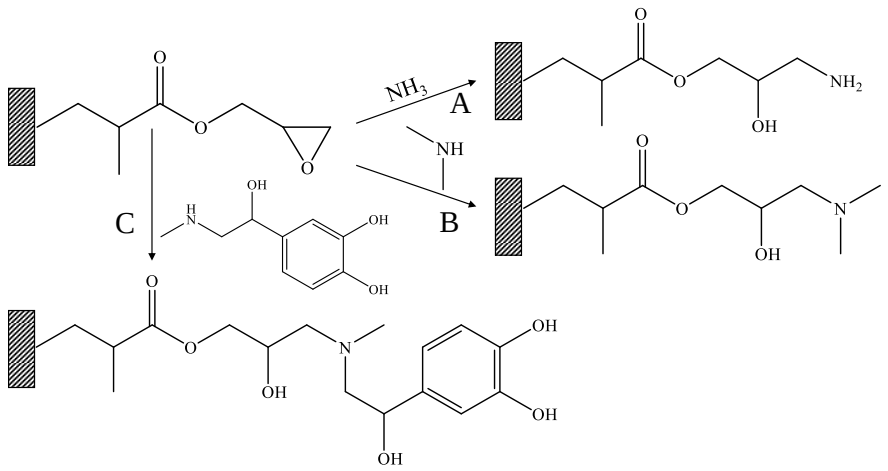

Fig. 6.1. Reaction schemes for the functionalization of poly(GMA-co-EDMA) monoliths with NH3 (A), DEA (B) and epinephrine (C). Reaction conditions as described in the experimental section.

The bulk monolithic materials (obtained from glass vials) were functionalized under similar preparation conditions as described above for the capillaries. Thus, powdered bulk material (5 mg) was mixed with the derivatization solutions, and the mixtures were stirred at 60ºC for 2 h. In particular, *ca*. 0.7 mL and 1.3 mL reagent mg^{-1} monolith were added for NH_3 and DEA, and for epinephrine, respectively.

6.2.5. Glycerol assay for the evaluation of the 2,3-epoxypropyl and 2,3-dihydroxypropyl groups

The reaction schemes used to determine the accessible 2,3-epoxypropyl and 2,3-dihydroxypropyl groups of parent and functionalized monoliths are given in Fig. 6.2 (paths A1, A2, B1, B2 and B3). In this figure, the alternative reactions C and D, which are commented below, are also shown. A syringe pump was used first to flush the parent capillary columns with 0.5 M aqueous sulfuric acid at 90 ºC for 2 h at 60 µL h^{-1}. This procedure, adapted from Hrudková *et al.* [15], resulted in the opening of the accessible epoxy groups. The monoliths were then washed with MeOH to remove the acid until reaching pH 7 at the outlet. Then, a reduction based on the well-known procedure for ester bond reductive break down with $LiAlH_4$ was used [26]. For this purpose, a syringe pump was used to force a dispersion containing 100 mM $LiAlH_4$ in hexane at room temperature for 2 h at a flow rate of 100 µL h^{-1}, while collecting the eluate in a micro-vial. Afterwards, using an HPLC pump, the column was rinsed with hexane, until collecting *ca.* 1 mL in the same micro-vial. The vial was weighed, and the weight was divided by the hexane density (0.66 g mL^{-1} at 22 ºC) to obtain the total volume. A proper amount of 100 µg mL^{-1} internal standard solution (diethylene glycol in hexane) was added up to reach 10 µg mL^{-1} and the mixture was injected in the GC-FID system.

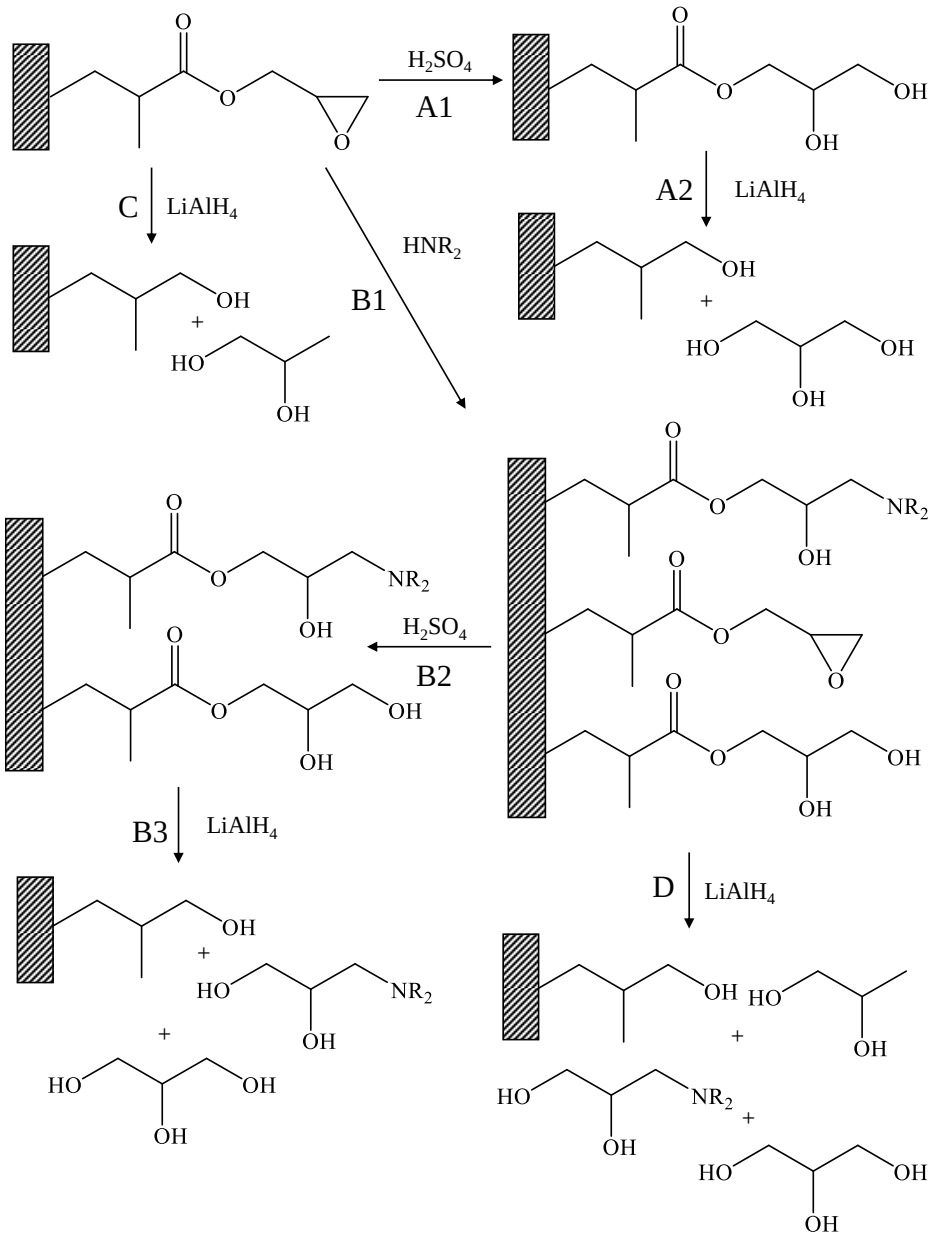

Fig. 6.2. Reaction schemes for the determination of 2,3-epoxypropyl and 2,3-dihydroxypropyl groups in underivatized and functionalized monoliths using H_2SO_4 followed by $LiAlH_4$ (reaction paths A1, A2, B1, B2 and B3). The alternative reaction paths when $LiAlH_4$ is used without previous opening of the epoxy rings with H_2SO_4 are also shown (C and D).

A similar procedure was used to study the bulk monoliths prepared in glass vials. Thus, powdered bulk material (5 mg) was mixed with the aqueous sulfuric solution (*ca*. 0.7 mL mg^{-1} monolith), and the mixture was stirred at 90ºC for 2 h. The material was repeatedly washed with MeOH, dried at 80ºC for 6 h, and stirred with the $LiAlH_4$ suspension (*ca*. 1.1 mL mg^{-1} monolith) for 2 h. The suspension was filtered and the filtrate was adequately diluted, and treated as above for GC-FID determination. The chromatograms of all the monoliths prepared both in the capillaries and glass vials showed the glycerol peak.

The initial temperature of the GC oven was 80 ºC, which was followed by rising to 180 ºC at 20 ºC min^{-1} with a final 180 ºC plateau for 10 min. The FID temperature was 250 ºC. The GC injection port was set at 225 ºC; the injection volume was 2 µL under splitless mode. Nitrogen was used as carrier at a constant flow rate of 3 mL min^{-1}. A calibration curve was constructed by mixing the adequate volumes of hexane solutions of glycerol containing diethylene glycol (as internal standard).

6.3. Results and discussion

6.3.1. Selection of the reaction steps

The monoliths, prepared as indicated in section 6.2.3, showed a high permeability (wide flow-through pores of around 1-2 µm), which enormously facilitated the rinsing steps. First, H_2SO_4 was used to open the epoxy rings of the 2,3-epoxypropyl groups to yield 2,3-dihydroxypropyl groups (Fig. 6.2, reaction paths A1 and B2). Second, glycerol was liberated by reducing the ester bonds with $LiAlH_4$ (Fig. 6.2, paths A2 and B3). Alternatively, the direct reduction of the ester bond of the 2,3-epoxypropyl groups with $LiAlH_4$, without previous opening of the epoxy ring with H_2SO_4, is also possible. This would liberate 1,2-propanediol instead of glycerol for parent monoliths (Fig. 6.2, path C). Besides, for functionalized monoliths, the direct use of $LiAlH_4$ would

release glycerol, 1,2-propanediol and the corresponding 2,3-propyldiol derivative of the ligand. The evaluation of the 1,2-propanediol GC peak for the parent monolith (path C) seems to be equivalent to the evaluation of the glycerol peak after paths A1 and A2; however, as next discussed, path C is not convenient for functionalized monoliths. As indicated above, a number of 2,3-epoxypropyl groups which have not been functionalized with the intended ligand could have been opened during functionalization. According to path D, it would provide three peaks, namely that of glycerol, 1,2-propanediol and its amine derivative. Thus, this reaction path would complicate the determination of the unfunctionalized 2,3-epoxypropyl and 2,3-dihydroxypropyl groups, since two calibration curves, one for glycerol and another for 1,2-propanediol, would be needed. This would also decrease the sensitivity of the procedure, since two GC peaks instead of a single one would be obtained. Instead of this, opening of the residual epoxy groups of functionalized monoliths with H_2SO_4, followed by reduction with $LiAlH_4$, yields only glycerol (Fig. 6.2, paths B2 and B3). With the proposed two-step reaction procedure, the initially available epoxy groups and the sum of the unreacted 2,3-epoxypropyl and 2,3-dihydroxypropyl groups of functionalized monoliths, will be both established by measuring the single peak of glycerol. On the other hand, for functionalized monoliths, and either with or without previous opening of the residual epoxy groups with H_2SO_4, reduction with $LiAlH_4$ will liberate the functionalization ligand with an attached 2,3-propyldiol chain. Thus, the chromatograms obtained with functionalized monoliths will show an additional peak if the resulting molecule has enough volatility (Fig. 6.2, paths B3 and D). This will also provide direct information about the functionalization yield. In this work, this was the case for NH_3 and DEA, but not for epinephrine.

6.3.2. Optimization of the reaction conditions for the two reactions

The flushing time for the reactions of parent monoliths with both H_2SO_4 and $LiAlH_4$ was optimized (Fig. 6.3). The ring opening of the 2,3-epoxypropyl groups of capillary monoliths was performed a 0.5 M H_2SO_4 solution at 90 ºC and 60 µL h^{-1}. Using a series of capillary columns, the effect of time on the total amount of liberated glycerol, while keeping constant working conditions for the subsequent reaction with $LiAlH_4$, was studied. As observed in Fig. 6.3A, it was necessary to flush the capillary for at least 1 h to achieve total hydrolysis of the 2,3-epoxypropyl groups. The experiments that follow were performed using 2 h. Then, the influence of the flushing time of the $LiAlH_4$ solution through the column was studied. For this purpose, a 100 mM $LiAlH_4$ solution was flushed through the column at room temperature 100 µL h^{-1}.The working conditions of the previous reaction with H_2SO_4 were kept constant. As shown in Fig. 6.3B, the reaction yield was higher when the $LiAlH_4$ was dissolved in hexane rather than in Et_2O. This could be due to the hygroscopicity of Et_2O; in fact, hydrogen bubbles were observed in the $LiAlH_4$ solution in Et_2O, but not in that prepared in hexane. Reduction of the traces of water present in Et_2O, or absorbed from the atmosphere, may reduce the amount of available $LiAlH_4$, which did not occur by using hexane as solvent. As also observed in Fig. 6.3B, it was necessary to flush the columns for at least 2 h to achieve a constant amount of released glycerol. This corresponds to a $LiAlH_4$ excess of 20 times with respect to the theoretical amount of 2,3-epoxypropyl groups present in the whole parent monolith. Thus, the conditions selected for ester bond reduction were flushing the column at room temperature with a 100 mM $LiAlH_4$ solution in hexane at 100 µL h^{-1} for 2 h.

6.3.3. Determination of the accessible 2,3-epoxypropyl and 2,3-dihydroxypropyl groups of capillary monoliths

The proposed procedure was next applied to the joint determination of the accessible 2,3-epoxypropyl and 2,3-dihydroxypropyl groups in the capillary monoliths (before and after functionalization of the monoliths). The GC-FID chromatograms obtained for parent monoliths and for columns functionalized with NH_3, DEA and epinephrine are shown in Fig. 6.4. All these chromatograms showed the peak of glycerol, as well as a small peak of ethylene glycol due to the reduction of the two ester bonds of EDMA bridges of the polymer structure. No peaks were observed in the chromatogram of the reagent's blank (not shown). In addition, for the capillary columns functionalized with NH_3 (Fig. 6.4, trace B) and DEA (Fig. 6.4, trace C), a peak due to 1-amino-2,3-propanediol (peak no. 2) and 1-dimethylamino-2,3-propanediol (peak no. 3), respectively, was observed. These compounds were due to the reduction of the ester bond at the polymer sites successfully functionalized with NH_3 and DEA (see also Fig. 6.2). An additional peak was not found for the monolith derivatized with epinephrine (Fig. 6.4, trace D), probably due to the lack of volatility of the released 2,3-propyldiol epinephrine derivative.

As shown in Table 6.1 for parent monoliths, the concentration of the 2,3-epoxypropyl groups was 5.98 mmol g^{-1} monolith, which was only slightly higher than the theoretically predicted value of 5.63 mmol g^{-1} [8,9,14]. In this case, the presence of 2,3-dihydroxypropyl groups is unlikely, and if present, their concentration should be negligible. The results obtained with the functionalized monoliths are also given in Table 6.1. As expected, the joint content of 2,3-epoxypropyl and 2,3-dihydroxypropyl groups in functionalized monoliths was smaller than the concentration of 2,3-epoxypropyl groups in the parent monoliths.

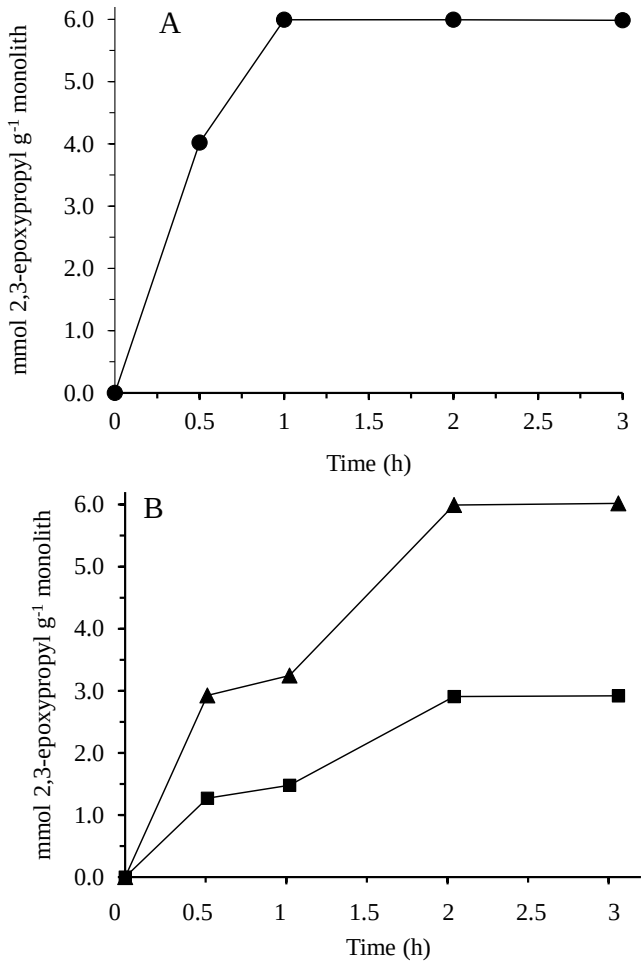

Fig. 6.3. Optimization of the flushing time for the first (ring opening) and second (reduction with $LiAlH_4$) reaction steps. A 0.5 M H_2SO_4 solution in water at 90 ºC and at a flow rate of 60 µL h^{-1}, and a 100 mM $LiAlH_4$ solution in either hexane (▲) or Et_2O (■) at room temperature and at a flow rate of 100 µL h^{-1}, were used. The flushing time for the first reaction was increased by keeping the flushing time of the $LiAlH_4$ solution in hexane at 2 h (A); then, the flushing time for the second reaction was increased by keeping the flushing time of the H_2SO_4 solution at 2 h (B).

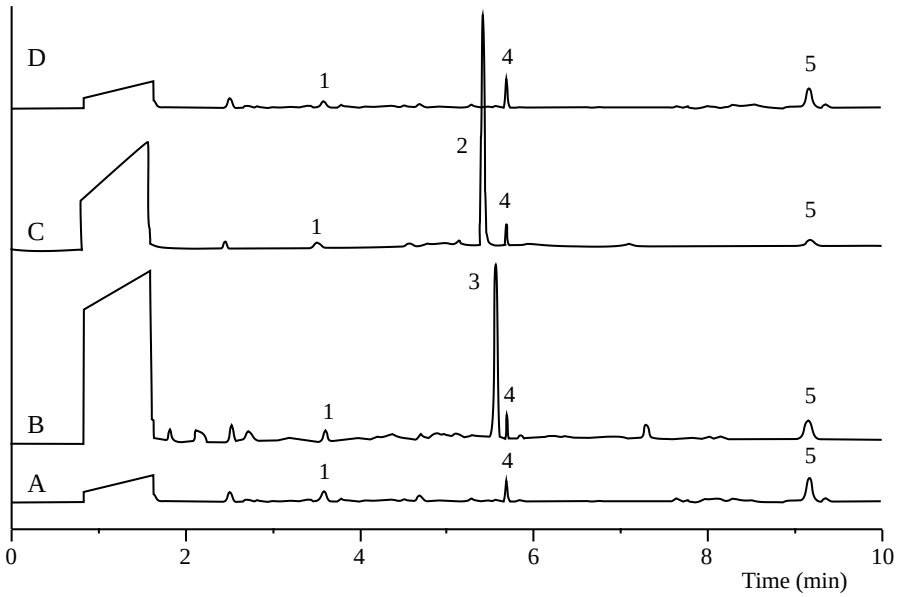

Fig. 6.4. Chromatograms obtained by applying the proposed method to parent capillary monoliths (A) and monoliths modified with NH_3 (B), DEA (C) and epinephrine (D). Chromatographic conditions are indicated in the section 2.5. Peak identification: ethylene glycol (1), 1-amino-2,3-propanediol (2), 1-dimethylamino-2,3-propanediol (3), diethylene glycol (4, internal standard) and glycerol (5).

From these values, the corresponding functionalization yields were calculated. As could be expected, the functionalization yield was much higher for NH_3 and DEA than for epinephrine. This could be attributed to steric hindrance, that is, to the greater difficulty for epinephrine to access to the monolith reaction sites when compared to NH_3 and DEA; further, the low percentage for epinephrine agrees with that found in a previous study [4]. The yield was higher for DEA than for NH_3 probably due to the stronger nucleophilic character of the secondary amine with respect to ammonia. In Table 6.1, the repeatability of the proposed method is also given. The parent monoliths showed a quite satisfactory 1.7 %. The derivatized monoliths gave values close to 3 %, which can be attributed to both the variability of the monolith functionalization reactions and to the smaller amounts of glycerol which were released.

Table 6.1. Sum of contents of 2,3-epoxypropyl and 2,3-dihydroxypropyl groups in parent and functionalized monoliths prepared in capillary tubes and glass vials, functionalization yields and repeatability (given as RSD % for *n* = 3 columns).

Monolith support	Modified with	Concentration (mmol g^{-1} monolith)[a]	Difference (mmol g^{-1} monolith)[b]	Functionalization yield (%)	RSD (%)
Capillary (100 µm I.D.)	Parent	5.98	-	-	1.7
	NH_3	3.59	2.39	39.9	2.7
	DEA	2.92	3.06	51.2	2.7
	Epinephrine	5.49	0.49	8.2	3.2
Glass vial (1.5 cm I.D.)	Parent	4.73	-	-	3.2
	NH_3	2.88	1.85	39.1	3.5
	DEA	2.33	2.40	50.7	3.5
	Epinephrine	4.45	0.29	6.1	3.7

[a] Initial and residual 2,3-epoxypropyl and 2,3-dihydroxypropyl groups which are released as glycerol upon opening of the epoxy ring followed by ester bond reduction.

[b] Difference between the reactive sites of the parent monolith and the non-functionalized sites of the functionalized monolith.

6.3.4. Capillary monoliths versus bulk material

As commented in the section 6.1, a variety of surface modifications of monoliths which are reported in the literature have been characterized by using bulk probes prepared in large diameter formats rather than in the capillaries. However, as discussed below, bulk monoliths may significantly differ from those prepared in a capillary. Evidence on the different properties of monoliths prepared in rather different formats can be provided by comparing the contents of the accessible 2,3-epoxypropyl and 2,3-dihydroxypropyl groups. The data obtained for the parent and functionalized bulk monoliths (prepared in glass vials) with the same polymerization mixture used for capillaries, are shown in Table 6.1. As observed, for all the monoliths, the joint content of 2,3-

epoxypropyl and 2,3-dihydroxypropyl groups was systematically lower for the bulk polymers than for the corresponding capillary monoliths. However, the percentages of functionalization were approximately the same. The differences in the concentrations of the accessible reactive and unfunctionalized groups should be attributed to the different structure of the bulk polymers with respect to the capillary monoliths. In capillaries, the effect of the polymer attached to the silanized inner wall of the capillary could be to reduce rather than to increase the concentration of the reactive groups of the monoliths, then this wall effect was probably negligible. Then, it can be deduced that, for unknown reasons, the monoliths in capillary formats have a larger accessible area than the monoliths synthetized in larger diameter supports. The differences between the two formats studied in this work were rather constant, reaching to a 25.0 ± 1.3 % area excess for all the monoliths prepared in capillaries (Table 6.1). Finally, the uncertainty of the measurements was somewhat worse for the monoliths prepared in the glass vials than for those prepared in the 100 µm I.D. capillaries (Table 6.1). This latter could be due to a lower reproducibility of the polymerization conditions within the glass vials.

The differences observed between the capillary and bulk monoliths could be due to self-screening of the UV radiation by the polymerization mixture during UV-curing. Since polymerization was performed in opened glass vials, the initiating process probably started faster at the free surface of the mixture than in the underneath liquid. This inhomogeneous distribution of initiating species could give rise to an overall reduction in the rate of polymerization, and probably, monoliths with different porous properties in both supports. However, the question about how a different reaction rate could affect the accessible monolith surface remains. Since globule growing depends on many factors, the answer is probably not simple.

These differences observed in UV initiation using different supports could not be much relevan in the case of thermal initiation. Although differences may arise due to convective movements of the polymerization mixture, which can

easily take place in supports with larger diameters but not in capillaries, the long polymerization times (20-24 h) employed level off such changes in monolithic structures.

6.4. Conclusions

A simple and quick method for the joint determination of 2,3-epoxypropyl and 2,3-dihydroxypropyl groups in poly(GMA-*co*-EDMA) monoliths has been developed. Application of the method to parent and functionalized monoliths provides a measure of the accessible 2,3-epoxypropyl groups and the unfunctionalized groups, respectively. Hence, the functionalization yield can be estimated. Further, evidence has been provided that the monoliths polymerized inside 100 µm I.D. capillaries have a *ca.* 25 % excess of reactive sites with respect to the equivalent monoliths obtained in glass vials, which could seem to be due to self-screening of the UV-radiation. Finally, rather common reagents and widely used instrumentation, as a gas chromatograph with a FID, are required to implement the proposed method. In any case, the method proposed in this work could be also useful to reveal possible differences in monoliths prepared in different supports using different initiating systems (photo, thermal, and chemical initiation).

Acknowledgements

Work supported by Project CTQ2014-52765-R (MINECO of Spain and FEDER funds). E.J.C-C. thanks the MINECO for an FPI grant.

References

[1] Y.Y. Li, H.D. Tolley, M.L. Lee, J. Chromatogr. A 1218 (2011) 1399.

[2] P.Y. Xin, Y. Shen, L. Qi, Talanta 85 (2011) 1180.

[3] H. Aoki, N. Tanaka, T. Kubo, K. Hosoya, J. Polym. Sci. Part A: Polym. Chem. 46 (2008) 4651.

[4] F. Svec, J.M.J. Fréchet, Anal. Chem. 64 (1992) 820.

[5] D. Sykora, F. Svec, J.M.J. Frechet, J. Chromatogr. A 852 (1999) 297.

[6] A. Podgornik, M. Barut, A. Strancar, D. Josic, T. Koloini, Anal. Chem. 72 (2000) 5693.

[7] W. Wieder, C.P. Bisjak, C.W. Huck, R. Bakry, G.K. Bonn, J. Sep. Sci. 29 (2006) 2478.

[8] E.J. Carrasco-Correa, G. Ramis-Ramos, J.M. Herrero-Martínez, J. Chromatogr. A 1298 (2013) 61.

[9] E.J. Carrasco-Correa, G. Ramis-Ramos, J.M. Herrero-Martínez, M. Laemmerhofer, J. Chromatogr. A 1367 (2014) 123.

[10] X. Dong, J. Dong, J. Ou, Y. Zhu, H. Zou, Electrophoresis 27 (2006) 2518.

[11] Y. Xu, Q. Cao, F. Svec, J.M.J. Fréchet, Anal. Chem. 82 (2010) 3352.

[12] M. Wang, J. Xu, X. Zhou, T. Tan, J. Chromatogr. A 1147 (2007) 24.

[13] Y. Ueki, T. Umemura, J. Li, T. Odake, K. Tsunoda, Anal. Chem. 76 (2005) 7007.

[14] B. Preinerstorfer, W. Bicker, W. Lindner, M. Laemmerhofer, J. Chromatogr. A 1044 (2004) 187.

[15] H. Hrudková, F. Svec, J. Kálal, Brit. Polym. J. 9 (1977) 238.

[16] Y. Wen, Y.Q. Feng, J. Chromatogr. A 1160 (2007) 90.

[17] B. Preinerstorfer, W. Lindner, M. Laemmerhofer, Electrophoresis 26 (2005) 2005.

[18] A. Messina, M. Flieger, F. Bachechi, M. Sinibaldi, J. Chromatogr. A 1120 (2006) 69.

[19] A. Messina, M. Sinibaldi, Electrophoresis 28 (2007) 2613.

[20] Y. Tian, C. Zhong, E. Fu, Z. Zeng, J. Chromatogr. A 1216 (2009) 1000.

[21] Y. Li, C. Song, L. Zhang, W. Zhang, H. Fu, Talanta 80 (2010) 1378.

[22] Y. Lv, D. Mei, X. Pan, T. Tan, J. Chromatgr. B, 878 (2010), 2461.

[23] S.D. Chambers, F. Svec, J.M.J. Fréchet, A 1218 (2011) 2546.

[24] E.C. Peters, M. Petro, F. Svec, J.M.J. Fréchet, Anal. Chem. 69 (1997) 3646.

[25] E.C. Peters, M. Petro, F. Svec, J.M.J. Fréchet, Anal. Chem. 70 (1998) 2288.

[26] R.F. Nystrom, W.G. Brown, J. Am. Chem. Soc. 69 (1947) 1197.

Chapter 7. Methacrylate monolithic columns functionalized with epinephrine for capillary electrochromatography applications

Journal of Chromatography A, 1298 (2013) 61–67

Contents lists available at SciVerse ScienceDirect

Journal of Chromatography A

journal homepage: www.elsevier.com/locate/chroma

Methacrylate monolithic columns functionalized with epinephrine for capillary electrochromatography applications☆

Enrique Javier Carrasco-Correa*, Guillermo Ramis-Ramos, José Manuel Herrero-Martínez*

Department of Analytical Chemistry, Faculty of Chemistry, University of Valencia, Dr. Moliner 50, 46100 Burjassot, Valencia, Spain

Epinephrine-bonded polymeric monoliths for CEC were developed by nucleophilic substitution reaction of epoxide groups of poly(GMA-*co*-EDMA) monoliths using epinephrine as nucleophilic reagent. Monolith functionalization was achieved in dynamic conditions. Bonding of epinephrine to the monolith surface was completed after passing a 10 mM epinephrine solution of pH 8.0 at 60 ºC for 120 min. Successful chemical modification of the monolith surface was ascertained by *in situ* Raman spectroscopy characterization. In addition, the amount of epinephrine groups that was bound to the monolith surface was evaluated by oxidation of the catechol groups with Ce(IV), followed by spectrophotometric measurement of unreacted Ce(IV). About 9% of the all theoretical epoxide groups of the parent monolith were bonded to epinephrine. The chromatographic behavior of the epinephrine-bonded monolith in CEC conditions was assessed with test mixtures of alkyl benzenes, aniline derivatives and substituted phenols. In comparison to the unfunctionalized poly(GMA-*co*-EDMA) monoliths, the epinephrine-bonded monoliths exhibited a much higher retention of non-polar and polar analytes, and a different selectivity. The epinephrine-bonded monolith was further modified by oxidation with a Ce(IV) solution. In comparison to the epinephrine-bonded monoliths, the resulting epinephrine-quinone-bonded monoliths showed a slightly higher retention of most test solutes, and a different selectivity. Reproducibility of the functionalized monoliths was better than 9% RSD.

Keywords: epinephrine-bonded monolith; epinephrine-quinone-bonded surface modification; monolithic columns; capillary electrochromatography

7.1. Introduction

The development of monolithic separation media in CEC and related techniques, initiated two decades ago is still attracting considerable interest [1-3]. Within the two main types of monolithic materials, the advantages of polymer-based over silica-based monoliths are a simpler and faster preparation, greater choices of surface functionalities, wider pH stability, and better biocompatibility. A variety of organic polymer-based monoliths based on polymethacrylate [4-5], or polyacrylate [6-7], polyacrylamide [8-9] and polystyrene [10-11] have been extensively investigated. Among them, poly(GMA-*co*-EDMA) monoliths enable straightforward and efficient derivatization at the epoxy group with nucleophilic reagents, by nucleophilic substitution reactions (SN_2) [12-24]. In contrast to the single step copolymerization, post-modifications of the monolith allow the independent tuning of mechanical and flow-through porous properties and surface chemistry of the parent monolith. Functionalization at the epoxy groups of GMA-based monoliths with amines [12-14], amino acids [15], poly(ethylene imine) [16], sodium sulfite [17], sodium hydrogen sulfide [18], sulfuric acid [19] and a variety of chiral reagents [20-24], to provide monoliths with different chromatographic properties (ion-exchange, hydrophobic/hydrophilic, chiral, etc.), have been described. Also, an important limitation in the development of hydrophobic monoliths has been the difficulty to copolymerize hydrophobic monomers with the hydrophilic ionizable monomers required for the generation of EOF in CEC [25]. Within this concern, the multi-step post-polymerization approach provides an excellent way of harmonizing incompatible reagents, including hydrophobic and hydrophilic, low solubility ion-pairs or oxidizers and reducers.

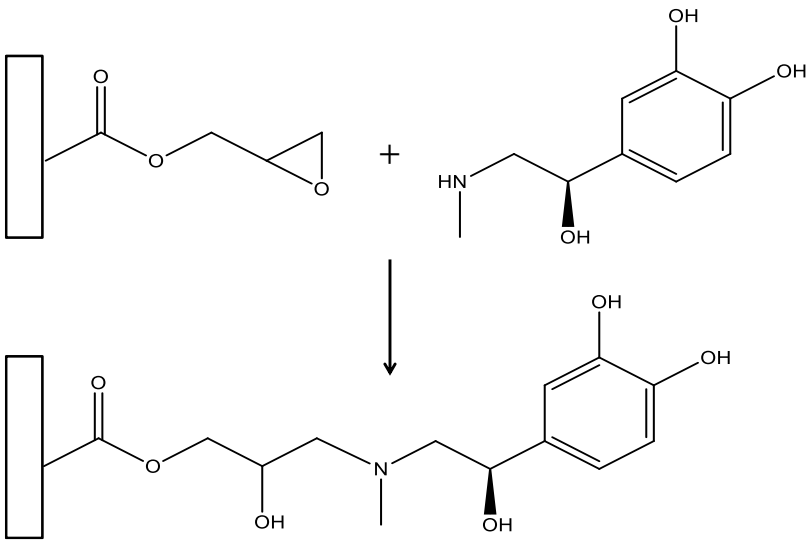

Fig. 7.1. Reaction scheme for the bonding of epinephrine to the surface of the poly(GMA-*co*-epinephrine-*co*-EDMA) monolith.

An important aspect of post-modification of epoxy groups is the evaluation of the yield of the functionalization reaction on the monolith surface, which should provide quantitative information about the amount of ligand bonded to the monolith surface; however, in most cases, this information is not available. To our knowledge, only one report [18] has afforded a procedure to determine the yield of the functionalization reaction of the monolith surface. Thus, the content of thiol groups bonded to a GMA-based monolith was evaluated by using a disulfide exchange reaction with excess dipyridyldisulfide. Bonding of thiol containing reagents to monoliths has been of utmost interest to further attach other chromatographic ligands as gold nanoparticles to the reactive thiol-substrates [26].

In this work, parent monolithic stationary phases based on GMA as reactive monomer and EDMA as crosslinker were functionalized with epinephrine, and the resulting monoliths were characterized for CEC applications. As shown in Fig. 7.1, functionalization with epinephrine adds to the monolith surface an aromatic ionizable catechol group, as well as an amino nitrogen, a chiral carbon atom and an extra hydroxyl. Thus,

hydrophobic/hydrophilic interactions, permanent and π-π induced dipole attraction and hydrogen bonding between this ligand and the analytes could be expected. In addition, bonded epinephrine can be easily oxidized to bonded epinephrine-quinone, which constitutes a simple way of modifying the properties of the stationary phase, including the chromatographic selectivity. The experimental conditions of the functionalization reaction of poly(GMA-*co*-EDMA) with epinephrine (involving epoxide groups opening) were optimized. The epinephrine-bonded monolith was morphologically characterized by SEM and Raman spectroscopy. Also, the concentration of the epinephrine bound to the monolith surface was determined by redox reaction between the catechol groups and Ce(IV), followed by spectrophotometric monitoring of the remaining Ce(IV). A Ce(IV) solution was also used to convert the bonded epinephrine to bonded epinephrine-quinone, giving rise to a monolith with different retention properties. The CEC performance of the epinephrine-bonded and epinephrine-quinone-bonded monolithic columns was evaluated by studying the separation of uncharged (alkyl benzenes) and ionizable (anilines and phenols) solutes. The modified monoliths were compared to the parent monolith. The run-to-run and column-to-column reproducibilities were also evaluated.

7.2. Materials and methods

7.2.1. Chemicals and other materials

GMA, EDMA, META (75% in water), γ-MPS, epinephrine, sodium tetraborate decahydrate and cerium(IV) ammonium nitrate were from Aldrich (Milwaukee, WI, USA). CYC, DOD, 1-PrOH, HPLC-grade ACN and MeOH were from Scharlau (Barcelona, Spain). AIBN and tris(hydroxymethyl)aminoethane (Tris) were from Fluka (Buchs, Switzerland). Thiourea as EOF marker, and several alkyl benzenes, anilines and phenols from Riedel-de Haën (Seelze, Germany), were used. Hydrochloric acid (37%) was

supplied by Panreac (Barcelona). Unless otherwise stated, other chemicals used were of analytical grade. Deionized water was obtained with a Barnstead deionizer (Sybron, Boston, MA, USA). Stock solutions of alkyl benzenes, anilines, phenols and thiourea prepared in ACN at 1 mg mL^{-1} each were kept at 4 ºC until use. Test mixtures of these solutions (100 µg mL^{-1} each analyte and thiourea) were prepared daily by dilution with the mobile phase.

Uncoated fused-silica capillaries of 33.5 cm total capillary length and 375 µm O.D. x 100 µm I.D with UV-transparent external coating (Polymicro Technologies, Phoenix, AZ, USA) were used. The effective monolithic bed length was 8.5 cm.

7.2.2. Instrumentation

An irradiation chamber (model CL1000) from UVP (Upland, CA, USA), equipped with UV lamps (5 × 8 W, 254 nm), was used to photo-initiate the polymerization. Conditioning steps and functionalization of the monolithic columns were achieved with an HPLC pump (1100 series, Agilent technologies). SEM images were taken with a scanning electron microscope (S-4100, Hitachi, Ibaraki, Japan) provided with a field emission gun, a back secondary electron detector and an EMIP 3.0 image data acquisition system (Rontec, Normanton, UK). Raman spectra were obtained with an "in viva" Renishaw spectrometer (Renishaw, Gloucestershire, UK) equipped with a Renishaw HPNIR laser (15 mW at 785 nm) and an Olympus microscope (Olympus, Hamburg, Germany). The absorbance of Ce(IV) solutions was measured with a model 8453 UV-VIS spectrophotometer (Agilent Technologies, Waldbrom, Germany) provided with a 1 cm optical-path quartz cell (Hellma, Müllheim, Germany). CEC experiments were performed on a HP^{3D}CE instrument (Agilent) equipped with a diode array UV detector, and pressurized at both capillary ends with an external nitrogen supply. Data acquisition was performed with the ChemStation Software (Rev.A.10.01,

Agilent). All mobile phases for CEC were degassed by ultrasonication.

7.2.3. Preparation of poly(GMA-co-EDMA) monolithic columns

Prior to the preparation of the columns, and in order to ensure covalent attachment of the monolith to the inner wall of the fused-silica capillaries, surface modification wit γ-MPS was performed as described [27, 28]. Monoliths were prepared from polymerization mixtures obtained by weighing GMA (20 wt%) EDMA (5 wt%), and a binary pore-forming solvent constituted by CYC (70 wt%) and DOD (5 wt%). AIBN (1 wt% with respect to the monomers) was added as polymerization initiator. After mixing and to obtain a clear solution, sonication for 10 min followed by purging with nitrogen for 10 more min was applied. The preconditioned capillary was filled with the mixture up to a length of 8.5 cm. Photo-polymerization was accomplished by irradiation of the capillaries within the UV irradiation chamber at 0.9 J/cm^2 for 30 min. After UV polymerization an HPLC pump was used to flush the columns for 30 min with MeOH to remove the pore-forming solvents and possible unreacted monomers.

7.2.4. Functionalization of poly(GMA-co-EDMA) with epinephrine

The reaction scheme of poly(GMA-*co*-EDMA) functionalization with epinephrine is given in Fig. 7.1. Chemical modification of the poly(GMA-*co*-EDMA) surface was performed under dynamic conditions, by flushing the capillary with continuous stream of derivatizing solution. For this purpose, the capillaries, placed in a thermostated water bath were allowed to react with a solution of epinephrine (10 mM in 100 mM sodium tetraborate at pH 8.0 at 60 ºC) for 2 h at a flow-rate of 4.0 μL min^{-1}. Then, the functionalized monoliths were flushed with MeOH for 30 min in order to remove the unreacted epinephrine, followed by mobile phase for 60 more min. An unfunctionalized

poly(GMA-*co*-EDMA) column (parent monolith) was also flushed with MeOH for 30 min followed by mobile phase for 60 min before injection of the test solutes.

7.2.5. Evaluation of the bonding of epinephrine on the monolith surface

For the determination of the amount of bonded epinephrine molecules bound to the monolith surface, the capillaries were flushed with a 2 mM Ce(IV) solution using a HPLC pump at flow rate of 4 μL min^{-1}. Several fractions (1 mL each) were collected at increasing time values along 12 h, and the unreacted Ce(IV) present in each fraction was spectrophotometrically measured at 320 nm. The scheme of the redox reaction, where bonded epinephrine is oxidated to bonded epinephrine-quinone is depicted in Fig 7.2. For comparison, an unfunctionalized monolith was also flushed with the Ce(IV) solution. The number of mols of Ce(IV) consumed in oxidizing the catechol group of bonded epinephrine was calculated as the difference between the total number of mols of Ce(IV) (initial mols present in absence of reaction) and those found in each collected fraction. For this purpose, calibration curves of Ce(IV) were constructed by measuring six standard solutions within 0.05-0.3 mM range. Straight lines with $r > 0.998$ were obtained. On the basis of the stoichiometry of the reaction, the content of epinephrine bound to the surface monolith was calculated. The chromatographic properties of the resulting epinephrine-quinone-bonded monoliths were also evaluated by injecting the test solutes.

7.2.6. CEC procedures

The monolithic column, placed in the CEC instrument, was equilibrated with the mobile phase by progressively increasing the applied voltage from 5 kV to 10 kV, until a constant current and a stable baseline were achieved.

Separations were performed at 25 ºC (at several voltages). In all cases, the inlet and outlet vials were pressurized at 1 MPa with nitrogen. The test mixtures were injected electrokinetically under 5 kV for 3 s. Detection was performed at 214 and 254 nm. Specific separation conditions for all mixtures are indicated in the figure captions.

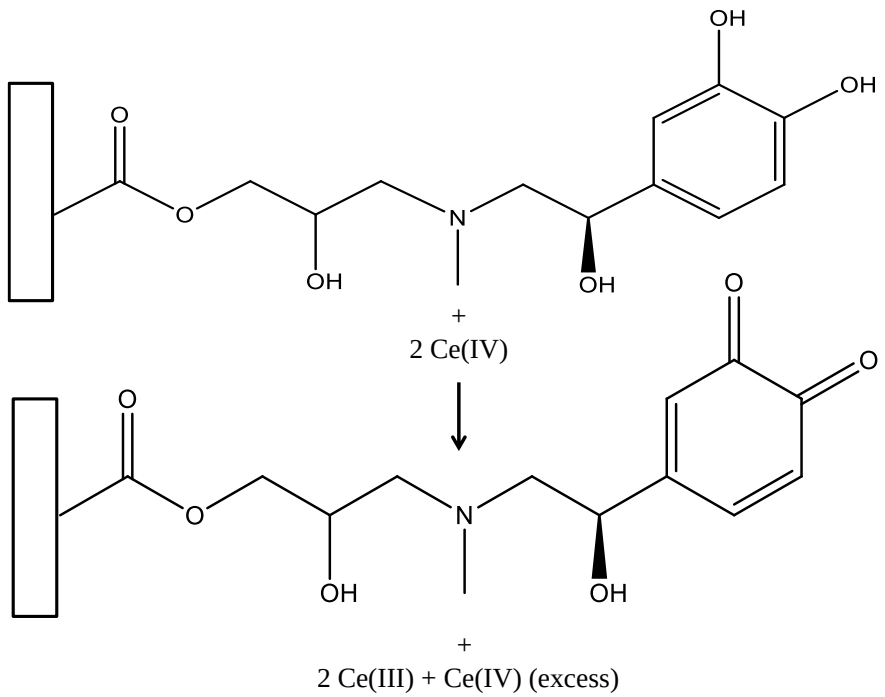

Fig. 7.2. Reaction scheme for the evaluation of the amount of bonded epinephrine on the monolith and oxidation of bonded epinephrine to bonded epinephrine-quinone with Ce(IV).

7.3. Results and discussion

7.3.1. Preparation of epinephrine-bonded monolithic stationary phases

The conditions to prepare photo-polymerized GMA-based monoliths were adapted from a previous work, where CEC columns were thermally polymerized using AIBN as initiator [15]. The selected composition of the

polymerization mixture was 20 wt% GMA as reactive monomer, 5 wt% EDMA as crosslinker, 70 wt% CYC and 5 wt% DOD. The resulting poly(GMA-*co*-EDMA) monolith (parent monolith) provided a sufficiently large number of reactive epoxide groups jointly with a high permeability. Afterwards, the opening of the epoxide groups of the monolith surface with epinephrine was investigated. For this purpose, the reaction conditions that favored the bimolecular nucleophilic substitution (SN_2) reaction of the epoxide ring opening with the secondary amine group of epinephrine, and concomitantly minimize the competitive hydrolysis (ring opening of epoxide with hydroxyl ions), were optimized. After the reaction, epinephrine becomes attached to the polymer surface through a tertiary amino nitrogen. This group is close to two -OH groups, which reduces the expected pK_a value for a tertiary amine; in fact, a pK_a value of 7.6 was predicted [29].

Several authors [15, 18] have found that the hydrolytic epoxide ring-opening side reactions prevail at pH > 8.0. Consequently, pH 8.0 was selected for further studies. In this work, immobilization of epinephrine was procured in dynamic conditions. For this purpose, the concentration of epinephrine and the flow rate were kept constant, at 10 mM and 4 µL min^{-1}, respectively, and both temperature and reaction time were optimized. The separation of a mixture of alkyl benzenes on a series of monolithic columns derivatized at increasing reaction temperatures is shown in Fig. 7.3A. These columns were obtained by flushing the epinephrine solution for 2 h. As observed, the retention of the alkyl benzenes increased from 25 ºC to 60 ºC, higher temperatures leading to a retention decrease. A possible explanation is that the hydroxyl attack to the epoxide group is kinetically favored over the attack of the amino group of epinephrine at temperatures over 60 ºC. Similar findings have been described in the literature by Preinerstorfer *et al.* [18]. The retention times of alkyl benzenes obtained with monolithic columns which were derivatized at 60 ºC using increasing reaction times, are shown in Fig. 7.3B. As observed, a plateau is reached after 2 h. This suggests the saturation of all accessible epoxide groups

with epinephrine. Then, a reaction time of 2 h was selected for the studies that followed. Thus, the optimal conditions for the epinephrine immobilization on GMA-based monoliths were: 10 mM epinephrine, 100 mM sodium tetraborate (pH 8.0) at 60 ºC for 2 h at 4 µL min^{-1}.

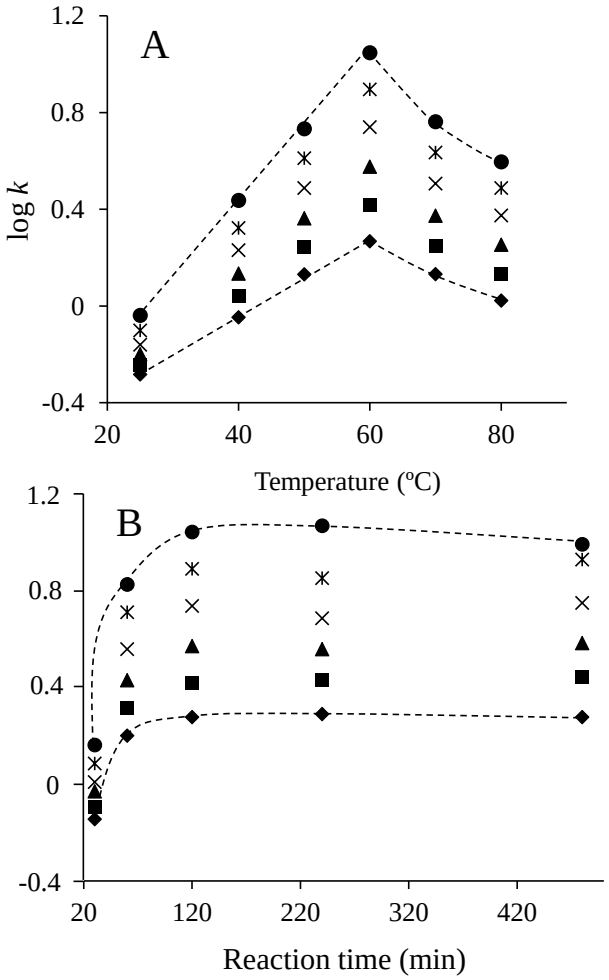

Fig. 7.3. Influence of (A) temperature and (B) reaction time on the functionalization of the monoliths with epinephrine. Retention times of the following test alkyl benzenes on the functionalization monoliths: (♦) toluene, (■) ethyl benzene, (▲) propyl benzene, (✕) butyl benzene, (✳) pentyl benzene and (●) hexyl benzene.

7.3.2. Characterization of epinephrine-bonded monolithic stationary phases

To characterize the epinephrine functionalized GMA-based monoliths, SEM images were first taken. A representative image is given in Fig. 7.4. No significant differences in monolith structures, i.e. the macropore and globule size morphology, between the functionalized and unfunctionalized (parent) monoliths were observed. Then, Raman spectroscopy was employed to probe the surface of the monoliths. Raman spectra were recorded directly on the monolith within the confines of the fused-silica capillaries (Fig. 7.5). Two bands in the epinephrine-bonded monoliths (Fig. 7.5B) which were absent in the unfunctionalized monoliths (Fig. 7.5, trace A) were observed. These two bands were attributed to stretch of the $C=N^+$ double bond (*ca.*1400-1500 cm^{-1}) and aromatic C=C double bond (*ca.* 1640-1660 cm^{-1}) [30, 31]. This provided further evidence regarding to the surface functionalization of the monoliths by epinephrine.

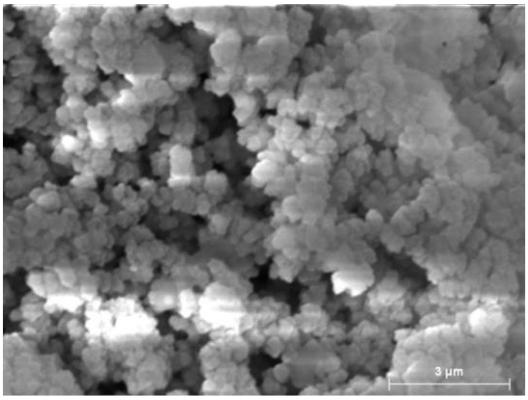

Fig. 7.4. SEM micrograph of epinephrine-bonded monolith.

Since the control of the yield of the surface functionalization reaction is of particular importance, it is desirable to determine the amount of epinephrine groups bound to the monolith surface. This was established by redox reaction of the phenolic groups of bonded epinephrine with Ce(IV) (see Fig. 7.2). This reaction is specific to catechols which are quantitatively oxidized to quinones

[32, 33]. Thus, as indicated in Section 7.2.5, the epinephrine-bonded monolith was flushed with a 2 mM Ce(IV) solution, and fractions were collected and measured spectrophotometrically. Successive fractions showed growing Ce(IV) concentrations, 2 mM being finally reached after more than 10 h. The number of mols of Ce(IV) required to quantitatively oxidize the catechol groups of bonded epinephrine was calculated as the difference between the number of mols of Ce(IV) (initial concentration present in absence of reaction, 2 mM) and those found in the collected fractions. Taking into account the stoichiometry relationship between Ce(IV) and epinephrine reaction (see Fig. 7.2), the amount of bonded epinephrine is easily derived. To check whether the Ce(IV) also attacks other sites of the monolith surface, (e.g., residual epoxy groups or the resulting glycol groups), an unfunctionalized monolith was also flushed with Ce(IV) solution. With this monolith, the number of mols of Ce(IV) consumed was rather small (two orders of magnitude lower than that found for epinephrine-bonded monoliths). Consequently, a blank correction was not made in the evaluation of the amount of bonded epinephrine groups.

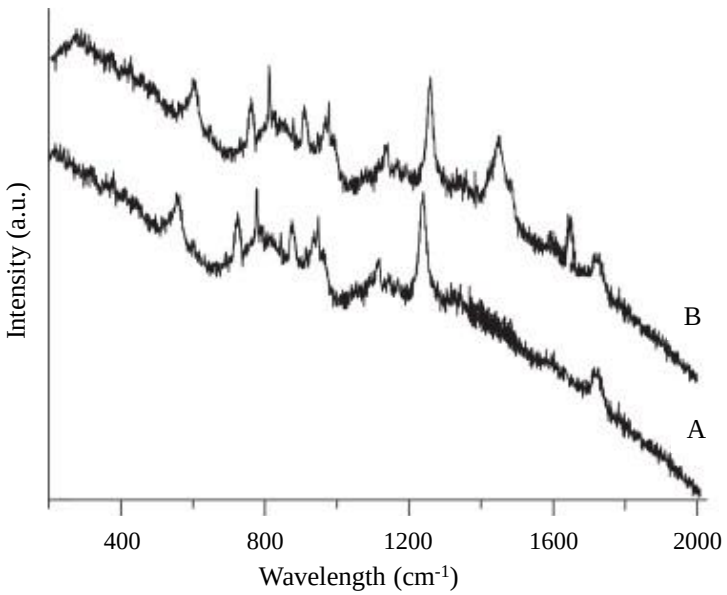

Fig. 7.5. Raman spectra for monolithic stationary phases. (A) parent monolith and (B) epinephrine-bonded monolith.

Thus, the surface coverage with epinephrine groups in the 8.5 cm long monolithic capillary columns of 100 µm i.d was *ca.* 0.08 ± 0.01 µmol (n = 3), which corresponds to about 0.5 mmol of bonded groups per gram of monolithic polymer. To calculate the percentage of epinephrine-bonded groups in the polymer, the total number epoxide groups in the whole polymer was theoretically calculated obtained by assuming a complete incorporation of the GMA into the polymer, and taking into account the density of the reaction mixture in the monolithic capillary column [18, 34]. As a molar fraction, the polymer turned out to have about 9% of all theoretical epoxide groups of the parent monolith bound to epinephrine molecules. It can be assumed that the other 91% of the epoxide groups are located inside micropores not accessible to the derivatizing epinephrine solution or well inside the bulk polymer matrix. These buried groups are not likely to participate in the functionalization process. As far as we know, there is no any method providing a description of the distribution of active surface groups in the open surface of the monoliths, and in pores of decreasing sizes, as well as within the bulk polymer matrix. If available, such a description would be of much interest to know at which limit of the pore diameter would corresponds a 9 % of the epoxidic groups.

The generation of EOF after chemical surface functionalization of GMA monolith with epinephrine was also studied. The presence of ionizable groups in epinephrine such as the tertiary amine (pK_a 7.6 [29]) or the catechol groups (pK_as 9.3 and 9.5 [29]) should be the responsible of EOF generation. Further, a dependence of the EOF with the pH of the mobile phase should be expected. Indeed, the absolute value of the anodic EOF decreased continuously from 3.3 $\times 10^{-8}$ m^2 V^{-1} s^{-1} at pH 2 to 1.8 $\times 10^{-8}$ m^2 V^{-1} s^{-1} at pH 10. Owing to the presence of the positively charged amino groups (with pK_a 7.6 [29], a decreasing anionic EOF was effectively expected at increasing pH values up to *ca.* 9.6, where only a 1% of the amino groups remained ionized. At the same time, deprotonation of catechol should be effective above pH 7.0. This should lead to the EOF suppression at same pH between 7.6 and 9.0 to be converted to a cationic EOF

over this range. Instead of this, a weak anionic EOF still remained at pH 10. However, no explanation was found for this anionic EOF.

7.3.3. Evaluation of chromatographic properties of the epinephrine-bonded monolithic stationary phase

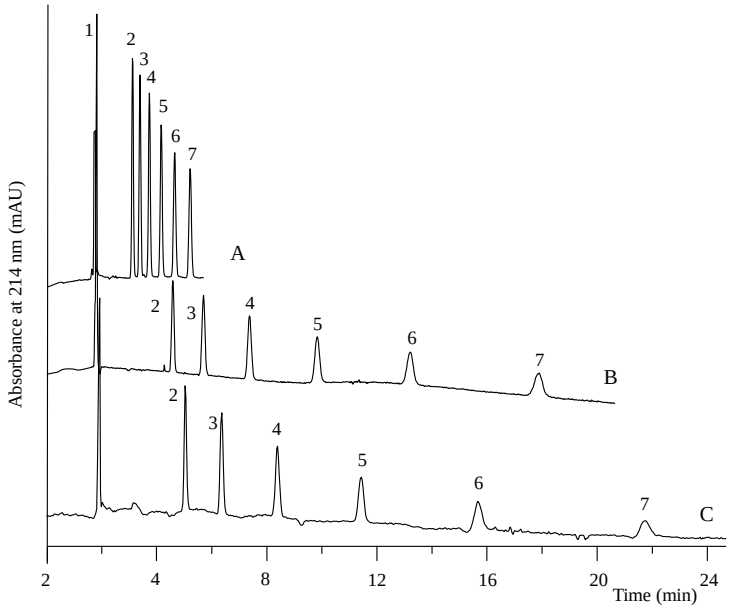

Fig. 7.6. Separation of alkyl benzenes on the (A) parent monolith, (B) epinephrine-bonded and (C) epinephrine-quinone bonded monolith. CEC conditions: mobile phase, 50:50 (v/v) ACN-water containing 5 mM acetate/acetic acid buffer of pH 3.0; electrokinetic injection, 5 kV for 3 s; separation voltage, 10 kV. Peak identification: (1) thiourea; (2) toluene, (3) ethyl benzene, (4) propyl benzene, (5) butyl benzene, (6) pentyl benzene and (7) hexyl benzene.

In order to test the chromatographic properties of poly(GMA-*co*-EDMA) monolith functionalized with epinephrine, the separation of mixtures of uncharged and ionizable solutes was investigated. For comparison, the test solutes were also chromatographied on the unfunctionalized monolith. To generate a similar EOF than that found in the epinephrine-bonded monolith, a

small amount of the cationic ionizable monomer META was added to the polymerization mixture of the unfunctionalized monolith. Separations were performed using hydro-organic mobile phases containing different ACN concentrations at varying pH values ($3 \leq pH \leq 10$).

A separation of alkyl benzenes using both the unfunctionalized and the epinephrine-bonded monolithic columns under the same CEC conditions (50% ACN and pH 3), is shown in Fig. 7.6. In both monoliths, alkyl benzenes were eluted in the order of increasing hydrophobicity; however, a large increase in retention was evidenced in the epinephrine-bonded monolithic column (Fig. 7.6B). This could be due to a combination of stronger hydrophobic interactions and induced dipole π-π attraction between bonded epinephrine and the analytes. Also, the efficiencies of both columns were evaluated by obtaining van Deemter curves for all the alkyl benzenes. Minimum plate heights comprised between 4.0–5.1 µm (at optimum *u*-values 0.58–0.62 mm/s) and 3.1–5.5 µm (*u*-values 0.65–0.73 mm/s) were obtained for the unfunctionalized and epinephrine-bonded monoliths, respectively. Thus, efficiency was essentially the same for the two column classes.

The separation of basic analytes (anilines) by CEC using both the unfunctionalized and epinephrine functionalized monoliths under the same conditions (50% ACN and pH 10), are compared in Fig. 7.7. At pH 10, the aniline derivatives are not charged and their retention should presumably result from hydrophobic, dipolar and acid-base interactions with the stationary phase. In the parent monolith (Fig. 7.7A), the anilines eluted in the order of increasing hydrophobicity. By plotting log k against log $P_{o/w}$ (1-octanol/water hydrophobicity coefficient) a straight-line with remarkable linearity ($r = 0.991$) was obtained. This suggests the presence of hydrophobic interactions between the analytes and the polymer skeleton. Experiments made at increasing ACN concentrations (chromatograms not shown) confirmed this behavior. For the epinephrine-bonded monolith, a higher retention of the aniline derivatives was observed (Fig. 7.7B).

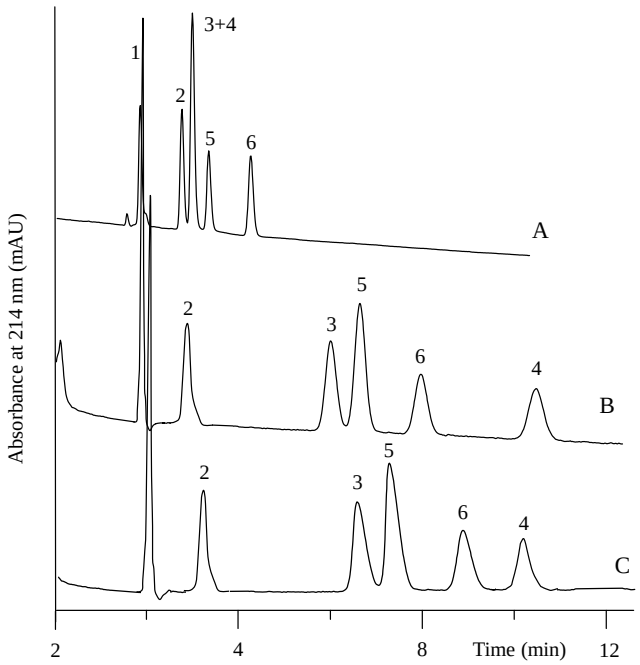

Fig. 7.7. Separation of anilines on the (A) parent monolith, (B) epinephrine-bonded and (C) epinephrine-quinone bonded monolith. CEC conditions as in Fig. 8.6, but using a 5 mM Tris buffer of pH 10.0. Peak identification: (1) thiourea; (2) pyridine, (3) aniline, (4) 4-nitroaniline, (5) 2,4,6-trimethylaniline and (6) N,N-diethylaniline.

The retention increase was small for pyridine but large for the other analytes. This indicates a strong interaction of the non-charged and anilines with the bonded epinephrine, which was attributed to induced π-π interactions. With the exception of p-nitroaniline which showed a rather high retention, the other analytes eluted in the order of increasing hydrophobicity (consistent with the log k - log $P_{o/w}$ plot). This reveals that hydrophobic interactions also contributed significantly to retention on the functionalized monolith. The low retention of pyridine could be explained by its low π-electron density due to the presence of the electronegative nitrogen in the ring; consequently, π-π interactions with bonded epinephrine were probably weaker than expected for a phenyl group. The behavior of 4-nitroaniline should be explained by the presence of the strongly polar nitro group, capable of strongly interacting with the catechol group. Thus, the epinephrine-bonded monolith showed a

remarkably large dipolar character, which makes it particularly adequate to separate strongly polar and polarizable analytes. As next discussed, this was confirmed by injecting a mixture of phenol derivatives.

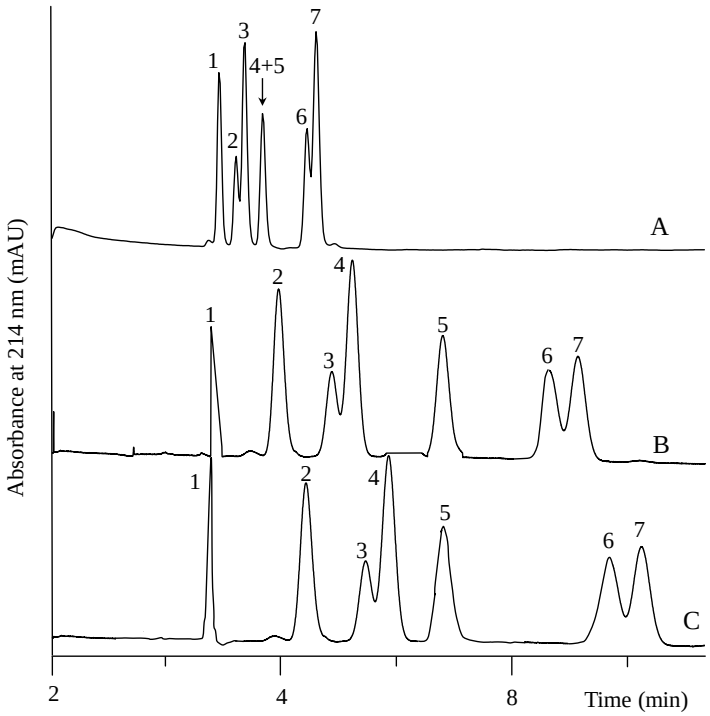

Fig. 7.8. Separation of phenols on the (A) parent monolith, (B) epinephrine-bonded and (C) epinephrine-quinone bonded monolith. CEC conditions: as in Fig. 7.6. Peak identification: (1) thiourea; (2) hydroquinone, (3) resorcinol, (4) catechol, (5) 4-nitrophenol, (6) o-cresol and (7) 2,4-dimethylphenol.

A separation of phenol derivatives is shown in Fig. 7.8 (50% ACN and pH 3). As observed, the phenol derivatives showed also a much higher retention on the epinephrine-bonded monolith than on the unfunctionalized monolith, whereas the elution order was the same. Thus for both monolith classes, retention of the three diphenols followed the order of increasing hydrophobicity: hydroquinone < resorcinol < catechol (peaks 2, 3 and 4, respectively in Fig. 7.8), retention of resorcinol and catechol being particularly large for the functionalized monolith. Retention of 4-nitrophenol (peak 5 of Fig.

7.8) also increased largely, revealing the importance of the interactions between the permanent dipoles of the nitro groups and the epinephrine catechol group. Finally, the large retention of the two phenols with methyl substituents (peaks 5 and 6 in Fig. 7.8) also indicated the large contributions of the hydrophobic interactions with the surface of the functionalized monolith.

As mentioned, the bonded epinephrine groups were further modified by oxidation to bonded epinephrine-quinone groups with Ce(IV). In this way, a column with a different surface functionality was easily generated. A separation of alkyl benzenes on an epinephrine-quinone-bonded monolith, obtained in the same conditions as in Figs. 7.6A and 7.6B, is shown in Fig. 7.6C. This column showed a slightly higher retention than that obtained with a non-oxidized epinephrine-bonded monolith (Fig. 7.6B). Retention of alkyl benzenes is produced both by hydrophobic interactions and via induced dipolar π-π interactions. Thus, the sum of the interactions of these two types increased only slightly by oxidizing the catechol group to a quinone group. Similarly, separations of the aniline derivatives and phenol derivatives on the epinephrine-quinone bonded column are shown in Figs. 7.7C and 7.8C, respectively. With respect to the chromatograms of Figs. 7.7B and 7.8B, which were obtained in the same working conditions, the chromatograms of Figs. 7.7C and 7.8C showed a slight increase in retention times. However, of much interest is the different selectivity. Thus, by comparing Figs. 7.7B and 7.7C, and 7.8B and 7.8C, retention of 4-nitroaniline and 4-nitrophenol decreased slightly or was the same by substituting the epinephrine-bonded monolith by the epinephrine-quinone-bonded monolith. Thus, the two functionalized monoliths showed a different selectivity, as well as a remarkably large dipolar character, which makes them particularly adequate to separate strongly polar and polarizable analytes.

A critical factor in column surface functionalization schemes is known to be the column-to-column reproducibility. Thus, the reproducibility of columns obtained with the optimized functionalization protocol was examined. For this

purpose, several CEC parameters, as well as the amount of epinephrine groups bonded to the surface monolith, were evaluated. The run-to-run repeatability was evaluated from series of six injections of the alkyl benzene test mixture at 10 kV performed on the unfunctionalized and functionalized columns of the two classes, while the column-to-column reproducibility was estimated by preparing three monoliths which were subjected to the optimal functionalization protocol with epinephrine both without and with further oxidation with Ce(IV). As observed in Table 7.1, for the tested parameters, satisfactory RSD values (below 9%) were obtained.

Table 7.1. CEC and functionalization properties of epinephrine-bonded monolith.

Parameter	Repeatability	Reproducibility	
	Run-to-run column (n = 6)	Day-to-day column (n = 6, 3 days)	Column-to-column (n = 3))
	RSD, %	RSD, %	RSD, %
t_{EOF} (min)	1.3	2.0	6.1
$k_{propylbenzene}$	1.5	2.5	6.4
H_{min} (μm)	2.6	4.4	7.6
mmol epinephrine/g monolith	-	-	8.4

7.4. Conclusions

An epinephrine-bonded monolithic stationary phase for CEC was prepared by a two-step procedure involving the synthesis of GMA-based monolith and subsequent on-column chemical modification by ring opening reaction of epoxide groups with epinephrine as nucleophilic ligand. The surface modification was demonstrated by Raman spectra of the resulting monoliths. Also, the amount of epinephrine molecules bound to the monolith surface was directly determined on the capillary columns by oxidation and spectrophotometric monitoring of the consumed Ce(IV). Bonded epinephrine was also oxidized to bonded epinephrine-quinone which yielded monoliths with a different functionality. These two functionalizated monoliths exhibited an increase retention of alkyl benzenes (alt: increase retention on alkyl benzenes), indicating and enhancement of hydrophobic interactions and π-π induced dipole attraction. Retention also increased remarkably for polar ionizable solutes having a variety of functional groups. In addition, oxidation of bonded epinephrine to bonded epinephrine-quinone provides a polar column with a different selectivity. Finally, the functionalized monolithic stationary phases exhibited a good reproducibility in column preparation (including the amount of bonded epinephrine) and chromatographic properties.

Acknowledgements

Work supported by Project CTQ2010-15335 (MINECO of Spain and FEDER funds). E.J.C-C. thanks the MINECO for an FPI grant. The authors would like to thank Patricia Concepción-Heydorn for performing the Raman experiments.

References

[1] F. Svec, J. Sep. Sci. 729 (2005) 28.

[2] M. R. Buchmeiser, Polymer 2187 (2007) 48.

[3] N. Smith, Z. Jiang, J. Chromatogr. A 416 (2008) 1184.

[4] V. Bernabé-Zafón, A. Cantó-Mirapeix, E.F. Simó-Alfonso, G. Ramis-Ramos, J. M. Herrero-Martínez, Electrophoresis 1929 (2009) 30.

[5] A. Cantó-Mirapeix, J. M. Herrero-Martínez, C. Mongay-Fernández, E. F. Simó-Alfonso, Electrophoresis 607 (2009) 30.

[6] A. Cantó-Mirapeix, J. M. Herrero-Martínez, C. Mongay-Fernández, E. F. Simó-Alfonso, Electrophoresis 3858 (2008) 29.

[7] A. Cantó-Mirapeix, J. M. Herrero-Martínez, C. Mongay-Fernández, E. F. Simó-Alfonso, Electrophoresis 599 (2009) 30.

[8] X. L. Dong, R. Wu, J. Dong, M. H. Wu, Y. Zhu, H. F. Zou, Electrophoresis 29 (2008) 919.

[9] V. Agustin, A. Jardy, P. Gareil, M.-C. Hennuin, J. Chromatogr. A 1119 (2006) 80.

[10] M. Petro, F. Svec, J. M. Fréchet, J. Chromatogr. A 752 (1996) 59.

[11] I. Gusev, C. Horváth, J. Chromatogr. A 948 (2002) 203.

[12] V. Frankovič, A. Podgornik, N. L. Krajnc, F. Smrekar, P. Krajnc, A. Štrancar, J. Chromatogr. A 1207 (2008) 84.

[13] W. Wieder, C. P. Bisjak, C. W. Huck, R. barky, G. K. Bonn, J. Sep. Sci. 29 (2006) 2478.

[14] G. Yang, H. Liu, Y. Zhang, S. Wang, J. Yin, B. Yin, Y. Chen, J. Chromatogr. A 1129 (2006) 231.

[15] X. Dong, J. Dong, J. Ou, Y. Zhu, H. Zou, Electrophoresis 27 (2006) 2518.

[16] M. wang, J. Xu, X. Zhou, T. Tan, J. Chromatogr. A 1147 (2007) 24.

[17] Y. Ueki, T. Umemura, J. Li, T. Odake, K. Tsunoda, Anal. Chem. 76 (2005) 7007.

[18] B. Preinerstorfer, W. Bicker, W. Lindner, M. Laemmerhofer, J. Chromatogr. A 1044 (2004) 187.

[19] Y. Wen, Y. Q. Feng, J. Chromatogr. A 1160 (2007) 90.

[20] A. Messina, M. Flieger, F. Bachechi, M. Sinibaldi, J. Chromatogr. A 1120 (2006) 69.

[21] B. Preinerstorfer, W. Lindner, M. Laemmerhofer, Electrophoresis 26 (2005) 2005.

[22] A. Messina, M. Sinibaldi, Electrophoresis 28 (2007) 2613.

[23] Y. Li, C. Song, L. Zhang, W. Zhang, H. Fu, Talanta 80 (2010) 1378.

[24] Y. Tian, C. Zhong, E. Fu, Z. Zeng, J. Chromatogr. A 1216 (2009) 1000.

[25] M. Guerrouache, M. C. millot, B. Carbonnier, J. Sep. Sci. 34 (2011) 2271.

[26] Y. Lv, F. Maya-Alejandro, J. M. J. Fréchet, F. Svec, J. Chromatogr. A 1261 (2012) 121.

[27] Peters, E. C., Petro, M., Svec, F., Fréchet, J. M. J., Anal. Chem. 1998, 70, 2288.

[28] Peters, E.C., Petros, M., Svec, F., Fréchet, J.M., Anal. Chem. 1997, 69, 3646.

[29] Sparc: http://archemcalc.com/sparc/

[30] M. D. morris, Anal. Chem. 47 (1975) 2453.

[31] W. J. Barreto, S. Ponzoni, P. Sassi, Spectrochim. Acta A 55 (1999) 65.

[32] W. R. Spencer, F. R. Duke, Anal. Chem. 26 (1954) 919.

[33] D. Ozyurt, B. Demirata, R. Apak, Talanta 71 (2007) 1155.

[34] Q. Cao, Y. Xu, F. Liu, F. Svec, J. M. J. Fréchet, Anal. Chem. 82 (2010) 7416.

Chapter 8. Phosphatidylcholine covalently linked to a methacrylate-based monolith as a biomimetic phase for capillary liquid chromatography

Journal of Chromatography A, XXXX (2015) XX-XX

Contents lists available at SciVerse ScienceDirect

Journal of Chromatography A [1]

journal homepage: www.elsevier.com/locate/chroma

Phosphatidylcholine covalently linked to a methacrylate-based monolith as a biomimetic stationary phase for capillary liquid chromatography

Dana Moravcová[a,*,#], Enrique Javier Carrasco-Correa[b,#], Josef Planeta[a], Michael Lämmerhofer[c], Susanne K. Wiedmer[d,*]

[a]Institute of Analytical Chemistry of the ASCR, v. v. i., Veveří 97, 60200 Brno, Czech Republic
[b]Department of Analytical Chemistry, University of Valencia, Dr. Moliner 50, 46100 Burjassot, Valencia, Spain
[c]Institute of Pharmaceutical Sciences, University of Tübingen, Auf der Morgenstelle 8, 72076 Tübingen, Germany
[d]Department of Chemistry, P.O. Box 55, 00014 University of Helsinki, Finland

[1] Accepted
* Corresponding authors
# The authors share first authorship

In this study a strategy to immobilize phospholipids onto a polymer-based stationary phase is described. Methacrylate-based monoliths in capillary format were modified by soybean phosphatidylcholine through 1-ethyl-3-(3-dimethylaminopropyl)carbodiimide coupling to obtain stationary phases suitable to mimic cell surface membranes. The covalent coupling reaction involves the phosphate group in phospholipids; therefore, the described methodology is suitable for all types of phospholipids. Immobilization of soy bean phosphatidylcholine on the monolith was confirmed by attenuated total reflectance (ATR) Fourier transform infrared (IR) spectroscopy and GC-MS of the fatty alcohol profile, generated upon reductive cleavage of the fatty acyl side chains of the phospholipid on the monolith surface with lithium aluminium hydride. The prepared stationary phases were evaluated through studies on the retention of low-molar mass model analytes including neutral, acidic, and basic compounds. Liquid chromatographic studies confirmed predominant hydrophobic interactions between the analytes and the synthesized stationary phase; however, electrostatic interactions contributed to the retention as well. The synthesized columns showed high stability even with fully aqueous mobile phases such as Dulbecco's phosphate-buffered saline solution.

Keywords: ATR-FTIR; capillary LC; analyte-membrane interaction; immobilized artificial membrane; monolithic column; phospholipids.

8.1. Introduction

Predictive models for drug absorption, distribution, excretion, and also metabolic pathways in living organisms are important in the field of drug discovery in pharmaceutical industry and medicine (drug screening). Although the octanol–water partition coefficient ($P_{o/w}$) proposed by Fujita et al. [1] as a model for biological partitioning is widely used and well accepted for evaluating the lipophilicity/hydrophobicity of compounds, there are still efforts to develop other systems providing better insight into biological partitioning processes. For example, the human intestinal Caco-2 cell line is often used as a simple reference model in prediction of cellular permeation of drug candidates [2]. Physico-chemical methods employing analytical separation methodologies based on immobilized (phospho)lipids or (phospho)lipid aggregates, especially capillary electromigration and liquid chromatographic techniques, are also indispensable for rapid screening of drug permeability. Comprehensive outlines of application of these techniques to analyte-membrane interactions studies are included, e.g., in reviews from Wiedmer et al. [3] or from Cserháti et al. [4].

Retention of analytes under the RP-LC conditions similarly as octanol–water partitioning do not consider the ionization of analytes and merely hydrophobicity alone is used for prediction of drug absorption [5]. However, since most drugs are charged at physiological pH values, the use of biomimetic stationary phases may provide better insight into their biological partitioning processes. These biomimetic stationary phases are prepared by modification of silica or soft gel particles such as sepharose. Surface modification can be based on covalent and non-covalent bonding of lipids. Non-covalent bonding methods include coating [6, 7] and hydrophobic binding [8, 9, 10, 11, 12]. The covalently bonded stationary phases possess improved stability over non-covalently bonded ones and cover sorbents such as cholesterol stationary phases [13, 14, 15], alkyl-phosphate stationary phases [16], phosphatidylcholine (PC) stationary phases [17], and sphingomyelin stationary phases [18].

Another approach to the synthesis of phospholipid-modified stationary phases was introduced by Gallagher et al. [19]. They stabilized a phospholipid bilayer containing small unilamellar vesicles (SUVs) on non-porous silica particles by UV- and redox polymerization. SUVs were prepared from a mixture of 1,2-dioleoyl-*sn*-glycero-3-phosphocholine and 1,2-bis[10-(2′,4′-hexadieoyloxy)decanoyl]-*sn*-glycero-2-phosphocholine (a phospholipid containing double bonds in its alkyl chains).

Despite a tremendous progress in synthesis of new LC chromatographic stationary phases, only the ones based on monolayers of phospholipids covalently bonded to aminopropyl silica particles (cf. immobilized artificial membranes, IAM) developed by Ch. Pidgeon [20, 21, 22] are commercially available.

Monolithic stationary phases have gained increased popularity during the last years due to their unique hydrodynamic properties and a wide variety of chemistries available for their synthesis. At present, monolithic polymer-based [23, 24], inorganic oxide-based [25], or hybrid organic-inorganic oxide-based [26] materials are synthesized and evaluated.

There are two fundamentally different ways to manufacture polymer-based monolithic columns with dedicated surface chemistry, namely, one-step in-situ polymerization and post-polymerization surface functionalization. A variety of in-situ prepared monoliths have been described for RP-LC [27], ion-exchange LC [28], and advanced chromatographic modes such as enantioselective [29] and affinity-type [30] separations. Concerning the chromatographic properties, the success of one-step in-situ polymerization strongly depends on a proper choice of both the monomers and the porogenic solvents in the polymerization mixture. Attempts to modify well-known polymerization mixtures by incorporating new monomers require careful re-optimization of the whole polymerization mixture to preserve the pore structure [31].

In contrast to single step copolymerization, post-modifications of the monolith allow the independent tuning of mechanical, flow-through porous properties, and also surface chemistry of the parent monolith. The use of GMA containing an epoxy group is particularly useful for preparing monoliths which can be easily functionalized. Using EDMA as a crosslinker, poly(GMA-*co*-EDMA) monoliths with a highly reactive surface are obtained. Monoliths with a variety of chromatographic properties (ion-exchange, hydrophobic/hydrophilic, chiral, etc.) have been obtained by bonding amines [32], amino acids [29], polymers [33], thiol derivatives [34], and chiral reagents [35] to the parent monolith.

The use of monolithic supports for preparation of chromatographic sorbents suitable for mimicking biological cell membranes is not common. Kuroda et al. [36] modified a silica-based monolithic column by capturing phospholipids (egg phosphatidylcholine and a mixture of 1,2-dimyristoyl-*sn*-glycero-3-phosphocholine and 1,2-dipalmitoyl-*sn*-glycero-3-phosphoserine) through hydrophobic interactions with octadecylsilane (C18) alkyl chains. Zhao et al. [37] prepared phospholipid functionalized capillary monolithic columns by in-situ copolymerization of 12-methacryloyl dodecylphosphatidylcholine, 12-methacryloyl dodecylphosphatidylserine, and ethylene dimethacrylate. The same approach for synthesis of a cholesterol-based polymeric monolithic column was reported by Szumski et al. [38], who used cholesteryl methacrylate as a functional monomer and trimethylolpropane trimethacrylate as a crosslinker in the polymerization mixture.

In our earlier paper we described a procedure for preparation of silica-based monolithic capillary columns covered by spherical unilamellar liposomes, in which immobilization was performed through amino groups via Schiff's base formation [39]. Due to the fact that, in general, secondary and tertiary amino groups do not undergo a Schiff's base reaction, only liposomes with primary amino group were able to react.

In this work we suggest another approach to synthesize biomembrane mimicking stationary phase using soy bean phosphatidylcholine as a model phospholipid. Immobilization was done onto a poly(GMA-*co*-EDMA) monolith. The reaction takes place via 1-ethyl-3-(3-dimethylaminopropyl)carbodiimide (EDC) coupling (a reaction commonly used for protein-conjugation to carboxylic acid linkers, e.g., in the preparation of enzyme reactors [40]), whereby a covalent phosphoramidate bond is created between amino groups present on the stationary phase and the phosphate group of a phospholipid. The developed stationary phases were characterized by ATR-FTIR, GC-MS, and cHPLC, confirming the presence of immobilized phospholipids onto the monolith.

8.2. Experimental part

8.2.1. Chemicals and reagents

ACN LC/MS-grade, alkylbenzenes (C_0-C_6), formic acid, oxalic acid, citric acid, drugs (Table 8.1), lidocaine, imidazole, glutaraldehyde (GA), sodium cyanoborohydride (SCBH), ammonium bifluoride (NH_4HF_2), GMA, EDMA, γ-MPS, $LiAlH_4$, and 1-octadecanol were purchased from Sigma-Aldrich (Vienna, Austria). HPLC-grade MeOH and IPA were from Scharlab (Barcelona, Spain). AIBN and EDC were from Fluka (Buchs, Switzerland). Hexamethylene-1,6-diamine (HMD) was from BASF (Ludwigshafen, Germany). L-α-phosphatidylcholine (PC) extracted from soy bean (hereafter called soyPC) was from Avanti Polar Lipids (Alabaster, AL, USA) and it has the following fatty acid distribution: 14.9 wt% of 16:0; 3.7 wt% of 18:0; 11.4 wt% of 18:1; 63.0 wt% of 18:2; 5.7 wt% of 18:3; 1.2 wt% of unknown lipids. Uncoated fused-silica capillaries 375 µm O.D. × 100 µm I.D. (Polymicro Technologies, Phoenix, AZ, USA) were used for preparation of monolithic columns.

Table 8.1. Physico-chemical parameters of studied compounds.

Compound	Type of compound/drug	Mw	pK_a	log $P_{o/w}$ (pH 7.4)*	log D (pH 7.4)*	Overall charge at pH 7.4
m-nitroaniline (1)	dye	138.12	2.46 ± 0.10	1.37	1.38	neutral
p-nitroaniline (2)	standard chemical	138.12	1.01 ± 0.10	1.39	1.31	neutral
salicylic acid (3)	analgesic/ anti-anflammatory/ antipyretic/keratolytic	138.12	3.01 ± 0.10	2.06	-0.77	negative
p-toluidine (4)	standard chemical	107.15	5.04 ± 0.10	1.40	1.47	neutral
aniline (5)	standard chemical	93.13	4.61 ± 0.10	0.94	1.17	neutral
m-nitrobenzoic acid (6)	standard chemical	167.12	3.48 ± 0.10	1.82	-1.23	negative
phenol (7)	antibacterial/antiinfective agent/antipruritic/disinfectant	94.11	9.86 ± 0.13	1.48	1.63	neutral
benzoic acid (8)	antifungal agent	122.12	4.20 ± 0.10	1.89	-1.00	negative
acetanilide (9)	analgesic/antipyretic	135.16	0.51 ± 0.50	1.08	1.24	neutral
phenazone (10)	analgesic	188.23	0.65 ± 0.65	0.27	0.72	neutral
theophylline (11)	bronchodilator agent/ vasodilator agent	180.16	8.60 ± 0.50; 1.64 ± 0.70	-0.17	0.11	neutral
acetylsalicylic acid (12)	analgesic/anti-inflammatory/antipyretic/ antirheumatic	180.16	3.48 ± 0.10	1.19	-1.69	negative

* The data was calculated using Advanced Chemistry Development (ACD/Labs) Software V11.02 (© 1994-2015 ACD/Labs).

8.2.2. Instrumentation

A syringe pump (Model 100, KD Scientific, New Hope, PA, USA) was employed to introduce the derivatization reagents into the monolithic capillary column. An HPLC pump (1100 series, Agilent Technologies, Waldbronn, Germany) was used for washing the prepared monolithic columns. FTIR was performed with a Jasco 4100 type A spectrophotometer (Jasco, Easton, MD) fitted with a single reflection ATR accessory. Spectra were accomplished from 4000 to 500 cm^{-1} in the absorbance mode at a 2 cm^{-1} resolution with 100 scans.

GC-MS analysis was done on a Focus DSQ II gas chromatograph provided with an AI 3000 autosampler and single quadrupole MS detector from Thermo Fisher Scientific. The analytical fused-capillary column was a TR-5MS (30 m, 0.25 mm I.D., 0.25 µm film thickness) from Thermo Fisher Scientific. The GC oven single ramp temperature program was operated as follows: the initial oven temperature 50ºC was kept for 2 min, the temperature was raised to 250ºC at rate 20ºC min^{-1} and hold at 250ºC for 5 min. The injector, transfer line, and ion source temperatures were set at 280°C. The injection volume was 1 µL under splitless mode. Ionization was done by electron impact at 70 eV. Ions within the *m/z* 50-800 range were monitored. Helium was used as the carrier gas at a flow rate of 1 mL min^{-1}.

The equipment used for HPLC-UV consisted of a syringe pump (100 DM with D-series controller, Teledyne Isco, Lincoln, NE), an electrically actuated E90-220 injection valve with a 60 nL inner loop (Valco, Houston, TX), and a T-splitter with a restrictor (fused silica capillary 0.025 mm I.D. × 150 mm length). The inlet part of the capillary monolithic column was inserted through the body of the splitter into the injection valve to minimize extra-column dispersion. The monolithic column outlet was connected to a Spectra 100 UV–Vis detector (Thermo Separation Products, Waltham, MA) via a 0.075 mm I.D. × 110 mm long fused silica capillary (with optical cell window) using a PTFE

sleeve. UV-detection was performed at 210 nm and 220 nm. Data were collected and processed using ChemStation software.

8.2.3. Mobile phases and samples

The LC mobile phase contained 10 or 20 mM (ionic strength) phosphate buffer at pH 7.4 and 0-50% v/v acetonitrile with addition of 0-200 mM of NaCl. Dulbecco's phosphate-buffered saline (DBS) solution consisting of 137 mM NaCl, 2.7 mM KCl, 10 mM Na_2HPO_4, and 2 mM KH_2PO_4 was used to evaluate drug partitioning into the synthesized stationary phase. DBS with or without 5% (v/v) of methanol was employed. Solutions of individual standards at a concentration of 1 – 5 mg mL^{-1} were prepared in methanol/water 1/2 (v/v).

8.2.4. Preparation of poly(GMA-co-EDMA) monolithic columns

The fused-silica capillaries were modified by γ-MPS [27, 41] prior to polymerization of a mixture containing GMA (20 wt%), EDMA (5 wt%), CYC (70 wt%), and DOD (5 wt%). AIBN (1 wt% with respect to the monomers) was added as a polymerization initiator [42]. This mixture was sonicated for 10 min, purged with nitrogen for 10 min, and then filled into the preconditioned capillary (200 x 0.1 mm I.D.). Thermal polymerization was accomplished in an oven at 60ºC for 20 h. The pore-forming solvents and remaining unreacted monomers were removed from the synthesized monolith by flushing with MeOH. The bulk monoliths were prepared inside 1.5 cm I.D. glass vials using 0.5 mL of polymerization mixture. The vials were located in the oven under same conditions as those used for the capillaries. After polymerization, the vials were broken and the bulk material was separated from the glass pieces. This material was repeatedly washed with MeOH on a Büchner funnel to remove the pore-forming solvents and unreacted monomers and dried at 80ºC for 6 h.

8.2.5. Functionalization of poly(GMA-co-EDMA) monolith with soyPC

Figure 8.1 displays the preparation procedure of soyPC modified capillary columns. The capillaries containing the monolithic substrate were flushed with water and then with 2M aqueous HMD solution at 60ºC for 2 h at a flow rate of 60 µL h^{-1}. After that, the column was filled with a 1 M aqueous GA solution. The column was closed with septum caps and held at room temperature for 12 h. Afterwards the column was flushed with water and MeOH. The modification step using a 2 M solution of HMD was repeated and, subsequently, the column was filled with a mixture containing 100 mM EDC and 150 mM soyPC dissolved in 0.1 M imidazole in MeOH. The column was closed with septum caps and left to react for 30 min at room temperature. After that the column was filled with an aqueous solution containing 0.2 M SCBH and left to react for 2 h at 4ºC. Finally, the column was washed with MeOH and IPA in order to eliminate any soyPC adsorbed to the monolith through Van der Waals interactions. The capillary columns (150 x 0.1 mm I.D.) were used in capillaryLC. Concerning the functionalization methodology, other procedures besides the reactions depicted in Figure 8.1 were tested. These are described in more details in the supplementary materials (Figure S8.1).

The bulk monolithic materials (obtained from glass vials) were functionalized under identical reaction conditions as described above for the capillaries. Thus, powdered bulk material (5 mg) was mixed with the derivatization solutions. The dynamic steps carried out in the capillary were done in static mode mixing the bulk material and adding the equivalent amount of solution. This reaction suspension was then stirred at the same temperature and for the same time as for the capillary reactions.

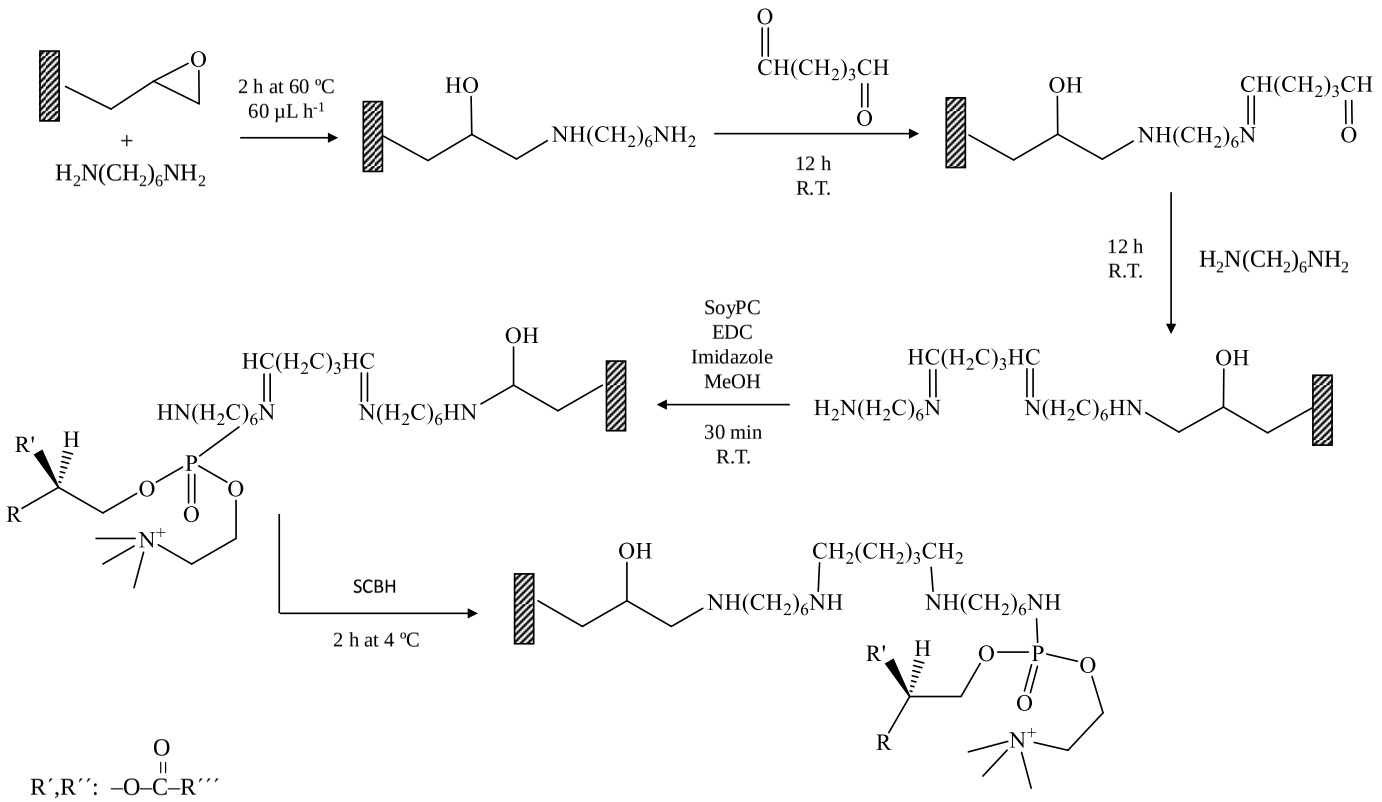

Figure 8.1. Reaction scheme for the functionalization of poly(GMA-*co*-EDMA) monoliths with soyPC. Reaction conditions as described in the experimental section.

8.2.6. ATR-FTIR characterization of soyPC columns

The bulk polymer was analyzed after each step of functionalization. It was ground into a fine powder with mortar and pestle and a small quantity of the monolithic material was placed into the instrument and the IR spectra were measured (Figure 8.2).

Monolithic capillary columns were also characterized by ATR-FTIR. A small piece of capillary was cut after each step of surface functionalization and used for ATR-FTIR characterization. To etch the silica capillary wall, the capillaries with monolithic polymer were cut into small pieces and submerged in 3 M aqueous NH_4HF_2 for 12 h under magnetic stirring at room temperature. Then, the monolith was repeatedly washed with MeOH on a Büchner funnel, further homogenized, and the finely ground material was used for FTIR measurements (see Figure S8.2).

8.2.7. GC-MS analysis

The powdered bulk material (5 mg) was mixed and stirred with a $LiAlH_4$ suspension in hexane (ca. 1.1 mL mg^{-1} monolith) for 2 h. The suspension was filtered and the filtrate used for GC-MS analysis [43] at the conditions described above (Section 8.2.2). Extracted ion current (EIC) chromatograms were obtained for the corresponding alcohol of the fatty acyl chains present in soyPC according to the supplier in order to prove successful immobilization of soyPC onto the monolith.

8.2.8. The total porosity of the synthesized columns

The value of total porosity of the synthesized columns was obtained from capillary LC data. It was calculated as a ratio of the hold-up volume of the column to the geometric volume of the empty fused silica capillary used to prepare the column. The hold-up volume of the column was obtained from the volumetric flow rate of the mobile phase (50/50 % (v/v) ACN/20 mM

phosphate buffer pH 7.4) and the column hold-up time, t_0, when the retention data were corrected for the extra-column instrumental contributions, e.g., the volume of the silica fused capillary connecting the monolithic column to the UV-detector. Uracil was employed as the t_0 marker.

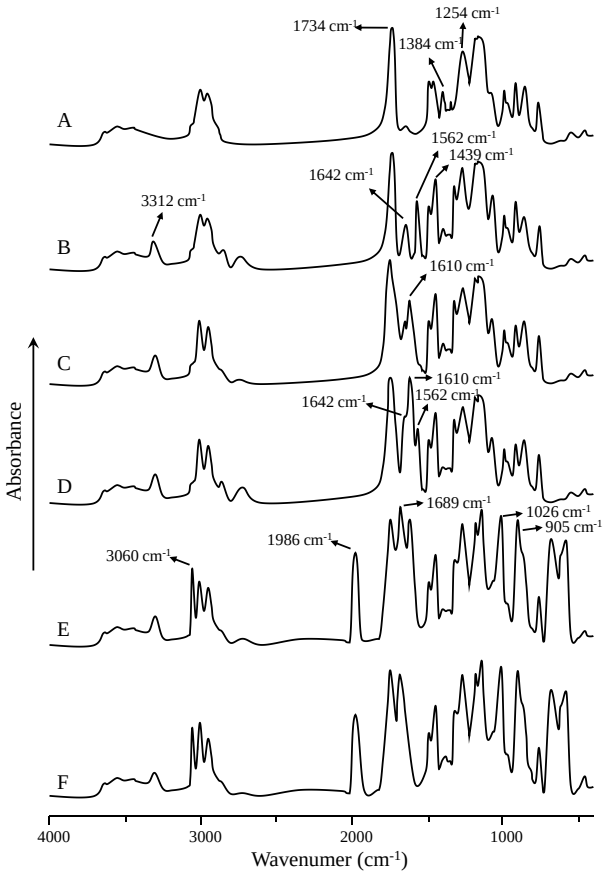

Figure 8.2. ATR-FTIR spectra of bulk material. A) poly(GMA-*co*-EDMA), B) after 1st modification step (HMD), C) after 2nd modification step (GA), D) after 3rd modification step (HMD), E) after 4th modification step (soyPC), and F) after SCBH reduction.

8.3. Results and discussion

8.3.1. Functionalization of poly(GMA-co-EDMA) monoliths with soyPC

A previously developed poly(GMA-*co*-EDMA) monolith [42] synthesized in fused silica capillaries was used to prepare the soyPC-modified columns. It possesses sufficient porosity, permeability, and efficiency for capillary LC (see Table 8.2**)**. Four different strategies to introduce the phospholipid ligand onto the poly(GMA-*co*-EDMA) monolith were tested (for detailed description see Figure 8.1 and Supplementary Material, Figure S8.1). The multistep monolithic surface modification strategy carried out according to the reaction scheme in Figure 8.1 gave the stationary phase with the highest amount of immobilized phospholipids. The oxirane ring from GMA was opened through reaction with HMD to create an amino stationary phase. After that, the amino monolith was modified by GA and HMD again, and phosphatidylcholine was covalently bound to it via an EDC coupling reaction. Finally, the formed imino groups were reduced by SCBH to stabilize the bonding.

Table 8.2. Porosity, permeability, and the height equivalent to the theoretical plate (*H*) for alkylbenzenes in poly(GMA-*co*-EDMA) bare column and soyPC modified column. Experimental conditions: Mobile phase, 50/50% (v/v) ACN/20 mM phosphate buffer pH 7.4; flow rate, 500 nL min^{-1}; columns. 150 x 0.1 mm.

	poly(GMA-*co*-EDMA) column	soyPC column
Compound	*H* [μm]	
Benzene	25.5	42.4
Toluene	27.9	57.5
Ethylbenzene	30.3	79.2
Propylbenzene	32.9	108.3
Butylbenzene	34.1	131.2
Pentylbenzene	34.3	138.7
Hexylbenzene	35.3	147.8
Porosity	0.828	0.732
Permeability [m^2]	3.63×10^{-14}	3.14×10^{-14}

This approach has several advantages over preparation procedures used earlier for column synthesis. First of all, soyPC is permanently immobilized to the functionalized poly(GMA-*co*-EDMA) monolith by covalent coupling. This provides improved stability of the stationary phase as compared to stationary phases prepared only by adsorption [6-10], especially when organic solvents are used as components of the mobile phase. Moreover, the used linking chemistry via a HMD-GA-HMD spacer arm allows a specific and controllable reaction compared to an adsorption methodology. The long spacer arm appears to be required to ensure unhindered accessibility to the reactive phosphate group, while in other tested approaches the spacer arm was too short and did not result in immobilized soyPC due to steric hindrance (Supplementary Material, Figure S8.1). Owing to the fact that the covalent bond is created via the phosphate group, also phospholipids without an amino group can be immobilized to the polymer surface, which is an additional great advantage over previously developed processes (involving, e. g., glutaraldehyde).

The presence of soyPC groups attached onto the surface of the poly(GMA-*co*-EDMA) monolith was demonstrated by ATR-FTIR of the bulk material (see Figure 8.2) and of the monolith prepared inside the capillary (Supplementary Material, Figure S8.2). The bands at 1734, 1254, and 1384 cm^{-1} corresponding to the C=O stretching, C-O(-C) stretching of the ester and the oxirane ring are present in the spectrum of both modified and non-modified monoliths. The multiple bands at about 3000 cm^{-1} originate from C-H stretching vibrations of CH, CH_2, and CH_3 groups of the polymer backbone. The presence of HMD bonded to the monolithic surface is demonstrated in Figure 8.2B. Several new bands arise upon modification of the epoxy monolith with HMD, amongst others at 3312, 1642, 1562, and 1439 cm^{-1}. The new band at 3312 cm^{-1} corresponds to the N-H stretch and clearly indicates the successful amination reaction. The other bands originate from deformation vibrations of NH_2, CH_2, and/or OH. The disappearance of the band at 1562 cm^{-1} (NH deformation) and a new band at 1610 cm^{-1} corresponding to the C=N bond as well as a shoulder

close to the band at 1734 cm^{-1}, indicating the presence of the aldehyde, confirm successful modification of the monolith by GA (Figure 8.2C). The third step of the reaction in which the aldehyde-terminated surface was modified by HMD caused the reappearance of the band at 1562 cm^{-1} and the intensification of the band at 1610 cm^{-1} (Figure 8.2D). Figure 8.2E shows the change in the ATR-FTIR spectrum of the monolith after the EDC coupling reaction with soyPC. Several bands demonstrate the presence of soyPC (905, 1026, 1689, 1986, and 3060 cm^{-1}). The bands at 905 and 1026 cm^{-1} correspond to the P–O–C phosphoester and P=O stretching vibrations from the phosphoramidate. In addition a band at 3100 cm^{-1} corresponding to a =C-H stretch from the unsaturated chains in soyPC also appeared. SoyPC and glycerol tripalmitate were also analyzed by ATR-FTIR (see Supplementary Material, Figure S8.3, where bands characteristic for phospholipids are observed) to confirm the successful immobilization of soyPC onto monolith. Comparing Figure 8.2E/8.2F with Figure S8.3 is apparent that some bands are hindered or slightly shifted by the presence of new bonds originating from poly(GMA-*co*-EDMA) monolith or modification. Finally, in Figure 8.2F, the disappearance of the band at 1610 cm^{-1} confirms the reduction of the imine (C=N) double bonds in the HMD-GA-HMD arm.

The same characterization by FTIR was carried out with the monoliths prepared inside the capillary at each step of surface functionalization. However, the reaction with NH_4HF_2 to remove the fused silica walls also modified the surface chemistry and led to alterations in the IR spectra as compared to the ones of the corresponding bulk polymer (Figure S8.2). Some of the bands disappeared due to chemical reaction and/or were shifted due to hydrogen bond formation. However, in general the same chemical alterations were observed in the spectra upon step by step surface derivatization as in the corresponding spectra of the bulk material.

Furthermore, GC-MS was used to confirm the immobilization of soyPC on the monolithic material. The fatty acyl chains were cleaved from the monolith surface by reduction of the ester to the corresponding alcohol using $LiAlH_4$ and the released alcohols were analyzed by GC-MS. The GC-MS chromatograms (Supplementary Material, Figure S8.4) revealed two peaks. The first one at 8.2 min was the 1-hexadecanol, the corresponding reduction product of 16:0 PC species with $LiAlH_4$. A second peak was found at 11.3 min corresponding to the 18:0, 18:1, 18:2, and 18:3 PC species but reduced by $LiAlH_4$ to corresponding alcohols with no, one, two, and three double bonds. Specific EICs for each alcohol clearly reveal their presence in accordance to the fatty acid profile in the employed soyPC (see Supplementary Material, Figure S8.4). The identification of the analytes was accomplished via NIST library search. It can be clearly seen by the presence of all fatty alcohols that soyPC was truly immobilized on the monolith surface by the reaction scheme outlined in Figure 8.1.

8.3.2 Capillary liquid chromatography

As mentioned before, SoyPC was chosen as a model compound for the synthesis of monolithic capillary columns. Therefore, the fatty acid chains originating from soyPC provide hydrophobic character to the prepared stationary phase, which can be used as a measure of soyPC-modification extent. All synthesized monolithic columns (Figure 8.1 and Supplementary Material, Figure S8.1) were evaluated in cLC under RP separation conditions utilizing alkylbenzenes as test analytes and acetonitrile–water as mobile phase. Unfortunately, columns prepared by methods A, B, and C (Supplementary Material, Figure S8.1) showed lower retention for alkylbenzenes than the original poly(GMA-*co*-EDMA) monolith. Since a multistep preparation procedure was used for the synthesis of the capillary columns, we investigated

the influence of all individual modification steps on the separation of analytes employing an alkylbenzene (C_0-C_6) mixture.

In Figure 8.3 the separation of a test mixture, containing uracil as a non-retained compound, benzene, and five n-alkylbenzenes, is compared for the original poly(GMA-*co*-EDMA) monolithic column (Figure 8.3A), a monolithic column before modification by soyPC when only the spacer is present on the stationary phase surface (Figure 8.3B), and for a soyPC modified poly(GMA-*co*-EDMA) capillary column (Figure 8.3C). Good separation of all tested compounds was obtained on the poly(GMA-*co*-EDMA) monolith within less than 11 minutes, confirming that the synthesized monolithic support has some hydrophobic character, mainly originating from the nature of the monomer and cross linker used for column synthesis. The poor separation of the sample mixture shown in Figure 8.3B confirms successful modification of the poly(GMA-*co*-EDMA) monolith with HMD and GA, through shielding of the original hydrophobic monolith by long hydrophilic spacer-bearing end amino groups (Figure 8.1). SoyPC covalently bonded to the modified monolithic support significantly improved the separation selectivity (hydrophobic) of the prepared stationary phase (Figure 8.3C). The retention factor of hexylbenzene is 4.5 times higher than on the original poly(GMA-*co*-EDMA) monolith; the retention factor of hexylbenzene was 2.8 on the poly(GMA-*co*-EDMA) monolith, whereas as high as 12.7 on the soyPC modified monolith. The chromatograms obtained for the monolithic column after the 1st and 2nd modification steps are not shown due to co-elution of analytes; thus, they were the same as in Figure 8.3B.

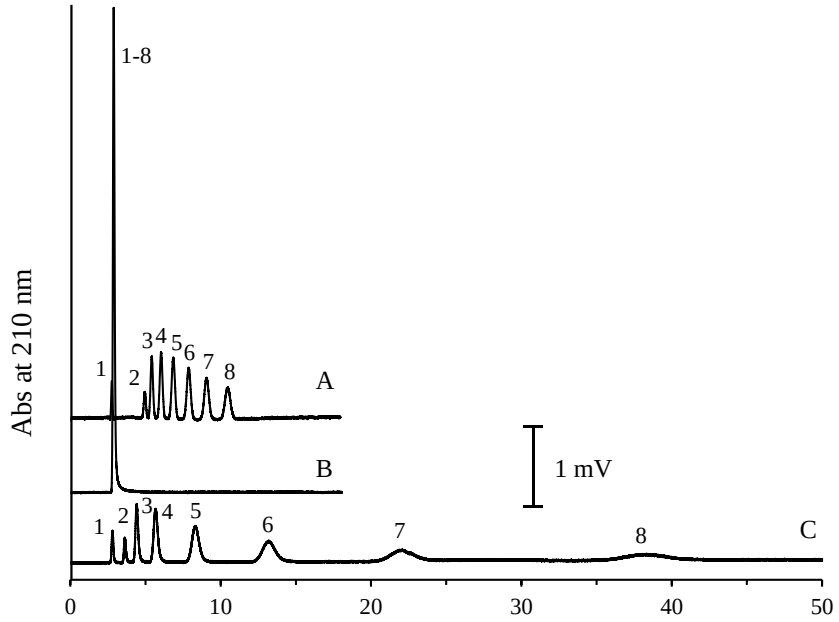

Figure 8.3. LC separation of a mixture containing uracil (non-retained compound), benzene, and five *n*-alkylbenzenes using A) the original poly(GMA-*co*-EDMA) monolithic column, B) a monolithic column with HMD-GA-HMD spacer arm before modification with soyPC, and C) a soyPC modified poly(GMA-*co*-EDMA) capillary column. The running conditions were as follows: mobile phase containing 50/50% (v/v) ACN/20 mM phosphate buffer pH 7.4; flow rate of 500 nL min^{-1}; UV-detection at 210 nm. Peak identification: 1) uracil, 2) toluene, 3) ethyl benzene, 4) propyl benzene, 5) butyl benzene, 6) pentyl benzene, and 7) hexyl benzene.

Table 8.2 summarizes the height equivalent to the theoretical plate (H) values for the alkylbenzene derivatives obtained on the original poly(GMA-*co*-EDMA) monolith and on the soyPC modified monolithic column. The increasing retention in the homologous series causes a significant decrease in the column efficiency of soyPC modified monolithic column while the plate heights for poly(GMA-*co*-EDMA) columns are almost independent of the solute type. Even though the column efficiency after multistep modification by soyPC was lowered, the column selectivity increased as is apparent from Figure 8.3. The immobilized layer of soyPC lowered also the total porosity and

permeability of the original monolith (Table 8.2). Figure 8.4 confirms the different characteristics of the soyPC stationary phase compared to the original poly(GMA-*co*-EDMA) monolith. The logarithm of the retention factors (log *k*) of individual alkylbenzenes increase linearly with the number of carbons in the alkyl chain (n_c); however, the slope is steeper for the soyPC column, providing lower retention for the C_{0-2} compounds (i.e., for benzene, toluene, and ethylbenzene) and higher retention for the C_{3-6} compounds (i.e., for propyl-, butyl-, pentyl-, and hexylbenzene).

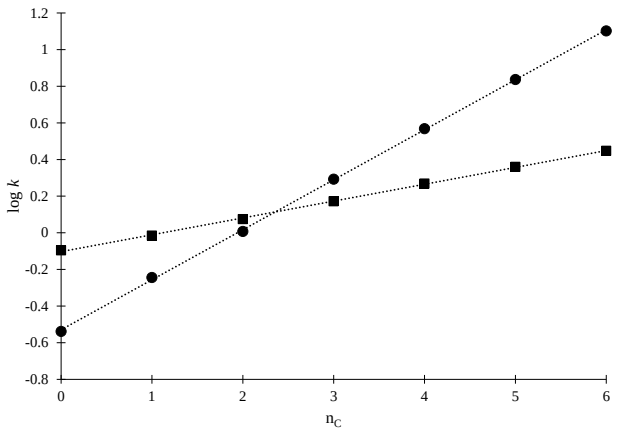

Figure 8.4. Comparison of log *k* vs. number of carbon in alkylbenzene molecule (n_c) for poly(GMA-*co*-EDMA) (■) and soyPC modified monolithic columns (●). The running conditions were as follows: mobile phase containing 50/50% (v/v) ACN/20 mM phosphate buffer pH 7.4; flow rate of 500 nL min^{-1}; UV-detection at 210 nm.

The interactions between analytes and the phospholipid stationary phase were observed utilizing test analytes like organic acids, lidocaine, and sulfanilamide. A mobile phase consisting of phosphate buffer at pH 7.4 and acetonitrile with or without NaCl was employed for column characterization. The variation of the retention of neutral, acidic, and basic compounds on the synthesized soyPC column was investigated by altering the ACN concentration in the mobile phase (0-50% v/v). Figure 8.5A demonstrates that increasing

concentration of organic solvent in the mobile phase accelerates more the elution of lipophilic compounds (steepest dependency) (Figure 8.5A) than retention of small organic acids (Figure 8.5B). This confirms the prevalence of hydrophobic interactions similarly as in the case of conventional RPLC stationary phases or biomimetic IAM stationary phases [44]. On the other hand, the synthesized columns can operate under fully aqueous phase conditions (see Figure 8.5 and Figure 8.6) and the resultant data do not need extrapolation to 100% aqueous conditions (buffer), as typically (but not always) done in IAM chromatography or in RP chromatography [5].

Figures 8.5C and 8.5D display the effect of increasing ionic strength of the mobile phase (concentration range 0-200 mM of NaCl) on the retention of the tested compounds. The retention of tested compounds gradually decreases with increasing ionic strength of the mobile phase. The discrepancy between log *k* values of tested compounds in 10 mM phosphate buffer and 10 mM phosphate buffer containing 50 mM of NaCl (i.e. the lower retention factor for acidic solutes than expected from the trend line by extrapolation to 0 mM NaCl) can be attributed to a salting out effect, inducing strengthened retention, once 50 mM NaCl is added; when the NaCl concentration is further increased, the shielding of the charges on the soyPC column and the anionic solutes causes a decrease of retention factors due to balanced ionic interactions [45, 46]. The higher retention and steepest dependency of log *k* vs. ionic strength of mobile phase for organic acids confirms that the phosphate group in phosphatidylcholine is partially blocked through a phosphoramidate bond and interactions can mainly take place with the amino groups and through hydrophobic interactions.

Drug partitioning into the synthesized stationary phases was evaluated under capillary LC conditions employing a set of unrelated analytes and Dulbecco's phosphate-buffered saline solution (DBS) as a mobile phase. DBS is an isotonic (physiological) saline solution suitable to mimic human body

conditions. The differences between retention of compounds in pure 10 mM phosphate buffer and 10 mM phosphate buffer with added NaCl are shown in Figure 8.5C and 8.5D.

Figures 8.6A and 8.6B present the relationship between the logarithm of the retention factor (log *k*) of the tested solutes (Table 8.1) and the logarithm of the corresponding octanol–water partition coefficients (log $P_{o/w}$) when only a Dulbecco's phosphate-buffered saline solution or this buffer solution containing 5% of methanol were employed as mobile phase. Figure 8.6A shows retention data for the bare poly(GMA-*co*-EDMA) monolith, where hydrophobic and electrostatic interactions (slightly negative charge) prevail. Organic acids such as benzoic acid (6), *m*-nitrobenzoic acid (8), and acetylsalicylic acid (12) had repulsive interactions with the column (k<0) when 5% v/v of methanol was added to the mobile phase and the hydrophobic interactions were lowered. There is no correlation between the measured data and log $P_{o/w}$ values for the poly(GMA-*co*-EDMA) monolith. SoyPC immobilized on the poly(GMA-*co*-EDMA) monolith caused changes in the retention factors of the tested solutes, which was confirmed by stronger hydrophobic interactions (Figure 8.3C) and by electrostatic interactions (slightly positive charge) between the tested compounds and the stationary phase (Figure 8.5). When rat intestinal drug absorption parameters [47] were applied to investigate interactions between the tested drugs and the soyPC monolith (Figure 8.6C), the correlation coefficient R^2 increased from 0.55 (Figure 8.6B) to 0.73 (Figure 8.6C).

The synthesized columns were stable for more than six months when they were evaluated employing mobile phases consisting of ACN and phosphate buffer at pH 7.4 of various ionic strengths or only Dulbecco's phosphate-buffered saline solution. The relative standard deviations (RSDs) for the retention times of alkylbenzenes (C_{0-6}) on a newly prepared soyPC capillary column and those obtained on the same column after all chromatographic tests (up to 900 injections) were less than 2.3% when 50/50% v/v ACN/20 mM

phosphate buffer pH 7.4 was used as mobile phase. On the contrary, stationary phases such as silica or zirconia-magnesia particles coated with PC are stable for ca 50 hours of continual use [7] and the IAM.PC.D column longevity is reported as approximately 7,000 column volumes of aqueous mobile phase like Dulbecco's phosphate-buffered saline solution [48].

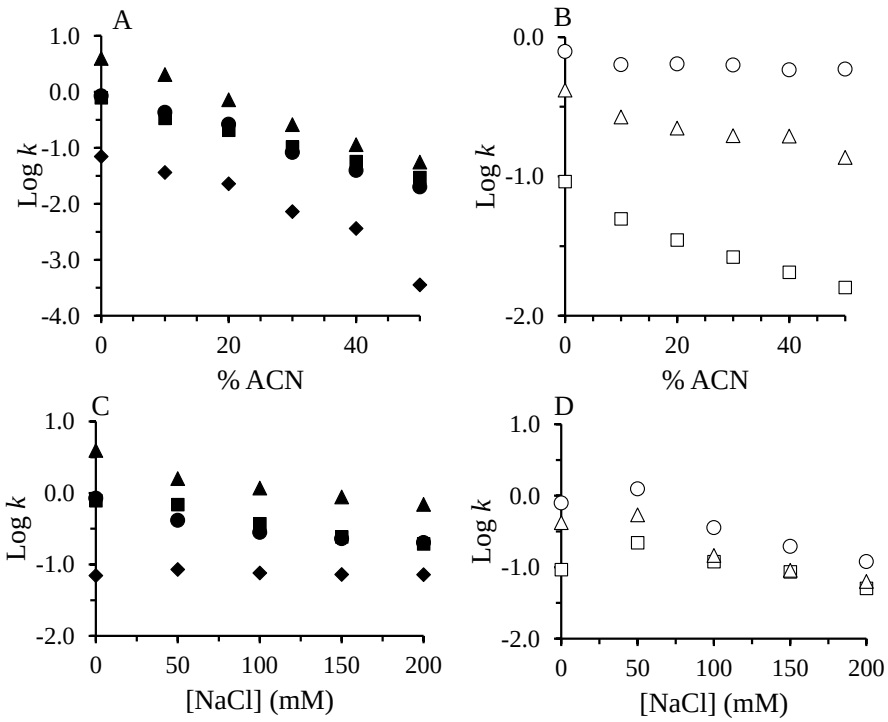

Figure 8.5. Effect of increasing concentration of ACN (0-50% v/v) and ionic strength (0-200 mM NaCl) of mobile phase on the retention of neutral, acidic, and basic compounds. The running conditions were as follows: A) and B) mobile phase containing 0-50% (v/v) ACN and phosphate buffer pH 7.4 (ionic strength 10 mM), C) and D) mobile phase containing phosphate buffer pH 7.4 (ionic strength 10 mM) with different concentrations of NaCl; flow rate of 1 µL min^{-1}; UV-detection at 220 nm. Sample: benzoic acid (■); *m*-nitrobenzoic acid (▲); lidocaine (●); sulfanilamide (♦), formic acid (□); oxalic acid (Δ); citric acid (○).

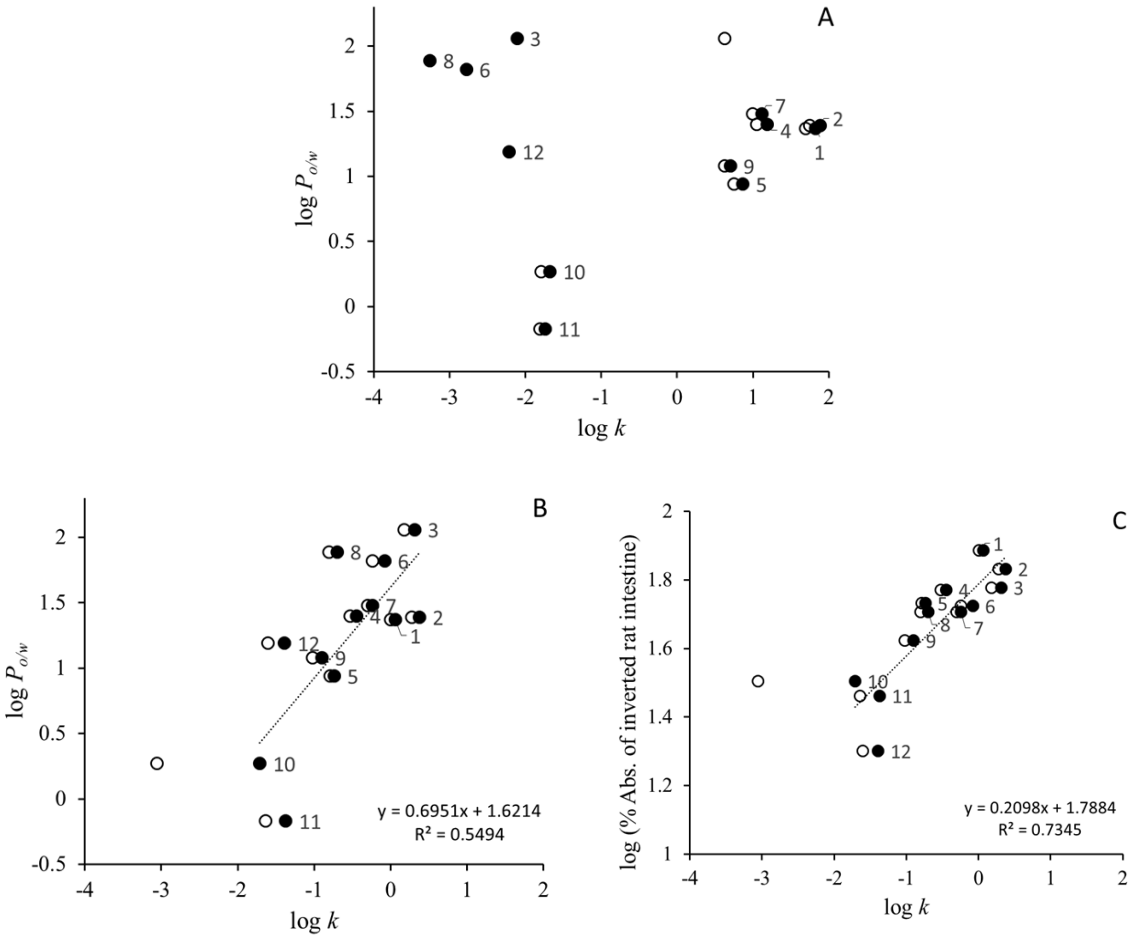

Figure 8.6. Relationship between the logarithms of retention factors (log *k*) of the tested solutes (see Table 8.1) and their hydrophobicities (log $P_{o/w}$ values, Table 8.1). A) Poly(GMA-*co*-EDMA) monolithic column; B) soyPC modified monolithic column; C) correlation between retention factors (log *k*) of tested solutes on the soyPC modified monolithic column and rat intestinal drug absorption. The running conditions were as follows: mobile phase was DBS (●, regression equations, correlation coefficients) and 5/95 % (v/v) methanol/DBS (○); flow rate of 1 µL min^{-1}; UV-detection at 220 nm.

8.4. Conclusion

This work presents a novel methodology for preparing biomembrane mimicking monolithic columns for cLC. Our data shows that the synthesized stationary phase, consisting of zwitterionic phosphatidylcholines covalently bonded to a poly(GMA-*co*-EDMA) monolith through EDC coupling, possesses improved stability in contrast to physically adsorbed phospholipid stationary phases. The suggested technique of column preparation through EDC coupling involves the phosphate group in the phospholipid in order to form a phosphoramidate linkage. Thus, this coating procedure enables to covalently immobilize all kinds of phospholipids, not only those containing (primary) amino groups. In addition, this means that part of the functional groups in the phospholipid polar head group is available for additional electrostatic interactions. The proposed methodology will strongly broaden the field of immobilized phospholipid stationary phases for chromatography, which is of importance for elucidating binding interactions between biologically relevant compounds and biomembranes.

Acknowledgements

This work was supported by the Ministry of the Interior of the Czech Republic (Project No. VG20112015021), by the Academy of Sciences of the Czech Republic (Institutional support RVO: 68081715), by the Magnus Ehrnrooth foundation (SKW), by the Academy of Finland (projects 276075 and 266342; SKW), and by Project CTQ2014-52765-R (MINECO of Spain and FEDER funds). E.J.C-C. thanks the MINECO for an FPI grant. ML is grateful to the German Academic Exchange Service for support (Project 54655966).

References

[1] T. Fujita, J. Iwasa, C. Hansch, J. Am. Chem. Soc. 86 (1964) 5175.

[2] P. Artursson, J. Karlsson, Biochem. Biophys. Res. Commun. 175 (1991) 880.

[3] S. K. Wiedmer, M. S. Jussila, M.-L. Riekkola, , Trends Anal. Chem. 23 (2004) 562.

[4] T. Cserháti, M. Szögyi, Biomed. Chromatogr. 24 (2010) 1265.

[5] K. Valkó, J. Chromatogr. A 1037 (2004) 299.

[6] K. Miyake, F. Kitaura, N. Mizuno, H. Terada, J. Chromatogr. A 389 (1987) 47.

[7] W. Zhang, Z. Hu, Y. Feng, S. Da, J. Sep. Sci. 33 (2010) 2990.

[8] E. Krause, M. Dathe, T. Wieprecht, M. Bienert, J. Chromatogr. A 849 (1999) 125.

[9] W. Hu, P.R. Haddad, K. Tanaka, M. Mori, K. Tekura, K. Hasebe, M. Ohno, N. Kamo, J. Chromatogr. A 997 (2003) 237.

[10] M. Hanna, V. De Biasi, B. Bond, P. Camilleri, A.J. Hutt, Chromatographia 52 (2000) 710.

[11] P. B. Ogden, J. W. Coym, J. Chromatogr. A 1218 (2011) 2936.

[12] H. Luo, Ch. Zheng, Y. Cheng, J. Chromatogr. A 1176 (2007) 100.

[13] C. Delaurent, V. Tomao, A. M. Siouffi, Chromatographia 45 (1997) 355.

[14] J. J. Pesek, M. T. Matyska, G. B. Dawson, A. Wilsdorf, P. Marc, M., J. Chromatogr. A 986 (2003) 253.

[15] M. A. Al-Haj, P. Haber, R. Kaliszan, B. Buszewski, M. Jezierska, Z., J. Pharm. Biomed. Anal. 18 (1998) 721.

[16] S. Bocian, A. Nowaczyk, B. Buszewski, Anal. Bioanal. Chem. 404 (2012) 731.

[17] Y. Watanabe, M. Abolhassani, Y. Tojo, Y. Suda, K. Miyazawa, Y. Igarashi, K. Sakuma, T. Ogawa, K. Muramoto, J. Chromatogr. A 1216 (2009) 8563.

[18] D. Verzele, F. Lynen, M. De Vrieze, A. G. Wright,.M. Hanna-Brown, P. Sandra, Chem. Commun. 48 (2012) 1162.

[19] E. S. Gallagher, S. M. Adem, Ch. A. Baker, S. N. Ratnayaka, I. W. Jones, H. K. Hall, S. S. Saavedra, C. A. Aspinwall, J. Chromatogr. A 1385 (2015) 28.

[20] C. Pidgeon, U.V. Venkataram, Anal. Biochem. 176 (1989) 36.

[21] S. Ong, C. Pidgeon, Anal. Chem. 67 (1995) 2119.

[22] D. Rhee, R. Markovich, W.G. Chae, X. Qiu, C. Anal. Chim. Acta 297 (1994) 377.

[23] F. Svec, J. Chromatogr. A 1217 (2010) 902.

[24] R. D. Arrua, M. Talebi, T. J. Causon, E. F. Hilder, Anal. Chim. Acta 738 (2012) 1.

[25] Z. Walsh, B. Paull, M. Macka, Anal. Chim. Acta 750 (2012) 28.

[26] T. Zhu, K. H. Row, J. Sep. Sci. 35 (2012)1294.

[27] E.C. Peters, M. Petro, F. Svec, J.M.J. Fréchet, Anal. Chem. 69 (1997) 3646.

[28] W. Wieder, C. P. Bisjak, C. W. Huck, R. Bakry, G. K. Bonn, J. Sep. Sci. 29 (2006) 2478.

[29] X. Dong, J. Dong, J. Ou, Y. Zhu, H. Zou, Electrophoresis 27 (2006) 2518.

[30] A. Messina, M. Flieger, F. Bachechi, M. Sinibaldi, J. Chromatogr. A 1120 (2006) 69.

[31] G. Yang, H. Liu, Y. Zhang, S. Wang, J. Yin, B. Yin, Y. Chen, J. Chromatogr. A 1129 (2006) 231-235.

[32] B. Carbonnier, M. Guerrouache, R. Denoyel, M.-C. Millot, J. Sep. Sci. 30 (2007) 3000.

[33] M. Wang, J. Xu, Z. Zhou, T. Tan, J. Chromatogr. A 1147 (2007) 24.

[34] B. Preinerstorfer, W. Bicker, W. Lindner, M. Laemmerhofer, J. Chromatogr. A 1044 (2004) 187-199.

[35] Y. Tian, C. Zhong, E. Fu, Z. Zeng, J. Chromatogr. A 1216 (2009) 1000.

[36] Y. Kuroda, R. Hamaguchi, T. Tanimoto, Chromatographia 77 (2014) 405.

[37] X. Zhao, W. Chen, Z. Liu, J. Guo, Z. Zhou, J. Crommen, R. Moaddel, Z. Jiang, J. Chromatogr. A 1367 (2014) 99.

[38] M. Szumski, D. Grzywiński, B. Buszewski, J. Chromatogr. A 1373 (2014) 114.

[39] D. Moravcová, J. Planeta, S. K. Wiedmer, J. Chromatogr. A 1317 (2013) 159.

[40] Hermanson G. T. (2008). Bioconjugate Techniques. 2nd Edition. pp. 969-1002, Academic Press, San Diego.

[41] E. C. Peters, M. Petro, F. Svec, J. M. J. Fréchet, Anal. Chem. 70 (1998) 2288.

[42] E. J. Carrasco-Correa, G. Ramis-Ramos, J. M. Herrero-Martínez, J. Chromatogr. A 1298 (2013) 61.

[43] E.J. Carrasco-Correa, G. Ramis-Ramos, J. M. Herrero-Martínez, J. Chromatogr. A 1379 (2015) 100.

[44] A. Taillardat-Bertschinger, C. A. Martinet, P.-A. Carrupt, M. Reist, G. Caron, R. Fruttero, B. Testa, Pharm. Res. 19 (2002) 729.

[45] L. Grumetto, C. Carpentiero, P. Di Vaio, F. Frecentese, F. Barbato, Journal of Pharmaceutical and Biomedical Analysis 75 (2013) 165.

[46] L. Grumetto, G. Russo, F. Barbato, European Journal of Pharmaceutical Sciences 65 (2014) 139.

[47] L.S. Schanker, D.J. Tocco, B.B. Brodie, C.A.M. Hogben, J. Pharmacol. Exp. Ther. 123 (1958) 81.

[48] G. W. Caldwell, J. A. Masucci, M. Evangelisto, R. White, J. Chromatogr. A 800 (1998) 161.

Supplementary Material

Short description of the work

A methodology for immobilizing soybean phosphatidylcholine onto a methacrylate-based monolith in capillary format was developed. The covalent 1-ethyl-3-(3-dimethylaminopropyl)carbodiimide coupling reaction involves the phosphate group in the phospholipid. Immobilization was confirmed by ATR-FTIR and GC-MS. Liquid chromatographic studies confirmed predominant hydrophobic interactions between the studied analytes and the synthesized stationary phase; however, electrostatic interactions contributed to the retention as well. The biomimetic phospholipid capillary column showed high stability even with fully aqueous mobile phases such as Dulbecco's phosphate-buffered saline solution.

Reaction pathways

Functionalization of poly(GMA-*co*-EDMA) with soyPC was performed by four different strategies. Only methods A-C are presented in Supplementary Material. The fourth method is described in the Experimental section of the main document.

Method A. First, a mixture containing HMD (15 mM), EDC (15 mM) and soyPC (150 mM) prepared in 0.1 M imidazole dissolved in MeOH was prepared. The mixture was left for 30 min at room temperature and then the solution was allowed to flow through the column at 60ºC for 2 h at a flow rate of 60 µL h^{-1}. Afterwards, using an HPLC pump, the capillaries were washed with MeOH and IPA.

Method B. The capillaries containing the poly(GMA-*co*-EDMA) monoliths were flushed and then with 2 M aqueous HMD solution at 60ºC for 2 h at a flow rate of 60 µL h^{-1}. After that, the column was filled with a mixture

containing EDC (100 mM) and soyPC (150 mM) in 0.1 M imidazole in MeOH. The column was closed with septum caps and left to react for 30 min at room temperature. Finally, an HPLC pump was used to wash the capillaries with MeOH and IPA.

Method C. The capillary containing the monolith were flushed with water and then with 2 M aqueous HMD solution at 60ºC for 2 h at a flow rate of 60 µL h^{-1}. After that, the column was filled with a 1 M aqueous GA solution. The column was closed with septum caps, held at room temperature for 12 h and afterwards the column was flushed with water and MeOH using an HPLC pump. Next, the column was filled with a 30 min aged mixture containing EDC (15 mM), HMD (15 mM), and soyPC (150 mM) in 0.1 M imidazole in MeOH. The column was closed with septum caps and left to react for 12 h at room temperature. The column was flushed with MeOH, water and then it was filled with an aqueous solution containing 0.2 M SCBH and left react for 2 h at 4ºC. Finally, the column was washed with MeOH and IPA (using an HPLC pump).

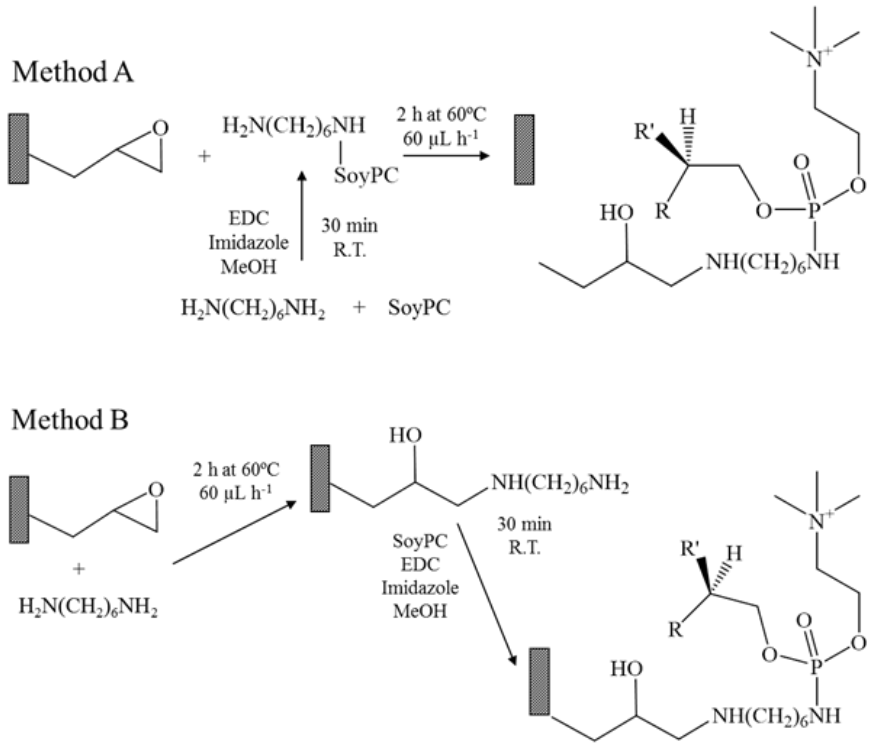

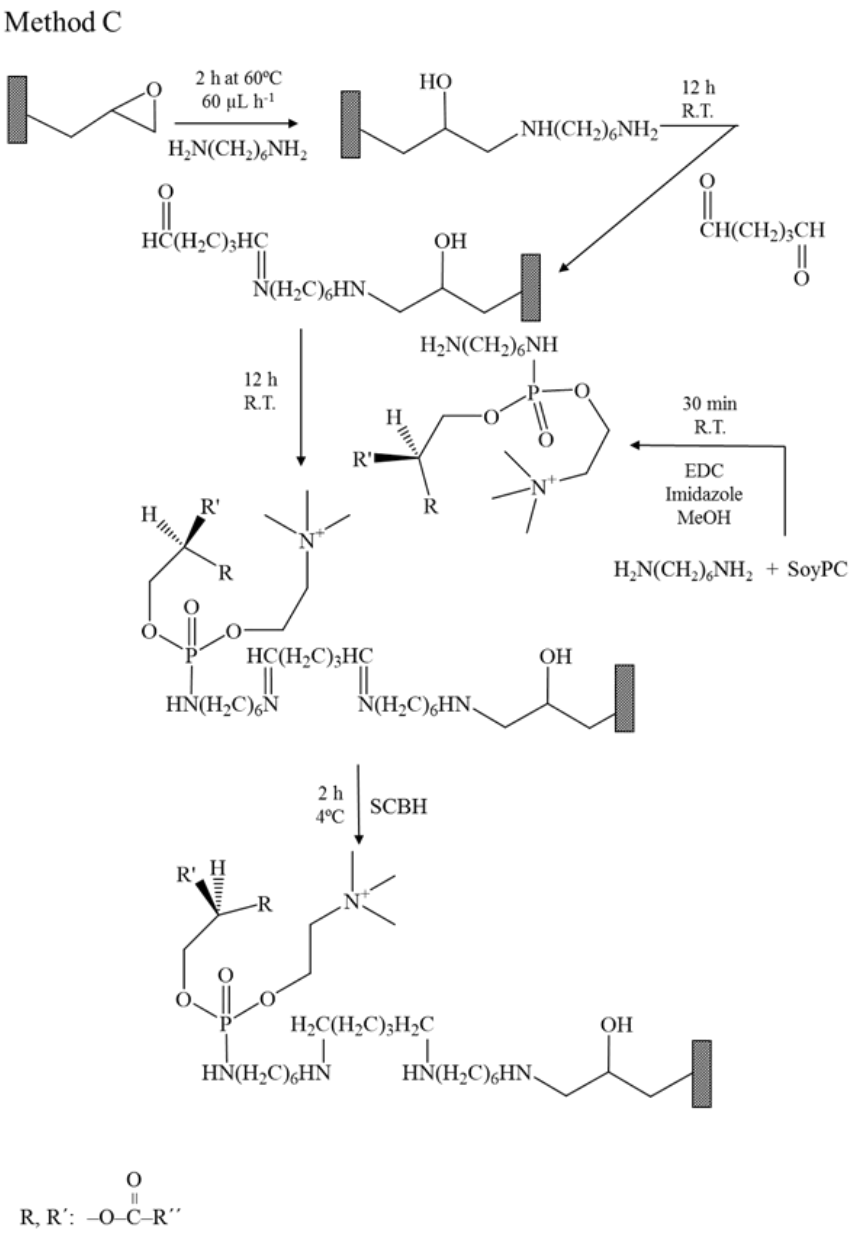

Figure S8.1. Reaction schemes for the functionalization of poly(GMA-*co*-EDMA) monoliths by methods A, B, and C.

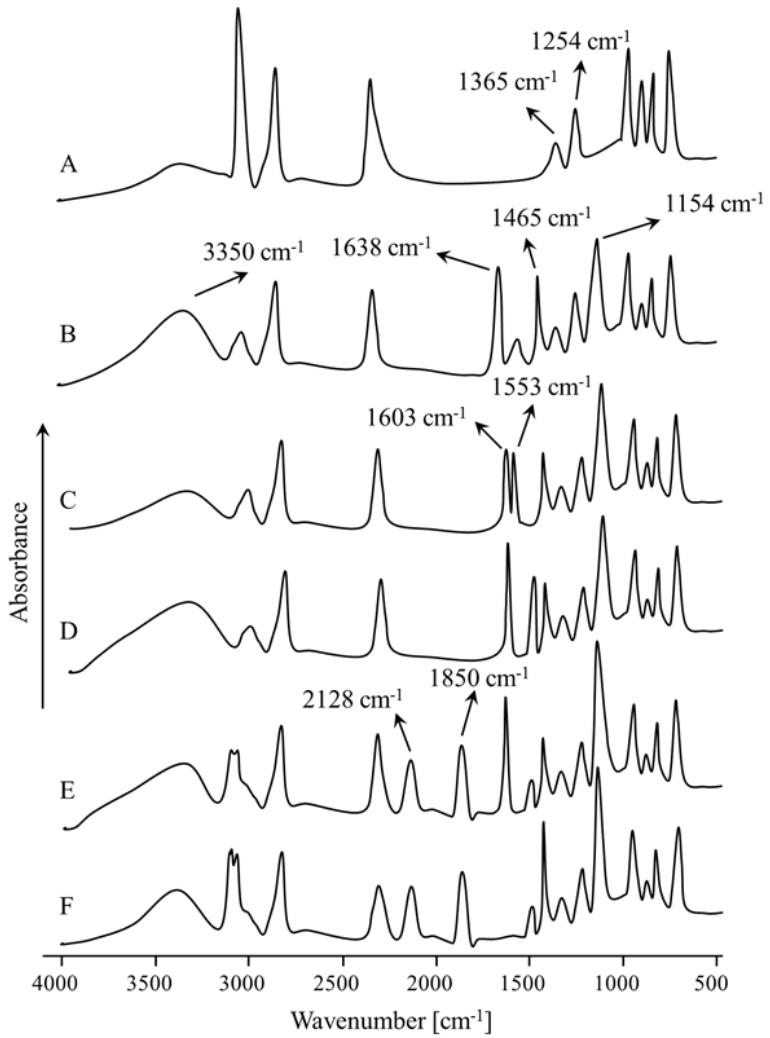

Figure S8.2. ATR-FTIR characterization of monoliths from capillaries A) poly(GMA-*co*-EDMA), B) after 1st modification step (HMD), C) after 2nd modification step (GA), D) after 3rd modification step (HMD), E) after 4th modification step (soyPC), and F) after SCBH reduction. Some bands are missing or shifted due to NH_4HF_2 treatment as compared to the spectra in Figure 8.2 without NH_4HF_2 treatment.

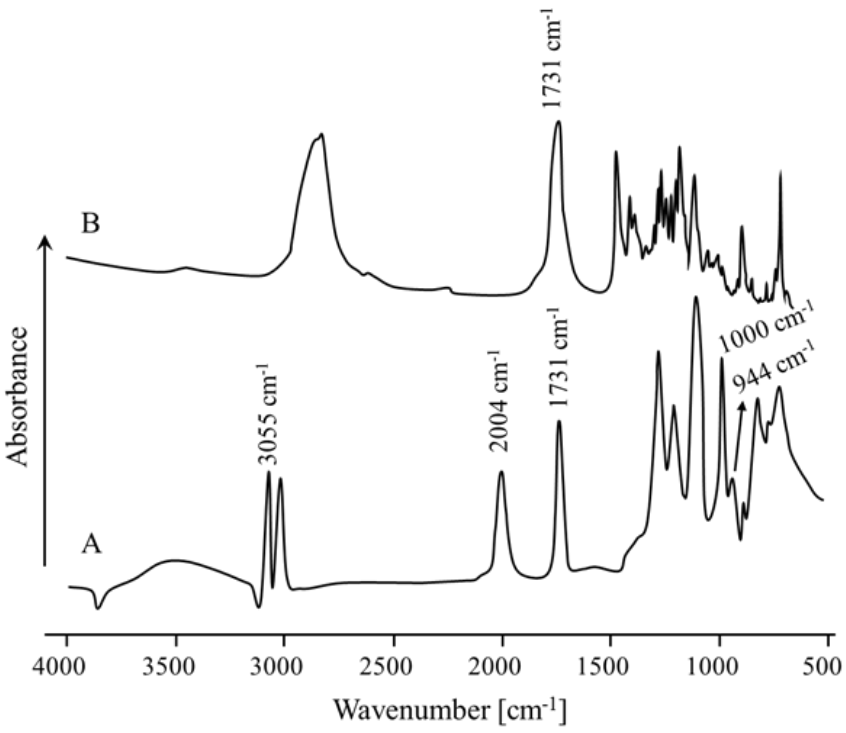

Figure S8.3. ATR-FTIR spectra of reference substances. A) soyPC and B) glycerol tripalmitate.

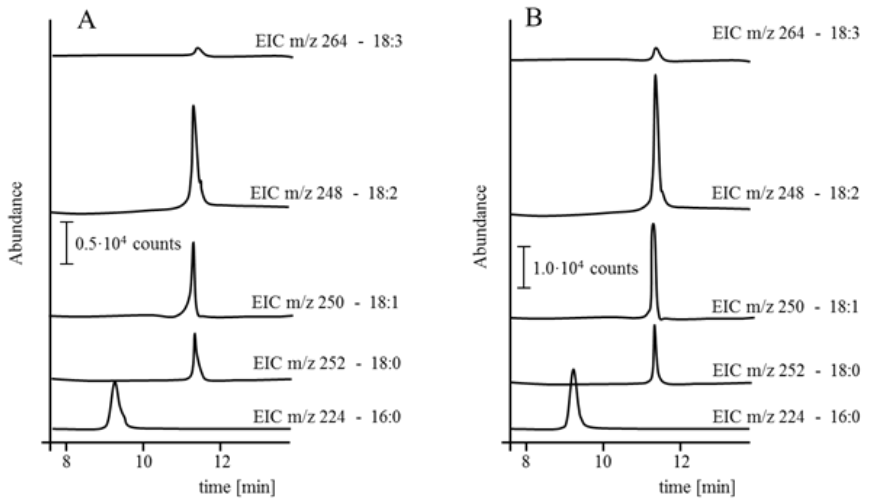

Figure S8.4. Extracted ion chromatograms (EICs) of (A) fatty alcohols of immobilized soyPC released by reductive cleavage of fatty acyls with $LiAlH_4$ and (B) fatty alcohols of soyPC standards in hexane released by reductive cleavage of fatty acyls with $LiAlH_4$. The chromatograms reflect the composition of soyPC. All fatty acyls (16:0, 18:0, 18:1; 18:2, and 18:3) were detected. The m/z values were specific for the respective compounds and selected based on spectra from the NIST library.

Chapter 9. Polymethacrylate monoliths with immobilized poly-3-mercaptopropyl methylsiloxane film for high-coverage surface functionalization by thiol-ene click reaction

Journal of Chromatography A, 1367 (2014) 123–130

Contents lists available at ScienceDirect

Journal of Chromatography A

journal homepage: www.elsevier.com/locate/chroma

Polymethacrylate monoliths with immobilized poly-3-mercaptopropyl methylsiloxane film for high-coverage surface functionalization by thiol-ene click reaction

Enrique Javier Carrasco-Correa[a], Guillermo Ramis-Ramos[a], José Manuel Herrero-Martínez[a], Michael Lämmerhofer[b,*]

[a] Department de Química Analítica, Universitat de València, Dr. Moliner 50, 46100 Burjassot, Valencia, Spain
[b] Institute of Pharmaceutical Sciences, University of Tübingen, 72076 Tübingen, Germany

In this work, new polythiol-functionalized macroporous monolithic polymethacrylate-polysiloxane composite materials are presented which can be useful substrates for highly efficient immobilization of (chiral) catalysts, chromatographic ligands, and other functional moieties by thiol-ene click reaction. poly(GMA-*co*-EDMA) monoliths were coated with a poly-3-mercaptopropyl methylsiloxane (PMPMS) film and subsequently the polymer was covalently immobilized by formation of crosslinks via nucleophilic substitution reaction with pendent 2,3-epoxypropyl groups on the monolith surface. This monolith, though, showed similar levels of surface coverage as a reference monolith obtained by opening of the epoxide groups with sodium hydrogen sulfide. However, a 3-step functionalization by amination of the epoxy monolith, followed by its vinylation with allylglycidyl ether and subsequent thiolation by coating of a thin polythiol (PMPMS) film and crosslinking by click reaction furnished a monolith with more than 2-fold elevated thiol coverage. Its further functionalization with a clickable chiral quinine carbamate selector clearly documented the benefit of highly dense thiol surfaces for such reactions and synthesis of functional materials with proper ligand loadings. The new monoliths were chromatographically tested in CEC mode using *N*-3,5-dinitrobenzoyl-leucine as chiral probe and the capillary column with the monolith having the highest selector coverage, produced from the precursor with the most thiols on the surface, showed the largest separation

factor. By performic acid oxidation the surface characteristic could be tuned and strongly altered due to a delicate balance of enantioselective and non-specific interactions.

Keywords: Poly-3-mercaptopropyl methylsiloxane, O-9-tert-buylcarbamoyl quinine, thiol-covered surfaces, reactive monolith, capillary column, thiol-ene click reaction

9.1. Introduction

Porous monolithic materials that have emerged in early 1990s have become popular as stationary phases for liquid chromatography and related separation techniques [1-4]. Monolithic columns have high permeability [5], which enables excellent performance for the fast separation of large molecules such as proteins [6], DNA [7], and synthetic polymers [4]. The major categories of monolithic columns are those prepared from (i) silica and (ii) organic polymers. However, advantages of polymer-based over silica-based monoliths comprise simple and faster preparation, greater choices of surface functionalities, wider pH stability, and better biocompatibility. A variety of organic polymer monoliths based on polymethacrylate, polyacrylate, polyacrylamide and polystyrene have been described [8-10].

In contrast to the single step copolymerization [11-17], post-modifications of the monolith allow the independent tuning of mechanical and flow-through porous properties and surface chemistry of the parent monolith. The use of GMA, which carries an epoxy group, as a monomer is particularly useful to obtain monoliths which can be easily functionalized. Using EDMA as a crosslinker, poly(GMA-co-EDMA) monoliths with a highly reactive surface are obtained. Monoliths with a variety of chromatographic properties (ion-exchange, hydrophobic/hydrophilic, chiral, etc.) have been obtained by bonding amines [11,18-20], amino acids [21], poly(ethylene imine) [22], sodium sulfite [23], sodium-hydrogen sulfide [24], sulfuric acid [25] and a variety of chiral reagents [26-30] to GMA-based monoliths.

Thiols are prone to react either via radical or catalyzed processes under very mild conditions with a multitude of substrates, which makes them suitable as reactive moieties on solid chromatographic supports for surface functionalization. Thus, the high potential reactivity of thiols has been widely used for click chemistry reactions in the last years [24, 31-34]. However, this type of reaction is not new but has been already proposed by Salvadori et al. [35] for surface modification of silica and has been extensively used over

decades by Lindner's group for the preparation of particulate silica-based chiral stationary phases and modification of monoliths [36-37]. However, the direct one-step radical addition copolymerization of a functional monomer having a thiol group would not lead to a material with free thiol groups for subsequent ligand attachment by thiol-ene click reaction, as thiols participate in radical addition reaction and would not be present after polymerization [38]. In contrast, poly(GMA-*co*-EDMA) monoliths with thiol groups were easily synthesized and subsequently modified with quinine or phosphonic acid derivatives and the resulting columns were used for enantioseparations [24]. Additionally, thiol groups can be functionalized by a variety of reactions including radical addition, nucleophilic substitution, disulfide formation, Michael addition, and by coverage of the surfaces with gold, silver and other nanoparticles [32-34, 36]. Along this line, several studies were reported in which surface epoxide groups of poly(GMA-*co*-EDMA) were modified with sodium hydrogen sulfide [24], cysteamine [33] and cystamine [31] providing columns with thiol coverage between 0.7 and 1.1 mmol g^{-1} of thiol groups. However, these thiol contents should be improved with the aim to achieve high-coverage thiol surfaces, which is a demanding issue in the development of new materials.

The (multi-step) post-polymerization approach provides an excellent way of harmonizing incompatible reagents, including hydrophobic and hydrophilic substances, low solubility ion-pairing agents and oxidizing and reducing agents. Moreover, by bonding reactive polymers instead of grafting small molecules onto the monolith surface, provides tentacle-like phases with high surface coverage of functional groups and concomitant potential of achieving enhanced sample loading capabilities.

In this work, with the aim of obtaining monolithic capillary columns with a higher coverage of thiol functionalities, PMPMS was coated and then bonded to the surface epoxide groups of a poly(GMA-*co*-EDMA) monolith by formation of crosslinks. Since only a small fraction of the thiol groups of the

PMPMS chains are used for crosslinking the polythiol to the monolith, a new surface with many reactive thiol groups was generated. The remaining free thiol groups of bonded PMPMS can be used to attach other ligands in order to further modify the surface and adapt it for any specific chromatographic mode. Two distinct methodologies were pursued in this work to functionalize poly(GMA-*co*-EDMA) monoliths with PMPMS: (i) a direct dynamic functionalization comprising the coating of the epoxy monolith with a thin film of the PMPMS polymer, and (ii) a three-step functionalization approach in which the epoxy monolith was preactivated first with ammonia and then allyl glycidyl ether followed by thiol-ene click-attachment of the coated PMPMS polymer. In this latter approach, a spacer arm was introduced between the monolith surface and the PMPMS coating (Fig. 9.1). For each monolith, the concentration of thiol groups generated on the surface was determined [24]. Thiol-ene click reaction was then used for the post-functionalization of the thiol-covered surfaces with chiral anion-exchange type chromatographic ligand, namely *O*-9-*tert*-butylcarbamoyl-quinine (*t*-BuCQN, a quinine derivative). Further variants of PMPMS-coating based chiral monolithic columns were subsequently obtained, after functionalization with *t*-BuCQN, by oxidation of free thiols to sulfonate groups using performic acid whereby accessible thioethers on the monolith surface were also oxidized to sulfones. The chromatographic performances of the new thiol- and t-BuCQN-functionalized monolithic materials were tested by CEC using neutral, acid, basic and chiral solutes.

9.2. Experimental

9.2.1. Materials and other materials

GMA, EDMA, γ-MPS, (*R*,*S*)-N-3,5-dinitrobenzoyl-leucine (DNB-Leu), allyl glycidyl ether (AGE), 2,2'-dipyridyl disulfide (Aldithriol-2, 98%, DPDS), 2-mercaptoethanol and sodium hydrogen sulfide were from Aldrich (Milwaukee, WI, USA). HPLC-grade ACN and MeOH were from Scharlab (Barcelona, Spain). AIBN was from Fluka (Buchs, Switzerland). Sodium

dihydrogen phosphate and ortophosphoric acid were from Merck (Darmstadt, Germany). Thiourea as EOF marker, and several alkyl benzenes, anilines and benzoic acids (Riedel-de Häen, Seelze, Germany) were used as probes. PMPMS was from ABCR (Karlsruhe, Germany). Uncoated fused-silica capillaries of 33.5 cm total length and 375 µm O.D. × 100 µm I.D. (Polymicro Technologies, Phoenix, AZ, USA) were used. The effective monolithic bed length was 25 cm.

9.2.2. Instrumentation

To introduce the derivatizing reagents into the monolithic capillary columns, a syringe pump (Model 100, KD Scientific, New Hope, PA, USA) was employed. The washing steps used for monoliths in capillaries were performed with an HPLC pump (1100 series, Agilent Technologies, Waldbronn, Germany). For the CEC experiments, an HP^{3D}CE instrument (Agilent) equipped with a diode array UV detector (Agilent Technologies), and pressurized at both capillary ends with an external nitrogen supply, was used. The HPLC experiments were carried out on a 1100 series HPLC system equipped with a quaternary pump, a thermostatic column compartment and a diode array detector (Agilent Technologies). A Kromasil C18 column (5 µm particle size, 15 cm × 4.6 mm ID) from Teknokroma (Barcelona, Spain) was employed for these experiments.

9.2.3. Preparation of poly(GMA-co-EDMA) monolithic columns

Prior to the preparation of capillary columns, to ensure covalent attachment of the monolith to the inner wall of the fused-silica capillaries, surface modification with γ-MPS was performed as described [17,38]. The monoliths were prepared from polymerization mixtures by weighing GMA (20 wt%), EDMA (5 wt%), and a binary pore-forming solvent constituted by CYC (70 wt%) and DOD (5 wt%). AIBN (1 wt% with respect to the monomers) was added as polymerization initiator [11]. To obtain a clear solution, sonication for

10 min followed by purging with nitrogen for 10 more min was applied. The preconditioned capillary was filled with the polymerization mixture up to a length of 25 cm. Thermal polymerization was accomplished in an oven at 60 ºC for 20 h. Then, an HPLC pump was used to flush the columns for 30 min with MeOH to remove the pore-forming solvents and remaining unreacted monomers.

9.2.4. Functionalization of poly(GMA-co-EDMA) with sodium hydrogen sulfide (Method A)

A 2 M sodium hydrogen sulfide (NaSH) solution was freshly prepared in a 20:80 (v/v) mixture of MeOH and 0.1 M aqueous sodium dihydrogenphosphate. The solution was sonicated for a few minutes, filtered through a 0.45 µm nylon membrane, and the pH was adjusted to 8.15 with 2 M orthophosphoric acid. Using an HPLC pump, the capillaries containing the poly(GMA-*co*-EDMA) monolith were washed with the 20:80 (v/v) MeOH–water mixture. Then, the capillaries were flushed with 60 µL of the 2 M NaSH solution. For this purpose, a Hamilton syringe driven by a syringe pump at a flow rate of 30 µL h^{-1} was employed. After 2 h, the capillaries were connected to an HPLC pump and rinsed with the 20:80 (v/v) MeOH–water mixture, then with MeOH and finally with ACN. These monolithic columns were identified as R-SH.

9.2.5. Direct functionalization of poly(GMA-co-EDMA) with PMPMS by nucleophilic substitution (Method B)

Sonication was used to freshly prepare a 10% (v/v) solution of PMPMS in acetone. The monolithic capillary columns were first rinsed with acetone employing an HPLC pump. They were then flushed with 60 µL of the PMPMS solution using a Hamilton syringe driven by a syringe pump at a flow rate of 30 µL h^{-1}. After 2 h, the capillaries were connected to an HPLC pump to be rinsed

with acetone and ACN. These columns were identified as R-PMPMS (see column B, Fig. 9.1).

9.2.6. Functionalization of poly(GMA-co-EDMA) with PMPMS by a three-step click chemistry reaction scheme (Method C)

The capillaries containing the poly(GMA-*co*-EDMA) monoliths were first flushed with MeOH, followed by flushing with aqueous 4.5 M ammonia at 60 ºC for 2 h at a flow rate of 60 µL h^{-1}. Then, they were washed with MeOH until reaching pH 7 at the outlet. Then, the syringe pump was used to force a 4% (v/v) AGE aqueous solution at 60 ºC for 2 h at a flow rate of 60 µL h^{-1}. Afterwards, using an HPLC pump, the capillaries were washed with MeOH and acetone, and filled with a freshly prepared 10% (v/v) PMPMS solution in acetone (this solution also contained 1% AIBN). The columns were sealed with GC septa and maintained in an oven at 60 ºC, where the radical addition occurred. After 24 h, the capillaries were removed from the oven, and rinsed with acetone and MeOH. These columns were identified as R-NH-AGE-PMPMS (See column C, Fig. 9.1).

9.2.7. Evaluation of the thiol groups bonded to the monolith surfaces (DPDS assay)

The procedure for the determination of the thiol concentration on the monolith surface was taken from a previous work [24] with slight modifications. Thus, the capillaries were filled up with a 1.19 M DPDS solution in ACN using a syringe pump. The disulfide-exchange reaction was allowed to occur for 1 h in the capillary. Then, using an HPLC pump, the capillary was rinsed with ACN, and the eluate was collected in an HPLC micro-vial. The total volume of the eluate was established by weighing the micro-vial. A calibration curve was constructed by mixing a 0.1 M DPDS solution in ACN with standard solutions containing increasing amounts of 2-mercatoethanol. For all the standards, the reaction was allowed to take place for 1 h at room temperature.

The reaction product (pyridine-2-thione) and non-reacted DPDS were separated by gradient elution RP-HPLC on a Kromasil C18 column. Linear gradients from 5% to 90% acetonitrile in 20 min were carried out. The flow rate was 1 mL min^{-1} and the column temperature was 25 ºC; 20 µL aliquots were injected. The reaction product was detected at 343 nm and the excess reagent at 254 nm.

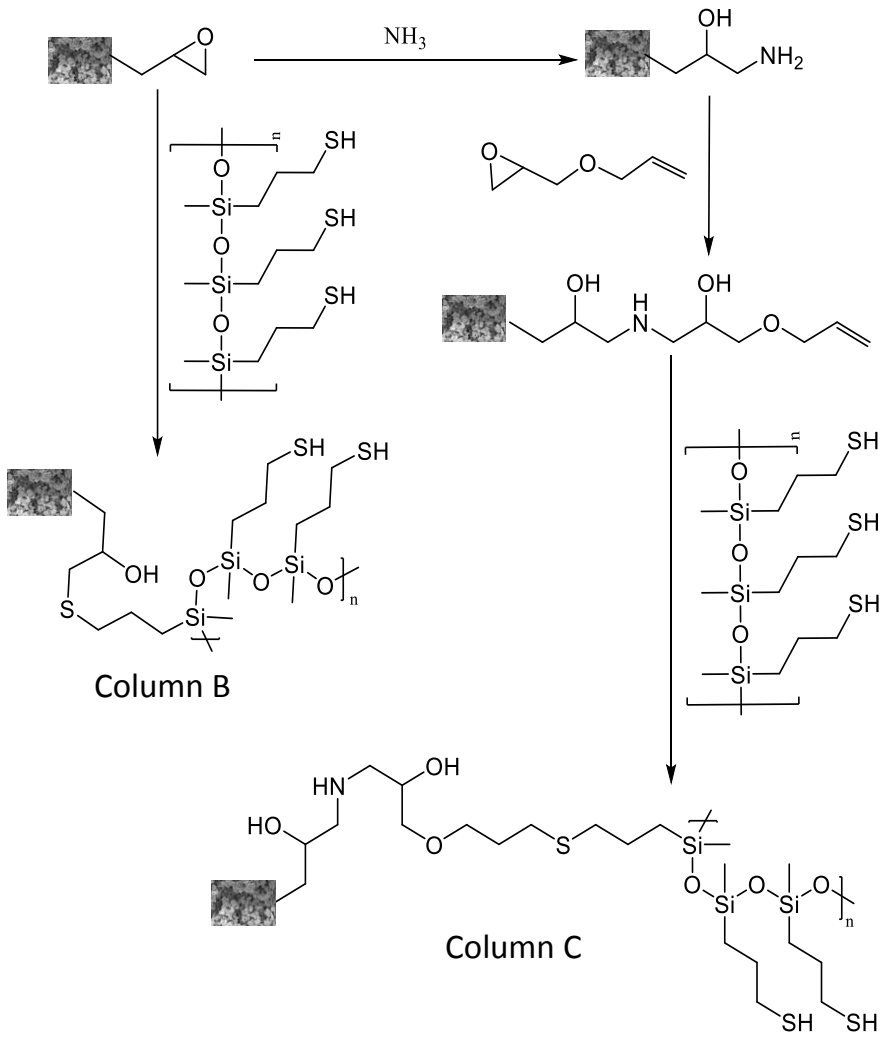

Fig. 9.1. Schemes used to bond PMPMS to the poly(GMA-co-EDMA) monolith surface.

9.2.8. In-column immobilization of t-BuCQN by radical addition

A 0.25 M *t*-BuCQN solution was prepared in MeOH and AIBN (6 mg mL^{-1}, 0.037 M) was added as radical initiator. The mixture was sonicated for 5 min, filtered through a nylon membrane and purged with nitrogen for 10 min. Then, the thiol-functionalized capillaries were filled up with the *t*-BuCQN solution using a syringe pump. The capillary ends were sealed with GC septa and the radical addition of the ligand was carried out in an oven at 60 ºC. After 24 h, the capillaries were removed from the oven and rinsed with MeOH (Fig. 10.2).

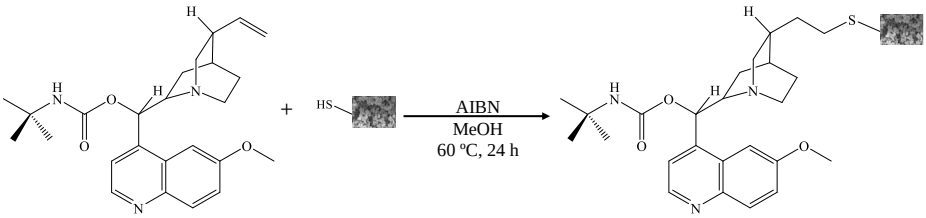

Fig. 9.2. Scheme used to bond the chiral selector (*t*-BuCQN) to the thiol modified surfaces.

9.2.9. Performic acid oxidation reaction

A performic acid solution was prepared by mixing formic acid (98%) and hydrogen peroxide (30% in water) (25:75; v/v). As a catalyst, orthophosphoric acid (1%) was added and the mixture was maintained at 40 ºC for 1 h. The capillaries containing the modified monoliths were first flushed for a few minutes with MeOH, followed by the performic acid solution for 2 h at room temperature at a flow rate of 60 µL h^{-1}. Then, the capillaries were washed with MeOH until reaching pH 7 at the outlet.

9.2.10. Chiral separations on the t-BuCQN-functionalized monolithic capillaries

(R,S)-DNB-Leu (1 mg mL^{-1} in the mobile phase) containing 100 µL of acetone as EOF marker was used as a probe for chiral separations. The mobile phase consisted of a 20:80 (v/v) MeOH-ACN mixture containing 400 mM

acetic acid and 4 mM triethylamine. Electrokinetic injections (10 kV for 10 s) were performed. The CEC separations were carried out at 10 kV and 25 ºC, and nitrogen was used to apply 10 bar on both capillary ends. Detection of the analytes at 230 nm and acetone at 280 nm was performed.

9.2.11. Non-chiral CEC separations using the t-BuCQN-functionalized monolithic capillaries

Mixtures of six alkyl benzenes (toluene and ethyl-, propyl-, butyl-, pentyl- and hexylbenzene), four benzoic acids (2,4-dihydroxybenzoic, 3,4-dihydroxy benzoic, vanillic and 4-nitrobenzoic acid) and four anilines (2-methoxy-4-nitroaniline, 2-amino-5-nitrotoluene, *N*,*N*-diethylaniline and 4-nitroaniline) were used as probes for RP-CEC separations in the presence of thiourea as EOF marker (100 µg mL^{-1} of each solute in the mobile phase). The mobile phase consisted of 50:50 (v/v) ACN-water containing 5 mM of an acetic acid/ammonium acetate buffer of pH 3. Electrokinetic injections (10 kV for 10 s) were performed. The electrochromatographic separations were carried out at 10 kV and 25 ºC, and nitrogen was used to apply 10 bar on both capillary ends. All the solutes were detected at 214 nm.

9.3. Results and Discussion

9.3.1. Functionalization of poly(GMA-co-EDMA) monoliths with PMPMS

9.3.1.1. Direct functionalization of poly(GMA-co-EDMA) monolith with PMPMS

A previously developed poly(GMA-*co*-EDMA) monolith [11] was used to prepare the thiol-modified columns. The polymerization mixture was constituted by 20 wt% GMA as reactive monomer, 5 wt% EDMA as crosslinker, and 70 wt% CYC and 5 wt% DOD as porogenic solvents. The monoliths prepared with this polymerization mixture showed a high permeability (large size flow-through pores of around 1–2 µm), which

enormously facilitated the rinsing steps employed in the surface modification procedures. However, the main advantage of this monolith was the higher epoxide concentration (5.63 instead of 4.22 mmol epoxide g^{-1} monolith) with respect to that described by Preinerstorfer *et al.* [24]. As discussed below, this difference was important in obtaining a higher density of reactive sites on the polymer surface. In this work, the epoxy groups were transformed into thiol groups by nucleophilic substitution and click chemistry reactions, respectively.

The yield of the surface modification reactions was controlled by determining the concentration of thiol groups bonded to the monolith surfaces. For this purpose, the DPDS assay (see section 9.2.7) was used to optimize the reaction conditions of surface functionalization with PMPMS in order to increase the density of reactive thiol groups on the surface of the modified monoliths [34].

A reference capillary column using the formerly employed approach of epoxy group derivatization with sodium hydrogen sulfide was prepared as well and will be henceforth referred to as capillary column of Method A. Thus, the poly(GMA-co-EDMA) monolith was first modified by rinsing with sodium hydrogen sulfide (NaSH) solution. The thiol content of the resulting R-SH (Method A) column, determined by the DPDS method, was 0.98 ± 0.03 mmol thiol g^{-1} monolith (n = 6 columns) versus the 0.70 mmol thiol g^{-1} monolith obtained in a previous work [24]. Thus, the monoliths prepared in this work effectively had a slightly larger density of reactive epoxy groups, which resulted in somewhat higher surface coverage with thiol groups. However, overall the thiol surface coverage found was still limited and rather similar to the values reported in the literature [24].

In order to further enhance the surface coverage, PMPMS was selected as new polythiol reagent to modify epoxy groups of the monolith. PMPMS is a viscous liquid at room temperature (*ca.* 175 cP), which generated high back pressures when it was pumped through the monolithic columns in pure

undiluted form. In order to reduce the viscosity of the reaction mixture, it was diluted with a solvent. The solubility of PMPMS was found to be too low in most common solvents (such as H_2O, ACN, MeOH, ethanol, dimethylsulfoxide and dimethylformamide). However, its solubility in acetone was excellent. Then, a 10% PMPMS (v/v) solution in acetone was used for monolith derivatization via SN_2 reaction (SN_2-type thiolation). This solution gave a back pressure compatible with syringe pump operation, and it was employed to perform functionalization studies at several temperatures and distinct reaction times.

Presumably, a part of the thiol groups of PMPMS were bound to the surface, and the unreacted thiol groups remain available for either solute interaction or further derivatization. After reaction of PMPMS with the monolith surface, the still available unreacted thiol groups on the monolith surface were determined by the DPDS assay. As observed in Fig. 9.3, at constant reaction time (2 h), the concentration of available thiol groups on the monolith surface slightly decreased as the capillary temperature in the course of PMPMS reaction was increased from 25°C to 40 and then 60°C. A possible explanation is the ocurrence of side-reactions, such as the formation of disulfides. However, even at 25 ºC, the concentration of thiol groups on the modified surface was limited (< 0.9 mmol thiol g^{-1} monolith) not exceeding the approach with NaSH (Method A). The problem could be due to a slow kinetics of the nucleophilic substitution reaction on the heterogeneous surface. Therefore, the reaction time was next increased by maintaining 25 ºC. However, the reaction yield did not improve by increasing the reaction time from 1 h up to 6 h. Further, these concentrations were lower than those achieved using sodium hydrogen sulfide as reagent (Method A) (R-SH columns, 0.98 mmol thiol g^{-1} monolith) instead of PMPMS. Possible reasons for this unexpected finding are: (i) low reactivity of the thiols at neutral conditions (as compared to basic catalysis of Method A), ii) hindered access of the large and bulky polymeric PMPMS molecules to the reactive epoxy groups on the

polymethacrylate surface, iii) excessive reaction of a large portion of the thiol groups of PMPMS, or iv) disulfide formation between thiols of adjacent pendent groups. To overcome the problem of limited thiol coverage, a different approach with a spacer arm in-between the monolith surface and the coated PMPMS layer was developed (*vide infra*). The columns obtained by direct functionalization with PMPMS, using the optimized conditions (2 h at 60 ºC), are below referred to as R-PMPMS (Method B) capillary columns.

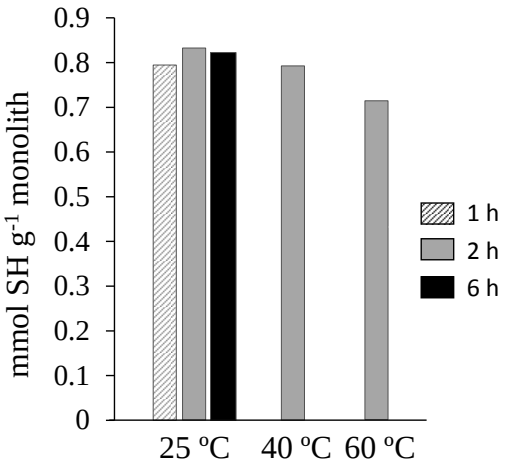

Fig. 9.3. Optimization of one-step direct functionalization of the poly(GMA-co-EDMA) monoliths with PMPMS. Effect of temperature (2 h reaction time) and time (at 25 ºC). The bars represent concentrations of reactive thiols bonded to the monolith.

9.3.1.2. Multi-step modification of poly(GMA-co-EDMA) monoliths with PMPMS

To increase the coverage of the monoliths with PMPMS, a surface functionalization procedure comprising the following three steps was developed (Method C): (i) conversion of the epoxy functionalities into amino moieties using ammonia (amination); (ii) attachment of allyl glycidyl ether (AGE) molecules to the ammonia groups (vinylation); and (iii) bonding of PMPMS thiol groups by means of a click reaction to the double bonds of AGE

(click-type thiolation). The key difference with respect to direct functionalization was the introduction of a spacing arm prior to bonding PMPMS and possibly a more efficient reaction type with higher yields (thiol-ene click reaction *versus* uncatalyzed SN_2 of Method B).

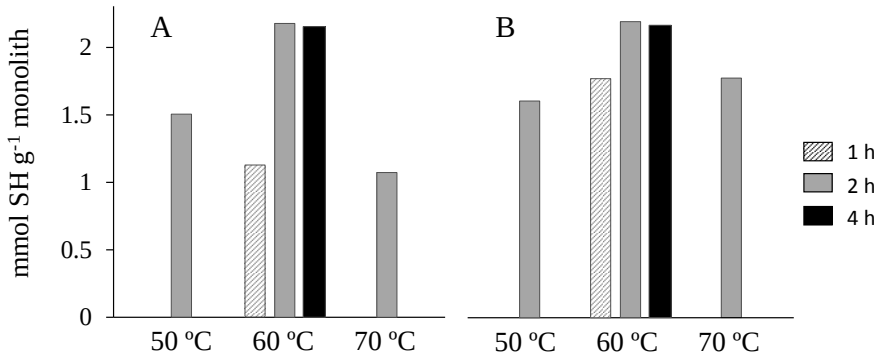

Fig. 9.4. Optimization of the 1st (amination) and 2nd (vinylation) steps of the monoliths. (A) Effect of temperature (2 h reaction time) and time (at 60 ºC) for the 1st step of the reaction scheme (attack to the surface epoxy groups with ammonia); the 2nd and 3rd steps were carried out at 60 ºC during 2 and 24 h. (B) Effect of temperature (2 h reaction time) and time (at 60 ºC) for the 2nd step of the reaction scheme, in which the bonded amino groups were derivatized with AGE; the 1st and 3rd steps were carried out at 60 ºC, during 2 h and 24 h, respectively. The bars represent final concentrations of reactive thiol groups bonded to the monolith after completing the reaction scheme.

The hypothesis was to increase the density of bonded PMPMS molecules by reducing the distance between the thiol groups of PMPMS and the reaction sites of the monolith. For this purpose, a first nucleophilic substitution step using 4.5 M ammonia in water was performed. The influence of both reaction temperature and time was also studied (Fig. 9.4A). For evaluation of these factors, the whole three-step derivatization procedure was carried out and the effect of the investigated factor was assessed by finally available thiol groups of the resulting monolith (after the 3rd step). All other factors, except for the one

explored, were kept constant. Thus, optimization of the 1st step (amination) was carried out by performing the 2nd (vinylation) and 3rd steps (click-type thiolation) at 60 ºC with reaction times of 2 h (vinylation) and 24 h (click-type thiolation), respectively. As can be seen from Fig, 9.4A, the concentration of available thiol groups increased from 50 ºC to 60 ºC (1.5 to 2.2 mmol thiol g^{-1} monolith), and decreased for 70 ºC. A possible explanation is that at temperatures over 60 ºC the competitive hydroxyl attack to the epoxide groups gets kinetically more important as side reaction. Similar findings have been described in previous works for the derivatization of epoxy groups with amines [11,24]. The effect of increasing the reaction time at 60ºC is also shown in Fig. 9.4A. As observed, a plateau was reached after 2 h (2.2 mmol thiol g^{-1} monolith) and no further gain in thiol concentration was found by doubling the reaction time to 4h. This indicated a maximal reaction yield for the amination step [11]. Thus, the selected conditions for the first (amination) step of the derivatization procedure were 4.5 M NH_3 (v/v) at 60 ºC for 2 h at a flow rate of 60 µL h^{-1}.

Optimization of the 2nd (vinylation) step of the procedure, namely nucleophilic substitution with a 0.34 M aqueous AGE solution at optimal amination and constant click-type thiolation conditions, is shown in Fig. 9.4B. A higher concentration of AGE in aqueous media was not possible due to miscibility problems. As can be seen from Fig. 9.4B optimal yields are furnished when the reaction was allowed to proceed with 0.34 M AGE solution in water at 60°C for 2 h with a flow rate of 60 µL h^{-1}.

Adopting optimal reaction conditions for the amination and vinylation step, the working conditions of the 3rd (click-type thiolation) step were finally optimized. The same 10% PMPMS solution (v/v) in acetone which was used for Method B was selected. However, a 1% AIBN (1:10 m/v ratio with respect to the PMPMS) was also added to start the click reaction [39]. Using a syringe pump, the PMPMS solution was flushed through the column at 60 µL h^{-1} for 30 min. First, a reaction time of 24 h was maintained, and the influence of the

reaction temperature was studied. As shown in Fig. 9.5, a plateau was reached between 60ºC and 70ºC (2.18 and 2.17 mmol thiol g^{-1} monolith, respectively). By maintaining 60ºC and increasing the reaction time from 24 to 48 h no further significant increase (2.18 and 2.24 mmol of thiol groups g^{-1} monolith, respectively) was observed. Thus, the selected conditions for the 3rd (click-type thiolation) step were 60ºC and 24 h. The columns obtained with this procedure are hence forth referred to as R-NH-AGE-PMPMS (Method C).

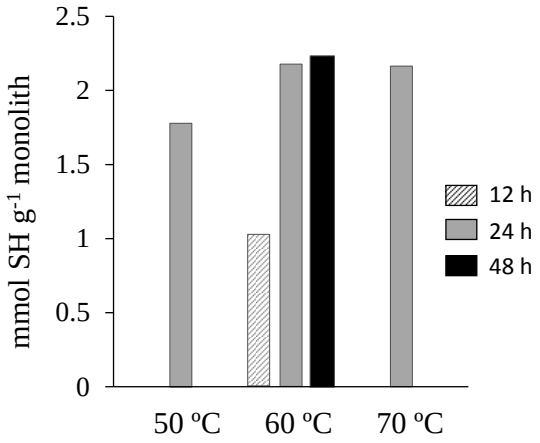

Fig. 9.5. Optimization of the 3rd step of the derivatization of the monoliths with PMPMS (derivatization of the double bond with PMPMS) (click-type thiolation step). Effect of temperature (24 h reaction time) and time (at 60 ºC). The 1st and 2nd steps were both carried out at 60 ºC, respectively, during 2 h; other details as in Figure 9.4.

In comparison to the R-SH (Method A) and R-PMPMS (Method B) columns, the R-NH-AGE-PMPMS (Method C) columns showed a *ca.* 2.7- and 2.3-fold increase in the concentration of available thiol groups, respectively. This novel thiol column also provided greatly enhanced reactive thiol coverages over those previously described in the literature for monoliths obtained with direct functionalization with sodium hydrogen sulfide [24] and thiol amino acids (3.2 and 2.1-fold, respectively) [32,33].

9.3.2. Post-functionalization with a clickable chiral selector

Above prepared monolithic supports could be valuable carriers for the synthesis of heterogeneous catalysts and chromatographic media as they offer high density of reactive functionalities for thiol-ene click functionalization. To document that elevated levels of reactive thiols can be beneficially translated into higher surface coverage of ligands accompanied with improved selectivity, a clickable chiral selector was bonded onto the thiol-monoliths obtained by Methods A, B and C. For this purpose, a quinine carbamate derivative, *t*-BuCQN, was selected.

According to a previous work, the immobilization yield of *t*-BuCQN on poly(GMA-co-EDMA) monoliths modified with sodium hydrogen sulfide (R-SH columns) was about 78% [24]. This value was calculated as the difference between the number of thiols found before and after the thiol-ene click reaction with *t*-BuCQN, divided by the number of thiols found before the reaction. In this work, similar percentage (77%) was found for the R-SH columns. Nevertheless, in absolute terms, the concentration of bonded *t*-BuCQN was much larger than that found in the previous work, *i.e.* 0.75 versus 0.55 mmol *t*-BuCQN g^{-1} monolith, respectively. This is in agreement with the higher concentration of epoxy groups on the surface of the monolith developed in this work. The relative *t*-BuCQN surface coverages were still higher for the R-PMPMS (Method B) and R-NH-AGE-PMPMS (Method C) columns than for the R-SH (Method A) columns, namely 82% (0.68 mmol *t*-BuCQN g^{-1} monolith) and 85% (1.85 mmol *t*-BuCQN g^{-1} monolith), respectively, instead of the 77% (0.75 mmol *t*-BuCQN g^{-1} monolith) for the reference R-SH (Method A) column. These incremental changes in the percentage of the surface coverage with *t*-BuCQN nicely correlated with the higher surface density of free thiol groups. Thus, in particular the new PMPMS-type surface functionalization according Method C is deemed to provide superior results in ligand-dependent chromatographic applications and represents a viable alternative to brush-type functionalization.

Table 9.1. CEC parameters for DNB-(R,S)-Leu in the investigated columns.

	Column [a]	t_1; t_2 (min) [b]	α (t_2/t_1)	N_1; N_2 (plates/m)	*Rs*	mmol SH g^{-1} monolith[c]	mmol *t*-BuCQN g^{-1} monolith[c]
Non-oxidized columns	R-S-*t*-BuCQN (A)	5.7; 6.4	1.1	13600; 10500	1.6	0.98	0.75
	R-PMPMS-*t*-BuCQN (B)	3.3; 4.5	1.4	1200; 200	0.8	0.83	0.68
	R-NH-AGE-PMPMS-*t*-BuCQN (C)	6.4; 10.6	1.7	1600; 1800	2.6	2.18	1.85
Oxidized columns	R-S(O_2)-*t*-BuCQN (A‘)	2.7; 3.2	1.2	47000; 16000	3.3	-	0.75
	R-PMPMS_{ox}-*t*-BuCQN (B‘)	1.75; 1.80	1.0	20000; 21000	0.5	-	0.68
	R-NH-AGE-PMPMS_{ox}-*t*-BuCQN (C’)	2.5; 3.3	1.3	1600; 2000	1.5	-	1.85

[a] The subscript “ox” indicates that the thio and thiol groups of PMPMS were oxidized.

[b] First eluted enantiomer always *R*-configuration.

[c] Thiol and chiral selector determined by the DPDS assay.

9.3.3. Performic acid oxidation subsequent to bonding of chromatographic ligand

Both, the polymethacrylate backbone as well as the polysiloxane film have some pronounced lipophilic character. It is well known from enantioselective chromatography that non-specific interactions with the support may deteriorate enantioselectivity [40-41]. Hydrophobic interactions between the lipophilic support surface of the polymethacrylate-polysiloxane composite material and chiral solutes such as the probe used herein might be detrimental. Consequently, it was considered to make the surface more polar by post-synthesis treatment with performic acid [42]. A performic acid solution was prepared as described by Showell et al. [43]. Thioether groups stemming from radical addition reactions between thiol and vinyl-moieties (thiolation reactions and ligand attachment) are thereby converted into sulfone groups, and free thiols are oxidized to sulfonic acid moieties. The more hydrophilic surface may show reduced non-specific interactions, e.g. due to repulsive electrostatic interactions with negatively charged test solutes such as DNB-Leu. The columns obtained by performic acid oxidation are, corresponding to their non-oxidized counterparts, denoted as A', B', and C', respectively.

9.3.4. Chromatographic characterization of the capillary column

The various quinine carbamate-bonded monolithic columns developed in this work were chromatographically evaluated with Dinitrobenzoyl-(*R,S*)-Leucine (DNB-(*R,S*)-Leu) in CEC mode. Test results for other probes (alkyl benzenes, benzoic acids and amines) are provided as Supplementary Material (Fig. S9.2 and Table S9.1). The test for enantiomer separation is the ultimate proof for the success of the surface functionalization because it needs sufficient surface coverage of chiral selector in order to furnish reasonable enantioselectivity. If the ligand density is too low, non-specific interactions with the support may become dominant which leads to a significant loss in

separation factors. The full set of test results on the various columns is summarized in Table 9.1 and chromatograms are given in Fig. 9.6.

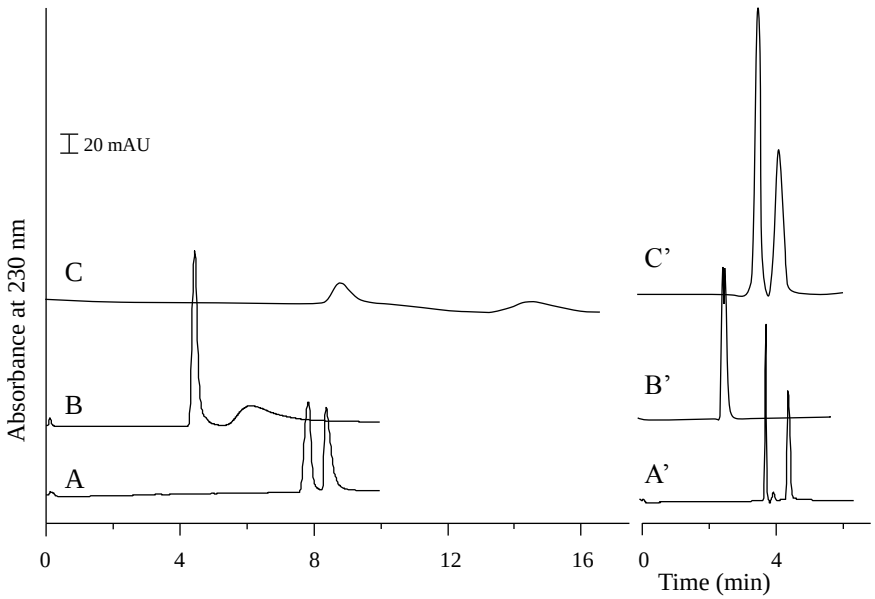

Fig. 9.6. Separation of DNB-(*R*,*S*)-Leu enantiomers on non-oxidized (left) and oxidized (right) R-SH (A, A'), R-PMPMS (B, B') and R-NH-AGE-PMPMS (C, C') columns. CEC conditions: mobile phase, 80:20 (v/v) ACN-MeOH containing 400 mM acetic acid and 4 mM triethylamine; electrokinetic injection, 10 kV × 10 s; separation voltage, 10 kV. First eluted peak was *R*-enantiomer and second one *S*-enantiomer.

It can be clearly seen from Fig. 9.6 and Table 9.1 that, before oxidation, the new PMPMS-based chiral capillary columns (prepared by Method B and C; see Fig. 9.6B and 9.6C, respectively) gave superior performance in terms of enantioselectivity as compared to the column synthesized by Method A (Fig. 9.6A). The highest separation factor was obtained for the chiral monolith prepared by Method C (α=1.7) (Fig. 9.6C). Not surprisingly, this is the column with the highest thiol and ligand coverages, respectively, clearly emphasizing the beneficial effect of the strategy to enhance the number of reactive entities

in the preactivation step for achieving higher selector densities which are important in affinity-type and chiral separations.

Oxidation perturbs these trends, yet the findings may be readily explained by the delicate interplay between non-specific interactions at the support backbone and enantioselective interactions at the chiral selector. The column obtained from Method A has presumably a low number of residual silanols. Thus, oxidation leads to a low number of oxidized species such as sulfonic acids. They can interact with the solute by electrostatic repulsion and reduce interactions of the acidic solute with the monolith backbone because they are electrostatically repelled. Yet, the interaction with the chiral selector moiety which is positively charged is still strong enough due to the low number of sulfonate groups. It leads to an improvement of separation factors upon oxidation of column A (α=1.1) to its oxidized counterpart column A' (α=1.2). The situation is different for columns C and C'. Due to the high thiol coverage, the residual thiol concentration after immobilization of the chiral selector is larger than the other columns. Hence, after oxidation repulsive electrostatic interactions with the solute may get dominant weakening the interactions at the chiral sites. The result is a decrease of both non-specific and enantioselective interactions as well with a more than over proportional effect of the weakened interactions at the chiral sites leading to significant loss in separation factors upon oxidizing column C to C' (Table 9.1). Details about the theoretical explanations of such a delicate interplay of enantioselective and non-specific interactions and their effect on observed separation factors can be found, among others [39]. Overall, the highest separation factor of all 6 tested columns was provided by column C, the column with the highest thiol and ligand loadings confirming our working hypothesis for this work.

Table 9.2. Repeatability and reproducibility (as RSD %) of functionalized monolith for column prepared by method C.

	Repeatability	Reproducibility	
Parameter	Run-to-run (same column) (n = 6)	Day-to-day (same column) (*n* = 6, 3 days)	Column-to-column (*n* = 3)
t_{EOF} (min)	1.2	2.2	5.8
k (propylbenzene)	1.3	2.7	6.7
H_{min} (μm)	1.9	3.3	8.1
mmol thiol groups g^{-1} monolith	-	-	2.4
mmol t-BuCQN g^{-1} monolith	-	-	3.2

t_{EOF}, elution time of electroosmotic flow marker; H_{min}, theoretical plate height at minimum of van Deemter curve as measured for propylbenzene (obtained from the van Deemter curve at different voltages from 2.5 to 15 kV (other conditions are in Fig. S9.1)

These results were compared with the copolymerized *t*-BuCQN monoliths with GMA and EDMA monomers [13]. As observed the non-oxidized column obtained from method C presents improves in the resolution of *ca.* 109 % and the efficiency was also improved in *ca.* 260 % [24]. On the other hand, the oxidized columns obtained from method C shows improvements in resolution and efficiency of 21 % and 300 %. Column reproducibility could be a critical factor. However, Table 10.2 clearly reveals that this is not the case. For all tested parameters, satisfactory RSD values (below 9%) were obtained for all synthesized columns.

9.4. Conclusions

Novel thiol-modified poly(GMA-*co*-EDMA) monoliths, obtained by coating PMPMS have been developed. The bonding chemistry involved a thiolation reaction by either nucleophilic substitution or thiol-ene click reaction. The direct functionalization of the GMA-based monoliths with the polythiol-film and SN_2-crosslinking reaction barely exceeded the approach of derivatizing epoxide groups using sodium hydrogen sulfide. However, when a three-step derivatization procedure (amination, vinylation with allyl glycidyl etherAGE and coating of the polythiol film by thiol-ene click reaction) was utilized a more than 2-fold molar increase in surface thiol concentrations could be accomplished. Such new polymethacrylate-polysiloxane composite materials with enhanced thiol coverage are supposed to be beneficial as substrates for materials like (chiral) catalysts and (affinity-type) adsorbents functionalized by thiol-ene click chemistry. Our proof of principle with a clickable chiral selector, viz. *t*-BuCQN quinine, confirmed this hypothesis. Elevated chromatographic ligand (i.e. chiral selector) densities could be accomplished which is of twofold importance, because i.) organic polymer monoliths have low surface areas due to absence of a dedicated mesoporous structure in their microglobules being accompanied by weak retention, and ii.) affinity-type and chiral separations need reasonable ligand coverages to achieve

sufficient selectivity and minimize the effect from non-specific interactions. In fact, the polythiol-based monolithic chiral column obtained by the three step synthesis procedure (highest thiol and ligand concentration) provided the largest separation factor for the DNB-(R,S)-Leu. Performic acid oxidation had a beneficial effect in the reference column but a negative effect for the polythiol-coated chiral monoliths indicating the sensitive interplay between enantioselective and non-specific interactions. Overall, the methodology presented here turns out to be an interesting and straightforward alternative for monolith functionalization and could be of great potential for synthesis of materials which exploit thiol-ene click reactions for functionalization of surfaces for various applications.

Acknowledgements

Project CTQ2010-15335 (MINECO of Spain and FEDER funds); E.J. C.-C. thanks the MINECO for an FPI grant and a bourse for a research stay in the University of Tübingen (Germany). M.L. acknowledges support by the "Struktur- und Innovationsfonds Baden-Württemberg (SI-BW)". This work was carried out at the laboratories of Tübingen (Germany) and University of Valencia (Spain).

References

[1] H. Aoki, N. Tanaka, T. KuBo, J. Polym. Sci. Part A: Polym. Chem., 46 (2008) 4651.

[2] R. Y. Zhang, G. L. Yang, P. Y. J. Xin, J. Chromatogr. A, 1216 (2009) 2404.

[3] M. Bedair, Z. E. Rassi, J. Chromatogr. A, 1079 (2005) 236.

[4] H. F. Wang, Y. Z. Zhu, J. P. Lin, Electrophoresis, 29 (2008) 952.

[5] Y. Y. Li, H. D. Tolley, M. L. Lee, J. Chromatogr. A, 1218 (2011) 1399.

[6] P. Y. Xin, Y. Shen, L. Qi, Talanta 85 (2011) 1180.

[7] S. Yamamoto, N. Yoshimoto, C. J. Tarmann, A. Jungbauer, J. Chromatogr. A, 1216 (2009) 2616.

[8] K. Štulík, V. Pacáková, J. Suchánková, P. Coufal, J. Chromatogr. B, 841 (2006) 79.

[9] V. Bernabé-Zafón, A. Cantó-Mirapeix, E.F. Simó-Alfonso, G. Ramis-Ramos, J. M. Herrero-Martínez, 30 (2009) 1929.

[10] A. Cantó-Mirapeix, J. M. Herrero-Martínez, C. Mongay-Fernández, E. F. Simó-Alfonso, 30 (2009) 607.

[11] E. J. Carrasco-Correa, G. Ramis-Ramos, J. M. Herrero-Martínez, J. Chromatogr. A, 1298 (2013) 61.

[12] M. Lämmerhofer, F. Svec, J.M.J. Fréchet, W. Lindner, J. Chromatogr. A, 925 (2001) 265.

[13] M. Lämmerhofer, E.C. Peters, C. Yu, F. Svec, J.M.J. Fréchet, W. Lindner, Anal. Chem., 72 (2000) 4614.

[14] M. Lämmerhofer, F. Svec, J.M.J. Fréchet, W. Lindner, Anal. Chem., 72 (2000) 4623.

[15] T. Koide, K. Ueno, J. Chromatogr. A, 909 (2001) 305.

[16] R. Hahn, A. Podgornik, M. Merhar, E. Schallaun, A. Jungbauer, Anal. Chem., 73 (2001) 5126.

[17] E.C. Peters, M. Petro, F. Svec, J.M.J. Fréchet, Anal. Chem., 69 (1997) 3646.

[18] V. Frankovič, A. Podgornik, N. L. Krajnc, F. Smrekar, P. Krajnc, A.

Štrancar, J. Chromatogr. A, 1207 (2008) 84.

[19] W. Wieder, C. P. Bisjak, C. W. Huck, R. Bakry, G. K. Bonn, J. Sep. Sci., 29 (2006) 2478.

[20] G. Yang, H. Liu, Y. Zhang, S. Wang, J. Yin, B. Yin, Y. Chen, J. Chromatogr. A, 1129 (2006) 231.

[21] X. Dong, J. Dong, J. Ou, Y. Zhu, H. Zou, Electrophoresis, 27 (2006) 2518.

[22] M. Wang, J. Xu, X. Zhou, T. Tan, J. Chromatogr. A, 1147 (2007) 24.

[23] Y. Ueki, T. Umemura, J. Li, T. Odake, K. Tsunoda, Anal. Chem., 76 (2005) 7007.

[24] B. Preinerstorfer, W. Bicker, W. Lindner, M. Laemmerhofer, J. Chromatogr. A, 1044 (2004) 187.

[25] Y. Wen, Y. Q. Feng, J. Chromatogr. A, 1160 (2007) 90.

[26] A. Messina, M. Flieger, F. Bachechi, M. Sinibaldi, J. Chromatogr. A, 1120 (2006) 69.

[27] B. Preinerstorfer, W. Lindner, M. Laemmerhofer, Electrophoresis, 26 (2005) 2005.

[28] A. Messina, M. Sinibaldi, Electrophoresis, 28 (2007) 2613.

[29] Y. Li, C. Song, L. Zhang, W. Zhang, H. Fu, Talanta, 80 (2010) 1378.

[30] Y. Tian, C. Zhong, E. Fu, Z. Zeng, J. Chromatogr. A, 1216 (2009) 1000.

[31] Y. Lv, Z. Lin, F. Svec, Analyst, 137 (2012) 4114.

[32] Y. Xu, Q. Cao, F. Svec, J. M. J. Fréchet, Anal. Chem., 82 (2010) 3352.

[33] Q. Cao, Y. Xu, F. Liu, F. Svec, J. M. J. Fréchet, Anal. Chem., 82 (2010) 7416.

[34] Y. Lv, F. Maya-Alejandro, J. M. J. Fréchet, F. Svec., J. Chromatogr. A, 1261 (2012) 121.

[35] C. Rosini, P. Altemura, D. Pini, C. Bertucci, G. Zullino, P. Salvadori, J. Chromatogr. A, 348 (1985) 79.

[36] E. Veigl, B. Boehs, A. Mandl, D. Krametter, W. Lindner, J. Chromatogr. A, 694 (1995) 151.

[37] M. Guerrouache, S. Mahouche-Chergui, T. Mekhalif, T. T. H. Dao, M. M. Chehimi, B- Carbonnier, Surf. Interface Anal., 46 (2014) 1009.

[38] E. C. Peters, M. Petro, F. Svec, J. M. J. Fréchet, Anal. Chem., 70 (1998) 2288.

[39] S. Constantin, W. Bicker, E. Zarbl, M. Lämmerhofer, W. Lindner, Electrophoresis, 24 (2003) 1668.

[40] J. Samuelsson, R. Arnell, T. Fornstedt, J. Sep. Sci., 32 (2009) 1491.

[41] R. J. Collins, C. N. Sukenik, Langmuir, 11 (1995) 2322.

[42] H. C. Kolb, K. B. Sharpless, Drug. Discover. Today, 8 (2003) 1128.

[43] J. S. Showell, J. R. Russell, D. J. Swern, J. Org. Chem., 27 (1962) 2853.

Supplementary Information

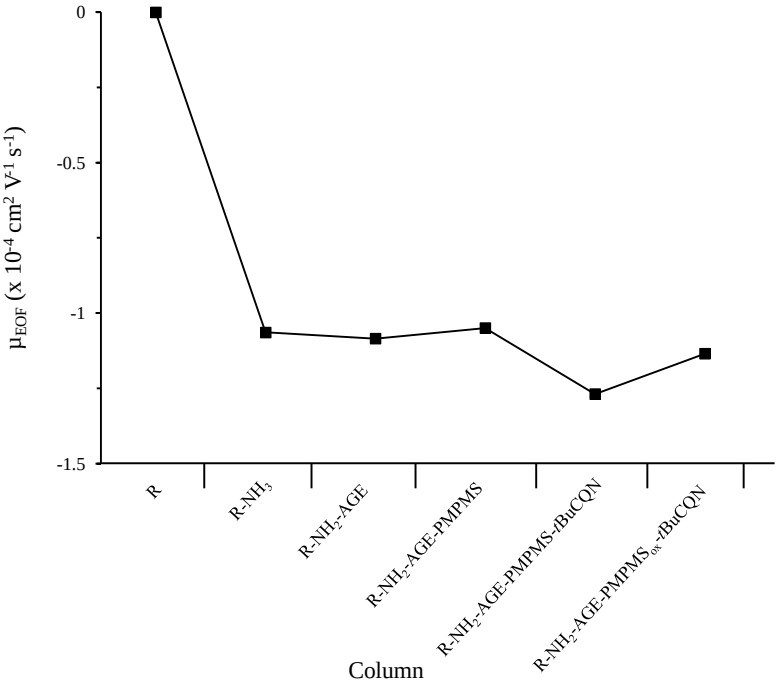

Figure S9.1. EOF measured after each step of surface functionalization with acetone as EOF marker. The mobile phase consisted of a 20:80 (v/v) MeOH-ACN mixture containing 400 mM acetic acid and 4 mM triethylamine. Electrokinetic injections (-10 kV for 10 s) were performed. The CEC separations were carried out at -10 kV and 25 ºC, and nitrogen was used to apply 10 bar on both capillary ends. Detection of acetone was performed at 280 nm.

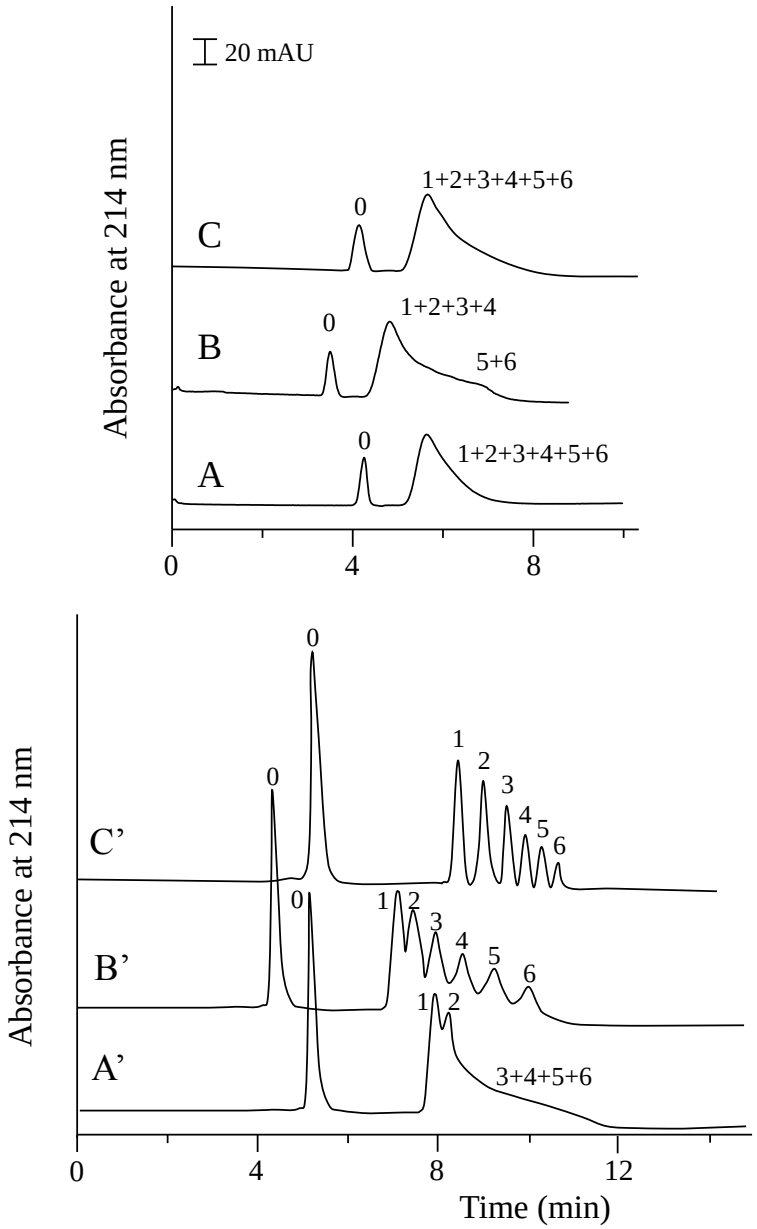

Figure S9.2. Separation of alkyl benzenes on the non-oxidized (up) and oxidized (down) R-SH (A, A'), R-PMPMS (B, B') and R-NH-AGE-PMPMS (C, C') columns. CEC conditions: mobile phase, 50:50 (v/v) ACN-water containing 5 mM acetic acid/acetate buffer of pH 3.0; electrokinetic injection, -5 kV × 3 s; separation voltage, -10 kV. Peak identification: (0) thiourea; (1) toluene, (2) ethyl benzene, (3) propyl benzene, (4) butyl benzene, (5) pentyl benzene and (6) hexyl benzene.

Table S9.1.

CEC parameters for alkyl benzenes, benzoic acid derivatives and anilines in the investigated columns[a]

		Column	t_1; t_6 (min) [b]	*N (plates/*m) [c]
Alkyl benzenes	Non-oxidized columns	R-S-*t*-BuCQN (A)	4.3; 4.3	300
		R-PMPMS-*t*-BuCQN (B)	3.5; 5.1	800
		R-NH-AGE-PMPMS-*t*-BuCQN (C)	4.0; 4.0	160
	Oxidized columns	R-S(O_2)-*t*-BuCQN (A‘)	5.7; 7.3	15000
		R-PMPMS$_{ox}$-*t*-BuCQN (B‘)	5.1; 7.3	37000
		R-NH-AGE-PMPMS$_{ox}$-*t*-BuCQN (C’)	6.1; 7.8	118000

		Column	t_1; t_4 (min) [b]	*N (plates/*m) [c]
Benzoic acids	Non-oxidized columns	R-S-*t*-BuCQN (A)	1.3; 1.4	1600
		R-PMPMS-*t*-BuCQN (B)	4.0; 4.5	3600
		R-NH-AGE-PMPMS-*t*-BuCQN (C)	5.5; 6.5	2000
	Oxidized columns	R-S(O_2)-*t*-BuCQN (A‘)	1.3; 1.8	1700
		R-PMPMS$_{ox}$-*t*-BuCQN (B‘)	1.5; 2.3	6400
		R-NH-AGE-PMPMS$_{ox}$-*t*-BuCQN (C’)	2.0; 3.0	58000

		Column	t_1; t_4 (min) [b]	*N (plates/*m) [c]
Anilines	Non-oxidized columns	R-S-*t*-BuCQN (A)	4.3; 4.3	2100
		R-PMPMS-*t*-BuCQN (B)	4.6; 4.6	5400
		R-NH-AGE-PMPMS-*t*-BuCQN (C)	5.9; 5.9	6200
	Oxidized columns	R-S(O_2)-*t*-BuCQN (A‘)	2.3; 2.3	2700
		R-PMPMS$_{ox}$-*t*-BuCQN (B‘)	2.2; 2.6	7000
		R-NH-AGE-PMPMS$_{ox}$-*t*-BuCQN (C’)	2.5; 2.9	40000

[a] Separation conditions and peak identification are indicated in Figures S1 (alkyl benzenes); other details as in Table 1.

[b] Retention times for the first and last eluted solutes.

[c] Maximal values of efficiency achieved for the solutes

[d] Maximal resolution achieved for the pairs of consecutively eluted solutes.

Chapter 10. Zwitterionic codeine-derived methacrylate monoliths for enantioselective capillary electrochromatography of chiral acids and chiral bases

Journal of Chromatography A,XXXX (2015) XX-XX

Contents lists available at SciVerse ScienceDirect

Journal of Chromatography A[1]

journal homepage: www.elsevier.com/locate/chroma

Zwitterionic codeine-derived methacrylate monoliths for enantioselective capillary electrochromatography of chiral acids and chiral bases

Enrique Javier Carrasco-Correa[a,b], Guillermo Ramis-Ramos[a], José Manuel Herrero-Martínez[a], Michael Lämmerhofer[b], Wolfgang Lindner[c,*]

[a]Department of Analytical Chemistry, University of Valencia, Dr. Moliner 50, 46100 Burjassot, Valencia, Spain
[b]Institute of Pharmaceutical Sciences, University of Tübingen, Auf der Morgenstelle 8, 72076 Tübingen, Germany
[c]Department of Analytical Chemistry, University of Vienna, Waehringer Strasse 38, 1090 Vienna, Austria

[1] **Submitted**

The preparation of a *de novo* designed low molecular mass chiral selector based on the thiol-ene click addition of *N*-acetyl-L-cysteine methyl ester to codeine, followed by reaction with allyl isocyanate and hydrolysis to the corresponding zwitterionic chiral selector, is described. This zwitterionic codeine-derived chiral selector was bonded to the surface of a methacrylate monolith by means of four successive reactions. First, the epoxy groups were converted into amine residues, followed by reaction with AGE. In this way, a spacer arm was bonded to the surface before coating and cross-linking PMPMS via radical addition (thiol-ene click reaction) to the surface. In order to improve the performance of the monolithic chiral stationary phase, thio ether and residual thiol groups were oxidized to sulfonyl and sulphonate groups, respectively. This novel chiral stationary phase (CSP) was evaluated by CEC using two chiral model compounds, namely DNB-(R,S)-Leu (retained by anion-exchange mechanism) and mefloquine (by cation-exchange process). The ion-exchange retention mechanism on the CSP was characterized for these two counterionic model solutes by varying the mobile phase composition, including the nature of solvents, the concentration of counter-ions and co-ions, and the acid-to-base ratio. A series of chiral β-blockers and amino acid derivatives was used to further check the performance of the modified monolith under the optimal conditions. In all cases, the pairs of enantiomers were

baseline resolved, with good peak efficiencies (up to 60000 theoretical plates per meter for the second eluted enantiomer).

Keywords: capillary electrochromatography; zwitterionic chiral stationary phase; mercaptopolysiloxane coating; high-density thiol covered methacrylate; codeine derivative; enantioselective ion-exchange.

10.1. Introduction

The development of monolithic separation media for CEC and related techniques, initiated two decades ago, is still attracting considerable interest. Within the two main types of monolithic materials, the advantages of polymer-based over silica-based monoliths are a simpler and faster preparation, greater choices of surface functionalities, wider pH stability and better biocompatibility. A variety of organic polymer-based monoliths based on different chemistries [1,2] have been extensively investigated. Among them, poly(GMA-*co*-EDMA), monoliths enable straightforward and efficient derivatization at the epoxy group by nucleophilic substitution reactions (SN_2) [3–29]. In contrast to single step copolymerization approaches, functionalization of the monolith surface allows the independent tuning of the mechanical and flow-through porous properties and of the surface chemistry of the parent monolith. Functionalization of GMA-based monoliths with amines [4–7], amino acids [8], sodium hydrogen sulfide [9], sulfuric acid [10] and a variety of chiral reagents [11,30–32], to provide monoliths with different chromatographic properties (ion-exchange, hydrophobic/hydrophilic, chiral, etc.), has been described. Besides such GMA-based chirally functionalized monoliths in-situ chiral organic monoliths [33–36] and chirally functionalized silica monoliths [37–40] have been described as reviewed recently [41]. Recently, a new strategy for functionalization of organic polymer monoliths by coating with PMPMS leading to monolithic composite materials with high surface coverage of reactive thiols for bonding of ligands by thiol-ene click chemistry has been disclosed [3]. Advantageously, only minute quantities of ligands are required due to the capillary format, which avoids preparing large amounts of chiral selectors for early functional tests, and enables use of expensive ligands as well as those requiring complicated multistep synthesis procedures.

Enantioselective chromatography or electrochromatography employing CSPs are major techniques for the separation of enantiomers [15–26,42–47]. At

the analytical level, enantioselective chromatography is a powerful tool for the analysis of racemic or enantio-enriched mixtures, including the determination of the enantiomeric excess. CSPs of many different types have been synthetized along the last decades, and a large number of them have become commercially available. Polysaccharide based materials are the most prominent type of commercial CSPs due to their very broad spectrum of enantioselectivity towards different classes of chiral compounds [27]. Other commercial CSPs are based on proteins [16,28], synthetic polymers [18], cyclodextrins [29], macrocyclic antibiotics [19,20], crown ethers [21,26], synthetic organic chiral molecules such as trans-1,2-diamino-cyclohexane derivatives [23] and 4-(3,5-dinitrobenzamido)-*1*,2,3,4-tetrahydrophenanthrene (Whelk O1) [46], and quinine derivatives [3,9,15,24,25].

In a continuous effort to develop more efficient chiral media and chromatographic conditions for direct stereoselective separations of ionic chiral solutes, ion-exchanger type CSPs with remarkably broad applicability for the dedicated class of chiral compounds have been developed [48–50]. Yet, applicability of chiral cation-exchangers is restricted to chiral bases [15] and that of chiral anion-exchangers to chiral acids [51,52]. It was only recently shown that application profiles of ion-exchangers can be combined by use of zwitterionic chiral selectors through hybridizing chiral cation- and chiral anion-exchanger functionalities into zwitterionic cinchona alkaloid derivatives [24,50,53]. However, the introduction of zwitterionic low molecular mass chiral selectors to organic monoliths and their use as chiral stationary phases in CEC has not been reported yet.

In this work, a new zwitterionic chiral selector is presented which has been derived from the morphinane alkaloid codeine (COD). It was immobilized on a parent GMA-based monolithic stationary phase, which was first functionalized with PMPMS via a three-step surface derivatization process followed by bonding of the chiral selector through thiol-ene click reaction according to a procedure described recently [3] (See Chapter 9). This process

of ligand immobilization gives rise to a surface with a high density of thiol groups and consequently also high chiral selector coverage [3]. The novel chiral selector, the codeine derivative, which was bound to the free thiol groups of PMPMS-based monolith, was prepared by coupling COD and *N*-acetyl-L-cysteine methyl ester (NACME) followed by reaction with allyl isocyanate (AIC). Prior to bonding to the monolith surface, hydrolysis of the methyl ester group of the NACME moiety into a free carboxylate group was carried out. Intermediates and final product of the synthesis of COD-NAC-AIC were purified by HPLC and analyzed by chiral HPLC, MS and ^{1}H and ^{13}C NMR. After bonding the chiral selector (CS) to the PMPMS-modified monolith surface, performic acid was used to oxidize thio ether (R-S-R') and free thiol groups, to sulfonyl and sulfonate groups, respectively. This post-modification treatment was useful to modulate the surface character and remove unwanted solute retention sites [3].

Resultant chiral selector and surface of the monolith, respectively, revealed zwitterionic nature, and thus, this monolith exhibited ion-exchange retention for both anions and cations. A series of both basic and acidic chiral solutes (Fig. 10.1) was used to test the CSP in CEC mode. In particular, DNB-(R,S)-Leu and mefloquine, were used for optimization of experimental conditions as well as to characterize the CSP. The influence of the mobile phase composition, including the nature of the solvents, and nature and concentration of the counterion and co-ion, respectively, and the acid-to-base ratio was investigated to reveal factors involved in the retention process, thus providing some insight into retention and separation mechanism of this chiral monolithic material.

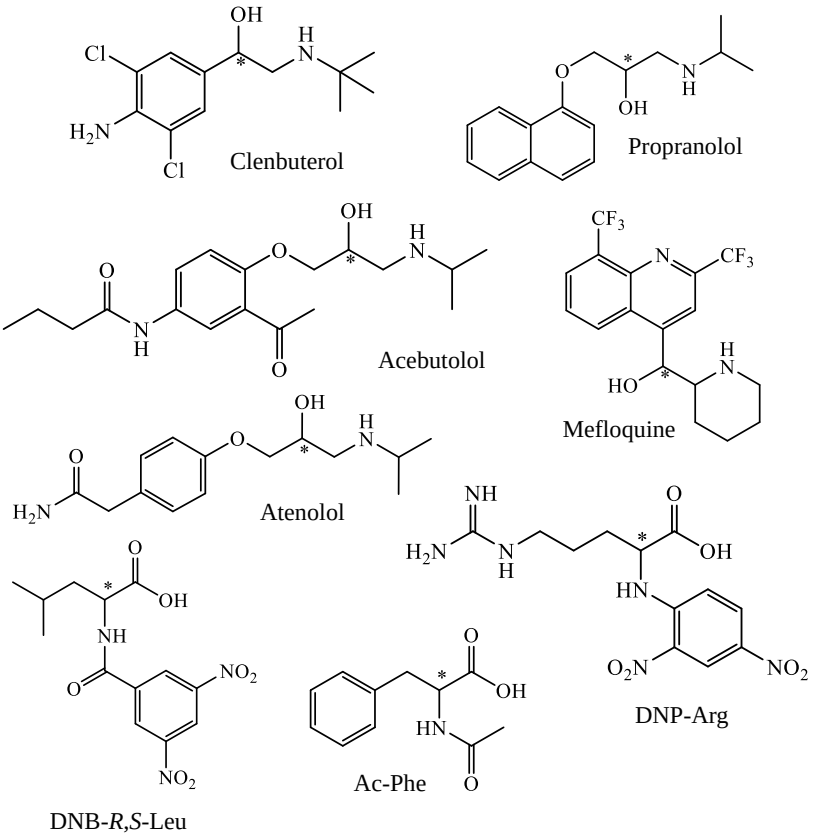

Fig. 10.1. Overview of chiral analytes used in the presented study. Abbreviations: dinitrobenzoyl-R,S-leucine (DNB-*R*,*S*-Leu); N-acetyl-R,S-phenylalanine (Ace-*R*,*S*-PheAla); N-(2,4-dinitrophenyl)-*R*,*S*-arginine (DNP-*R*,*S*-Arg).

10.2. Materials and methods

10.2.1. Chemicals and other materials

GMA, EDMA, γ-MPS, COD ((*5R*,*6S*,*9R*,*13S*,*14R*)-4,5-epoxy-3-methoxy-*N*-methyl-7-morphinen-6-ol), *N*-acetyl-L-cysteine methyl ester (NACME), AIBN, formic acid (FA), HAcO, DEA, triethylamine (TEA), AGE, DPDS, 2-mercaptoethanol and AIC were from Aldrich (Milwaukee, WI, USA). PMPMS was from ABCR (Karlsruhe, Germany). CYC, DOD, 1-PrOH, HPLC-grade ACN and MeOH were from Merck (Darmstadt, Germany). All chemicals used for synthesis were of reagent grade quality or higher, purchased from Sigma-

Aldrich and used without further purification. Chiral solutes, including basic and acidic compounds were used as test solutes (Fig. 10.1). All the test solutes were either commercially available or kindly donated by pharmaceutical companies. Uncoated fused-silica capillaries of 33.5 cm total capillary length and 375 µm O.D. x 100 µm I.D (Polymicro Technologies, Phoenix, AZ, USA) were used. The effective monolithic bed length was 25 cm.

10.2.2. Instrumentation

To introduce the derivatizing reagents into the monolithic capillary columns, a syringe pump (Model 100, KD Scientific, New Hope, PA, USA) was used. Conditioning of the monolithic columns was carried out with an HPLC pump (1100 Series, Agilent Technologies). CEC experiments were performed on a $HP^{3D}CE$ instrument (Agilent) equipped with a diode array UV detector, and pressurized at both capillary ends with an external nitrogen supply. The HPLC experiments were carried out on an HPLC system (1100 Series, Agilent) equipped with a quaternary pump, a thermostatic column compartment and a diode array detector. An Agilent Eclipse XDB-C18 column (5 µm, 15 cm × 4.6 mm ID) and a *t*-BuCQN) modified silica column (5 µm, 15 cm × 4.6 mm ID), commercially available as Chiralpak QN-AX (Chiral Technologies Europe, Illkirch, France), were also used. Data acquisition was performed with the ChemStation Software (Rev.A.10.01, Agilent). All mobile phases for CEC were degassed by ultrasonication.

10.2.3. Preparation of poly(GMA-co-EDMA) monolithic columns

Prior to the preparation of the columns, to ensure covalent attachment of the monolith to the inner wall of the fused-silica capillaries, surface modification with γ-MPS was performed as described [54,55]. The monoliths were prepared from polymerization mixtures by weighing GMA (20 wt%), EDMA (5 wt%), and a binary pore-forming solvent constituted by CYC (70

wt%) and DOD (5 wt%). AIBN (1 wt% with respect to the monomers) was added as polymerization initiator. To obtain a clear solution, sonication for 10 min followed by purging with nitrogen for 10 additional min was applied. The preconditioned capillary was filled with the polymerization mixture up to a length of 25 cm. Thermal polymerization was accomplished in an oven at 60 ºC for 20 h. Then, an HPLC pump was used to flush the columns for 30 min with MeOH to remove the pore-forming solvents and remaining unreacted monomers.

10.2.4. Synthesis of the chiral selector

The chiral selector, (*2R*)-2-acetamido-3-{[(*5R,6R,7R,9R,13S,14R*)-6-allylcarbamoyloxy-4,5-epoxy-3-methoxy-*N*-methyl-morphinan-7-yl]-thio}-propanoic acid (COD-NAC-AIC) was prepared as depicted in Fig. 10.2. First, methyl (*2R*)-2-acetamido-3-{[(*5R,6R,7R,9R,13S,14R*)-6-allylcarbamoyloxy-4,5-epoxy-3-methoxy-*N*-methyl-morphinan-7-yl]-thio}-propanoate (COD-NACME) was prepared from a solution of COD (1.05 g, 3.5 mmol) by reaction with NACME in MeOH (10 mL). The COD solution was doped with 10 mg AIBN (0.06 mmol, 1% with respect to codeine), and 0.88 g NACME (5 mmol) was added. The mixture was placed in an oven at 60 ºC for 24 h. The stereoisomeric purity of COD-NACME was controlled by RP-HPLC and chiral chromatography (see section 10.2.5). Only one stereoisomer of the compound was found. Then, the product was purified by preparative RP-HPLC (see section 10.2.5). For this purpose, fractions were collected, combined and dried overnight with a rotatory evaporator. The solid was recrystallized from THF affording off-yellow crystals (1.58 g, 94.8%). ^{1}H NMR [DMSO-d6]: δ = 8.32 (s, 1H), 6.60 (d, J = 7.5 Hz, 1H), 6.55 (d, J = 7.5 Hz, 1H), 5.37 (s. 1H), 4.70 (d, J = 7.0 Hz, 1H), 4.31 (m, J = 7.8, 9.0 Hz, 1H), 3.92 (d, J = 7.8 Hz, 1H), 3.82 (s, 3H), 3.66 (s, 3H), 3.05 (m, J = 12.4, 7.0 Hz, 2H), 2.91 (m, J = 12.4, 7.0, 2H), 2.48 (m, J = 9.0, 11.9, 11.9 Hz, 1H), 2.46 (m, J = 12.4, 7.1 Hz, 2H), 2.26 (s, 3H), 2.23 (m, J = 7.0, 7.0 Hz, 1H), 1.84 (m, J = 12.4, 11.9, 12.1 Hz, 4H), 1.73

(m, J = 12.4, 7.1 Hz, 2H), 1.59 (m, J = 12.4, 11.9, 12.1 Hz, 1H), 1.25 (m, J = 7.0, 12.1; 12.1 Hz, 1H). ^{13}C NMR: δ = 178.6 (C), 171.5 (C), 147.7 (C), 142.5 (C), 126.8 (C), 126.2 (C), 120.4 (CH), 113.7 (CH), 95.4 (CH), 79.2 (CH), 67.2 (CH), 56.5 (CH), 56.1 (CH3), 51.9 (CH3), 48.2 (C), 47.7 (CH2), 45.1 (CH), 43.7 (CH3), 33.8 (CH2), 31.6 (CH2), 26.8 (CH), 25.3 (CH2), 23.3 (CH3), 20.4 (CH2). MS (ESI, positive): 477.2 $[M + H]^+$, 302.2 $[M – C6H9NO3S]^+$. HRMS (ESI-TOF) *m/z*: $[M+H]^+$ Calcd $C_{24}H_{33}N_2O_6S$: 477.2059; Found: 477.2111.

Next, a solution of the COD-NACME product (1.5 g, 3.15 mmol) in 10 mL of anhydrous THF was mixed with an excess of AIC (1 g, 12 mmol), and 0.1% TEA was added as a catalyst. The solution was stirred at 35 ºC for 5 h and the mixture was left overnight at room temperature. Then, the solution was dried in a rotatory evaporator to eliminate the excess of AIC.

Afterwards, the product (COD-NACME-AIC) was purified by RP-HPLC (see section 10.2.5). Thus, fractions were collected, combined and subsequently evaporated to dryness with a rotary evaporator (1.27 g, 72.2%). ^{1}H NMR [DMSO-d6]: δ = 8.32 (s, 1H) 8.25 (s, 1H), 6.60 (d, J = 7.5 Hz, 1H), 6.55 (d, J = 7.5 Hz, 1H), 5.84 (m, J = 6.2; 16.8, 10.0 Hz, 1H), 5.38 (m, J = 7.8, 9.1 Hz, 1H), 5.19 (m, J = 1.0, 2.1, 16.8 Hz, 1H), 5.06 (m, J = 1.0, 2.1, 10.0 Hz, 1H), 4.70 (d, J = 7.0 Hz, 1H), 4.51 (d, J = 7.8 Hz, 1H), 4.04 (m, J = 6.2, 1.0, 1.0 Hz, 2H), 3.82 (s, 3H), 3.66 (s, 3H), 3.07 (m, J = 9.1, 11.9, 11.9 Hz, 1H), 3.05 (m, J = 12.4, 7.0, 2H), 2.91 (m, J = 12.4, 7.0 Hz, 2H), 2.46 (m, J = 12.4, 7.1 Hz, 2H), 2.26 (s, 3H), 2.23 (m, J = 7.0, 7.0 Hz, 1H), 1.84 (m, J = 12.4, 11.9, 12.1 Hz, 4H), 1.73 (m, J = 12.4, 7.1 Hz, 2H), 1.59 (m, J = 12.4, 11.9, 12.1 Hz, 1H), 1.25 (m, J = 7.0, 12.1, 12.1 Hz, 1H). ^{13}C NMR: δ = 178.6 (C), 171.5 (C), 158.6 (C), 147.7 (C), 142.5 (C), 134.2 (CH), 126.8 (C), 126.2 (C), 120.4 (CH), 117.4 (CH2), 113.7 (CH), 91.8 (CH), 81.1 (CH), 67.2 (CH), 56.5 (CH), 56.1 (CH3), 51.9 (CH3), 48.4 (C), 47.7 (CH2), 43.7 (CH3), 43.4 (CH2), 41.5 (CH), 33.5 (CH2), 31.3 (CH2), 26.5 (CH), 25.5 (CH2), 23.3 (CH3), 20.4 (CH2).

MS (ESI, positive): 560.3 $[M + H]^+$, 477.2 $[M – C_4H_4NO]^+$, 385.2 $[M – C_6H_9NO_3S]^+$, 302.2 $[M – C_{10}H_{14}N_2O_4S]^+$. HRMS (ESI-TOF) *m/z*: $[M+H]^+$ Calcd $C_{28}H_{38}N_3O_7S$: 560.2430; Found: 560.2562.

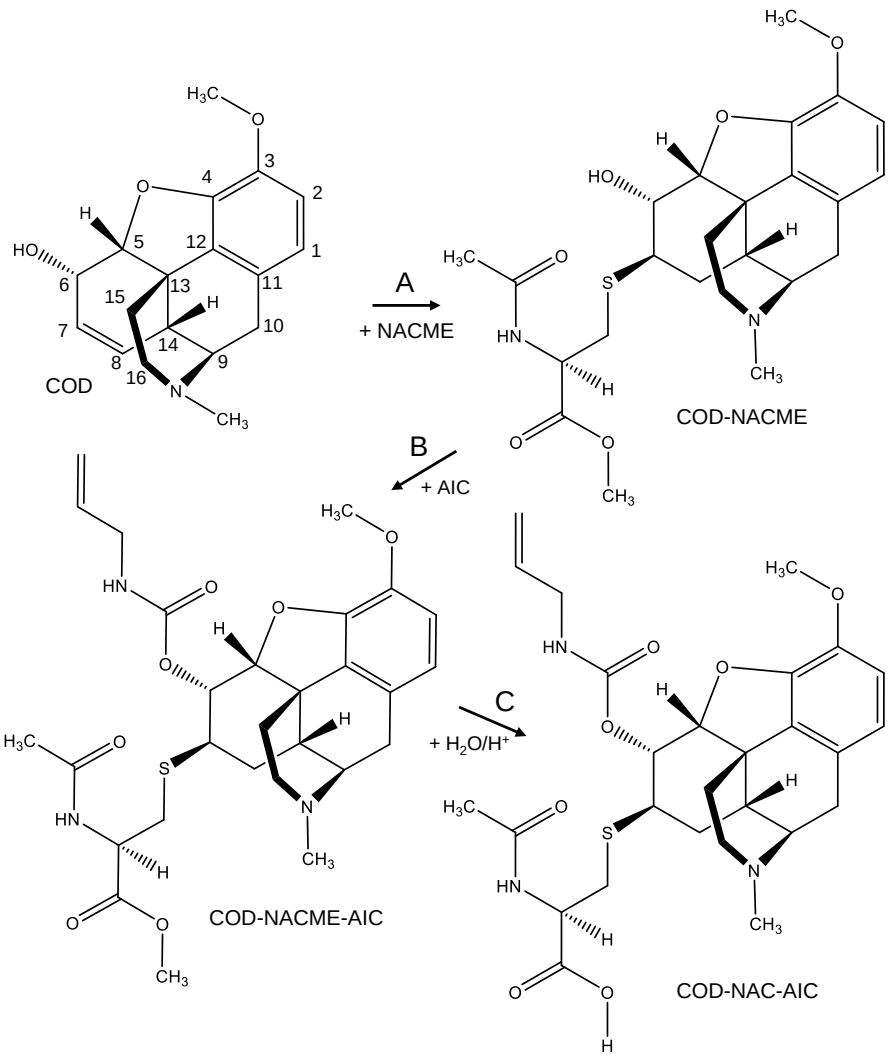

Fig. 10.2. Synthesis of COD-NAC-AIC, where: (A) reaction of COD with NACME in MeOH at 60 ºC for 24 h; (B) reaction of COD-NACME with AIC in THF at 35 ºC for 5 h; (C) hydrolysis of the methyl ester of the NACME moiety in 1:1 MeOH/water in the presence of 1% H_2SO_4 at room temperature for 1 h.

The COD-NACME-AIC product (1.20 g, 2.15 mmol) was dissolved in 10 mL of 1:1 MeOH/water containing 1% H_2SO_4. The solution was stirred at room temperature for 1 h, followed by neutralization with ammonia until pH 7.0 and purification by RP-HPLC (section 10.2.5). Again, fractions were collected, combined, and the solution evaporated to dryness with a rotary evaporator to obtain pure COD-NAC-AIC (1.11 g, 94.9%). ^{1}H NMR [DMSO-d6]: δ = 12.40 (s, 1H), 8.32 (s, 1H), 8.25 (s, 1H), 6.60 (d, J = 7.5 Hz, 1H), 6.55 (d, J = 7.5 Hz, 1H), 5.84 (m, J = 6.2; 16.8, 10.0 Hz, 1H), 5.38 (m, J = 7.8, 9.1 Hz, 1H), 5.19 (m, J = 1.0, 2.1, 16.8 Hz, 1H), 5.06 (m, J = 1.0, 2.1, 10.0 Hz, 1H), 4.74 (d, J = 7.0 Hz, 1H), 4.51 (d, J = 7.8 Hz, 1H), 4.04 (m, J = 1.0, 1.0, 6.2 Hz, 2H), 3.82 (s, 3H), 3.07 (m, J = 9.1, 11.9, 11.9 Hz, 1H), 2.93 (m, J = 12.4, 7.0 Hz, 2H), 2.91 (m, J = 12.4, 7.0 Hz, 2H), 2.46 (m, J = 12.4, 7.0 Hz, 2H), 2.26 (s, 3H), 2.23 (m, J = 7.0, 7.0 Hz, 1H), 1.84 (m, J = 12.4, 11.9, 12.1 Hz, 4H), 1.73 (m, J = 12.4, 7.1 Hz, 2H), 1.59 (m, J = 12.4, 11.9, 12.1 Hz, 1H), 1.25 (m, J = 7.0, 12.1, 12.1, 1H). ^{13}C NMR: δ = 178.8 (C), 178.6 (C), 158.6 (C), 147.7 (C), 142.5 (C), 134.2 (CH), 126.8 (C), 126.2 (C), 120.4 (CH), 117.4 (CH2), 113.7 (CH), 91.8 (CH), 81.1 (CH), 67.2 (CH), 57.7 (CH), 56.1 (CH), 48.4 (C), 47.7 (CH2), 43.7 (CH3), 43.4 (CH2), 41.5 (CH), 33.5 (CH2), 31.0 (CH2), 26.5 (CH), 25.5 (CH2), 23.3 (CH3), 20.4 (CH2). MS (ESI, positive): 546.2 $[M + H]^+$, 464.2 $[M – C4H4NO]^+$, 385.2 $[M – C5H7NO3S]^+$, 302.2 $[M – C9H12N2O4S]^+$. HRMS (ESI-TOF) *m/z*: $[M+H]^+$ Calcd $C_{27}H_{36}N_3O_7S$: 546.2274; Found: 546.2347.

10.2.5. Chromatographic analysis and purification of synthesis product and intermediates

Synthesis intermediates and final product were characterized and purified by RP-HPLC. For this purpose an 1100 Series HPLC system (Agilent) equipped with a binary pump, a thermostatic column compartment and a DAD was used. An Eclipse XDB-C18 (Agilent) was utilized as column and the mobile phase was composed of water (A)/ACN (B) mixtures each containing 0.1% FA. Gradient elution was carried out from 10 to 30% B in 15 min. After

each synthesis step, the crude residue obtained after evaporation of solvent was dissolved in ACN/water (1:9; v/v). First, to assign the peak of the synthesis intermediate, 20 µL of this solution was injected in triplicate. Then, a series of 80 successive injections of 100 µL was programmed. For each injection, the eluate fraction between the front and tail end of the peak was collected. The following fraction collection times were programmed: COD-NACME, 4.5 to 5.7 min; COD-NACME-AIC, 6.2 to 7.2 min; COD-NAC-AIC, 5.8 to 6.6 min. Product yields of each step are specified above.

The stereochemical purity of the intermediates and final product was also examined by HPLC with chiral stationary phase. For this purpose, Chiralpak QN-AX was used as column and the isocratic mobile phase was composed of ACN/MeOH (80:20; v/v) mixture containing 400 mM HAcO and 4 mM TEA. Solutions of the purified products in MeOH were injected in triplicate. The flow rate was 1 mL min^{-1}, and the injection volume was 20 µL. The detection wavelength was 254 nm.

10.2.6. Synthesis of the chiral stationary phase

Capillaries containing poly(GMA-co-EDMA) monolith were successively flushed with MeOH and aqueous 4.5 M ammonia at 60 ºC for 2 h at a flow rate of 60 µL h^{-1}. Then, they were washed with MeOH until reaching pH 7 at the outlet. The syringe pump was used to force a 4% (v/v) aqueous AGE solution at 60 ºC for 2 h at a flow rate of 60 µL h^{-1} through the capillary column. Afterwards, using an HPLC pump, the capillaries were washed with MeOH and acetone, and filled with a freshly prepared 10% (v/v) PMPMS solution in acetone (this solution also contained 1% AIBN (m/v) as radical initiator). The columns were sealed with GC septa and maintained in an oven at 60 ºC. After 24 h, the capillaries were removed from the ovenrinsed with acetone and MeOH. Next, a 0.25 M COD-NAC-AIC solution was prepared in MeOH, and AIBN (6 mg mL^{-1}, 0.037 M) was added. The mixture was sonicated for 5 min, filtered through a nylon membrane and purged with nitrogen for 10 min. Then,

the capillaries functionalized with PMPMS were filled up with the COD-NAC-AIC solution using a syringe pump. The capillary ends were sealed with GC septa and the radical addition of the chiral selector was carried out in an oven at 60 ºC. After 24 h, the capillaries were removed from the oven and rinsed with MeOH. Finally, a performic acid solution was prepared by mixing formic acid (98%) and hydrogen peroxide (30% in water) (25:75, v/v). As a catalyst, orthophosphoric acid (1%, v/v) was added, and the mixture was maintained at 40 ºC for 1 h. The capillaries were flushed for a few minutes with MeOH, followed by flushing with the performic acid solution for 2 h at room temperature at a flow rate of 60 µL h^{-1}. Finally, the capillaries were washed with MeOH until reaching pH 7 at the outlet.

10.2.7. Determination of the chiral selector coverage on the monolith surface

The procedure for evaluating the concentrations of the residual thiol groups and the chiral selector bound on the monolith surface, obtained by the difference of thiols before and after derivatization with COD-NAC-AIC, was adapted from literature [3,9]. Three non-derivatized and derivatized columns with the synthesized COD-NAC-AIC were analyzed. Briefly, the capillaries were filled with a 1.19 M DPDS solution in ACN, and the thiol/disulfide-exchange reaction was allowed to proceed for 1 h. Then, using an HPLC pump, the capillaries were rinsed with ACN, and the eluates were collected in HPLC micro-vials. The total volume of the eluate obtained from each capillary was established by weighing the micro-vials. A calibration curve was also constructed by mixing a 0.1 M DPDS solution in ACN with standard solutions containing increasing amounts of 2-mercaptoethanol (n = 6 points). In all the vials, the reaction product, pyridine-2-thione, and non-reacted DPDS were separated by RP-HPLC on a Kromasil C18 column using water (channel A) and ACN (B) as mobile phase. Linear gradient elution from 5% to 90% ACN in 20 min was carried out. The flow rate was 1 mL min^{-1} and the column

temperature was 25 ºC; 20 µL aliquots were injected. The reaction product was detected at 343 nm and the excess reagent at 254 nm.

10.2.8. CEC procedures

The monolithic columns, installed in the capillary cartridge of the CEC instrument, were first equilibrated with the mobile phase by progressively increasing the applied voltage from 5 to 10 kV until a constant current and a stable baseline were achieved. Solutions of chiral analytes (1 mg mL^{-1} in MeOH) containing 6 drops of acetone as EOF marker were used for capillary column testing. Separations were performed at 10 kV and 25 ºC. In all cases, the inlet and outlet vials were pressurized at 6 bar with nitrogen. The test mixtures were injected electrokinetically under 10 kV for 10 s. Detection of the analytes at 214 and 230 nm, and acetone at 280 nm, was performed.

10.3. Results and discussion

10.3.1. Preparation of the chiral stationary phase

10.3.1.1. Synthesis of chiral selector

The zwitterionic CSP was prepared as outlined in Fig. 10.2 using established methodologies. Thus, COD was firstly reacted with NACME in presence of AIBN via thiol-ene click chemistry (Fig. 10.2, step A) [3,15]. During this synthesis step, the C6 carbon atom changes its absolute configuration from *6S* in codeine to *6R* in the reaction product due to a change in the CIP priorities. NACME instead of *N*-acetyl-L-cysteine (NAC) was used, since in NACME the carboxylic group is protected with a methyl group, which hinders the possible reaction (in step B) between AIC and the hydroxyl group of NAC. The COD-NACME reaction proceeded with high yield (ca. 95%). Four possible stereoisomers can be formed. In general, the thiol group of NACME to the double bond of the C ring of the morphinene skeleton of COD

can attack the double bond at the C7 or C8 position. Furthermore, the thiol substituent could adopt an equatorial or axial arrangement in the reaction product. RP-HPLC revealed that a single isomer was formed as reaction product in this radical addition reaction. The chemical shifts of the ^{1}H NMR demonstrated that the attack of NACME on the double bond occurred exclusively on the carbon atom C7 (in close proximity to the hydroxyl group) as shown in Fig. 10.2. This position seems to be sterically favored over attack at carbon atom C8. On the other hand, information about the possible equatorial or axial arrangement of the thiol substituent was deduced from the dihedral coupling constants of the hydrogen at C8 ($^{3}J_{H7H8}$) with a chemical shift at 3.07 ppm. The NMR spectra showed J-couplings of 9.1, 11.9 and 11.9 Hz for this hydrogen, which corresponded to the axial position. For the equatorial position, J-couplings of 10.5, 11.9 and 11.9 Hz should be expected, but the former frequency was not observed in the NMR spectra. The resultant E (trans) arrangement of the thiol substituent with respect to the 6-hydroxyl group is sterically favorable over Z (cis) arrangement in the boat conformation of the C-ring of COD.

Subsequently, the secondary hydroxyl group of ring C of COD was derivatized with AIC furnishing a urethane functionality as to introduce a hydrogen-donor/acceptor system for interaction with solutes and a linker for immobilization of the chiral selector by thiol-ene click reaction, respectively (step B of Fig. 10.2). For this purpose, the product was dissolved in anhydrous THF, and AIC in presence of TEA as catalyst was added [56]. The reaction product, COD-NACME-AIC, gave again a single peak in RP-HPLC. In the last step (step C of Fig. 10.2), the methylester of cysteine was hydrolyzed to obtain the zwitterionic codeine-derived chiral selector (COD-NAC-AIC) [57]. A single peak in RP-HPLC and stereoselective HPLC with a chiral anion-exchanger (Chiralpak QN-AX) which has proven broad stereoselectivity for chiral *N*-derivatized amino acid derivatives confirmed, along with corresponding NMR spectra, the presence of a single stereoisomer.

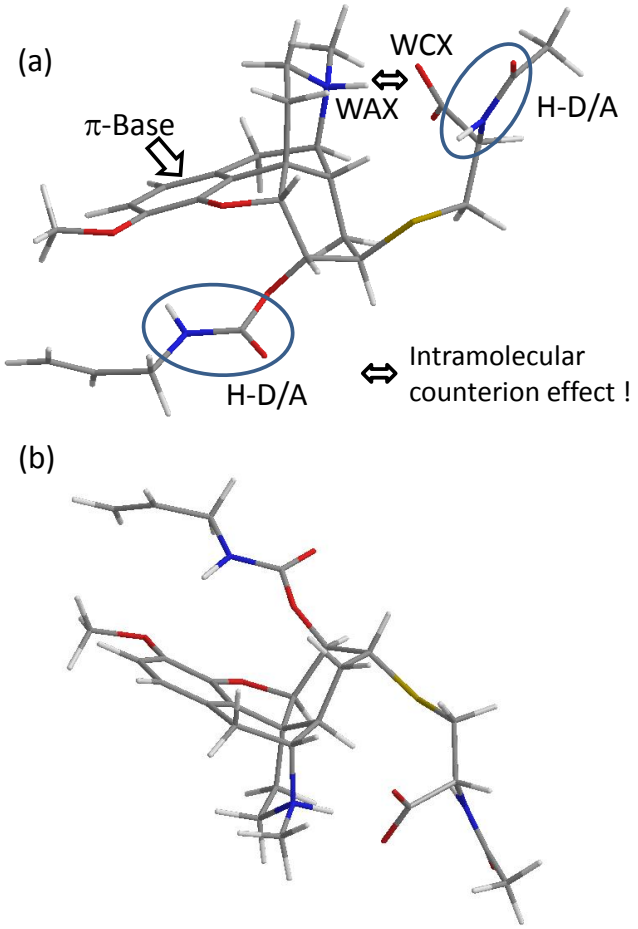

Fig. 10.3. Model of zwitterionic chiral selector

The resultant zwitterionic codeine-derived selector (Fig. 10.3) has 6 centers of chirality embedded in a rigid backbone (*5R,6R,7R,9R,13S,14R*) with a conformationally flexible chiral NAC side chain harboring another stereogenic center (*2R*) and a further achiral allylcarbamoyl substituent acting as linker for immobilization. The tert-amine of the COD backbone represents a weak anion-exchange (WAX) site (pK_a 7.72; calculated by ACD software) and the carboxylic group of cysteine constitutes the weak cation-exchange (WCX) site (pK_a 3.24; ACD). The corresponding calculated isoelectric point is 5.48. The two ionic functionalities may serve either as fixed-charge of the ion-exchange site for binding of the counterionic solute or as intramolecular

counterion in the opposite ion-exchange mode (*vide infra*). In addition to these primary ion-exchange sites, this chiral selector possesses a π-π-interaction site (π-base in A-ring of morphinene backbone) as well as two hydrogen donor/acceptor systems (carbamate at C6 and amide of NAC) as supportive interaction sites. The A and C-rings are arranged perpendicular to each other and form a cleft for analyte insertion driven by ion-pairing at counterionic ion-exchange site whereas complex stabilization is supported by directed π-π-interactions and hydrogen bonds of adjacent binding sites.

10.3.1.2. Immobilization of chiral selector

The procedure for thermal polymerization of the GMA-based monoliths was adapted from a previous work [7]. This monolith provided a tailored macroporous structure and a high quantity of epoxy groups which represented the anchor groups for further surface functionalization. Since enantioselective chromatography requires a substantial amount of chiral moieties on the surface, a new approach of thiolation of the monolith surface for subsequent bonding of the chiral selector by thiol-ene click reaction was pursued (Fig. 10.4). In the first step, the epoxy groups were converted into primary amino groups using ammonia. The amino groups were derivatized with AGE. Onto the surface of this allyl-modified monolith, a thin film of PMPMS was obtained by binding to the allyl groups from the prior bonded AGE linker through thiol-ene click reaction [3]. This multi-step surface modification strategy produced thiol coverages by a factor of about 2 higher than derivatization of epoxy groups with hydrogen sulfide [3]. The large quantity of free thiols could then be utilized for bonding of the codeine-derived chiral selector via click chemistry with a methanolic solution of COD-NAC-AIC in presence of AIBN.

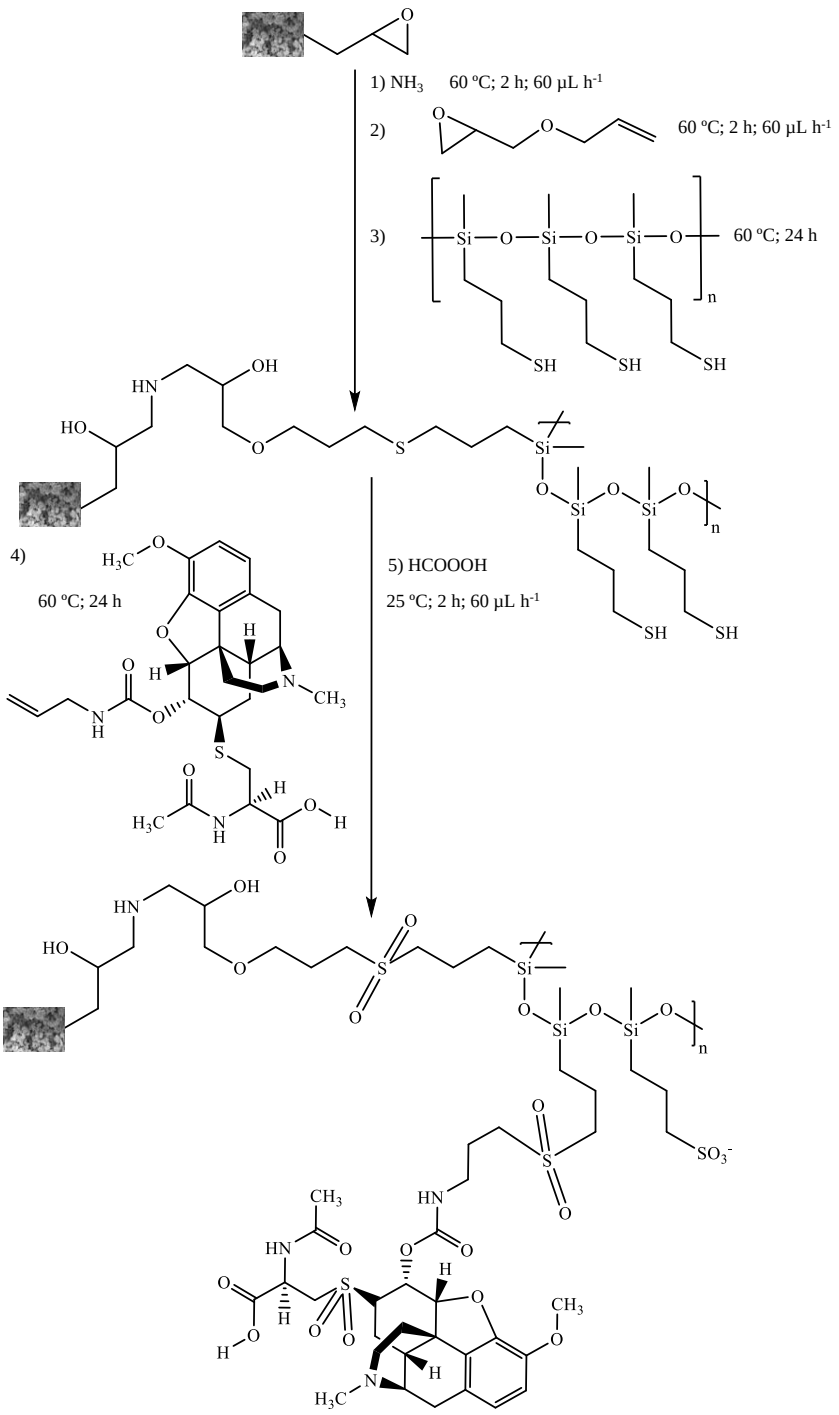

Fig. 10.4. Reaction scheme for immobilization of chiral selector on thiolated monolith surface.

To evaluate the coverage of the monolith with PMPMS and the CS, the DPDS assay was used. First, the thiol concentration of the monoliths modified with PMPMS was determined. The amount of free thiol groups on the monolith surface was 2.21 mmol SH g^{-1} of monolith. After reaction with COD-NAC-AIC, the total free thiol groups amounted to 0.38 mmol SH g^{-1} of monolith. Hence, the yield of the thiol derivatization, calculated from the difference between the free thiol groups before and after the reaction, was 83%. This corresponded to 1.83 mmol COD-NAC-AIC g^{-1} monolith. This high selector coverage should help to assure a sufficient number of enantioselective interactions and reduce non-enantioselective adsorption to the monolith surface.

This zwitterionic chiral monolith showed good enantioselectivity in both the cation-exchange mode for chiral bases (e.g. for mefloquine) as well as the anion-exchange mode for chiral acids (e.g. for DNB-Leu), yet surprisingly, poor efficiency (Fig. 10.5, upper traces). Hence, the monolith surface was finally treated with performic acid to convert the residual free thiol groups of PMPMS and the thioether groups of both PMPMS and COD-NAC-AIC into sulphonate and sulfonyl groups, respectively. This zwitterionic chiral monolith provided much better efficiencies in CEC (Fig. 10.5, lower traces).

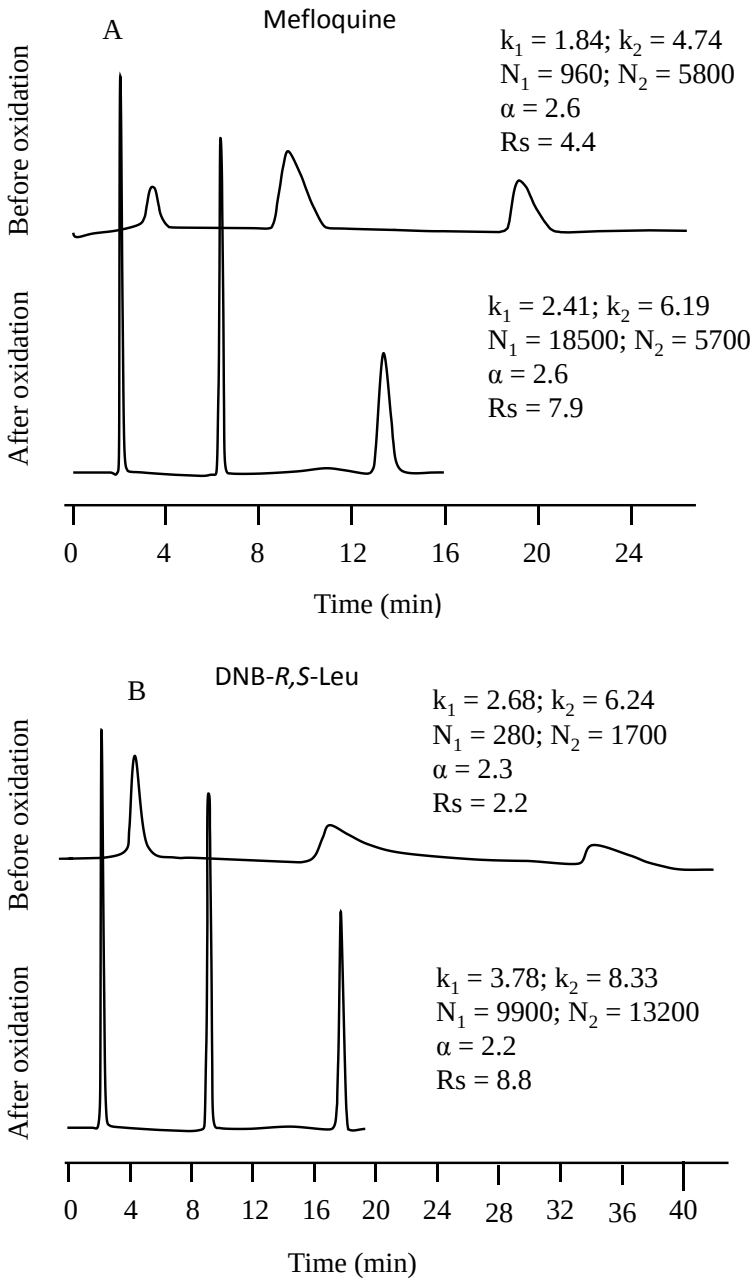

Fig. 10.5. CEC performance of chiral monolith before (upper traces) and after performic acid oxidation (lower traces) for mefloquine (A) and DNB-*R,S*-Leu (B). CEC conditions: mobile phase, 80:20 (v/v) ACN-MeOH containing 25 mM HAcO and 12.5 mM DEA; electrokinetic injection, 10 kV for 10 s; separation voltage, 10 kV.

10.3.2. Electrochromatographic evaluation of the CSP

10.3.2.1. Variation of the counterion concentration

Retention of acidic and basic analytes on zwitterionic CSPs in non-aqueous media is supposed to be governed by ion-pairing interactions with respective counterionic functionalities of the zwitterionic surface. As result, ion-exchange retention processes are dominating the adsorption mechanism at the CSP surface for both types of ionic solutes. To evaluate these processes, CEC experiments were made using protonated DEA and acetate as counterions with respect to the carboxylate and amino groups of the CSP, respectively. These were first used at a molar ratio of 1:1 (HAcO:DEA), and their concentration was varied within the concentration range of 6.25-50 mM. A study of the retention of acidic DNB-*R,S*-Leu and basic mefloquine is shown in Fig. 10.6. As observed, retention decreased with increase of counterion concentration. Further, plots of log *k* versus the logarithm of the counterion concentration (log *c*) revealed linear dependencies of the two pairs of enantiomers for each type of chiral solute in accordance with a stoichiometric displacement model [15]. This is a clear indication that retention takes place by ion-exchange processes, i.e. anion-exchange for DNB-Leu and cation-exchange for mefloquine. According to the stoichiometric displacement model, the slope of log *k* – log *c* plots retrieves or shows information on the charges involved in ion-exchange, which should be 1 for the ion-exchange interaction between fully dissociated monovalent solute ions and counterions. However, the slopes found were 0.62 and 0.66 for the enantiomers of DNB-*R,S*-Leu, and 0.26 and 0.28 for those of mefloquine, indicating deviation from 1:1 charge interactions. In a mobile phase containing equimolar amounts of DEA and HAcO, significant ionization of the amino and carboxylate groups of both the solutes and the CSP can be expected. Besides ionic interactions at the zwitterionic selector, non-enantioselective binding to ionic moieties of the monolith backbone and oxidized polysiloxane coating may contribute to retention. Their individual contributions to overall retention cannot be

deconvoluted easily. These non-specific interactions, due to zwitterionic nature as well, partly neutralize each other and are supposed to represent low affinity sites due to missing simultaneous supportive interactions. Whatsoever, the data clearly show that interaction at the zwitterionic codeine selector is dominant and occurs highly enantioselectively. Since the slopes are proportional to the effective charges involved in ion-exchange (slope ~ $z_{eff\ (solute)}$ / $z_{eff\ (counterion)}$), it can be concluded that DNB-Leu involves stronger ionic interactions than mefloquine, probably originating mainly from specific dissociation states of corresponding functionalities of solute and respective counterions, in other words incomplete dissociation may be responsible for the deviations from slope values of 1. On the other hand, the two enantiomers of each corresponding pair showed almost identical slopes indicating a rather similar response to changes in counterion concentration. The independence of enantioselectivity from the counterion concentration has been previously reported for other chiral ion-exchangers [15], allowing the adjustment of retention times without affecting enantioselectivity.

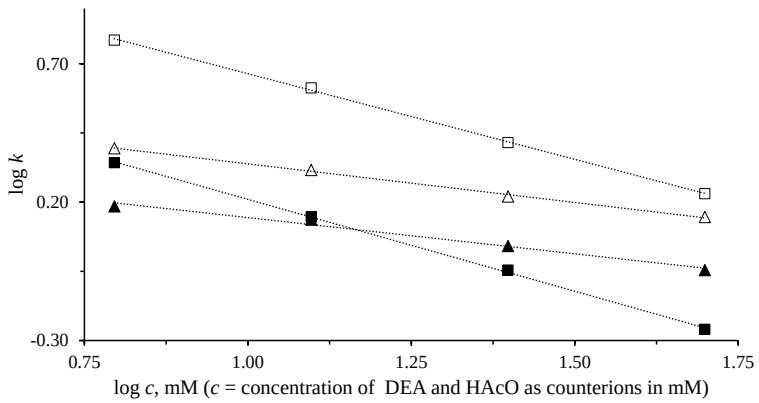

Fig. 10.6. Influence of the counterion concentration on the retention of two pairs of enantiomers. CEC conditions: mobile phase, 80:20 (v/v) ACN-MeOH containing 6.25-50 mM HAcO and 6.25-50 mM DEA in 1:1 ratio; electrokinetic injection, 10 kV for 10 s; separation voltage, 10 kV. Compound identification: (■) *R*-DNB-Leu; (□) *S*-DNB-Leu, (▲) (–)-mefloquine, (Δ) (+)-mefloquine. HAcO or DEA was the counterion for DNB-*R,S*-Leu and mefloquine, respectively.

There is another point which deserves mentioning. The solutes can be eluted on this zwitterionic codeine CSP with relatively mild conditions regarding ionic strength. Low concentrations of counterions are sufficient to balance the ionic interactions, as opposed to mere anion- and cation-exchange systems which need elevated counterion concentrations for efficient elution of solutes. This can be explained by the presence of both an ion-exchange site and an intramolecular counterion functionality on the CSP in close proximity. The carboxylate of the NAC moiety serves as intramolecular counterion for acidic solutes such as DNB-Leu which primarily interact via anion-exchange at the tertiary amino group of codeine, and the *tert*-amino group of the codeine moiety acts as intramolecular counterion for basic solutes such as mefloquine which bind primarily via cation-exchange at the carboxylic group of NAC. This intramolecular counterion effect assures fast separations at mild conditions in terms of ionic strength which is beneficial for CEC and MS detection.

10.3.2.2. Variation of the acid-to-base ratio

The ion-exchange processes also depend on the proton activity of the non-aqueous mobile phases [15], which regulates the dissociation states of solutes, ion-exchanger functionalities and mobile phase electrolytes (co- and counterions). In order to explore suitable CEC operation conditions, the dependence of the overall performance of the CSP on different acid-to-base ratios, as a way of controlling the proton activity in the nonaqueous medium, was investigated. For this purpose, in addition to the molar ratio (HAcO:DEA) 1:1, the basic 1:2 (6.25 mM HAcO with 12.5 mM DEA), and the acidic 2:1 and 4:1 ratios (25 mM and 50 mM HAcO, respectively, with 12.5 mM DEA), were used. The effects of the acid-to-base ratio on retention and efficiency for the *R* and *S* enantiomers of DNB-Leu and the (+) and (–) enantiomers of mefloquine are shown in Fig. 10.7. Acidic conditions are on the right hand side of the x-axis while basic conditions (excess of DEA) are on the left hand side (excess of HAcO).

As observed in Fig. 10.7, the electroosmotic mobility is positive over the entire investigated range and points towards an overall slightly negative net charge of the surface under given conditions. There is only an insignificant alteration with variation of acid-to-base ratio (Fig. 10.7A). It can be further seen that retention factors of the two solutes were maximal for the acid-to-base ratio 2:1, i.e. under weakly acidic conditions, while they decreased at both lower and higher acid-to-base ratios (Fig. 10.7B). According to its molecular structure, the tertiary amino group of the CSP should get more and more deprotonated the lower the acid-to-base ratios. Thereby, the CSP loses its anion-exchange capacity although acidic solutes are dissociated to larger degree. This could explain the decrease of retention of DNB-*R*,*S*-Leu at 1:1 and 1:2 acid-to-base ratios with respect to the 2:1 ratio (Fig. 10.7B). Lack of charge on mefloquine at these low acid-to-base ratios could also explain its low retention, in spite of a high degree of dissociation of the carboxylic group of the *N*-acetylcysteine moiety of the zwitterionic selector. On the other hand, the carboxylate group of the CSP will get increasingly protonated the larger the acid-to-base ratios, which should lead to loss of its cation-exchange capacity. This could explain the decrease of retention of mefloquine at the 4:1 acid-to-base ratio (Fig. 10.7B). Concerning DNB-*R*,*S*-Leu, lack of negative charge due to protonation of the carboxylic acid function could explain the decrease of its retention at the highest acid-to-base ratio. As also observed in Fig. 10.7C, enantioselectivity (bars) and enantiomeric resolution (symbols) were only slightly modified when the acid-to-base ratio increased. According to Fig. 10.7D, there is some minor effect of the proton activity in the eluent on efficiency of DNB-Leu, while the effect was significant for mefloquine. The latter shows maximal plate numbers at acidic conditions when the acid-to-base ratio increased up to 4:1.

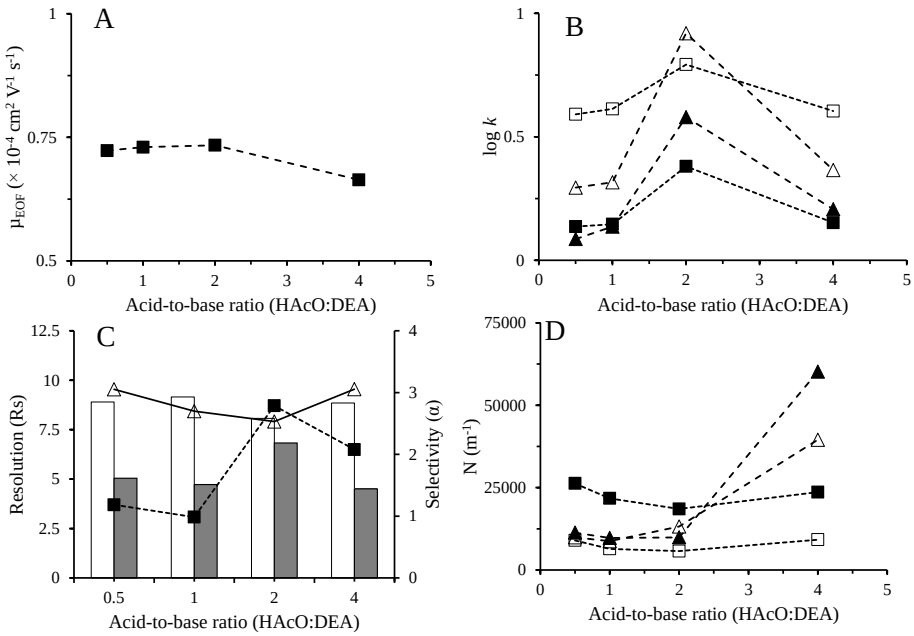

Fig. 10.7. Effect of acid-to-base ratio on (A) electroosmotic mobility, (B) log k, (C, bars) selectivity and (C, symbols) resolution and (D) efficiency (as plate numbers) of two pairs of enantiomers. CEC conditions: mobile phase, 80:20 (v/v) ACN-MeOH containing 6.25-50 mM HAcO and 12.5 mM DEA; electrokinetic injection, 10 kV for 10 s; separation voltage, 10 kV. Compound identification in (B) and (D): (■) R-DNB-Leu; (□) S-DNB-Leu, (▲) (–)-mefloquine, (Δ) (+)-mefloquine; in (C): (■) and grey bars DNB-Leu; (Δ) and white bars mefloquine.

10.3.2.3. Variation of the nature of counterion and co-ion

Counterions, which act as competitors for the solutes bound at the ion-exchange centers, play a crucial role in ion-exchange retention processes. For this reason, both the nature and concentration of the counterion in the mobile phase can be used to control retention and other electrochromatographic parameters. As commented above, the CSP developed in this work was both a cation- and an anion-exchanger. According to its charge and preference for a site of interaction, either an anion or a cation of the mobile phase would represent the counterion with respect to the retained solute.

First, the influence of counterions on the elution of mefloquine was studied by using the following compounds (12.5 mM each): NH_3 (pK_a 9.3), DEA (pK_a 10.8) and TEA (pK_a 11.0). The co-ion was kept constant in this series of experiments (25 mM HAcO). As shown in Fig. 10.8A, retention of mefloquine displayed a strong dependence on the nature of the counterion, whereby the elution strength increased in the order: TEA < DEA < NH_3. This trend was also observed previously with chiral cation-exchangers in HPLC [15]. The co-ion (acidic component) effect was negligible (data not shown).

Secondly, elution of DNB-*R*,*S*-Leu was studied in the presence of the following counterions (always 25 mM): FA (pK_a 3.8), HAcO (pK_a 4.8) and TFA (pK_a 0.2). The co-ion was 12.5 mM DEA in all experiments. As shown in Fig. 10.8B, elution strength for DNB-*R*,*S*-Leu increased in the following order: FA < HAcO < TFA. While the relative elution strength for FA and HAcO was the same as observed in chiral anion-exchange HPLC, TFA showed the lowest elution strength contradictory to chiral anion-exchange HPLC where it has the highest elution strength of the three employed acids. The effect is not fully understood, but complete disruption of the intramolecular counterion effect could be an explanation. As above, the change of the nature of the co-ion did not produce any significant effect on the elution of DNB-*R*,*S*-Leu (data not shown).

As a result of the elution strength obtained with various counterions, suitable mobile phase compositions for isoeluotropic elution can be deduced. Ion-exchange retention can be regulated by changing either the nature of the counterion or its concentration; however, the former also significantly modulates enantioselectivity. The best compromise in terms of broad applicability for chiral acids and chiral bases as well as with regards to high efficiencies, satisfactory resolutions and reasonable retention times was obtained for mobile phases with DEA and HAcO as co- and counterions, respectively. They were therefore found to be optimal to resolve a larger set of chiral test compounds (*vide infra*).

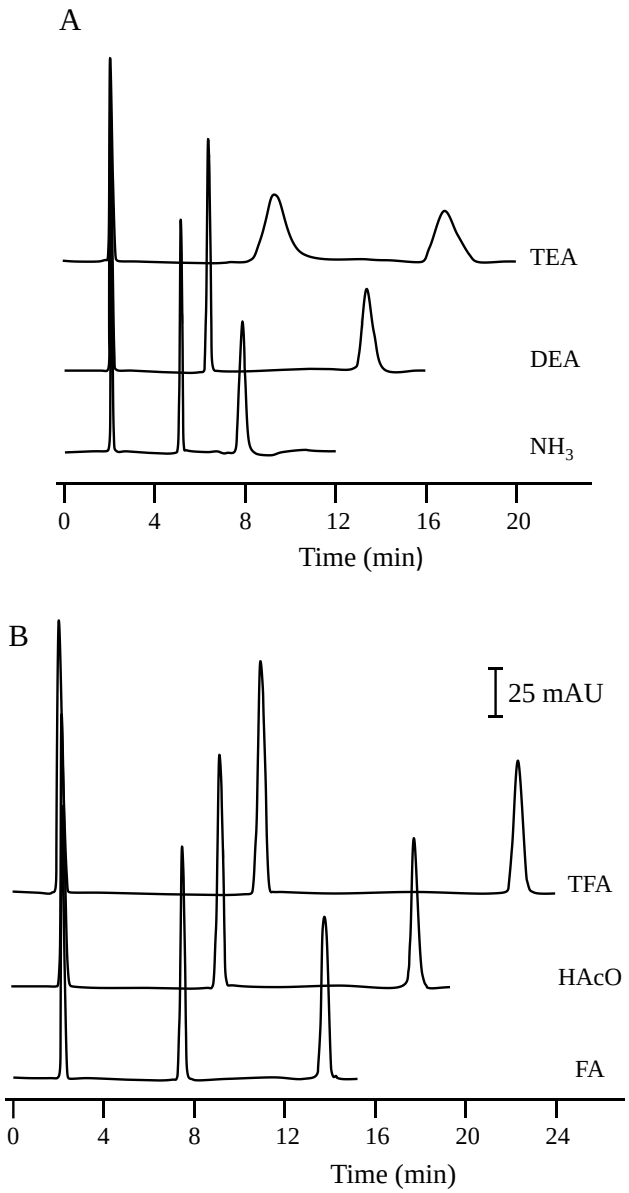

Fig. 10.8. Effect of the nature of the counterion for (A) mefloquine and (B) DNB-*R,S*-Leu. CEC conditions: mobile phase, 80:20 (v/v) ACN-MeOH containing (A) 25 mM HAcO and 12.5 mM NH_3, DEA or TEA, and (B) 25 mM FA, HAcO or TFA and 12.5 mM DEA; electrokinetic injection, 10 kV for 10 s; separation voltage, 10 kV.

10.3.2.4. Influence of the ratio of protic and aprotic solvents

ACN and MeOH are frequently used as bulk solvents in nonaqueous liquid chromatography and CEC separations. ACN is an aprotic solvent that is known to disrupt π–π interactions [58], whereas MeOH is a protic solvent which can interfere with H-bonding. Hence, it is of interest to investigate whether the ratio of these two solvents has an impact on the chromatographic behavior of the developed CSP. For this purpose, the proportions of ACN and MeOH in the mobile phase were varied (100, 50, 20, 10 and 0% MeOH in ACN) under otherwise identical conditions. The resultant effects on the electroosmotic mobility, μ_{EOF}, enantiomeric selectivity and resolution, and on efficiency in the separation of DNB-*R,S*-Leu and mefloquine enantiomers, are shown in Fig. 10.9.

The EOF in the capillary column gradually decreased with increase of methanol in the mobile phase, an effect that is mainly driven by the viscosity change (Fig. 10.9A). As observed, rather poor values of enantioselectivity, resolution and efficiency were obtained in 100% ACN (Figs. 10.9B and 10.9C). This can be due to improperly balanced solute-adsorbent (H-bond or dipole) interactions owing to absence of proton donors and resultant slow desorption kinetics, respectively [15]. When a protic solvent was present in sufficient amounts (e.g. 10% MeOH) the CSP worked properly. Both the weakly acidic and weakly basic sites of the CSP, as well as the weak acid or basic solutes, should be ionized. Thus, the presence of a protic solvent like MeOH seems to be essential to mediate acid-base equilibria and hence to also sustain the ion-exchange processes between the chiral selector, solutes and counterions. When MeOH concentration increased, the selectivity, resolution and efficiency also increased up to a maximum. Thus, protic solvents such as MeOH are required, but polar aprotic solvents like ACN generally improve the CSP performance. The latter can be used in large proportions, up to 90% of the mobile phase.

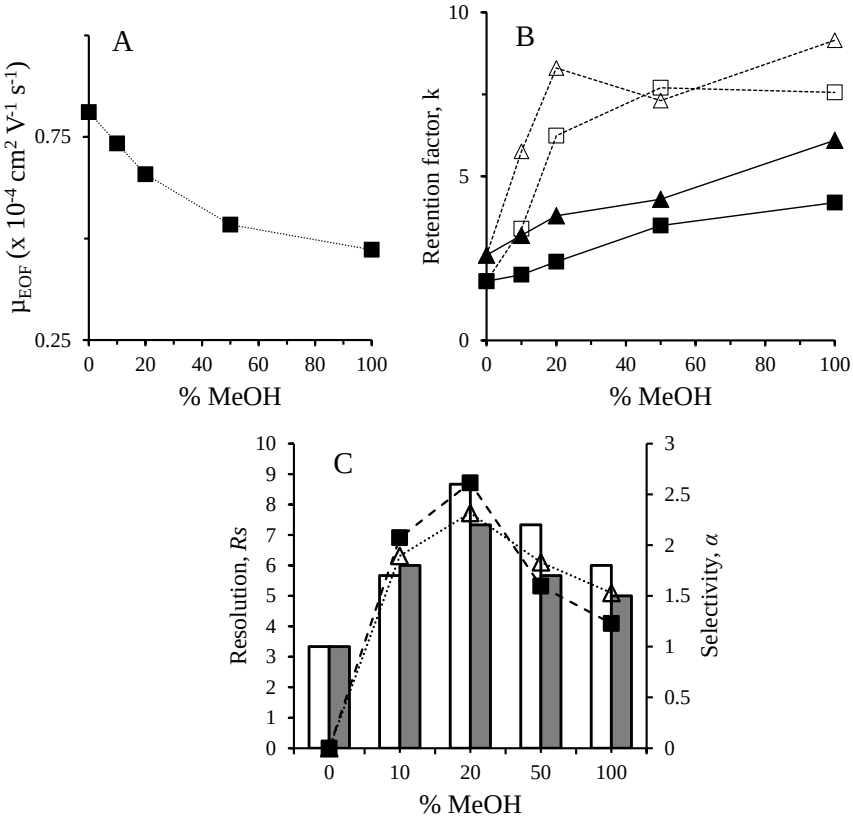

Fig. 10.9. Effect of the proportion of MeOH in the bulk solvent (mixture of ACN and MeOH) on the (A) electrophoretic mobility, (B) retention factor and (C, bars) selectivity and (C, symbols) resolution of two pairs of enantiomers. CEC conditions: ACN-MeOH mixtures containing 25 mM HAcO and 12.5 mM DEA; electrokinetic injection, 10 kV for 10 s; separation voltage, 10 kV. Compound identification in (B): (■) R-DNB-Leu; (□) S-DNB-Leu, (▲) (–)-mefloquine, (Δ) (+)-mefloquine; in (C): (■) and grey bar DNB-Leu; (Δ) and white bars mefloquine; in (C): (■) and grey bars DNB-Leu; (Δ) and white bars mefloquine.

10.3.2.5. Enantiomeric separation of several β-blockers and amino acid derivatives

Several chiral solutes were additionally tested to explore the CEC performance of the CSP with optimized conditions for a structurally broader solute set. β-Blockers and amino acid derivatives carrying a variety of functional groups were examined. A summary of the chromatographic data is given in Table 10.1, and three representative chromatograms are shown in Fig. 10.10. All tested racemates were fully baseline separated with high selectivity and resolution (*e.g.* mefloquine: α = 2.6, R_S = 7.9) and exhibited also excellent peak efficiencies (e.g. > 30000 theoretical plates per meter for atenolol, propranolol and DNP-*R*,*S*-Arg).

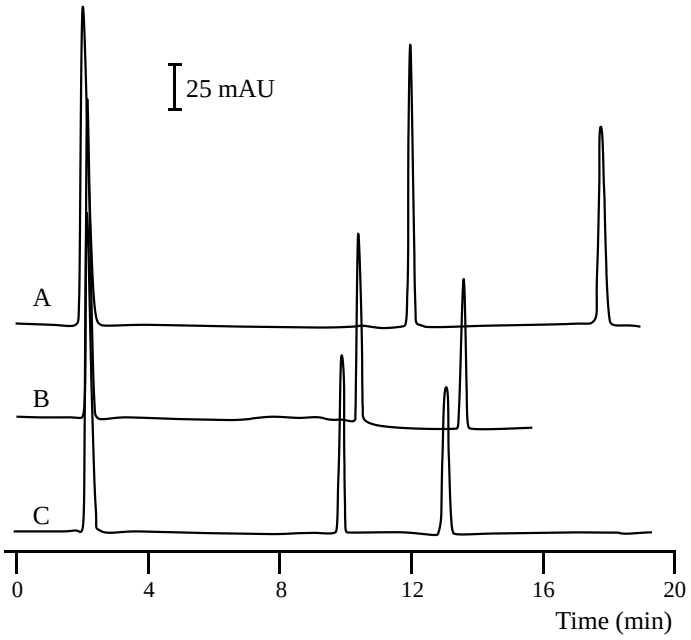

Fig. 10.10. Electrochromatograms of (A) atenolol, (B) propranolol and (C) DNP-*R*,*S*-Arg. CEC conditions: mobile phase, 80:20 (v/v) ACN-MeOH containing 25 mM HAcO and 12.5 mM DEA; electrokinetic injection, 10 kV for 10 s; separation voltage, 10 kV.

Table 10.1

CEC enantiomer separation of various solutes on the zwitterionic codeine-derived ion-exchanger CSP

Solute	Elution order	k_1	k_2	α	R_S	N_1 (m^{-1})	N_2 (m^{-1})
Atenolol	R-S	5.31	8.32	1.6	10.3	41000	50300
Propranolol	R-S	4.42	6.12	1.4	8.8	75000	62300
Clenbuterol	R-S	7.03	12.1	1.7	9.7	23500	28200
Mefloquine	(+)-(-)	2.41	6.19	2.6	7.9	18500	5700
Acebutolol	(–)-(+)	5.12	11.3	2.2	8.2	12300	8600
DNB-Leu	R-S	3.78	8.33	2.2	8.8	9900	13200
Ac-Phe	R-S	6.23	9.32	1.5	7.3	27300	28200
DNP-Arg	R-S	4.23	5.87	1.4	6.8	42000	38700

[a] Conditions: mobile phase, 80:20 (v/v) ACN-MeOH; other conditions as in Fig. 10.6.

10.4. Conclusions

A successful zwitterionic monolithic CSP for CEC enantiomer separations has been developed. This CSP is based on rather common and cheap low molecular mass chiral selectors, namely codeine and *N*-acetylcysteine, which was attached to codeine by thiol-ene click reaction to the double bond of ring C of the morphinane skeleton. A single stereoisomer resulted from the synthesis. The zwitterionic codeine-derived chiral selector was bonded to a polymethacrylate monolith which was coated with a thin film of PMPMS previously bonded to the monolith surface. The CSP performs both as a weak cation-exchanger and weak anion exchanger, expanding its applicability to chiral acids and chiral bases. The CEC evaluation of the novel CSP was carried out with nonaqueous polar organic mobile phases. In such media, detailed investigations of the operating conditions in terms of proton activity, nature of counterion and co-ion, concentration of the counterion, and nature of the bulk solvent (protic/aprotic balance) were carried out. Thereby, ion-exchange was

the dominant retention mechanism. Insights into the mechanisms for enantiodiscrimination were also provided. Furthermore, optimized mobile phase conditions were established using both basic and acidic solutes, and applied to the chiral separations of test solutes comprising a variety of functional groups. The findings presented here are promising and demonstrate the potential of enantioselective zwitterionic ion-exchangers for combining application profiles of chiral anion-exchangers and chiral cation-exchangers.

Acknowledgements

G. R.-R. and J.M. H.-M. acknowledge support by Project CTQ2014-52765-R (MINECO of Spain and FEDER funds). E.J.C-C. thanks the MINECO for an FPI grant. M.L. is grateful for support by the “Struktur- und Innovationsfonds Baden-Württemberg (SI-BW)”.

References

[1] K. Stulík, V. Pacáková, J. Suchánková, P. Coufal, J. Chromatogr. B. Analyt. Technol. Biomed. Life Sci., 841 (2006) 79.

[2] P. Jandera, J. Chromatogr. A, 1313 (2013) 37.

[3] E.J. Carrasco-Correa, G. Ramis-Ramos, M. Lämmerhofer, J.M. Herrero-Martínez, J. Chromatogr. A, 1367 (2014) 123.

[4] V. Frankovic, A. Podgornik, N.L. Krajnc, F. Smrekar, P. Krajnc, A. Strancar, J. Chromatogr. A, 1207 (2008) 84.

[5] W. Wieder, C.P. Bisjak, C.W. Huck, R. Bakry, G.K. Bonn, J. Sep. Sci., 29 (2006) 2478–2484.

[6] G. Yang, H. Liu, Y. Zhang, S. Wang, J. Yin, B. Yin, et al., J. Chromatogr. A, 1129 (2006) 231.

[7] E.J. Carrasco-Correa, G. Ramis-Ramos, J.M. Herrero-Martínez, J. Chromatogr. A, 1298 (2013) 61.

[8] X. Dong, J. Dong, J. Ou, Y. Zhu, H. Zou, Electrophoresis, 27 (2006) 2518.

[9] B. Preinerstorfer, W. Bicker, W. Lindner, M. Lämmerhofer, J. Chromatogr. A, 1044 (2004) 187.

[10] Y. Wen, Y.-Q. Feng, J. Chromatogr. A, 1160 (2007) 90.

[11] A. Messina, M. Flieger, F. Bachechi, M. Sinibaldi, J. Chromatogr. A, 1120 (2006) 69.

[12] B. Preinerstorfer, W. Lindner, M. Lämmerhofer, Electrophoresis, 26 (2005) 2005.

[13] A. Messina, M. Sinibaldi, Electrophoresis, 28 (2007) 2613.

[14] Y. Tian, C. Zhong, E. Fu, Z. Zeng, J. Chromatogr. A, 1216 (2009) 1000.

[15] C. V. Hoffmann, M. Laemmerhofer, W. Lindner, J. Chromatogr. A, 1161 (2007) 242.

[16] J. Haginaka, J. Chromatogr. A, 906 (2001) 253.

[17] N.M. Maier, P. Franco, W. Lindner, J. Chromatogr. A. 906 (2001) 3.

[18] S.G. Allenmark, S. Andersson, P. Muller, D. Sanchez, Chirality, 7 (1995) 248.

[19] D.W. Armstrong, Y. Tang, S. Chen, Y. Zhou, C. Bagwill, J.-R. Chen, Anal. Chem, 66 (1994) 1473.

[20] I. Ilisz, R. Berkecz, A. Péter, J. Sep. Sci., 29 (2006) 1305.

[21] M.H.O. Hyun, Y.J.A.E. Cho, Y. Song, H.E.E.J. Choi, B.U.S. Kang, 81 (2007) 74.

[22] C.J. Welch, J. Chromatogr. A. 666 (1994) 3.

[23] G. Cancelliere, I. D'Acquarica, F. Gasparrini, M. Maggini, D. Misiti, C. Villani, J. Sep. Sci., 29 (2006) 770.

[24] F. Ianni, Z. Pataj, H. Gross, R. Sardella, B. Natalini, W. Lindner, et al., J. Chromatogr. A, (2014) 10.1016/j.chroma.2014.03.060.

[25] B. Preinerstorfer, C. Hoffmann, D. Lubda, M. Lämmerhofer, W. Lindner, Electrophoresis, 29 (2008) 1626.

[26] Y. Machida, H. Nishi, K. Nakamura, H. Nakai, T. Sato, J. Chromatogr. A, 805 (1998) 85.

[27] Y. Okamoto, E. Yashima, Angew. Chemie - Int. Ed., 37 (1998) 1021.

[28] E.J. Franco, H. Hofstetter, O. Hofstetter, J. Sep. Sci., 29 (2006) 1458.

[29] C. Gu, S.A. Shamsi, Electrophoresis, 32 (2011) 2727.

[30] B. Preinerstorfer, W. Bicker, W. Lindner, M. Lämmerhofer, J. Chromatogr. A, 1044 (2004) 187.

[31] B. Preinerstorfer, W. Lindner, M. Lämmerhofer, Electrophoresis, 26 (2005) 2005.

[32] X. Dong, R. Wu, J. Dong, M. Wu, Y. Zhu, H. Zou, Electrophoresis, 29 (2008) 919.

[33] E.C. Peters, K. Lewandowski, M. Petro, F. Svec, J.M.J. Fréchet, Anal. Commun., 35 (1998) 83.

[34] M. Lämmerhofer, E.C. Peters, C. Yu, F. Svec, J.M.J. Fréchet, W. Lindner, Anal. Chem., 72 (2000) 4614.

[35] T. Koide, K. Ueno, J. Chromatogr. A, 893 (2000) 177.

[36] M.G. Schmid, N. Grobuschek, O. Lecnik, G. Gübitz, A. Végvári, S. Hjertén, Electrophoresis, 22 (2001) 2616.

[37] B. Preinerstorfer, D. Lubda, W. Lindner, M. Lämmerhofer, J. Chromatogr. A, 1106 (2006) 94.

[38] B. Chankvetadze, C. Yamamoto, N. Tanaka, K. Nakanishi, Y. Okamoto, J. Sep. Sci., 27 (2004) 905.

[39] B. Chankvetadze, T. Kubota, T. Ikai, C. Yamamoto, M. Kamigaito, N. Tanaka, et al., J. Sep. Sci., 29 (2006) 1988.

[40] X. Dong, J. Dong, J. Ou, Y. Zhu, H. Zou, Electrophoresis, 28 (2007) 2606.

[41] M. Lämmerhofer, A. Van Eec, CRC Press, Boca Raton, DL, USA, 2010.

[42] W.F. N. M. Maier, W. Lindner, E. In, Chirality in Drug Research, Wiley-VCH, Winheim, 2006.

[43] W.L. M. Lämmerhofer, Recent Developments in Liquid Chromatographic Enantioseparation, K. Valko, Elsevier, Amsterdam, 2000.

[44] Z. Aturki, M.G. Schmid, B. Chankvetadze, S. Fanali, Electrophoresis. (2014) 10.1002/elps.201400085.

[45] S. Fanali, G. D'Orazio, T. Farkas, B. Chankvetadze, J. Chromatogr. A, (2012) 136.

[46] D. Kotoni, A. Ciogli, I. D'Acquarica, J. Kocergin, T. Szczerba, H. Ritchie, et al., J. Chromatogr. A, (2012) 226.

[47] R.M. Woods, D.C. Patel, Y. Lim, Z.S. Breitbach, H. Gao, C. Keene, et al., J. Chromatogr. A, 1357 (2014) 172.

[48] A.F.G. Gargano, M. Kohout, P. Macíková, M. Lämmerhofer, W. Lindner, Anal. Bioanal. Chem., 405 (2013) 8027.

[49] S. Wernisch, O. Trapp, W. Lindner, Anal. Chim. Acta, 795 (2013) 88.

[50] C. V Hoffmann, R. Reischl, N.M. Maier, M. Lämmerhofer, W. Lindner, J. Chromatogr. A, 1216 (2009) 1147.

[51] M. Lämmerhofer, W. Lindner, J. Chromatogr. A, 741 (1996) 33.

[52] M. Lämmerhofer, W. Lindner, Adv. Chromatogr. 46 (2008) 1.

[53] C. V Hoffmann, R. Pell, M. Lämmerhofer, W. Lindner, Anal. Chem. 80 (2008) 8780.

[54] E.C. Peters, M. Petro, F. Svec, J.M.J. Fréchet, Molded Rigid Anal. Chem., 70 (1998) 2296.

[55] E.C. Peters, M. Petro, F. Svec, J.M.J. Fréchet, Anal. Chem., 69 (1997) 3646.

[56] S.L. Reegen, K.C. Frisch, J. Polym. Sci. Part A-1 Polym. Chem., 8 (1970) 2883.

[57] L.G. Wade, Organic Chemistry, Prentice Hall, Walla Walla, WA, 2002.

[58] C.A. Hunter, K.R. Lawson, J. Perkins, C.J. Urch, J. Chem. Soc. Perkin Trans., 2. (2001) 651.

Chapter 11. Polymeric monolithic columns with a high coverage of silver nanoparticles for chromatographic separations

Polymeric monolithic columns with a high coverage of silver nanoparticles for chromatographic separations

Enrique Javier Carrasco-Correa, María Jesús Lerma-García, Ernesto F. Simó-Alfonso, Guillermo Ramis-Ramos, José Manuel Herrero-Martínez*

Department of Analytical Chemistry, University of Valencia, Dr. Moliner 50, 46100 Burjassot, Valencia, Spain

In preparation

A methodology to prepare polymeric monoliths with enhanced surface coverage with silver nanoparticles (SNPs) is described. For this purpose, the pore surface of parent monolith, poly(GMA-*co*-EDMA), was functionalized with PMPMS, a polythiol, using a three-step procedure. Subsequently, the monolith was successively coated with two SNP layers. The second SNP layer was attached to the first one through a self-assembly process driven by a dithiol. The synthetized hybrid materials were characterized using thermogravimetry analysis and energy dispersive X-ray spectroscopy. The SNP content, which was 63.0 wt% (with respect to the whole monolith) for the first SNP layer, increased up to 95.7 wt% after attachment of the second SNP layer. The monolithic columns modified with two SNP layers were finally functionalized with an alkanethiol. Aromatic hydrocarbons and proteins were used to evaluate the chromatographic performance of these novel materials. The monoliths covered with SNPs showed increased retention of aromatic compounds with respect to the parent monolith. Further, after coverage with the last alkylthiol layer, good resolution of a mixture of three proteins was also achieved.

Keywords: Polymeric monoliths; silver nanoparticles; thiol-covered surfaces: self-assembly processes; multi-layer coverage

11.1. Introduction

Monolithic columns consisting of rigid synthetic polymers emerged in the early 1990s as an alternative to packed chromatographic columns. Their easy in situ preparation, high permeability and biocompatibility, stability along wide pH-ranges, and readily modifiable surface chemistries make these materials to be a competitive alternative to the conventional particle-based stationary phases [1]. Because of their singular porous structure, monolithic columns provide for rapid conventional mass transport with very low resistance to flow. As a result, these stationary phases have been used in HPLC [2] and capillary electromigration techniques [3-4]. Nevertheless, these monoliths have low surfaces areas due to the absence of an adequate mesoporous structure, which results in reduced separation efficiency and weak retention.

On the other hand, an important feature of polymeric monoliths is the access to a variety of surface chemistries which are easily available by direct copolymerization of functional monomers [2, 5], or by grafting of functional polymer chains onto the surface of pores [6-7] which allows the chemical modification of preformed reactive monoliths [3-4, 8-9]. In addition, the grafting approach enables the independent control of both porous structure and final surface chemistry. Functionalization of the pore surface using NPs is a recent approach in the development of polymeric stationary phases. The bonding of NPs on the monolith surface provides several immediate advantages, such as the enlargement of the surface [10], and opens many possibilities, including new surface chemistries, the construction of multilayers and the easily exchangeable chemistries.

Monolithic structures coated with NPs of latex [11-12], hydroxyapatite [14], carbon nanotubes [14], GNPs [10, 15-16], SNPs [17] and other metals [18-19] have been described and used in chromatographic separations. It is well-known that SNPs have some distinctive properties relative to other nanostructured metal particles, such as electrical conductivity [20], antimicrobial effects [21], and optical properties [22]; however, SNPs have not

been extensively used for analytical applications. Thus, the use of SNPs for affinity probes of peptides and proteins [23], sulfur drugs, and biothiols [24] in MALDI-MS has been reported. SNPs have been also used as preconcentrating supports of hydrophobic peptides and proteins [25]. Owing to its surface plasmon resonance, SNPs suspended in the BGE [26] or photodeposited [27] on the inner wall of capillary have been employed for on-column surface-enhanced Raman spectroscopy detection in CE. Also, suspensions of poly(ethylene oxide)-stabilized SNPs have been reported as effective pseudostationary phases for the CE separation of proteins [28]. Recently, monoliths with immobilized SNPs were used for the removal of excess radioiodine from radiolabelled pharmaceuticals [29].

Sulfur containing functionalities are known to strongly interact with noble metals and this property has been widely used in analytical chemistry [29]. Thus, several authors [10, 30-31] have studied the attachment of GNPs and SNPs on the pore surface of reactive polymer-based monolithic supports. In particular, poly(GMA-co-EDMA monoliths have been functionalized with cysteamine to afford a pore surface with thiol groups, to which GNPs or SNPs were attached. These monolithic columns have been used for the capture and separation of cysteine containing peptides [15] and as platforms to facilitate further variations in surface functionalities [10]. Another interesting approach developed by Paull's group was the photografting of poly(butyl methacrylate-co-ethylene dimethacrylate) monolith with poly(2-vinyl-4,4-dimethylazlactone), followed by reaction with cysteamine or ethylenediamine, as ligands, and posterior attachment of GNPs [16]. However, the drawback of surface modification reactions including cysteamine is that both amine and thiol groups can react with epoxide or azlactone functionalities. While reaction with the amine group affords desirable free thiol groups at the pore surface, reaction with the thiol group leads to a thioether with reduced affinity for gold or silver NPs. In addition, both bifunctional reagents used previously, i.e. cysteamine and ethylenediamine, may form crosslinks via a reaction of both of their end

functionalities with epoxide or azlactone functionalities. These side effects lead to a reduction in pore surface coverage with these noble metal NPs. Consequently, more efficient approaches are required to prepare polymer monoliths with enhanced coverage of immobilized GNP or SNPs. In this way, another strategy developed by Svec's group [32] to increase the thiol functionalities was the use of cystamine as reagent followed by a reduction of disulfide bonds with tris(2-carboxylethyl)phosphine hydrochloride. This leads to linking of the ligands exclusively through the amine groups, then leaving the thiol groups free for further bonding.

In this work, a different strategy was adopted to achieve a high thiol pore surface coverage of a preformed monolith using a multi-step functionalization method involving click reactions. In a previous work [4], a GMA-based monolith was derivatized by a three-step procedure, namely amination, vinylation with allyl glycidyl ether, and coating of a thin polythiol (PMPMS) film by click reaction. This thiol polymer provides tentacle-like phases with high surface coverage of unreacted thiol groups and, thus with concomitant potential of achieving grafting of further ligands and ultimately enhanced sample loading capabilities. In fact, the developed stationary phases afforded a more than 2-fold molar increase in surface thiol contents than previously reported. Then, this novel polythiol composite material with enhanced thiol coverage constitutes an excellent substrate for coverage with further ligands including NPs.

On the other hand, the preparation of multi-layers of nanomaterials using self-assembly processes with a variety of multifunctional reagents has emerged as a versatile tool for the development of materials with high coverage of NPs [33]. Thus, much work has been undertaken on the self assembly of GNPs onto surfaces presenting dithiol and diamine groups due to its potential applications in optoelectronics [34], microelectronics [35], and bioscience [36]. However, few studies have been conducted using this approach in the chromatographic

area, efforts being focused on the development of packing materials for HPLC [37] and open-tubular CEC [38].

The aim of this study was the development of a novel stationary phase with an enhanced surface coverage of SNPs through of a dithiol self-assembly methodology for chromatographic separations. First, to obtain a high coverage of thiol functionalities, the PMPMS polymer was bonded to the poly(GMA-co-EDMA) monolith by the aforementioned three-step functionalization process. Then, SNPs were attached onto the thiol active monolith surface, next modified with a dithiol ligand, and subsequently covered with a second SNPs layer. Finally, the surface of the attached SNPs was functionalized with an alkanethiol. The chromatographic performance of these novel materials was evaluated by using aromatic hydrocarbons and proteins.

11.2. Materials and methods

11.2.1. Reagents and other materials

GMA, EDMA, γ-MPS, 1-hexanethiol (HMT) and 1,6-hexanedithiol (HDT), AGE, DPDS, 2-mercaptoethanol, aromatic hydrocarbons (benzene, naphthalene, anthracene and benz[a]anthracene) and proteins (ribonuclease A from bovine heart, cytochrome C from bovine pancreas and myoglobin from equine heart) were from Aldrich (Milwaukee, WI, USA). Cyclohexanol, 1-dodecanol, HPLC-grade ACN, MeOH and EtOH were from Scharlau (Barcelona, Spain). AIBN was from Fluka (Buchs, Switzerland). PMPMS was from ABCR (Karlsruhe, Germany). SNP suspension with particle size of 20 nm was from Alfa Aesar (Lancashire, United Kingdom). Unless otherwise stated, other chemicals were of analytical grade. Deionized water was obtained with a Barnstead deionizer (Sybron, Boston, MA, USA). Stock solutions of aromatic hydrocarbons, prepared in ACN at 1 mg mL^{-1} each, were kept at 4 ºC until use. Test mixtures of these solutions (containing 100 µg mL^{-1} each analyte and uracil) were prepared daily by dilution with the mobile phase. Proteins were

dissolved in water at a concentration of 1.0 mg mL^{-1}. Uncoated fused-silica capillaries of 33.5 cm total length and 375 µm O.D. × 100 µm I.D. with UV-transparent external coating (Polymicro Technologies, Phoenix, AZ, USA) were used.

11.2.2. Instrumentation

To photoinitiate polymerization, the capillaries were placed into an UV crosslinker chamber (Model CL1000, UVP, Upland, CA, USA) equipped with five UV lamps (5 × 8 W, 254 nm). To introduce the functionalizing reagents into the monolithic capillary columns, a syringe pump (Model 100, KD Scientific, New Hope, PA, USA) was employed. The washing steps were performed with an HPLC pump (1100 Series, Agilent Technologies, Waldbronn, Germany). The SNP dispersion was pumped through the monolithic capillary columns using the HPLC pump provided with a manual six-port sample injection valve (7725i, Rheodyne, Bensheim, Germany), a 350 µL sample loop was used to avoid contamination of the pump with the SNPs. For the nanoLC experiments, an HP3DCE instrument (Agilent) equipped with a diode array UV detector (Agilent Technologies) was employed. Nitrogen was used to flush the mobile phase through the column by the external pressure system. A Hitachi S-4800 integrated with backscattered electron detector and a QUANTAX 400 energy dispersive spectrometer (Bruker, Germany) was employed to obtain SEM/backscattered electron (BSE) images and energy dispersive X-ray (EDAX) analysis. For these measurements, the monoliths were coated with a very thin-layer of conductive carbon instead of the more usual Au/Pd coating. Thermogravimetric analysis (TGA) was carried out using a Pyris Diamond instrument (PerkinElmer Instruments, Shelton, CT, USA) in a temperature range of 30-800 ºC.

11.2.3. Preparation of poly(GMA-co-EDMA) monoliths

For the preparation of monoliths in capillary format, and prior to polymerization, the inner wall of the fused-silica capillaries was modified to provide covalent attachment of the monolith. For this purpose, wall modification with γ-MPS was performed as described [39]. The polymerization mixtures were prepared by weighing GMA (20 wt%), EDMA (5 wt%), and a binary pore-forming solvent constituted by CYC (70 wt%) and DOD (5 wt%). AIBN (1 wt% with respect to the monomers) was added as initiator [40]. To obtain a clear solution, sonication for 10 min followed by purging with nitrogen for 10 more min was applied. The preconditioned capillary was filled with the polymerization mixture up to a length of 8.5 cm. Photopolymerization was accomplished by irradiation of the capillaries within the UV chamber at 0.9 J cm^{-2} for 15 min. Then, an HPLC pump was used to flush the columns for 30 min with MeOH to remove the pore-forming solvents and remaining unreacted monomers.

11.2.4. Functionalization of poly(GMA-co-EDMA) with PMPMS

The capillaries containing the poly(GMA-co-EDMA) monoliths were first flushed with MeOH, followed by flushing with aqueous 4.5 M ammonia at 60 ºC for 2 h at a flow rate of 60 µL h^{-1}. Then, they were washed with MeOH until reaching pH 7 at the outlet. Afterwards, the syringe pump was used to force a 4% (v/v) AGE aqueous solution at 60 ºC for 2 h at a flow rate of 60 µL h^{-1}. Afterwards, using an HPLC pump, the capillaries were washed with MeOH and acetone, and filled with a freshly prepared 10% (v/v) PMPMS solution in acetone (this solution also contained 1% AIBN). The columns were sealed with GC septa and maintained in an oven at 60 ºC, where the radical addition occurred. After 24 h, the capillaries were removed from the oven, and rinsed with acetone and MeOH. The yield of the surface modification reaction with

PMPMS was controlled by determining the concentration of thiol groups bonded to the monolith surfaces using the DPDS assay [8].

11.2.5. Preparation of monolithic columns with multi-layer SNPs

The capillaries containing the PMPMS-modified monoliths were flushed with EtOH (as mobile phase) using a HPLC pump with a T-splitter to achieve a flow rate of 2 µL min^{-1}. The 350 µL loop attached to the six-port injection valve was filled with the SNPs solution. Upon switching the valve, this solution was passed through the column until it turned dark red and yellow drops appeared at the column outlet.

The columns, covered with a first SNP layer, were flushed with 5 mL of pure HDT using a syringe pump at 120 µL h^{-1}. Then, the resulting monolithic columns were modified again with a second SNP layer. For this purpose, the procedure described above for attachment with the SNPs was applied. Finally, the second SNP layer was further modified by forcing 3 mL of pure HMT through the column at a flow rate of 120 µL h^{-1}. The detailed scheme of the successive reactions is depicted in Fig. 11.1.

11.2.6. Evaluation of the silver content in the SNP-modified monoliths using TGA

The silver content of the SNP-modified monoliths was established using TGA. The TGA curves were obtained within the 30-800 ºC range, at a heating rate of 5ºC/min, in an argon atmosphere (flow rate 10 mL min^{-1}). The capillaries were cut to the same length with a weight of ca. 5 mg. It was observed that the PTFE coating of the UV-transparent capillaries decomposed at around 450 ºC, while the monolithic polymer decomposed at about 360 ºC. In the Ar atmosphere, the residue obtained after heating at 800 ºC should contain SiO_2 (from the capillary walls and the PMPMS) and probably carbon and sulfur

compounds; however, it can be assumed that silver is mostly present in the metal reduced state. This is because Ag_2O decomposes at low temperatures [41] and also because silver alkyl-mercaptides when heated in a polystyrene matrix give rise to metallic silver NPs at temperatures as low as 250 ºC [42]. Assuming that most silver is in the reduced metallic form, the silver content in the monoliths was calculated as follows:

$$Ag\ (wt\%) = \left[\frac{W_{SB}-W_{EB}}{W_{SI}-W_{EI}}\right] \times 100 \qquad (11.1)$$

where W_{SB} is the weight of monolithic capillary column with attached SNP after burning the organic polymer and the capillary coating by heating, W_{EB} is the weight of the empty capillary after burning the coating, W_{SI} is the initial weight of the monolithic capillary column with attached SNP before its burning, and W_{EI} is the initial weight of the empty capillary, also before burning.

11.2.7. Nano-LC procedure

Extra-column effects are a major point in nano-LC due to the very low variance of chromatographic peaks. In order to test the multi-layer monolithic columns in nano-LC, the chromatographic experiments were carried out with a CE system by applying external pressure to the capillary end to pump the mobile phase. For this purpose, a constant pressure of 0.1-1.2 MPa (1-12 bar) was used. In situ hydrodynamic injection by applying pressure for a few seconds and UV monitoring without taking the mobile phase out of the capillary are other advantages of using a CE system for nanoLC separations. On-column injection and on-column detection helps reducing extra-column dispersion when compared with a classical HPLC system. Thus, the monolithic column, placed in the CE system, was equilibrated with the mobile phase by applying 1 MPa at the outlet (short-end injection) until a stable baseline was achieved. Separation was performed at 25 ºC (at several applied pressures). The test

mixtures were hydrodynamically injected under 1 MPa for 10 s. Detection was performed at 214 and 254 nm. The specific separation conditions for the test mixtures are indicated in the corresponding figure captions.

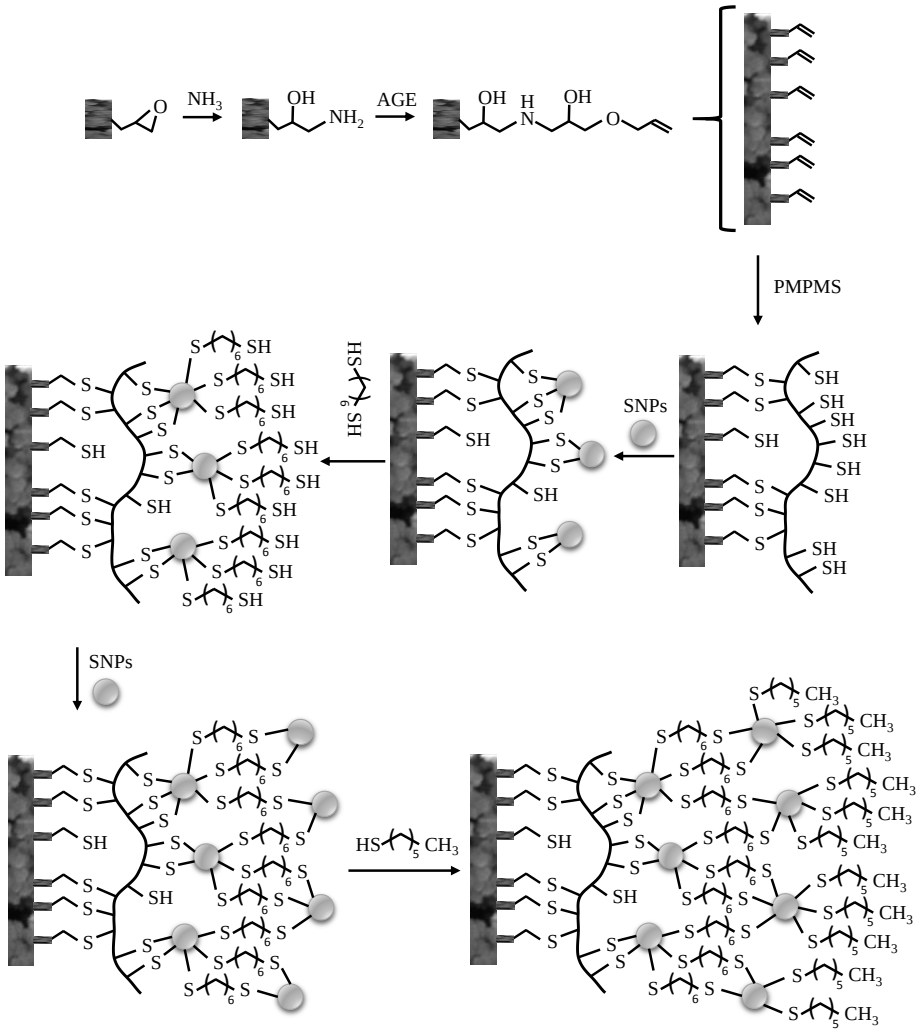

Fig. 11.1. Scheme for the surface of modification of poly(GMA-*co*-EDMA) monoliths with ammonia, AGE, bonding of PMPMS, attachment of the 1st SNP layer, coating with HDT, attachment of the 2nd SNP layer, and final coverage with HMT.

11.3. Results and discussion

11.3.1. Preparation and characterization of monolithic columns with multi-layer SNPs

The epoxide functionalities of a previously developed poly(GMA-co-EDMA) monolith [3] were used to prepare the thiol modified column. The monoliths prepared with the optimized poly(GMA-co-EDMA) polymerization mixture showed a high permeability [43], which enormously facilitated the rinsing steps employed in surface modification. However, the main advantage of this monolith was the high concentration of accessible epoxide groups (5.98 mmol epoxide g^{-1} monolith [43]). This is important because of the high density of reactive sites on the polymer surface. In order to further enhance the surface coverage with reactive groups, the poly(GMA-co-EDMA) monoliths were used to prepare PMPMS-modified monoliths. For this purpose, the multi-step procedure indicated above was applied (Section 11.2.6) [4]. These monoliths provided dense coverages with reactive thiol groups (2.32 mmol thiol g–1 monolith), more than two-fold denser than other functionalization protocols described in the literature using sodium hydrogen sulfide [39] and thiol amino acids [16].

After the desire high density of thiol groups was generated on the polymer surface, a SNP dispersion was pumped through the monolithic column. When the 20 nm SNPs were attached to the monolith, its color changed from white to dark red. When SEM micrographs of this monolith were taken with a BSE detector, an excellent surface coverage with SNPs (spots randomly distributed) was observed (Fig. 11.2A). Elemental analysis using EDAX indicated the presence of 59.8 wt% silver, and TGA was consistent with this value (Eq. 11.1, 62.9 wt% silver). In addition, this content was much higher than that previously reported for SNPs (12.1 wt% using 4 nm SNPs) [44] and even higher than that achieved for GNPs with a similar size (44.8-53.2 wt% Au using 15-20 nm GNPs) [10, 45]. The accessible surface of the SNPs was then functionalized by

flushing the column with pure liquid HDT at 120 µL h^{-1}. The required volume to achieve a complete SNPs coverage with this bifunctional reagent was studied. For this purpose, a mixture of aromatic hydrocarbons was injected into the column and pressure was applied to the outlet for nano-LC separation. Fig. 11.3A shows the retention factors of aromatic hydrocarbons (benzene and benz[a]anthracene) versus the HDT volume (mL) flushed through the column. A plateau was reached after 5 mL, indicating saturation of all accessible SNPs with HDT. SEM/BSE micrographs of these SNP-modified monoliths treated with HDT are shown in Fig. 11.2B. As observed, SNPs were not detected on monolith the surface, probably because they were covered by a layer of bonded alkanedithiol. Then, this column was flushed again with a SNP dispersion by following the procedure described above. In this way, HDT performed as a crosslinker for making a multilayer SNP film. After this treatment, an enhancement of the dark red color of the column was evidenced. The SEM/BSE image (Fig. 11.2C) also showed an excellent and remarkably regular coverage of the polymer surface with the SNPs. This confirmed the linkage of the SNPs on the HDT layer. The coverage of SNPs was estimated by both EDAX and TGA. Again, the comparison of data from both techniques revealed Ag contents much higher than those achieved by linking a single SNP layer and also similar to each other (90.2 wt% and 95.7 wt%, respectively). It is interesting to observe that EDAX gave rise again to a slightly lower percentage than TGA.

In any case, both the EDAX and TGA data indicate that the presence of second SNPs layer produced an increase of ca. 30 wt% in the Ag content of the monolith with respect to the Ag content due to the first SNP layer. The smaller increment due to the second SNP layer indicated a lower bonding capacity of the first layer when compared to the formerly used PMPMS layer.

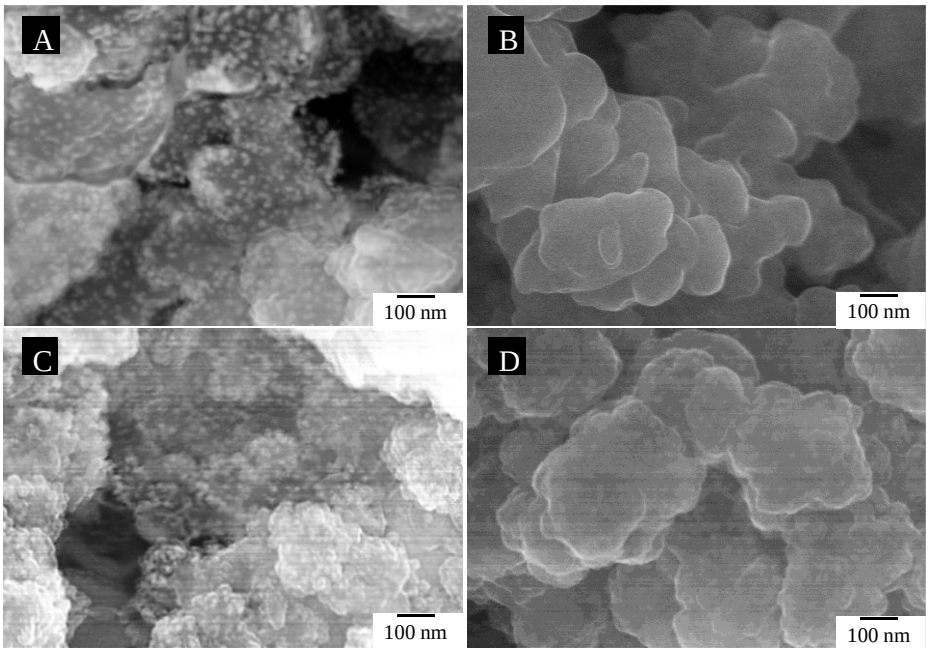

Fig. 11.2. SEM/BSE micrographs of poly(GMA-*co*-EDMA) monoliths functionalized with PMPMS and modified with: a 1st SNP layer (A); the 1st SNP layer coated with HDT (B); attachment of a 2nd SNP layer (C); as in C after final coverage with HMT (D). The images were obtained at 100k magnification. The white spots in traces A, C and D are the SNPs.

The surface of the monolithic column with the SNP multilayer film was finally modified with an alkanethiol (HMT). In order to achieve a complete coverage of this second SNP layer, the volume of this ligand to be forced through the column at 120 µL h^{-1} was also optimized. Fig. 11.3B shows the retention factors of aromatic hydrocarbons obtained at increasing HMT volumes. A plateau was reached after flushing the column with 3 mL of the pure reagent, which indicated the saturation of the accessible SNP surfaces present in the second SNP layer. Then, 3 mL HMT was selected for the studies that followed. As shown in Fig. 11.2D, the presence of the bonded HMT hindered the observation of the second SNP layer.

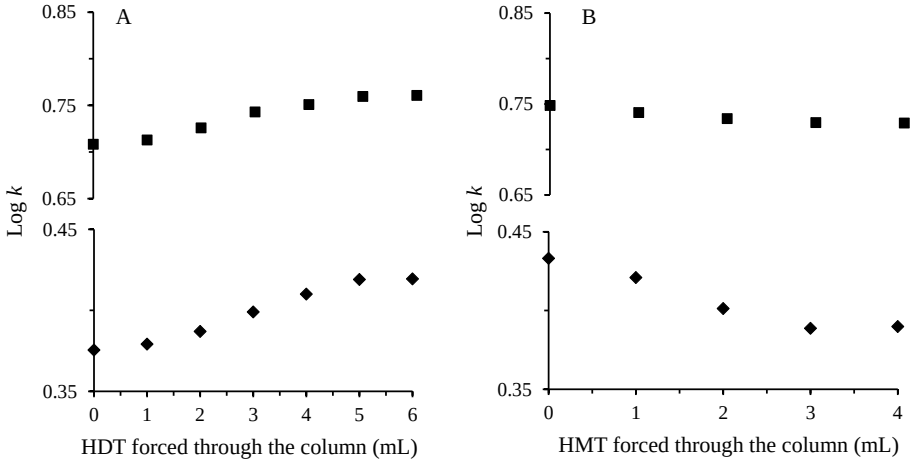

Fig. 11.3. Effect of increasing the volume of thiol reagent used for derivatization of the monoliths: (A) HDT and (B) HMT. Retention factors of benzene (♦) and benz[a]anthracene (■). Mobile phase, 50:50 (v/v) ACN-water containing 5 mM acetic acid (pH 3.0); hydrodynamic injection, 10 bar × 10 s; mobile phase pumped at 10 bar; UV detection at 254 nm.

11.3.2. Chromatographic performance of monolithic columns covered with a SNP multi-layer

The chromatographic performance of the different monolithic columns described in this work was tested using small molecules (aromatic hydrocarbons) and proteins. Fig. 11.4 shows the separations of aromatic hydrocarbons (benzene, naphthalene, anthracene and benz[a]anthracene) obtained using different monoliths at functionalization stages. Using the generic poly(GMA-co-EDMA) (Fig. 11.44A), and in spite of the low hydrophobicity of GMA-based monoliths, the test compounds were well resolved with efficiencies ranging from 2300 to 21000 plates m^{-1} within a short analysis time (< 15 min). On the contrary, the monoliths functionalized with PMPMS were not able to separate the analytes which coeluted as a single peak (data not shown). The separation changed dramatically after the attachment of

the first SNP layer (Fig. 11.4B). As observed in this figure, the retention of the analytes increased largely. This can be explained by the higher affinity of π-electron systems towards the silver atom. In fact, retention increased according to the degree of unsaturation of the test solute (e.g. see retention time of anthracene and benz[a]anthracene). Thus, the affinity of SNPs toward solutes with electron-rich unsaturated bonds has been described [46]. When this monolithic column was functionalized with HDT, a decrease in the retention, particularly remarkable for the late eluting compounds, was evidenced (Fig. 11.4C). Also, a slight improvement in efficiency was observed. This could be explained by a reduction in the direct interaction of the aromatic compounds with the Ag surface after attachment of HDT. However, the presence of this ligand was not enough to hinder retention of the aromatic solutes by the SNP layer. As suggested [45], for sterical reasons, the attached ligand always covers only a small fraction of the external surface area of the NP; consequently, most of the surface remains available for interactions with small molecules.

The strong interaction between unsaturated compounds and SNPs was again evidenced after attachment of the second SNP layer (see Fig. 11.4D), giving rise to an increase of retention and peak broadening. However, the chromatographic effects were smaller than those observed after bonding the first SNP layer. When this column was treated with HMT, efficiency increased and an improvement in peak shape was again observed (Fig. 11.4E), giving higher efficiencies than those modified with HDT. This could be due to the high density of the last coverage with HMT and consequently also to the increase in the surface homogeneity.

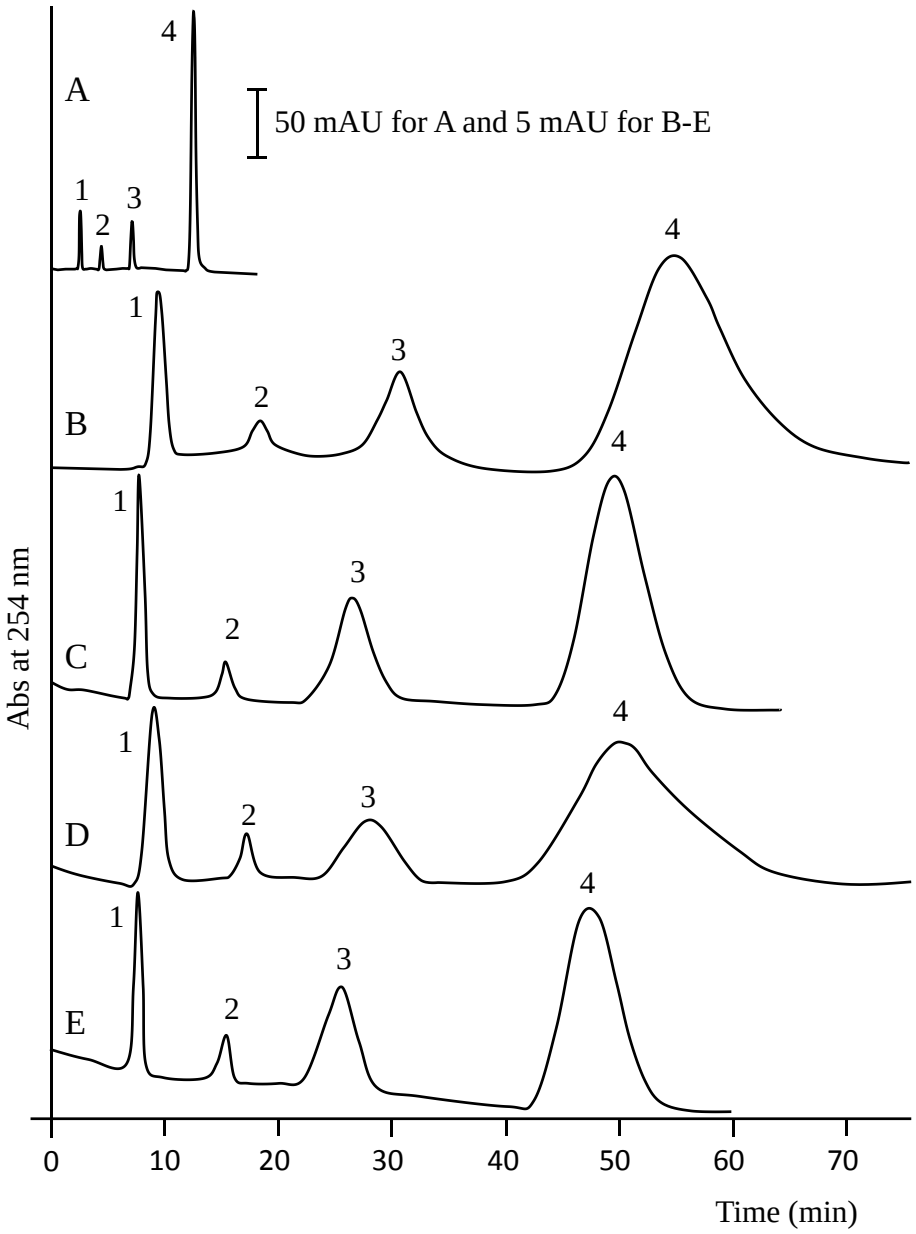

Fig. 11.4. Chromatographic separation of aromatic compounds using several poly(GMA-*co*-EDMA) monoliths: parent column (A) and GMA-based monoliths functionalized with PMPMS and further modified with: a 1st SNP layer (B); a 1st SNP layer coated with HDT (C); as in C after attachment of a 2nd SNP layer (D); as in D after final coverage with HMT (E). Other conditions as in Fig. 11.3.

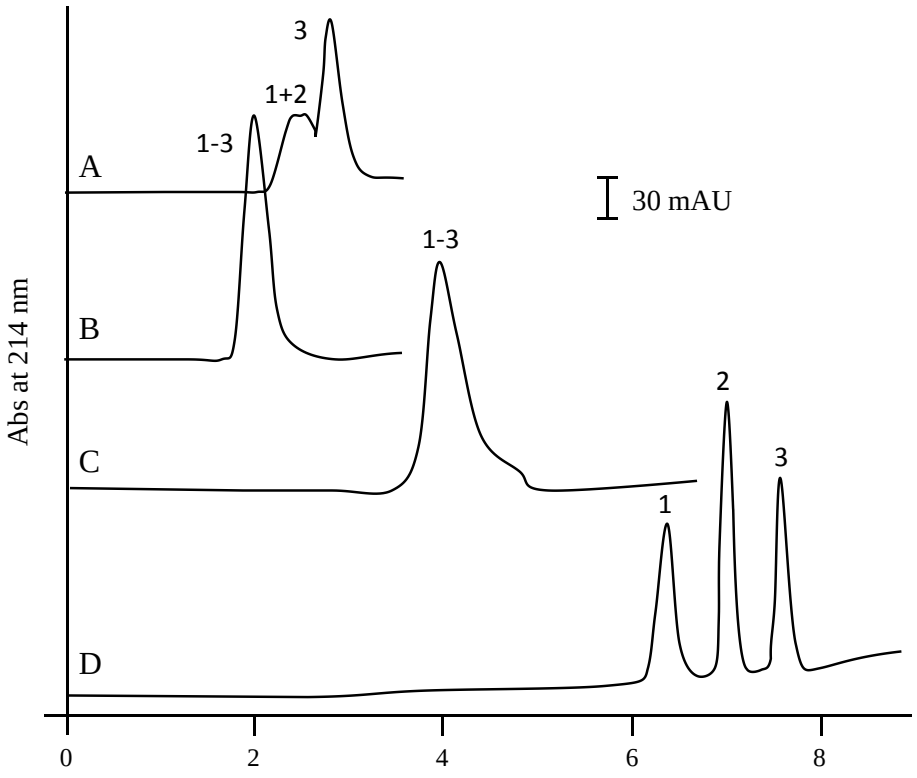

Fig. 11.5. Chromatographic separation of proteins using several poly(GMA-*co*-EDMA) monoliths: parent column (A) and GMA-based monoliths functionalized with PMPMS (B) and further modified with: a 1st SNP layer (C) and after attachment of two successive layers by HDT self-assembling procedure and with a final HMT coverage (D). Peak identification: 1, ribonuclease A; 2, cytochrome C; 3, myoglobin. Other conditions as in Fig. 11.3.

The performance of the parent and functionalized monoliths was also evaluated using a mixture of proteins (ribonuclease A, cytochrome C and myoglobin). Fig. 11.5A shows that the parent monolith provided a rather poor separation of these proteins. On the other hand, the PMPMS-modified monolith (Fig. 11.5B), as well as those modified with a first SNP layer (Fig. 11.5C), then further covered with HDT and with a second SNP layer without further modification (data not shown), led to the coelution of all proteins in a single peak. However, the columns modified with two SNP layers and finally

functionalized with HMT (Fig. 11.5) showed a successful separation of the three proteins in reversed phase mode. The elution order was produced in order of increasing hydrophobicity, as expected for reversed phase behavior. These results can be favorably compared to those reported for the same proteins using monolithic columns containing GNPs functionalized with 1-octanethiol [47] or with higher alkanethiol and mercaptoalkanoic acid ligands [45]. Nevertheless, it should be mentioned that in our case the separation was successfully achieved under isocratic conditions and using a final layer of HMT, which has an alkyl chain length much shorter than those used in the reported studies.

11.4. Conclusions

Novel monolithic stationary phases with a significant enhanced surface coverage of SNPs, prepared through a self-assembly methodology, have been developed. Previous preparation of the parent monolith surface by covering with a spacer arm first and with PMPMS, a polythiol, afterwards, provided an excellent platform for the subsequent coverage with SNPs. Thus, due to the high density of available thiol groups and the flexibility of the bonded polythiol skeleton, a SNP content as high as 63 wt% was achieved for the first SNP layer. This value was increased up to 93.7 wt% after attachment of a second SNP layer by means of a dithiol self-assembly process. The final modification of the bonding of an alkanethiol on the second SNP layer, thus to achieve a largely homogeneous hydrophobic layer. The developed materials were applied to the nano-LC separation of aromatic hydrocarbons and proteins. The monoliths covered with SNPs showed an enhanced retention of aromatic compounds, which was in agreement with the strong affinity of unsaturated compounds for the silver surfaces. On the other hand, the monolithic columns modified with two SNP layers and finally functionalized with an alkanethiol showed satisfactory retention and resolution for the mixture of aromatic compounds, as well as a satisfactory separation of proteins under RP elution conditions. Therefore, this work constitutes a significant advance within the field of the

modification of monoliths with NPs. The procedures here described to achieve large SNP coverage of monoliths can further be extended to the preparation of stationary phases covered with other NPs, also providing new promising surface for the enhanced separation of small and large molecules.

Acknowledgements

Work supported by Project CTQ2014-52765-R (MINECO of Spain and FEDER funds). E.J.C-C. thanks the MINECO for an FPI grant. The authors thank Dr. E. Navarro-Raga from Servei Central de Suport a la Investigació Experimental (SCSIE) of University of Valencia for his assistance with SEM/BSE measurements.

References

[1] Y.Y. Li, H.D. Tolley, M.L. Lee, J. Chromatogr. A, 1218 (2011) 1399.

[2] Q. Wang, F. Svec, J.M.J. Fréchet, Anal Chem., 65 (1993) 2243-2248.

[3] E.J. Carrasco-Correa, G. Ramis-Ramos, J.M. Herrero-Martínez, J. Chromatogr. A, 1298 (2013) 61.

[4] E.J. Carrasco-Correa, G. Ramis-Ramos, J.M. Herrero-Martínez, M. Lämmerhofer, J. Chromatogr. A, 1367 (2014) 123.

[5] E.C. Peters, M. Petro, F. Svec, J.M.J. Fréchet, Anal. Chem., 70 (1998) 2288.

[6] C. Viklund, F. Svec, J.M.J. Fréchet, K. Irgum, Biotechnol. Prog. 13 (1997) 597.

[7] T. Toht, E.F. Hilder, J.J. Donovan, F. Svec, J.M.J. Fréchet, Macromolecules 36 (2003) 1677.

[8] D. Moravcová, E.J. Carrasco-Correa, J. Planeta, M. Lämmerhofer, S.K. Wiedmer, J. Chromatogr. A, DOI: 10.1016/j.chroma.2015.05.004

[9] F. Svec, J.M.J. Fréchet, J. Chromatogr. A, 702 (1995) 89.

[10] Q. Cao, Y. Xu, F. Liu, F. Svec, J.M.J. Fréchet, Anal. Chem., 82 (2010) 7416.

[11] E.F. Hilder, F. Svec, J.M.J. Fréchet, J. Chromatogr. A, 1053 (2004) 101.

[12] P. Zakaria, J.P. Hutchinson, N. Avdalovic, Y. Liu, P.R. Haddad, Anal. Chem., 77 (2005) 417.

[13] J. Krenkova, N.A. Lacher, F. Svec, Anal. Chem., 82 (2010) 8335.

[14] Y. Li, Y. Chen, R. Xiang, D. Ciuparu, L.D. Pfefferie, C. Horváth, J.A. Wilkins, Anal. Chem., 77 (2005) 1398.

[15] Y. Xu, Q. Cao, F. Svec, J.M.J. Fréchet, Anal. Chem., 82 (2010) 3352.

[16] D. Connolly, B. Twanley, B. Paull, Chem. Commun., 46 (2010) 2109.

[17] J. Liu, I. White, D.L. DeVoe, Anal. Chem., 83 (2011) 2119.

[18] E. Guihen, J.D. Glennon, Anal. Lett., 36 (2014) 3309.

[19] D. Connolly, S. Currivam, B. Paull, Proteomics, 12 (2012) 2901.

[20] L.T. Chang, C.C. Yen, J. Appl. Polym. Sci., 55 (1995) 371.

[21] Q.L. Feng, F.Z. Cui, T.N. Kin, J. Mater. Sci. Lett., 18 (1999) 559.

[22] W. Fritzsche, H. Porwol, A. Wiegand, S. Bornmann, J. Köhler, Nanostruct. Mater., 10 (1998) 89.

[23] L. Hua, J. Chen, L. Ge, S.N. Ta, J, Nanopart. Res., 9 (2007) 1133.

[24] K. Shrivas, H.-F. Wu, Rapid Commun. Mass Spectrom., 22 (2008) 863.

[25] K. Shrivas, H.-F. Wu, Anal. Chem., 80 (2008) 2583.

[26] K. Prikryl, K. Klepárnik, F. Foret, J. Chromatogr. A, 1226 (2012) 43.

[27] W.F. Nirode, G.L. Devault, M.J. Sepaniak, Anal. Chem., 72 (2000) 1866.

[28] W. Qin, J. Tursen, Anal. Sci., 25 (2009) 333.

[29] D. Sykova, V. Kasicka, I, Miksik, P. Rezanka, K. Zaruba, P. Matejka, V. Kral, J. Sep. Sci., 33 (2010) 372.

[30] M. Guerrouache, S. Mahouche-Chergui, M.M. Chehimi, B. Carbonnier, Chem. Commun., 48 (2012) 7486.

[31] Y. Lv, Z. Lin, T. Tan, F.Svec, Bioteck. Bioeng., 111 (2014) 50.

[32] Y. Lv, Z. Lin, F. Svec, Analyst, 137 (2012) 4114.

[33] S.A. Jadhav, J. Mater Chem., 22 (2012) 5894.

[34] A.N. Shipway, E. Katz, I. Willner, Chem. Phys. Chem., 1 (2000) 18.

[35] F.K. Liu, Y.C. Chang, F.H. Ko, T.C. Chu, B.T. Dai, Microelectron. Eng., 67-68 (2003) 702.

[36] T.B. Dubrovsky, Z.Z. Hou, P. Stroeve, N.L. Abbott, Anal. Chem., 71 (1999) 327.

[37] Q.-S. Qu, Z.-X. Zhang, Z.-Z. Zhao, Z.-Y. Hu, X. Yan, J. Chromatogr. A, 1198-1199 (2008) 95.

[38] F.-K- Liu, Y.-T- Hsu, J. Chromatogr. A, 1083 (2005) 205.

[39] B. Preinerstorfer, W. Bicker, W. Lindner, M. Lämmerhofer, J. Chromatogr. A, 1044 (2004) 187.

[40] K. Štulík, V. Pacáková, J. Suchánková, P. Coufal, J. Chromatogr. B, 841 (2006) 79.

[41] B.V. L'vov, Thermochim. Acta, 333 (1999) 13.

[42] G. Carotemuto, Polymer Eng. Sci., 46 (2006) 1016.

[43] E.J. Carrasco-Correa, G. Ramis-Ramos, J.M. Herrero-Martínez, J. Chromatogr. A, 1379 (2015) 100.

[44] O. Sedlacek, J. Kucha, F. Svec, M. Hruby, J. Sep. Sci., 37 (2014) 798.

[45] L. Terborg, J.C. Masini, L. Michelle, K. Lipponen, M.-L- Riekolla, F. Svec, J. Adv. Res., 6 (2015) 441.

[46] Z. D. Pozun, K. Tran, A. Shi, R.H. Smith, G. Henkelman, J. Phys. Chem. C, 115 (2011) 1811.

[47] Y. Lv, F.M. Alejandro, J.M.J. Fréchet, F. Svec, J. Chromatogr. A, 1261 (2012) 121.

Chapter 12. Hybrid methacrylate monolithic columns containing magnetic nanoparticles for capillary electrochromatography

Journal of Chromatography A, 1385 (2015) 77–84

Contents lists available at ScienceDirect

Journal of Chromatography A

journal homepage: www.elsevier.com/locate/chroma

Hybrid methacrylate monolithic columns containing magnetic nanoparticles for capillary electrochromatography☆

Enrique Javier Carrasco-Correa, Guillermo Ramis-Ramos, José Manuel Herrero-Martínez*

Department of Analytical Chemistry, University of Valencia, Dr. Moliner 50, 46100 Burjassot, Valencia, Spain

Vinylized iron oxide magnetic nanoparticles (VMNPs) were incorporated into polymethacrylate monolithic columns to develop novel stationary phases with enhanced separation performance. The VMNPs were dispersed in a polymerization mixture containing GMA and EDMA as monomers, CYC and DOD as porogens and AIBN as initiator. The stability of the VMNPs in the polymerization mixture was investigated at several VMNP contents. Using short UV-polymerization times, polymeric beds with homogenously dispersed VMNPs were obtained. The novel stationary phases were characterized by scanning electron microscopy. The chromatographic performance of these hybrid monoliths was evaluated using alkyl benzenes and organophosphorous pesticides as test solutes. Using CEC, efficiencies up to 130,000 plates/m were achieved. The increase of the specific surface area of hybrid monoliths led to an increase in the retention of all the test analytes, and an enhancement of efficiency. The resulting hybrid monolithic columns exhibited satisfactory column to-column and batch-to-batch reproducibilities with RSDs values below 6%.

Keywords: magnetic nanoparticles, hybrid monolithic columns, UV initiation, capillary electrochromatography, organophosphorous compounds

12.1. Introduction

In the last years, with the rapid development of nanotechnology, a wide variety of new nanomaterials have provided a bridge between bulk materials and atomic or molecular structures. The impact of nanomaterials in fields such as material sciences, chemistry, physics and many others is large. The scientific interest in separation science of these nanomaterials relies on its large surface-to-volume ratios as well as multiform morphologies, which can be used to increase retention and to speed up mass transfer, thus improving the efficiency, as well as modify the selectivity in chromatographic separation [1,2]. In spite of these benefits, the use of ultra-high pressure during column packing and separation process has limited its use in chromatography and even in CEC [3]. Thus, the applications of nanomaterials in CEC were mostly focus on new pseudostationary phases [4] and open-tubular CEC [5, 6]. However, these applications are respectively hindered by light scattering of NPs and the low stationary to mobile phase ratios.

Organic monolithic stationary phases, that emerged in the early 1990s, have attracted increasing attention due to their easy in situ preparation, good permeability and biocompatibility, wide pH stability, and readily available surface chemistries [7-9]. Traditionally, approaches tailoring the surface chemistry of monoliths include adoption of functional monomers [10,11], chemical modification [12,13], and grafting of functional polymer chains [14,15]. Nevertheless, these monoliths have low surface areas due to the absence of an adequate mesoporous structure, which results in weak retention. For this reason, new functionalization methods consisting of adding nanoparticles to the monoliths have emerged as a way of increasing the surface-to-volume ratio, as well as to serve as new platforms to further or more efficiently modify the surface chemistries [16-25].

Within nanomaterials, iron oxide magnetic nanoparticles (MNPs) have been one of the most explored smart materials for a wide range of applications including biosensing [26], medical [27-28], and chemistry technologies [29-

33]. It should be pointed out that MNPs tend to agglomerate. To address this problem, tailored functional groups have been anchored to the MNP surface. One important characteristic of iron oxide MNPs is the capability to covalently bind silane-coupling materials such as γ-MPS [34-36], 3-aminopropyltrimethoxysilane [37] and *p*-aminophenyltrimethoxysilane [38]. Moreover, silanization endows the MNPs with an easily modifiable surface, which can be used to further grafting other desirable functional groups. Thus, derivatized MNPs can be incorporated to silica, methacrylate and other acrylate materials. The incorporation of MNPs to a polymer is expected to alter its properties (mechanical, thermal and others) [39]. This has encouraged many research oriented to develop polymer/magnetite materials for a variety of technological applications; however, the combination of MNPs and polymeric monoliths to form hybrid materials with potential application in chromatography and other separation techniques has been still scarcely explored. Krenkova et al. [40, 41] have recently proposed the use of pipette tips with methacrylate-based monoliths including iron oxide nanoparticles in their structure for the extraction of phosphopeptides.

In this work, MNPs were first silanized to link vinyl groups on their surfaces. Then, hybrid polymeric monoliths containing different amounts of the resulting vinylized magnetic nanoparticles (VMNPs) were prepared by copolymerization. Poly(GMA-co-EDMA), which is a well studied material, was chosen as the polymer matrix, being their chains generated by fast UV-initiated polymerization in the presence of VMNPs. The incorporation of increasing amounts of VMNPs into the composites and their effects on the CEC separation of test analytes (alkyl benzenes and organophosphorous pesticides) was investigated.

12.2. Materials and methods

12.2.1. Chemicals and materials

Iron(II) chloride tetrahydrate, iron(III) chloride hexahydrate, GMA, EDMA, META, γ-MPS, were from Sigma-Aldrich (Milwaukee, WI, USA). AIBN was from Fluka (Buchs, Switzerland). CYC, DOD, HPLC-grade ACN, MeOH and acetic acid were from Scharlau (Barcelona, Spain). Thiourea as EOF marker, alkyl benzenes from Riedel de Haën (Seelze, Germany) and the OPs chlorpyrifos, methylchlorpyrifos, quinalphos, malathion, profenofos, fensulfothion, suprofos and dialifos (Sigma-Aldrich) as probes, were used. Deionized water was obtained with a Barnstead deionizer (Sybron, Boston, MA, USA).

Fused-silica capillaries of 33.5 cm length and 375 μm O.D. × 100 μm I.D. with UV-transparent external coating (Polymicro Technologies, Phoenix, AZ, USA) were used. The effective monolithic bed length was 8.5 cm.

12.2.2. Instrumentation

CEC experiments were performed with an HP^{3D}CE instrument (Agilent Technologies, Waldbronn, Germany) equipped with a diode-array UV detector and connected to an external nitrogen pressure supply. Data acquisition was performed with the ChemStation Software (Rev.A.10.01, Agilent). Prior to use, all mobile phases for CEC were degassed with a D-78224 ultrasonic bath (Elma, Germany). To photoinitiate polymerization, the capillaries were placed into an UV crosslinker chamber (Model CL1000, UVP, Upland, CA, USA) equipped with five UV lamps (5 × 8 W, 254 nm). SEM/ EDAX of monolithic materials was performed with a scanning electron microscope (S-4800, Hitachi, Ibaraki, Japan) provided by a field emission gun, an EMIP 3.0 image data acquisition system, and a microanalysis system (Rontec, Normanton, UK). TEM images of MNPs and VMNPs were obtained using a Jeol (Tokyo, Japan)

model JEM-1010 microscope operated at 100 kV. For this purpose, the nanoparticles were dispersed in pure ethanol by sonication, and 0.05 mL of this suspension was placed on a 200-mesh Cu grid coated with a holey amorphous carbon film. The ethanol was evaporated prior to TEM analysis. Images were obtained using a MegaView III camera provided with the AnalySIS® image data acquisition system. FTIR spectra of powdered magnetic nanostructures (MNPs and VMNPs) were obtained with a Jasco 4100 type A spectrophotometer (Jasco, Easton, MD) fitted with a single reflection attenuated total reflectance (ATR) accessory. Spectra were accomplished from 4000 to 500 cm^{-1} in the absorbance mode at a 2 cm^{-1} resolution with 100 scans. The sedimentation of suspensions of VMNPs in the polymerization mixtures was monitored turbidimetrically. For this purpose, an UV-Vis spectrophotometer (Model 8453, Agilent Technologies) provided with a 1 mm optical-path quartz cell (Hellma, Müllheim, Germany) was used.

12.2.3. Preparation and characterization of VMNPs

Fe_3O_4 MNPs were first prepared by coprecipitation according to literature [42]. Thus, 180 mL of an aqueous solution containing 11.2 mmol Fe^{3+} and 5.6 mmol Fe^{2+} was heated to 50 °C. Then 12.5 mL of aqueous ammonia was added under vigorous stirring. After 30 min, the temperature was increased to 90 °C and kept for 30 min more. Nitrogen was used as the protective gas in the whole experiment. After completion of the reaction, the black precipitate was collected with the help of an external magnetic field, washed with water and ethanol, and dried under vacuum.

To modify the surface of the MNPs with bonded vinyl groups, 4 mL γ-MPS was dropwise added into 1 mL ethanol-water (1:1, v/v) containing 50 mg of dispersed MNPs, and the reaction was kept for 12 h at 40 °C under a N_2 atmosphere [32]. Then, the product was isolated, washed with ethanol for several times, and dried under vacuum.

The presence of vinyl groups attached onto the surface of MNPs was demonstrated by ATR-FTIR (see Fig. S12.1). Both the non-vinylized and vinylized nanoparticles showed a band at 562 cm^{-1} which corresponded to the Fe–O vibration of the magnetic core. The VMNPs also showed a strong band at 1718 cm^{-1}, which was characteristic of stretching of the carbonyl of the ester group of γ-MPS, as well as bands at 1633 and 3004 cm^{-1}, which were probably due to stretching of the terminal C=C and C–H bonds of the γ-MPS., respectively. Additionally, TEM characterization of MNPs and VMNPs showed diameters of *ca*. 12 and 15 nm, respectively (see Fig. S12.2). The increase in diameter upon silanization also suggested the presence of the bonded ligand on the nanoparticle surface.

12.2.4. Preparation of poly(GMA-co-EDMA) monoliths with incorporated VMNPs

To ensure covalent attachment of the monolithic beds to the inner capillary wall, the wall surface was previously modified with γ-MPS [11]. For the preparation of monoliths, a polymerization mixture containing 19.9 wt% GMA, 4.8 wt% EDMA, 0.3 wt% META, 70 wt% CYC, 5 wt% DOD and AIBN (1 wt% with respect to the monomers) as initiator was prepared [13]. Different amounts of VMNPs were added to the polymerization mixture to give a final content in the mixtures ranging from 0.5 to 5 wt%. Then, the mixtures were vortexed, sonicated for 10 min, purged with N_2 for 5 more min and vortexed again. The silanized capillary was filled with the polymerization mixture up to a length of 8.5 cm using a syringe pump. Polymerization was accomplished by irradiation of the capillaries within the UV crosslinker chamber at 0.9 J/cm^2 for 15 min. After polymerization and using an HPLC pump, the resulting columns were flushed first with MeOH, thus to remove the pore-forming solvents and any possible unreacted monomers, and then with the mobile phase.

To monitor the stability of the VMNP suspensions in the polymerization mixture, the 1 mm optical-path quartz cell was filled with the mixture up to about two thirds of its total volume. In this way, most of the light beam of the spectrophotometer passed through the solution and part of it over its surface. The region immediately below the free surface was further delimited with a 5-mm round hole mask attached to the cell. The wavelength was set at 500 nm and the decrease of scattering (apparent absorbance) just below the surface was monitored.

To obtain enough amounts of monolithic materials for nitrogen-adsorption experiments, polymerization of the same mixtures was carried out in quartz tubes (50 mm × 3 mm I.D). After polymerization, the monolithic material was removed from the tube, cut into small pieces with a razor blade, and Soxhlet extraction was carried out with MeOH for 24 h, followed by drying at 50 ºC for 4 h.

12.2.5. CEC procedures

After flushing, the columns were placed in the CEC instrument and equilibrated with mobile phase by applying a stepwise increase in voltage from 5 up to 15 kV, until both a stable current and a flat baseline were observed. Separations were performed at 25 ºC at several voltages. In all cases, N_2 was used to pressurize both the inlet and outlet vials at 0.8 MPa. To evaluate the CEC performance of columns, mixtures of alkyl benzenes and organophosphorous pesticides were used. Mixtures containing 100 µg mL^{-1} of each analyte and thiourea as EOF marker were prepared in the mobile phase. The test mixtures were injected electrokinetically using 5 kV for 6 s. Detection was set at 214 and 230 nm. The separation conditions for each mixture are indicated in the figure captions.

12.3. Results and discussion

12.3.1. Preparation and characterization of UV-polymerized poly(GMA-co-EDMA) monoliths with VMNPs

The dispersion of nanoparticles in the monolithic matrix can affect pore structure, separation retention and efficiency, and repeatability. Therefore, it is necessary to homogenously distribute NPs in the polymerization mixtures to obtain stationary phases with uniform properties. The monoliths prepared with the polymerization mixture indicated in section 12.2.4 showed a high permeability (large flow-through pores of around 1–2 μm in size), which enormously facilitated the flow properties of the monolithic columns.

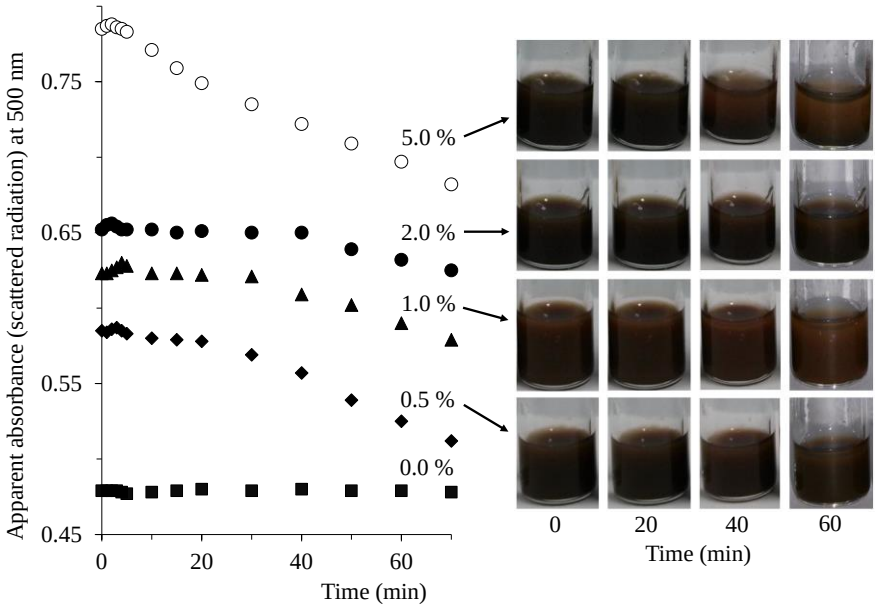

Fig. 12.1. Turbidimetric monitoring of polymerization mixtures prepared with increasing VMNP contents (percentages as indicated at the traces); at the right, images of vials containing the same mixtures at increasing time values after preparation.

Next, the stability of the VMNP suspensions in the polymerization mixture was studied. For this purpose, light scattering was used to monitor suspensions

containing between 0 and 5 wt% VMNPs (see section 12.2.4). As deduced from Fig. 12.1, polymerization mixtures with contents comprised between 0.5 and 2 wt% VMNPs were quite stable, showing negligible sedimentation for at least 20 min (up to 45 min for the 2 wt% mixture). On the contrary, for the mixture having 5 wt% VMNPs, sedimentation was perceptible after *ca.* 6 min. The different behavior of this mixture respecting those having lower VMNPs percentages could be due to a higher agglomeration rate. The results obtained by monitoring scattered light agreed with that visually observed (Fig. 12.1, images). Thus, stability of the suspensions containing up to 2 wt% VMNPs was considered to be quite safe in relation to the *ca.* 15 min that is required for UV polymerization [13]. Within this time, it could be assured than the VMNPs had no time to agglomerate and segregate. Accordingly, several monolithic columns were prepared by incorporating from 0.5 to 2 wt% VMNPs in the polymerization mixture. A monolith without VMNPs (control monolith) was also prepared for comparison.

SEM images of all the monoliths were obtained at different magnification powers. Images corresponding to monoliths obtained in the absence and presence of 2.0 wt% VMNPs are shown in Fig. 12.2. From the images at 60k magnification, the overall globule structure of monoliths was not modified by the presence of the VMNPs; however, the globules obtained in the absence of VMNPs (Fig. 12.2A) showed a smoother surface when compared to the rougher surface of the monoliths prepared with VMNPs (Fig. 12.2B). A larger magnification (150k) provided further evidence about this. The globules containing the VMNPs exhibit more protuberances than that observed in the absence of VMNPs (Fig. 12.2C and 12.2D). This can be also deduced from the more wavy edges (Fig. 12.2D). On the other hand, SEM/EDAX analysis confirmed the presence of VMNPs in the monoliths. As an example, the hybrid monoliths prepared with 2 wt% VMNPs showed contents of carbon (66.1 atom%), oxygen (14.3 atom%), silicon (17.5 atom%) and iron (2.1 atom%), whereas a control monolith contained only carbon (85.9 atom%) and hydrogen

(14.1 atom%). Thus, SEM/EDAX provided evidence of the incorporation of the VMNPs to the monoliths. Further evidence about the higher surface roughness of the resulting modified monoliths was achieved by measuring the BET surface area. In fact, the analysis of hybrid monoliths containing VMNPs showed significantly larger values (up to 17.8 m^2 g^{-1}) in comparison to that of the control monolith (5.1 m^2 g^{-1}). This remarkable increase in surface area will benefit the column retention and efficiency, which will be described in details below.

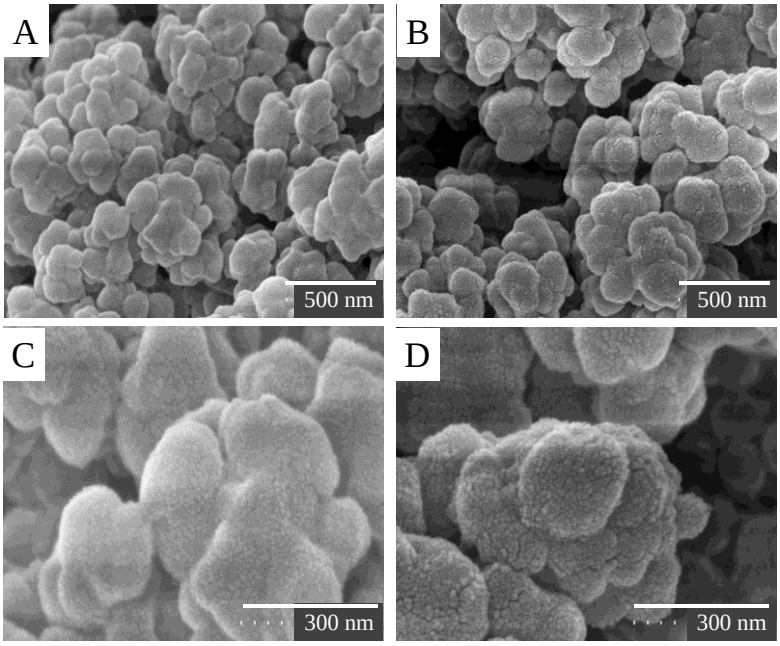

Fig. 12.2. SEM micrographs of monoliths prepared using polymerization mixtures in the absence of VMNPs (A, C) and containing 2 wt% VMNPs (B, D); the images were obtained at 60k (A, B) and 150k (C, D) magnification.

12.3.2. Electrochromatographic evaluation of hybrid monolithic columns

The CEC performance of the hybrid monolithic columns containing incorporated VMNPs was evaluated using different mixtures of test analytes. Fig. 12.3 shows the separation of a mixture of alkyl benzenes using a control

monolith and a monolith prepared with 1 wt% VMNPs under the same experimental conditions. Also, a series of chromatograms for organophosphorous pesticides using monoliths prepared in the presence of increasing VMNP contents were obtained (Fig. 12.4). As observed, for all the test analytes, the retention on the monoliths copolymerized with VMNPs was significantly higher than that obtained on the control monolith. For instance, the retention factors for propyl benzene on monoliths prepared with 0.5-2 wt% VMNPs ranged from 3.0 to 3.4, whereas the control monolith gave 1.7. Similar differences were observed for the other alkyl benzenes. Concerning to the organophosphorus pesticides, the increase of retention at higher VMNPs contents was also evidenced (see Table 12.1).

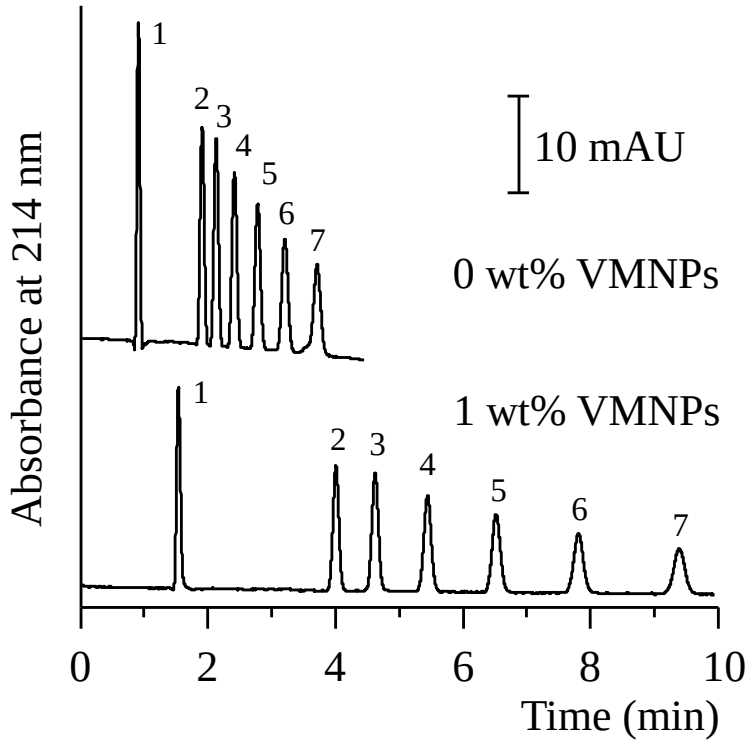

Fig. 12.3. Separation of alkyl benzenes by CEC using monoliths prepared in the absence and presence of 1 wt% VMNPs; peak identification: 1, thiourea; 2, toluene; 3, ethyl benzene; 4, propyl benzene; 5, butyl benzene; 6, pentyl benzene and 7, hexyl benzene.

Table 12.1

Retention factors (k) and efficiency (N, plates m^{-1}) for the organophosphorous pesticides using monolithic columns prepared in the absence and presence of increasing amounts of VMNPs [a]

% VMNPs	Quinalphos impurity		Fensulfothion		Malathion		Profenofos+ Quinalphos	
	k	N (m^{-1})	k	N (m^{-1})	k	N (m^{-1})	k	N (m^{-1})
0.0	0.12	11000	0.17	7000	0.61	8500	1.19	17000
0.5	0.14	7000	0.30	7300	0.95	8500	1.79	12100
1.0	0.15	27000	0.32	20600	0.97	17700	1.91	22400
2.0	0.16	53600	0.41	38300	1.47	27600	2.74	57000

% VMNPs	Dialifos		Methylchlorpyrifos		Chlorpyrifos		Sulprofos	
	k	N (m^{-1})	k	N (m^{-1})	k	N (m^{-1})	k	N (m^{-1})
0.0	2.36	15600	2.43	17400	2.88	11000	3.81	14400
0.5	3.81	5700	3.81	5700	4.51	7500	6.01	12300
1.0	3.77	23400	3.87	22400	4.57	20700	6.07	22600
2.0	6.32	43700	6.32	43700	7.71	64600	10.70	72400

[a] Working conditions as in Fig. 12.3.

An increase of retention can be due to a higher affinity of the analytes for the stationary phase as well as to an increase of the stationary to mobile phase ratio. Since the VMNPs were vinylized, they were probably covered by poly(GMA-*co*-EDMA). Covering of the VMNPs by the polymer would also explain why, in spite of the well-known affinity between iron and many phosphorus compounds, the selectivity was not modified when VMNPs were introduced in the monolith (see the k-values in Table 12.1). Thus, it is probably that the chemistry of the polymer surface was not modified by the presence of the VMNPs. On the contrary, both the SEM images and the BET measurements pointed out to an increase of the surface area of the monoliths due to the

presence of the VMNPs as the responsible for the increased retention. In addition, a non-linear decrease in the EOF mobility was observed at increasing VMNP contents, from $5.0 \cdot 10^{-4}$ (control monolith) to $2.6 \cdot 10^{-4}$ (monolith with 2 wt% VNMPs) $cm^2\ V^{-1}\ s^{-1}$ (see Fig. S12.3). This should be attributed to a decrease of the density of the quaternary ammonium functionalities of META (ionizable monomer) on the monolith surface. A reduction of the EOF to half its value is not justified by the dilution produced in the mixture by the presence of up to a 2 wt% of material (VMNPs), which do not contain META. A possible explanation is that a larger proportion of VMNPs is located close to the monolith surface in comparison to its concentration in the monolith core. This could effectively reduce the proportion of META at the monolith surface in a proportion much larger than a 2 wt% or less. Then, a series of experiments were performed in order to study the retention mechanisms in the hybrid monoliths. For this purpose, the monolith prepared with 1 wt% VMNPs was used, and the ACN content in the mobile phase was stepwise increased from 30 to 70%. The mixture of alkyl benzenes was first injected. A plot of log *k* versus the ACN concentration showed a linear behavior ($r = 0.992$), retention decreased when the ACN percentage increased (data not shown). In addition, plots of log *k* versus the 1-octanol-water coefficient (log $P_{o/w}$) showed positive correlations ($r > 0.999$ for alkyl benzenes). Therefore, the main retention mechanism was hydrophobic attraction (van der Waals interactions). A typical RP mechanism was reported for the CEC retention of neutral compounds in polymeric monolithic stationary phases [7, 11, 13].

Then, the test mixture of organophosphorous compounds was injected. These compounds also showed a decrease of retention as the ACN concentration increased, thus also indicating predominant RP mechanism. Also, the plots log *k* vs $P_{o/w}$ [43] for the OPs pesticides in monolithic columns prepared in the absence and presence of 2 wt% VMNPs were obtained (Fig. 12.5). A satisfactory linearity was achieved ($r > 0.962$) in both monoliths. The deviations from linearity could be explained by considering other interaction

mechanisms in addition to hydrophobicity. Thus, the ester and epoxy groups of the surface of the monoliths may interact with the analytes via dipole-dipole attraction. In any case, the slope of log *k* *vs* log $P_{o/w}$ plots was higher for the monoliths prepared with VMNPs (Fig. 12.5B), than for the control monolith (Fig. 12.5A). This could be due to the larger surface area of the hybrid monolith.

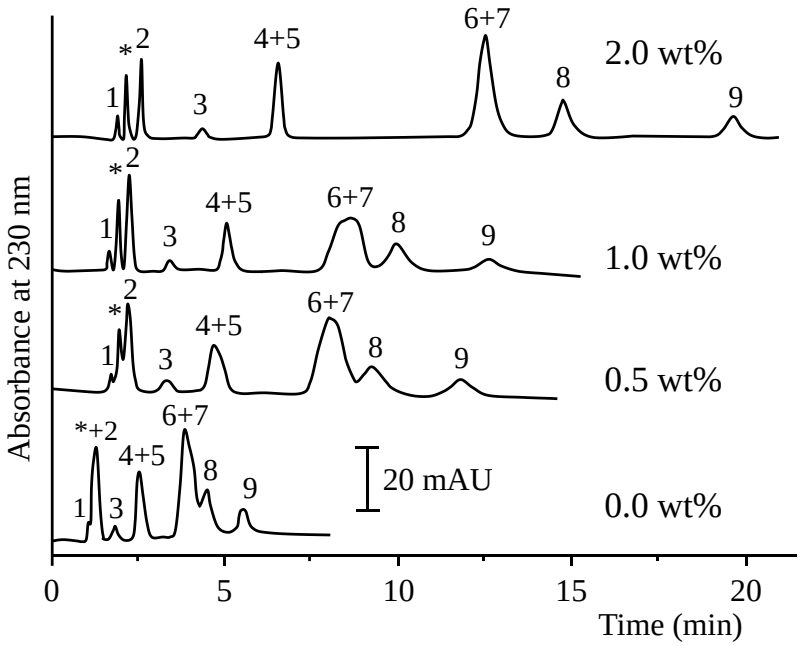

Fig. 12.4. Separation of OPs on UV-polymerized monoliths prepared at increasing VMNP contents÷ (percentages as indicated at the traces). CEC conditions as in Fig. 3; peak identification: 1, uracil; 2, fensulfotion; 3, malathion; 4, prophenofos; 5, quinalphos; 6, dialifos; 7, methylchlorpyrifos; 8, chlorpyrifos; 9, sulprofos. Peak labelled as asterisk was an impurity of quinalphos.

To evaluate the efficiency in columns prepared with different VMNP contents, van Deemter curves for propyl benzene (as representative analyte) were obtained (Fig. 12.6). As observed, the monolith prepared with 1 wt% VMNPs gave the best minimum plate heights (H_{min}). Thus, for the monoliths containing 1 wt% VMNPs, the H_{min} values were within the 6.6-9.4 µm range (130,000-82,000 plates/m), whereas for the control monolith obtained in absence of VMNPs, the H_{min} values ranged between 14.8 and 21.0 µm (67,700-

47,000 plates/m). Monoliths with 0.5 and 2 wt% VMNPs gave similar efficiencies to those obtained with 1 wt% VMNPs. Then, all the monoliths copolymerized with VMNPs showed significantly higher efficiencies than the control monolith. Additionally, the hybrid monoliths also showed lower mass transfer contributions (*C*-term) (0.003 ms) than that obtained with the control monolith (0.089 ms).

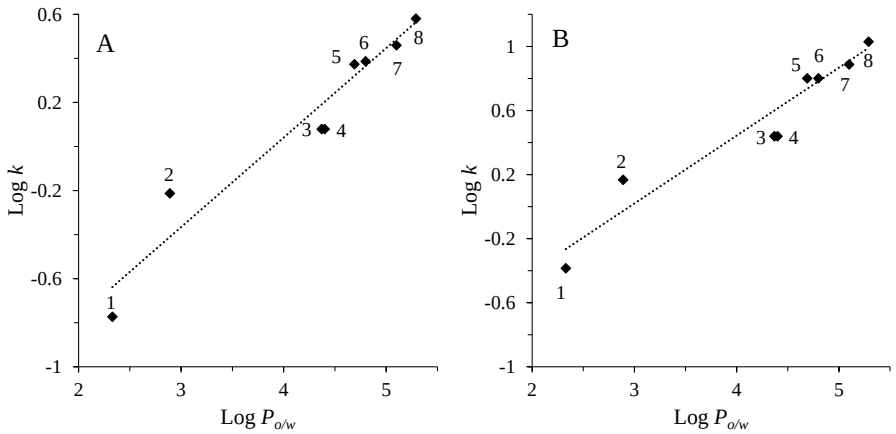

Fig. 12.5. Plots of log *k* against log $P_{o/w}$ for organophosphorous pesticides. The log *k* values were obtained using UV-polymerized monoliths prepared in the absence (A) and presence of a 2.0 wt% VMNPs (B). Other conditions as in Fig. 3; compound identification (in the order of increasing log $P_{o/w}$ values): 1, fensulfothion; 2, malathion; 3, prophenofos; 4, quinalphos; 5, dialifos; 6, methylchlorpyirfos; 7, chlorpyrifos; 8, sulprofos.

Concerning to OPs, and as shown in Table 12.1, an increase in the plate number for all analytes was produced at increasing VMNP percentages. The resolution (R_s) between the successive peak pairs of the pesticides, obtained with the monoliths with increasing contents of VMNPs, is plotted in Fig 12.7. As observed, in almost all cases, resolution increased when the percentage of VMNPs in the monolith increased. The best separation of organophosphorous pesticides was achieved by using the hybrid monolith containing 2 wt% VMNPs (Fig. 12.4D).

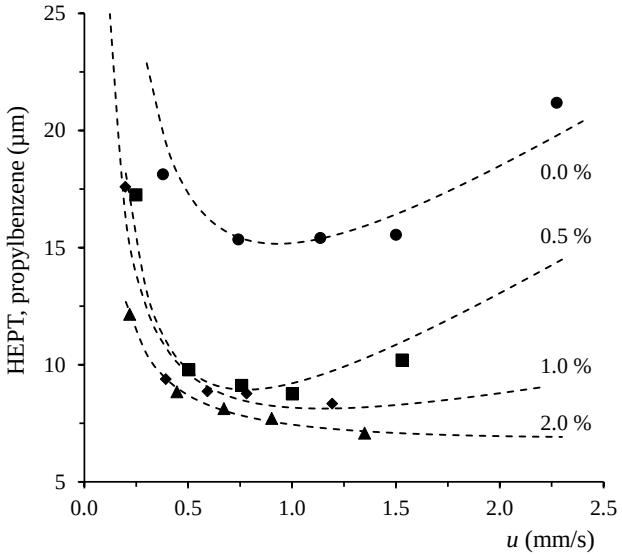

Fig. 12.6. Van Deemter plots for propyl benzene using monoliths with increasing amounts of VMNPs (percentages as indicated at the traces). CEC conditions: mobile phase, ACN:10 mM acetate buffer (pH 3.0) (50/50 v/v); UV detection at 214 nm; applied voltage, 10 kV; injection, 5 kV for 6 s.

A comparison in terms of efficiency with other polymeric monoliths was also performed. Thus, the efficiency values obtained were similar to the 120,000 plates/m reported for benzene derivatives (at optimum flow rates, 0.25 mm/s) using BMA-based monoliths and CEC [44]. It should be also remarked that these reported values were obtained with much longer monoliths (30-120 cm) than that used in this work (8.5 cm). The monoliths prepared with 1-2 wt% VMNPs also showed very low *C*-term values (Fig. 12.6) compared to reported values [45]. Therefore, using the monoliths containing VMNPs, the CEC analysis time can be largely reduced by increasing the applied voltage up to the maximum without losing efficiency. On the other hand, efficiencies were lower than those reported for PAHs (up to 400,000 plates/m at *ca.* 2 mm/s) using CEC and a 30 cm packed bed containing 1.5 µm non-porous octadecylsilica particles [44]. However, it should be mentioned that the construction of CEC packed columns is still quite problematic (reproducible synthesis of retaining frits, bubble formation, etc) [7, 11, 13].

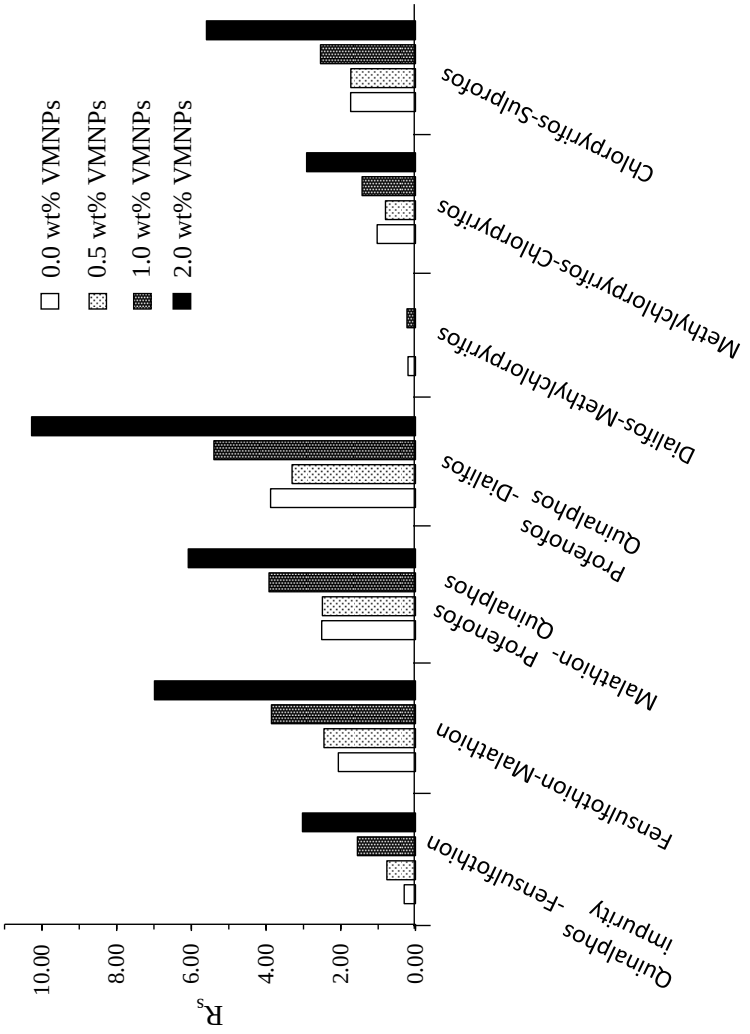

Fig. 12.7. Resolution (R_s) of organophosphorous compounds obtained with monoliths containing increasing amounts of VMNPs (see plot legend). CEC conditions as in Fig. 12.3.

Finally, the reproducibility of preparation of hybrid columns with VMNPs was examined. The run-to-run repeatability was evaluated from series of six injections of propyl benzene and fensulfothion as representative analytes, while the column-to-column reproducibility was estimated with three columns prepared from the same polymerization mixture. The batch-to-batch reproducibility was estimated from three batches of three columns each. Both the retention time and peak areas were evaluated. As shown in Table 12.2, RSD values for run-to-run were below 1.2%, whereas the column-to-column and batch-to-batch reproducibility gave values within the 1.2-5.5% and 1.8-6.1%, respectively.

Table 12.2

Repeatibility and reproducibility (RSD %) of poly(GMA-*co*-EDMA) monoliths with incorporated VMNPs for CEC separation[a,b]

Analytes	Parameter	Run-to-run column (n = 6)	Column-to-column (n = 3)	Batch-to-batch (n = 3)
Alkyl benzenes	t_R (min)	0.6-0.9	1.9-2.0	2.5-2.7
	Peak area	1.0-1.1	4.2-5.5	5.9-6.1
Organophosphorous pesticides	t_R (min)	0.7-0.8	1.2-1.4	1.8-2.0
	Peak area	1.1-1.2	3.1-3.3	4.4-4.9

[a] The VMNP contents in the hybrid monoliths were 1 and 2 wt% for alkyl benzenes and organophosphorous pesticides, respectively.
[b] Working conditions as in Fig. 12.3.

12.4. Conclusions

Novel hybrid monolithic columns containing copolymerized VMNPs have been developed. The stationary phases were prepared by simply dispersing the VMNPs in the polymerization mixture before UV irradiation. Experimental preparation conditions were carefully optimized to assure homogenous distribution of the VMNPs in the polymeric matrix. The combination of good dispersion with the short polymerization times used in UV-initiation avoided the segregation of the VMNPs. The synthetized smart materials were applied

to the CEC separation of test mixtures of alkyl benzenes and OPs. with increased retention and high column efficiency in comparison to the control monolith. The higher retention seems to be due to the increase of the surface area of the monolith, produced by the presence of VMNPs. The hybrid monolithic columns also showed a satisfactory batch-to-batch reproducibility. The intrinsic characteristics of VMNPs such as large surface area and its feasible dispersion in polymerization mixture make the nanocomposites reported in this work, attractive materials for the enhanced separation performance of small molecules in chromatographic techniques.

Acknowledgements

Work supported by Project CTQ2014-52765-R (MINECO of Spain and FEDER funds). E.J.C-C. thanks the MINECO for an FPI grant.

References

[1] E. Guihen, J.D. GlennonAnal. Lett., 36 (2003) 3309.

[2] C. Nilsson, S. Birnbaum, S. Nilsson, J. Chromatogr. A, 1168 (2007) 212.

[3] R. Tian, J. Sun, H. Zhang, M. Ye, C. Xie, J. Dong, J. Hu, D. Ma, X. Bao, H. Zou, Electrophoresis, 27 (2006) 742.

[4] C. Nilsson, P. Viberg, P. Spégel, M. Jörntén-Karlsson, P. Petersson, S. Nilsson, Anal. Chem., 78 (2006) 6088.

[5] Y.L. Hsieh, T.H. Chen, C.Y. Liu, Electrophoresis, 27 (2006) 4288.

[6] Q. Qu, D. Liu, D. Mangelings, C. Yang, X. Hu, J. Chromatogr. A, 1217 (2010) 6588.

[7] Y.Y. Li, H.D. Tolley, M.L. Lee, J. Chromatogr. A, 1218 (2011) 1399.

[8] P.Y. Xin, Y. Shen, L. Qi, Talanta, 85 (2011) 1180.

[9] H. Aoki, N. Tanaka, T. KuBo, J. Polym. Sci. Part A: Polym. Chem., 46 (2008) 4651.

[10] M. Lammerhofer, E.C. Peters, C. Yu, F. Svec, J.M.J. Frechet, W. Lindner, Anal. Chem., 72 (2000) 4614.

[11] E.C. Peters, M. Petro, F. Svec, J.M.J. Frechet, Anal. Chem., 70 (1998) 2288.

[12] S. Xie, F. Svec, J.M.J. Frechet, J. Chromatogr. A, 775 (1997) 65.

[13] E.J. Carrasco-Correa, G. Ramis-Ramos, J.M. Herrero-Martínez, J. Chromatogr. A, 1298 (2013) 61.

[14] T. Rohr, E.F. Hilder, J.J. Donovan, F. Svec, J.M.J. Frechet, Macromolecules, 36 (2003) 1677.

[15] C. Viklund, A. Nordstrom, K. Irgum, F. Svec, J.M.J. Frechet, Macromolecules, 34 (2001) 4361.

[16] S.D. Chambers, F. Svec, J.M.J. Fréchet, J. Chromatogr. A, 1218 (2011) 2546.

[17] J. Krenkova, N.A., Lacher, F. Svec, Anal. Chem., 82 (2010) 8335.

[18] M. Rainer, H. Sonderegger, R. Bakry, C.W. Huck, S. Morandell, L.A. Hubert, D.T. Gjerde, G.K. Bonn, Proteomics, 8 (2008) 4593.

[19] K. Yao, J. Yun, S. Shen, L. Wang, X. He, X. Yu, J. Chromatogr. A, 1109 (2006) 103.

[20] E.F. Hilder, F. Svec, J.M.J. Frechet, J. Chromatogr. A, 1053 (2004) 101.

[21] P. Zakaria, J. P. Hutchinson, N. Avdalovic, Y. Liu, P.R. Haddad, Anal. Chem., 77 (2005) 417.

[22] Y. Xu, Q. Cao, F. Svec, J.M.J. Frechet, Anal. Chem. 82 (2010) 3352.

[23] Q. Cao, Y. Xu, F. Liu, F. Svec, J.M.J. Frechet, Anal. Chem., 82 (2010) 7416.

[24] D. Connolly, B. Twamley, B. Paull, Chem. Commun., 46 (2010) 2109.

[25] J.P. Hutchinson, E.F. Hilder, M. Macka, N. Avdalovic, P.R. Haddad, J. Chromatogr. A, 1109 (2006) 10.

[26] M.M. Miller, G.A. Prinz, S.F. Cheng, S. Bounnak, S. Appl. Phys. Lett., 81 (2002) 2211.

[27] T.K. Jain, M.A. Morales, S.K. Sahoo, D.L. Leslie-Pelecky, V. Labhaserwar, Mol. Pharm., 2 (2005) 194.

[28] J.W. Bulté, Methods Mol. Med., 124 (2006) 419.

[29] G. Viau, P. Toneguzzo, A. Pierrard, O. Acher, F. Fiévet-Vincent, F. Fiévet, Scr. Mater., 44 (2001) 2263.

[30] S. Yu, G.M.J. Chow, Nanosci. Nanotechnol., 6 (2006) 2135.

[31] A.K. Giri, K.M. Chowdary, S.A. Majetich, Mater. Phys. Mech., 1 (2000) 3026.

[32] P. Qu, J. Lei, L. Zhang, R. Ouyang, H. Ju, J. Chromatogr. A, 1217 (2010) 6115.

[33] X. Kan, Z. Geng, Y. Zhao, Z. Wang, J.-J. Zhu, Nanotechnology 20 (2009) 165601 (7pp).

[34] S. Sun, C.B. Murray, D. Weller, L. Folks, A. Moser, Science, 287 (2000) 1989.

[35] M.J. Lerma-García, M. Zougagh, A. Ríos, Microchim. Acta, 180 (2013) 363.

[36] M. Bouri, M.J. Lerma-García, R. Salghi, M. Zougagh, A. Ríos, Talanta, 99 (2012) 897.

[37] M. Yamaura, R.L. Camilo, L.C. Sampaio, M.A. Macêdo, M. Nakamura, H.E. Toma, J. Magn. Magn. Mater., 279 (2004) 210.

[38] R.A. Whithead, M.S. Chagnon, E.V. Groman, L. Josephson, U.S. Patent 4,695,392, 1987.

[39] D. Lopez, I. Cendoya, F. Torres, J. Tejada, C. Mijangos, Polym. Eng. Sci., 41 (2001) 1845.

[40] J. Krenkova, F. Foret, Anal. Bioanal. Chem., 405 (2013) 2175.

[41] J. Krenkova, F. Foret, J. Sep. Sci., 34 (2011) 2106.

[42] C. Yang, G. Wang, Z. Lu, J. Sun, J. Zhuang, W. Yang, J. Mater. Chem., 15 (2005) 4252.

[43] E. Benfenati, G. Gini, N. Piclin, A. Roncaglioni, M.R. Vari, Chemosphere, 53 (2003) 1155.

[44] E.C. Peters, M. Petro, F. Svec, J.M.J. Frechet, Anal. Chem., 70 (1998) 2288.

[45] R. Dadoo, R.N. Zare, C. Yan, D.S. Anex, Anal. Chem., 10 (1998) 4787.

Supplementary Material

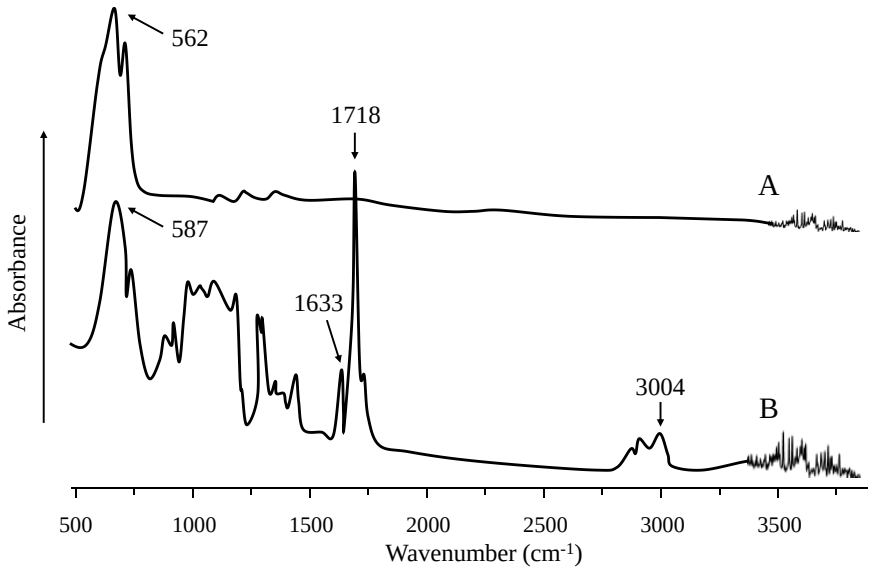

Fig. S12.1. ATR-FTIR spectra of the MNPs (A) and VMNPs (B).

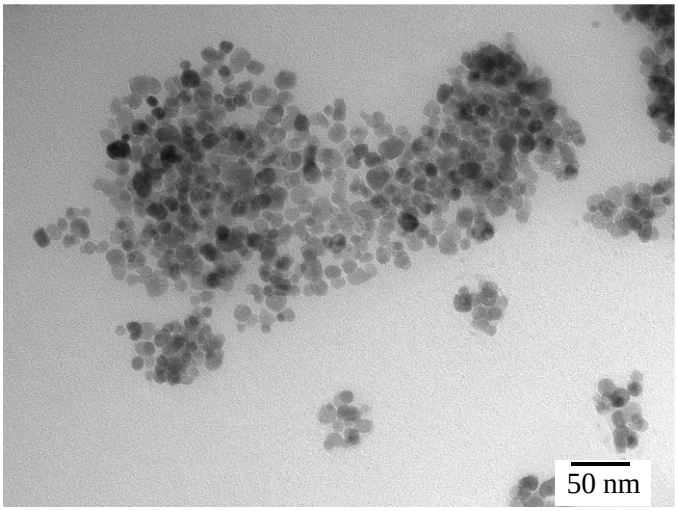

Fig. S12.2. TEM image of VMNPs.

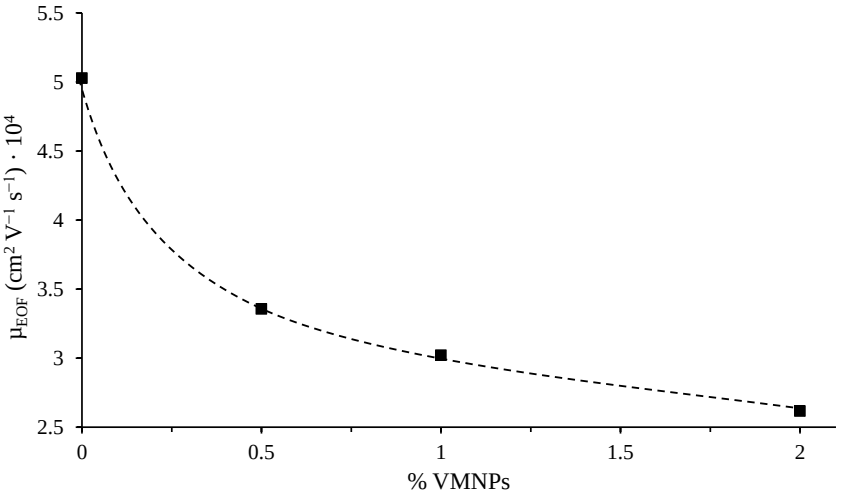

Fig. S12.3. Influence of VMNPs content (%wt) of hybrid monoliths on the EOF mobility.

SECTION III. CHARACTERIZATION OF RAW MATERIALS

Chapter 13. Evaluation of molecular mass and tacticity of polyvinyl alcohol by non-equilibrium capillary electrophoresis of equilibrium mixtures of a polymer and a dye

Journal of Chromatography A, 1218 (2011) 2334–2341

Contents lists available at ScienceDirect

Journal of Chromatography A

journal homepage: www.elsevier.com/locate/chroma

Evaluation of molecular mass and tacticity of polyvinyl alcohol by non-equilibrium capillary electrophoresis of equilibrium mixtures of a polymer and a dye

Enrique Javier Carrasco-Correa, Miriam Beneito-Cambra, José Manuel Herrero-Martínez, Guillermo Ramis-Ramos*

Departament de Química Analítica, Universitat de València, Dr. Moliner 50, 46100 Burjassot, Valencia, Spain

Non-equilibrium capillary electrophoresis of equilibrium mixtures (NECEEM) has been used to characterize polyvinyl alcohol (PVA). Commercial PVA samples with different molecular masses, from M_w = 15 up to 205 kDa, were used. According to the ^{13}C NMR spectra, the samples also differed in tacticity (stereoregularity). Mixtures of PVA and the anionic azo-dye CR were injected in the presence of a borate buffer. The electropherograms gave a band and a peak due to the residual PVA-CR complex and the excess dye, respectively, plus a superimposed exponential decay due to the partial dissociation of the complex during migration. The stoichiometry of the PVA-CR complex, q = [monomer]/ [dye], reached a maximum, q_{sat}, which depended on both M_w and tacticity of PVA. Thus, q_{sat} decreased from a molar ratio of ca. 4.9 to 3.6 at increasing M_w values, this variation also being largely dependent on tacticity. A similar dependence of the electrophoretic mobility of the complex on both M_w and tacticity was also observed. A possible explanation, based on the formation of a stack of CR ions inside the PVA-CR complex, was proposed and discussed. Finally, at increasing M_w values, the stability constant of the complex increased slightly (from log $K_s \approx$ 2.5 to 4.0), and the pseudo-first order dissociation rate of the complex decreased (from ca. 0.06 to 0.02 s^{-1}), this later parameter also showing a dependence on both M_w and tacticity.

Keywords: Azo-dyes; Non-equilibrium capillary electrophoresis; Polyvinylalcohol characterization; Polymer-dye complexes; Polymer molecular mass evaluation; Tacticity evaluation

13.1. Introduction

A variety of nonaqueous and aqueous CE methods for the characterization of synthetic polyelectrolytes, including CZE, CGE and capillary isoelectric focusing, have been described [1-5]. Using CE, information about size, shape, surface charge and formation of intramolecular associates can be gained [4]. Further, polyelectrolytes have been separated by CGE using solutions of nonionic polymers as sieving media [3-8]. Models describing the electrophoretic mobility of polyampholytes in free solution CZE have been developed [9], and CZE has been also used to study both the polymerization degree and sulfonation rate of polyestyrenesulfonates [10]. MEKC has been used to characterize highly charged polysaccharides (heparins) [11], and polyacrylic acids [12], as well as to study the synthesis progress and composition of ionic copolymers [13]. However, the characterization of non-charged polymers using CE has been scarcely investigated. In this connection, polyethylene glycols have been analyzed by CZE previous derivatization with an anhydride, which provides chromophore groups and electrical charges at both polymer ends [14-15]. In a previous work [16], we described a CZE method to characterize and evaluate PVP; for this purpose, we used the azo-dye CR which forms a charged and colored PVP-CR complex. The electropherograms of PVP-CR mixtures were interpreted at the light of the theory of NECEEM, which was developed by Krylov *et al*. [17-22] to obtain information about proteins and DNA fragments using fluorescent markers.

PVA is a synthetic polymer which is widely used for a variety of purposes within the fields of cosmetic, pharmaceutical and food technologies. Depending on the route of synthesis, PVA with a different tacticity is obtained. Tacticity or stereoregularity is a characteristic feature of those polymers which have repeating adjacent chiral centers along the main chain. Tacticity depends on the class percentages of pairs of adjacent monomers or diads. The two possible classes of diads are: *m* or meso (with the same orientation) and *r* or racemic (with opposite orientation). Accordingly, three clases of units constituted by

three adjacent monomers or triads can exist: *mm*, *mr* and *rr*. The relative percentages of *mm*, *mr* and *rr* triads, established by ^{1}H NMR, or preferably by ^{13}C NMR, are normally used to evaluate PVA tacticity [23-27].

As far as we know, CE methods for PVA characterization have not been reported, and the possibility of evaluating the tacticity of polymers using CE methods has not been investigated either. In this work, we have applied the NECEEM principles to the study of the electropherograms obtained by injecting PVA-CR mixtures. The formation of complexes between PVA and azo-dyes has been known for decades [28-32]. When excess borate was added to both the injected PVA-CR mixtures and the BGE, the expected NECEEM pattern for a mixture of a non-charged macromolecule and a charged marker was obtained. Commercial PVA samples with different molecular masses, also differing in tacticity, were studied. The electropherograms of PVA-CR mixtures provided information about the electrophoretic mobility, maximal stoichiometry, thermodynamic stability constant and pseudo first-order dissociation rate constant of the PVA-CR complex. These parameters were observed to depend on both molecular mass and tacticity of PVA.

13.2. Experimental

13.2.1. Reagents

PVA samples having the following average molecular masses (M_w) and percentages of residual acetylated monomers (n_{ac} x 100%, given between parenthesis) were used: 15 (0.0%), 49 (0.1%) and 100 (12.5%) kDa (Fluka, Buchs, Switzerland), and 31 (10.8%), 61 (1.5%), 130 (10.8%), 145 (0.6%) and 205 (10.8%) kDa (Sigma-Aldrich, Steinheim, Germany). CR (Panreac, Barcelona, Spain), sodium tetraborate decahydrate (borax, Sigma-Aldrich), acetone as EOF marker (Scharlau, Barcelona, Spain), deuterated dimethyl sulfoxide (DMSO-d_6, Sigma-Aldrich), and other analytical grade reagents, as

well as deionized water (Barnstead deionizer, Sybron, Boston, MA, USA), were also used.

13.2.2. Instrumentation and procedures

An HP3D CE system (Agilent Technologies, Waldbronn, Germany) provided with a diode-array detector, and uncoated fused-silica capillaries (Polymicro, Phoenix, AZ, USA) of 33.5 cm (25 cm effective length) x 50 μm ID (375 μm OD), were used. New capillaries were successively flushed with 1 and 0.1 M NaOH and water at 60 ºC for 10 min each. Daily before use, the capillary was successively rinsed with 0.1 M NaOH and water for 5 min each, followed by the running BGE for 10 more minutes. After each working day, the capillary was successively flushed with water, 0.1 M HCl (10 min each), water (5 min) and NaOH 1 M, followed by more water (20 min each). Between runs, it was flushed with 0.1 M NaOH and water for 2 and 3 min, respectively, followed by the BGE for 5 more minutes. The BGE, containing 25 mM borax, was adjusted to pH 9.0 with 0.1 M HCl. Before injection, all solutions were passed through 0.45 μm pore-size nylon filters (Albet, Barcelona, Spain); however, solutions containing PVA were injected without filtering to avoid retention of the polymer by the filter material. Triplicate injections at 50 mbar x 3 s were always performed throughout all this work. Separations were conducted at 25 ºC using 15 kV. Detection was set at 500 nm, close to the maximum of the absorption band of the dye in the absence of PVA; however, full spectra were also stored.

Stock solutions of the azo-dye (5 mM) and the PVA samples (10 mg mL^{-1}, 227 mM in monomers), and their mixtures, were prepared and diluted with the appropriate buffer solutions. To record UV-vis absorption spectra with the CE instrument, the capillary was filled up with 20 mM borax solutions also containing 4 mM CR and increasing PVA concentrations (49 kDa sample). The spectra were compared with those obtained with a model 8453 UV-vis

spectrophotometer (Agilent Technologies) provided with a 1 mm quartz cell (Hellma, Müllheim, Germany). For this purpose, the solutions were diluted to 1:40 (0.1 mM CR). The pre-equilibration time of the PVA-CR complexes was also studied both spectrophotometrically and by CZE.

13.2.3. NMR evaluation of the tacticity of the PVA samples

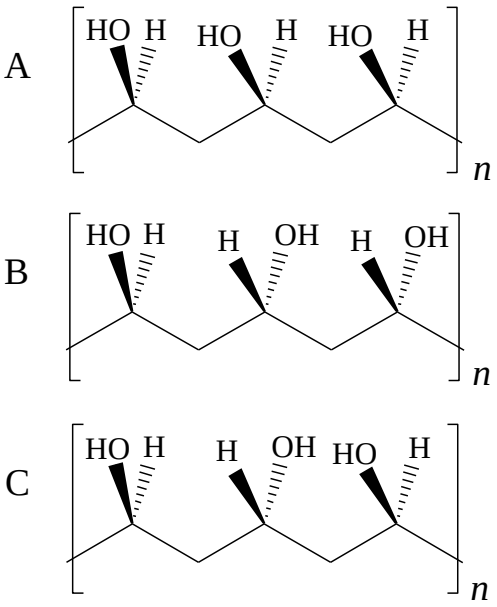

Fig. 13.1. The three possible classes of triads in a PVA chain: (A) *mm*, (B) *rm* and (C) *rr*.

The tacticity (stereoregularity) of the PVA samples was established by recording the ^{13}C NMR spectra with an Ultrashield DRX 400 NMR spectrometer (Bruker, Silberstreifen, Germany). For this purpose, the PVA samples were dehydrated in a centrifugal vacuum evaporator for 8 h at 60 ºC (MiVac, Genevac, Ipswich, UK); then, DMSO-d_6 to prepare 1% PVA solutions was added and sonication was applied; in all cases, $2x10^4$ spectra were accumulated. The structures of the three possible *mm*, *mr*+*rm* and *rr* triad classes in a PVA chain are depicted in Fig. 13.1. The percentages of triad

classes were estimated from the relative areas of the three multiplets found within the *ca.* 64 – 69 ppm range [24-27].

In Fig. 13.2, the *rr* triad percentages found in the samples are plotted against the *mm* triad percentages. In the same figure, several literature data are also given [24-27]. As observed in this figure, the PVA samples showed different tacticities, with *rr*/ *mm* ratios ranging from 1.72 to 1.39 for a group of three samples, from 1.09 to 1.04 for another group of three samples, and finally, the two samples with the largest molecular masses showed the lowest *rr*/ *mm* ratios, namely, 0.85 and 0.71. To facilitate the discussion that follows, these groups were qualitatively named according to the *rr*/ *mm* ratio as H (high), M (medium) and L (low).

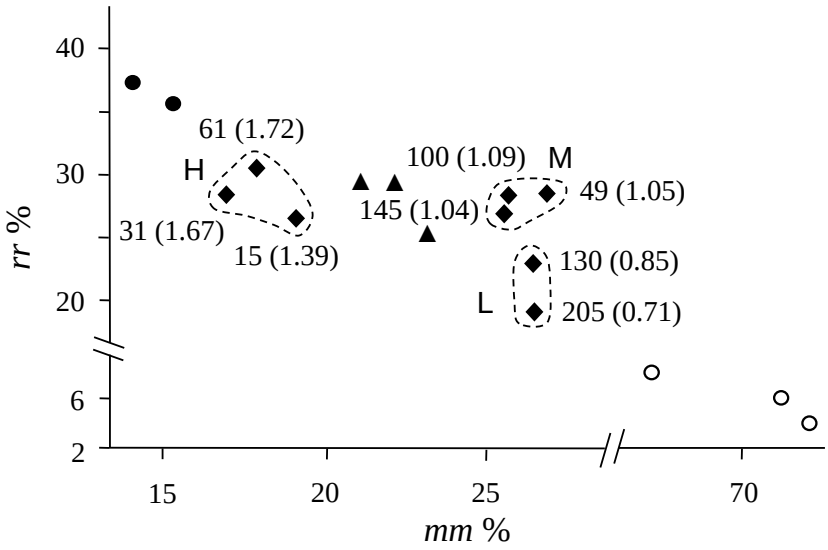

Fig. 13.2. Percentages of *rr* and *mm* triads found in the PVA samples used in this work (♦), as estimated by ^{13}C NMR. The numbers at the diamonds are molecular masses (kDa) and *rr*/ *mm* ratios (these within parenthesis). Other symbols correspond to literature data [24-27] for highly syndiotactic (●), atactic (▲) and highly isotactic (○) PVA.

13.3. Results and discussion

13.3.1. Effect of PVA on the UV-vis absorption spectrum of CR

The formation of PVA-CR complexes has been described [28-32]. As indicated in section 13.2.2, the formation of the complexes was first studied by filling the capillary with PVA-CR mixtures containing 20 mM borax. As illustrated in Fig. 13.3 for the 49 kDa PVA sample, the UV-vis spectrum of a 4 mM CR solution was largely modified when the mixture also contained increasing PVA concentrations. Thus, from q = [monomer]/ [dye] = 0 to 6, the molar absorptivity at the maximum of the main absorption band increased in a ca. 30%, and a large bathochromic shift of about 40 nm was also observed (from 479 to 519 nm). Similarly, an intensity increase of ca. 55% and a batochromic shift of ca. 50 nm (from 489 to 539 nm) were observed with a conventional spectrophotometer when 0.4 mM PVA was added to a 0.1 mM CR solution (spectra not shown). This implies a major change in the physico-chemical environment of CR [33]. The large modification of the CR spectrum could be partially due to replacing of water molecules attached to the polar locations of CR by the polar groups of the polymer; however, as discussed below in section 13.3.4, another possible reason is the stacking of dye ions in close proximity to each other within the structure of the PVA-CR complex. An absorptivity decrease at all wavelengths was also observed when $q > 6$. This could be due to an increase of the refraction index of the solution or to the optical screening of the dye in the presence of a large polymer excess.

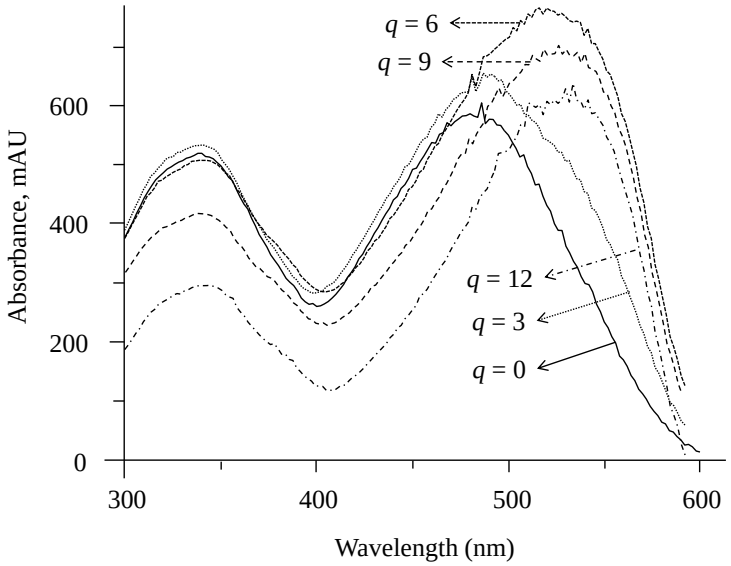

Fig. 13.3. UV-vis absorption spectra obtained by filling the capillary with solutions containing 20 mM borax, 4 mM CR and the following PVA concentrations (49 kDa) from A to E: 0, 12, 24, 36 and 48 mM (the resulting *q* values are indicated on the traces).

13.3.2. Selection of working conditions

In Fig. 13.4, traces A-D, electropherograms of mixtures of CR (4 mM) and PVA (15 kDa, increasing concentrations obtained in a BGE containing 25 mM borax are given. The injected mixtures were also equilibrated with borax; however, 20 mM borax was used to preserve sample stacking. Pre-equilibration with borax improved peak repeatability. In Fig. 13.4, traces E and F, electropherograms obtained by injecting 2.5 and 4 mM CR solutions, respectively, in the absence of PVA, are also shown. Truncation of the peak for the 4 mM CR solution was attributed to the local concentration increase produced by stacking, followed by precipitation of the dye. Truncation of this peak was not observed when PVA was present in the injected solution with at least $q \geq 1$. According to the NECEEM theory, when a solution containing an uncolored macromolecule and a colored charged marker is injected into the capillary, two peaks with a superimposed exponential decay region in the

middle should be observed [17-22]. Thus, in Fig. 13.4, traces A-D, the first band was attributed to the PVA-CR complex, and the peak that followed was assumed to be contributed by both the initial CR excess in free form and the dye released by the complex during migration (contributing mainly to the left half of the peak). As q increased (from traces A to D), the area of the band due to the PVA-CR complex increased, and the area of the peak due to the free dye decreased. Above $q \approx 4$ the electropherograms showed the single band of the complex, which progressively widened when q further increased (trace D). In addition, a BGE containing 20 mM Na_2HPO_4 (pH 10) instead of borax was tried. Mixtures containing 4 mM CR and 16 mM PVA (q = 4) were injected; however, a low intensity wide band due to the PVA-CR complex, and a large peak and exponential decay due to the free dye, were observed (electropherograms not shown). Thus, owing to the better shape and higher intensity of the complex band, the BGE containing a borax excess was preferred.

The time required to equilibrate the mixtures before injection was studied. For this purpose, aliquots of a solution containing 20 mM borax, 4 mM CR and 16 mM PVA monomers (49 kDa, q = 4) were injected at regular time intervals after mixing the reagents. The area due to the remaining complex, $A_{PVA\text{-}D}$, was estimated as indicated in Fig. 16.4, traces A-D, by doubling the area of the left half of the complex band. The rest of the area, due to both the initial free dye and the dye released by the complex during migration, was measured as $A_{Total} - A_{PVA\text{-}D}$. A slow increase of $A_{PVA\text{-}D}$ (ca. 8%), a decrease of the rest of the area (ca. 20%), and a small increase of the electrophoretic mobility of the complex (ca. 4%), were observed during the first two hours after mixing the reagents (sequence of electropherograms with time, not shown). This suggested a slow reorganization of the complex involving an increase of complex stability and compactness, or a decrease in its dissociation rate, or both processes at a time. Thus, to obtain reproducible electropherograms in the experiments that

followed, sample injection was performed with a delay of *ca.* 2 - 3 hours after mixing the reagents.

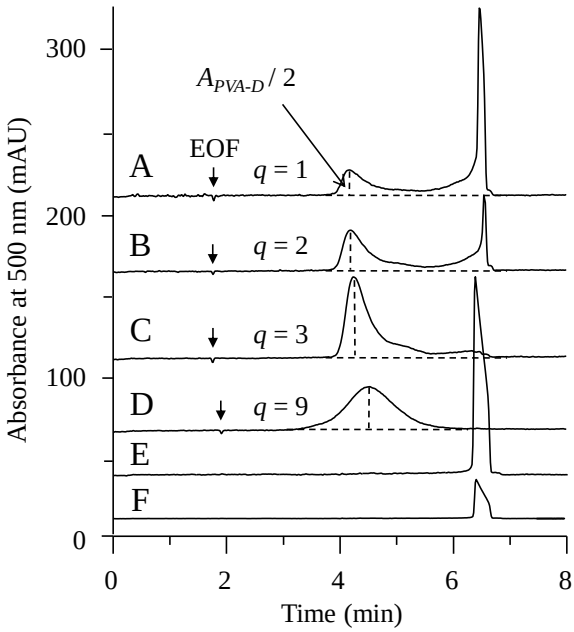

Fig. 13.4. From A to D: electropherograms of mixtures of CR (4 mM) and PVA (15 kDa, increasing concentrations). The *q* values are monomer/ dye molar ratios. The procedure used to calculate $A_{PVA\text{-}D}$ (used to construct Fig. 13.5) is indicated on the traces. Traces E and F are electropherograms of 2.5 and 4 mM CR, respectively. The BGE contained 25 mM borax (pH 9), and all the injected solutions contained 20 mM borax.

13.3.3. Maximal stoichiometry of the PVA-CR complex and its relationship with log M_w and tacticity

Series of electropherograms also obtained with 4 mM CR and increasing PVA concentrations (increasing *q* values) were used to estimate the saturation point or maximal stoichiometry of the PVA-CR complexes, q_{sat}, for all the PVA samples. As shown in Fig. 13.5 for the 15 kDa PVA sample, when *q* was increased the area of the PVA-CR complex, $A_{PVA\text{-}D}$, increased linearly up to $q \approx$

4, and the rest of the total area decreased proportionally. When $q \geq 5$, that is, above the saturation point, the peak due to the excess dye was not observed any longer, and $A_{PVA\text{-}D}$ decreased steadily. This agreed with the decrease in the absorptivity of the complex which was observed by recording spectra at large q values (Fig. 13.3). The other PVA samples behaved similarly, although with differences in the location of the saturation point indicating the maximal stoichiometry of the complex. In order to establish the saturation point of PVA complexes, q_{sat}, as accurately as possible, mixtures with q values close to the expected q_{sat} values were injected; however, repeatability of the electropherograms was poor when $q \approx q_{sat}$. Therefore, the q_{sat} values used in the discussion that follows were established for the different PVA samples as the point where the linear extrapolation of the decrease of $A_{Total} - A_{PVA\text{-}D}$ crossed zero (Fig. 13.5, dashed line).

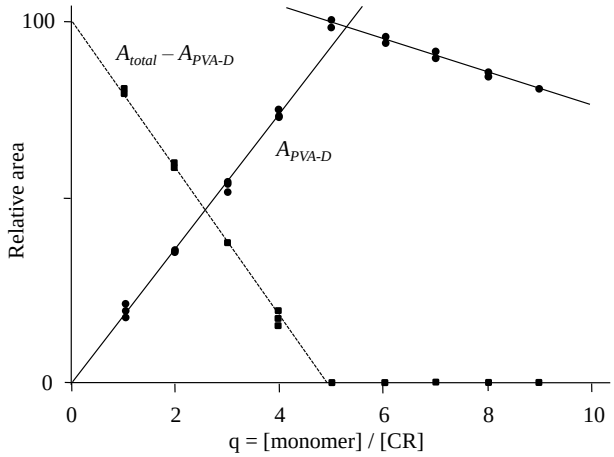

Fig. 13.5. Relative areas obtained from electropherograms of a series of solutions containing 4 mM CR and increasing PVA (15 kDa) concentrations in the presence of 20 mM borax. Other conditions as in Fig. 13.4. The continuous and dashed lines join points corresponding to the area assigned to the PVA-CR complex ($A_{PVA\text{-}D}$, estimated as indicated in Fig. 13.4) and the rest of the area under the peaks, respectively.

In Fig. 13.6 (full symbols), the q_{sat} values obtained in this way for the PVA samples were plotted against log M_w. As observed, H samples formed a clearly resolved group with respect to the M+L samples. Also, within each tacticity group, q_{sat} decreased as log M_w increased. Further, the upper and lower limits of the q_{sat} range were similar for the H and M+L sample groups, starting at q_{sat} ≈ 4.9 at a low molecular mass, and decreasing down to q_{sat} ≈ 3.5 at a large molecular mass. The two L samples, which had very large molecular masses, gave both q_{sat} values close to 3.5. Thus, q_{sat} decreased from ca. 4.9 to ca. 3.5 at increasing molecular masses, but this variation took place at different log M_w values depending on tacticity.

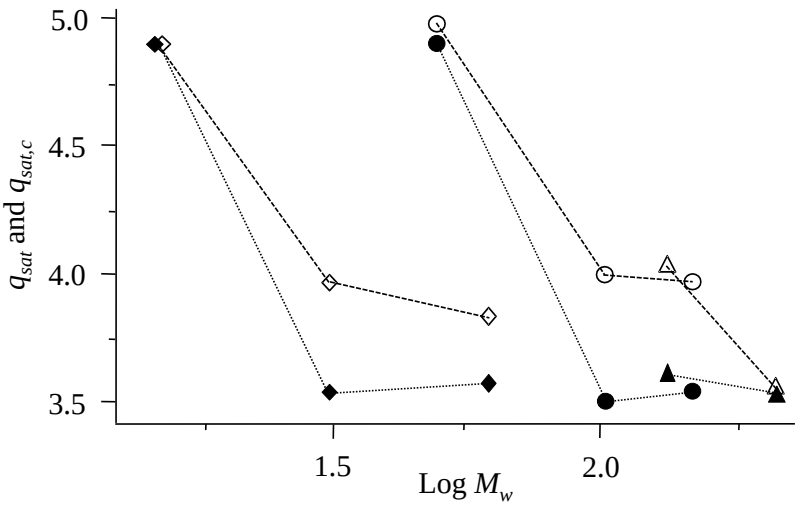

Fig. 13.6. Plots of the maximal stoichiometry of the complex against log M_w without (q_{sat}, full symbols) and with correction for the acetyl percentage ($q_{sat,c}$, empty symbols). Symbols indicating tacticity groups: H (diamonds), M (circles) and L (triangles).

Next, a correction of the q_{sat} values, thus to take into account the different proportions of residual acetyl groups in the PVA samples was tried. The molar proportions of residual acetyl groups per mol of monomers, n_{ac}, for the PVA samples used in this work, were given in section 13.2.1. In a PVA molecule,

acetyl groups could reduce the number of OH groups which are actually available to link the dye ions. Thus, in n_{ac} x 100% acetylated PVA, only (1- n_{ac}) x 100% of the monomers would be available for bonding; however, this should not reduce the complexing capacity of PVA in an equivalent (1- n_{ac}) x 100% factor, since acetylated monomers can also perform as nonbonding bridges between bonded monomers. Nevertheless, we studied next the effect which would have on q_{sat} the extreme situation in which the complexing capacity of PVA would be reduced in a full (1- n_{ac}) x 100% factor. Thus, the correction applied was: $q_{sat,c} = q_{sat} / (1 - n_{ac})$. As shown in Fig. 13.6 (empty symbols), full correction for the acetyl percentage essentially confirmed the conclusions obtained above using uncorrected q_{sat} values concerning both the decrease of q_{sat} at increasing molecular masses and the noticeable difference between the H and M+L tacticity groups.

13.3.4. Structure of the complex

When $q_{sat} \approx 4.9$, each dye ion could be bonded by a maximum of four and probably a minimum of two monomers (since CR is a symmetrical structure), leaving an average of 0.9 - 2.9 non-bonded monomers per dye ion, respectively. Similarly, when $q_{sat} \approx 3.5$, each dye ion could be bonded by a maximum of three and a minimum of two monomers, leaving an average of 0.5 - 1.5 non-bonded monomers per dye ion, respectively. In both cases, a small number of non-bonded monomers are available to perform as bridges between adjacent dye ions. Thus, in all the possible scenarios, the number of non-bonded monomers per dye ion is very low, which suggests a close proximity between the dye ions. As depicted in the temptative structure of Fig. 13.7, stacks of dye ions by pairs, or by groups constituted by a higher number of dye ions, could be formed. As proposed in this figure, it seems reasonably to stack the dye ions by alternating the sulfonate and amino groups, rather than putting together all the sulfonate groups at one side and all the amino groups at the other side of the stack. Also,

from a geometrical point of view, it seems reasonably to link the PVA monomers with the alternated sulfonate and amino groups though hydrogen bonds. As indicated in the literature, the azo groups are also possible sites for hydrogen bonding [30,33]; however, below the saturation point, and owing to the low stoichiometry, the number of available monomers per dye ion is rather short. Then, hydrogen bonding of the PVA monomers with both amino and azo groups, which are located in outer and inner sites of the dye ion, respectively, seems to be less likely than the structure proposed in Fig. 13.7. However, the probability of bonding the OH groups with azo groups should increase after the saturation point, when an excess of monomers are available.

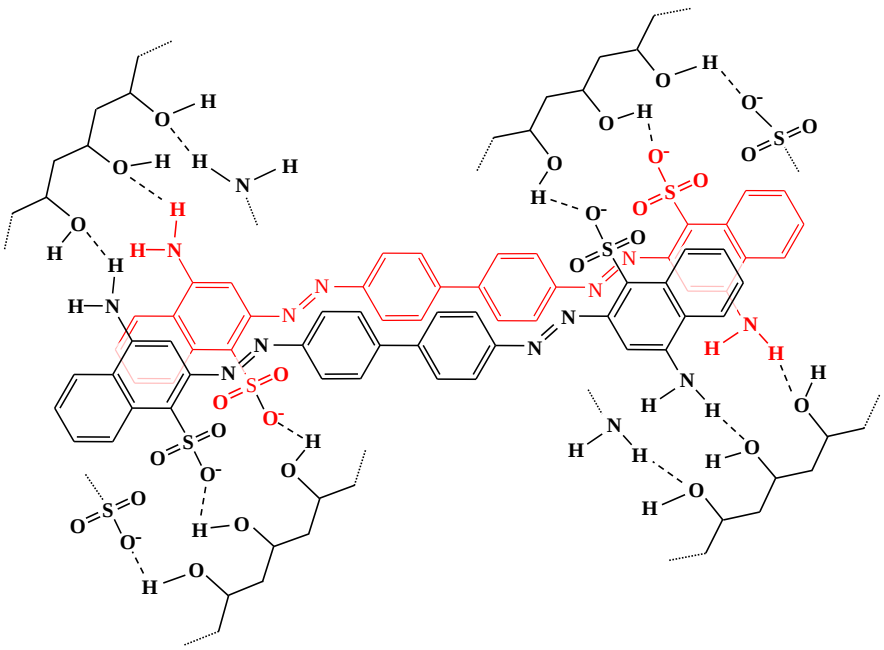

Fig. 13.7. Temptative structure for two adjacent PVA-CR complex units (with two stacked dye ions).

Dye stacking, resulting in a large absorptivity increase and blue shifting of the absorption maximum, has been described in solutions of plant pigments when certain ligands and Mg^{2+} are present [34]. Thus, dye stacking could explain both the low q_{sat} values of Fig. 13.6 and the very large modification of the absorption spectrum when PVA is added to CR solutions (Fig. 13.3).

Further, the distance between donor-acceptor atoms in adjacent stacked dye ions should be constricted by the distances between pairs of adjacent OH groups along the PVA chain, and these later are longer for *r* than for *m* diads. Thus, in PVA samples having a larger proportion of *r* diads, adjacent dye ions could be stacked at longer distances from each other than in samples with larger proportions of *m* diads. As discussed below, this could also explain the correlations found between other electrophoretic parameters and PVA tacticity as established by ^{13}C NMR.

The complex is probably compelled to adopt a given structure when an excess of either dye ions or unbound monomers is present. This could explain the excellent reproducibility of the electropherograms when $q < q_{sat}$ or $q > q_{sat}$, respectively. Therefore, poor reproducibility of the electropherograms when $q \approx q_{sat}$ could be due to the different ways the dye ions could be arranged within the complex when the available monomers are either in a small defect or a small excess with respect to q_{sat}.

13.3.5. Influence of molecular mass and tacticity on the electrophoretic mobility of the complex

Electropherograms obtained with PVA samples of increasing molecular mass, also corresponding to different tacticities, are shown in Fig. 13.8. These electropherograms were obtained with a small CR excess with respect to the saturation point. Thus, traces A and C, which correspond to complexes with q_{sat} = 4.51 were obtained at q = 4, and the other traces, which correspond to complexes with q_{sat} = 3.51 were obtained at q = 3. As further commented in section 3.6, this was important to distinguish the A_D area from that of the exponential decay contribution, A_e. As observed in Fig. 13.8, the electropherograms of M+L samples (traces C-E) showed a sharper complex band than that of the H samples (traces A-B). In addition, within each tacticity group, the electrophoretic mobility of the complex was reduced at increasing

molecular mass (A-B and C-D pairs). The relationships among electrophoretic mobility of the complex formed in the presence of an excess dye, molecular mass and tacticity are better recognized in Fig. 13.9 (full symbols). Within each tacticity group, the absolute electrophoretic mobility decreased slightly at increasing log M_w values. Therefore, electrophoretic mobilities indicated that charge density of the complexes decreased at increasing molecular masses. In addition, absolute mobility increased when the *rr*/ *mm* ratio decreased between the H and M sample groups. Therefore, absolute mobility increased when the average distances between the OH groups of adjacent monomers decreased as a result of the reduction of the proportion of *r* diads, probably giving rise to an increase of complex compactness. In free solution, the electrophoretic mobility of polyelectrolytes with the same linear structure but with different molecular masses is very similar [2, 9-10]. This is due to the almost identical charge-to-volume ratio which is achieved when units with a given charge-to-volume ratio are increasingly added to the polyelectrolyte. This electrophoretic behavior of polyelectrolytes has been called the free draining regime [10]. As occurs with polyelectrolytes, the mobility of the PVA-CR complexes could also reach a constant value at increasing molecular masses, not further dependent on the molecular mass of PVA. However, in the case of the PVA-CR complexes formed in the presence of an excess CR, to increase the molecular mass of the polymer is not the only factor to be taken into account for a free draining regime to be reached.

At increasing molecular masses, both the stoichiometry and apparent charge density of the saturated complex, q_{sat}, should be also maintained constant. As discussed above in section 13.3.3, stoichiometry of the complex formed in an excess dye varied with both molecular mass and tacticity; however, to show if a free draining regime is approached at high molecular masses, a model taking into account the stoichiometry variations can be constructed. For this purpose, the concept of average electrophoretic mobility per complex unit, μ_{unit}, can be used. This parameter was defined as the mobility

due to a unit constituted by a single dye ion and the average number of monomers directly attached to that ion, plus the average share of monomers which are necessary to link the complexed dye ion to the neighboring complex units. The mobility per complex unit, μ_{unit}, should be directly proportional to the charge of a dye ion, 2, and inversely proportional to the volume of the complex unit:

$$\mu_{unit} = \frac{2f}{V_D + q_{sat} V_m} \tag{13.1}$$

where f is a coefficient of proportionality, V_D is the volume of a dye ion bound to the polymer chain, and V_m is the average volume of a monomer in the complex. If both sides of Eq. (1) are multiplied by the electrophoretic mobility of the complex, μ, and the equation is reorganized, we have:

$$\frac{2f\,\mu}{V_m\,\mu_{unit}} = \mu\left[q_{sat} + \left(V_D / V_m\right)\right] \tag{13.2}$$

therefore, if a free draining regime would be reached at large molecular masses, the product $\mu\,[q_{sat} + (V_D / V_m)]$ would also reach a constant value. Since the V_D / V_m ratio was unknown, two approximations were used: first, V_D / V_m was taken as the ratio of the molecular masses of the dye ion and the monomers, 651/ 44 ≈ 15, and second, V_D / V_m was taken as the ratio of the total number of C, H, O and N atoms involved, 68/ 7 ≈ 10. These two values of V_D / V_m are rough approximations; however, as shown below, the use of any of them led to essentially the same conclusions. In Fig. 13.9 (empty symbols), product $\mu\,[q_{sat} + (V_D / V_m)]$ was plotted against log M_w. As observed in this figure, the differences among tacticity groups were enhanced upon correction of the electrophoretic mobility of the complex by the effects of complex stoichiometry. This correction confirmed the independent reduction of the absolute mobility at increasing log M_w values for the H and M+L tacticity groups. Therefore, both a higher molecular mass and a higher *rr*/ *mm* ratio implied a larger volume of the monomer-dye complex units, that is, a smaller

packing density of the complex. This agreed with the longer distances between the OH groups in *r* diads compared to *m* diads. On the other hand, the corrected mobilities of Fig. 13.9 also indicated that the complex did not reach a free draining regime at increasing molecular masses. This meant that coefficient *f* in Eq. (2) was not constant within any molecular mass range, that is, packing density of the complex decreased at increasing molecular masses for all the PVA samples used in this work.

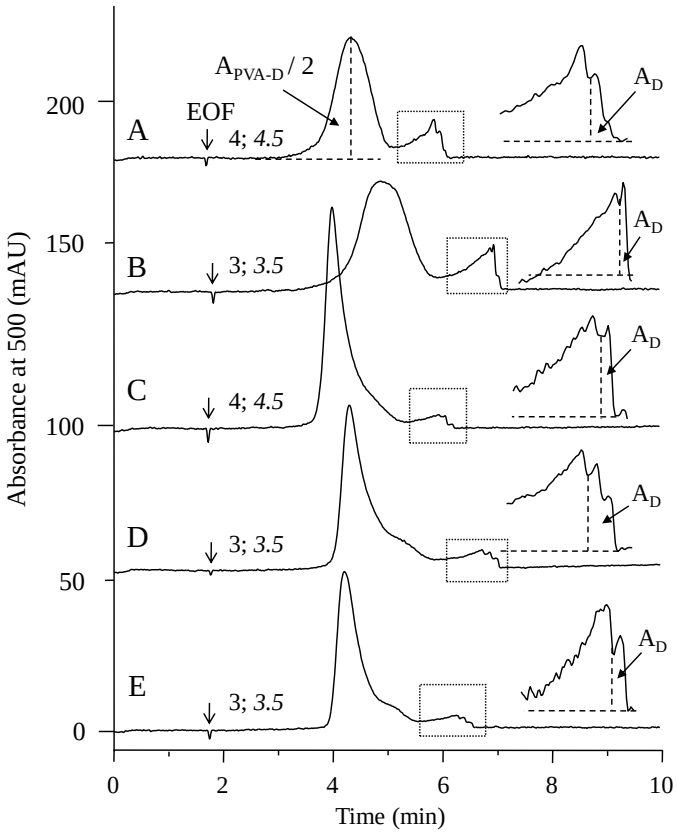

Fig. 13.8. Electropherograms of PVA-CR mixtures containing 20 mM borax, 4 mM CR and the following PVA monomer concentrations: (A, C) 16 mM and (B, D, E) 12 mM. The molecular masses were: (A) 15, (B) 31, (C) 49, (D) 100 and (E) 205 kDa. Sample tacticities: H (A, B), M (C, D) and L (E). The numbers on the traces are q and q_{sat} values (in italics). The expanded parts show how the A_D areas were

estimated; $A_{PVA\text{-}D}$ values were estimated as indicated in trace A. Other conditions as in Fig. 13.4, traces A-D.

13.3.6. Stability and dissociation rate constants of the complex

In Fig. 13.8, it can be also observed that the area of the peak due the free dye was larger for the H (A-B traces) than for the M+L (C-E traces) tacticity groups. This indicated either a higher complex stability or a slower dissociation rate, or both features at a time, for the H group in comparison to the M+L groups. Thus, next the stability and dissociation rate constants of PVA-CR complexes were estimated. For this purpose, three areas are needed: (i) $A_{PVA\text{-}D}$, due to the PVA-CR complex; (ii) A_D, due to the free dye present in the initial equilibrium conditions; and (iii) A_e, generated by the dye released by the complex during migration. In the electropherograms of Fig. 13.4, A_D could not be distinguished from A_e.

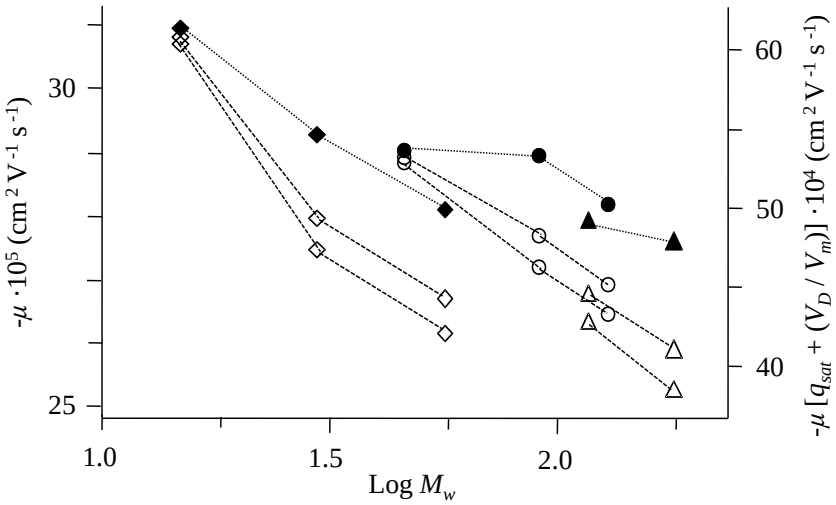

Fig. 13.9. Electrophoretic mobility of the PVA-CR complex against log M_w, without (full symbols, dotted lines and axis at the left) and with correction for the complex stoichiometry (empty symbols, dashed lines and axis at the right); correction was performed with both V_D / V_m = 15 and 10. Symbols indicating tacticity groups: H (diamonds), M (circles) and L (triangles). Other conditions as in Fig. 13.8.

This was attributed to the use of q values far from the maximal stoichiometry of the complexes, q_{sat}. Thus, the free dye concentration should be very low at large values of q, and conversely, at low q values, the large initial concentration of the free dye made also difficult to distinguish its contribution from that due to the dye released during complex migration. However, as shown in the expanded regions of the electropherograms of Fig. 13.8, at q values slightly lower than q_{sat}, it was possible to distinguish between these two contributions. Therefore, the maximum of the PVA-CR complex peak was located, and as indicated in the same figure (trace A), the area of the left half of the band was taken as $A_{PVA\text{-}D}$ / 2. In this band half, the contribution to the area due to the dye released during migration was assumed to be negligible (since the free dye migrates towards increasing migration times). Then, the area at the right of the first depression of the free dye peak (see the expanded parts in Fig. 13.8) was assigned to A_D, and A_e was calculated as the total area minus the contributions of the complex and initially free dye: $A_e = A_{Total} - (A_{PVA\text{-}D} + A_D)$. These assignments probably implied a systematic error in the estimation of A_D, and therefore also in the calculation of the stability constants; however, this made possible to compare the constants obtained with the different PVA samples. To estimate stability constants, the equilibrium molar concentration of free dye, $[D]_{eq}$, was obtained as:

$$[D]_{eq} = \frac{A_D}{b\varepsilon_D} \tag{13.3}$$

where $b\varepsilon_D$ is the optical path multiplied by the molar absorptivity of the dye. The equilibrium molar concentration of the complex is given by:

$$[PVA-D]_{eq} = \frac{A_{PVA-D}}{b\varepsilon_{PVA-D}} + \frac{A_e}{b\varepsilon_D} \tag{13.4}$$

where $\varepsilon_{PVA\text{-}D}$ is the molar absorptivity of the complex. Instead of reasoning about complex formation in terms of q_{sat} monomers per dye ion, calculations are much simpler if the formation of a 1:1 complex is assumed, being the

"ligand" the complexing units formed by groups of q_{sat} monomers. The stability constant, K_s, is then given by:

$$K_s = \frac{1+R}{[C]_0\left(1+\frac{1}{R}\right)-[D]_0} \tag{13.5}$$

where $[C]_0$ and $[D]_0$ are the total analytical molar concentrations of the complexing polymer units and the dye, respectively, and where R is given by:

$$R = \frac{[PVA-D]_{eq}}{[D]_{eq}} = \frac{A_{PVA-D}\left(\frac{\varepsilon_D}{\varepsilon_{PVA-D}}\right)+A_e}{A_D} \tag{13.6}$$

The value of $[C]_0$ can be calculated as:

$$[C]_0 = \frac{n}{q_{sat}}\,[PVA]_0 \tag{13.7}$$

where n is the average number of monomers along the polymer chains, and where $[PVA]_0$ is the total analytical molar concentration of the polymer in mol L^{-1}. The molar absorptivity ratio ε_D / $\varepsilon_{PVA\text{-}D}$ = 0.77 was obtained with a spectrophotometer at 500 nm by measuring several PVA-CR mixtures with q values sligthly lower than the respective q_{sat} values; in these conditions, the formation of a predominant complex with a 1:1 stoichiometry, in which the "ligand" was constituted by q_{sat} monomers, was assumed. In Fig. 13.10, part A, the resulting values of log K_s for q = 2 and 3 (full and empty symbols, respectively) were plotted against log M_w. Contrary to that observed for other CZE parameters, log K_s values did not show any significant trend concerning to either molecular mass or tacticity.

The electropherograms with q = 2 used to obtain log K_s were further processed to estimate pseudo-first-order rate constants for the dissociation of the PVA-CR complexes. For this purpose, half-life measurements were made,

and rate constants were estimated as $k = \ln 2 / t_{1/2}$, where $t_{1/2}$ is the half-life. The exponential decay curve within the region close to the peak of the excess dye, where the contribution of the remaining PVA-CR complex was small, was used. Five measurements of the half-life were made by selecting 5 different starting points on the decay curve of each electropherogram of series of triplicated injections. The starting points were evenly spaced from each other in about 5 s. Estimations of k were obtained with low uncertainties (*ca.* 4.3%). In Fig. 13.10, part B, the average values of k were plotted against log M_w. Within each tacticity group, the dissociation rate constant of the complex was reduced at increasing molecular masses; in addition, H samples showed differences with respect to the M+L samples.

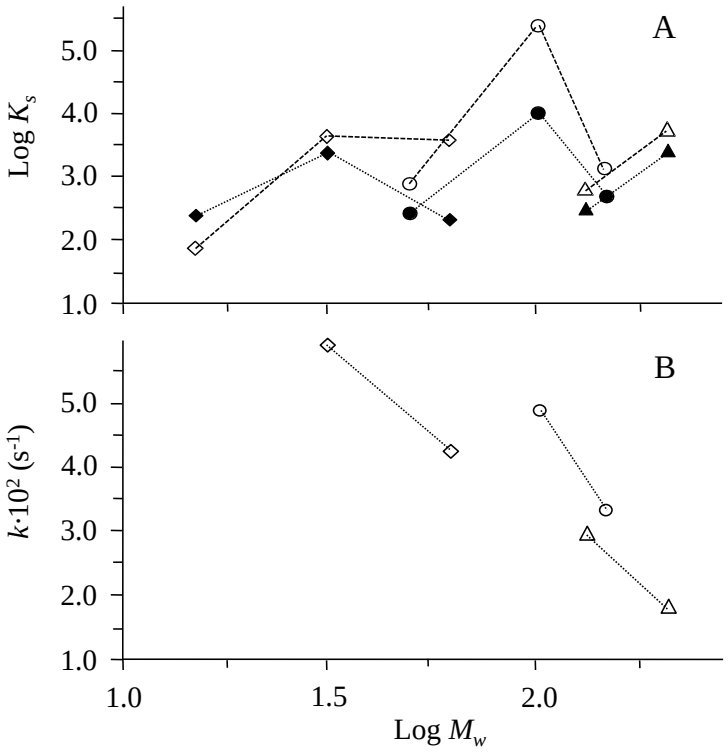

Fig. 13.10. Plots of (A) log K_s and (B) k vs log M_w. Data were calculated from electropherograms obtained with (A) q = 3 and 2 (full and empty symbols, respectively) and (B) q = 2. Symbols indicating tacticity groups: H (diamonds), M (circles) and L (triangles). Other conditions as in Fig. 13.8.

13.4. Conclusions

A PVA-CR complex is immediately formed when a PVA solution containing borate and a CR solution are mixed. Complex formation produced a large increase of the molar absorptivity and a remarkable bathochromic shift of the main band of the UV-vis absorption spectrum of CR. Using positive polarity, electropherograms of PVA-CR mixtures containing a CR excess showed the pattern predicted by the NECEEM theory for a complex formed by an uncharged macromolecule and an anionic marker. The area of the complex band increased linearly, and the areas due to the excess dye and to the dye released by the complex during migration decreased, when the PVA concentration increased up to the saturation point. The variation of the areas at increasing monomer/ dye molar ratios (q values) was used to estimate the maximal stoichiometry of the complex. This ranged from q_{sat} ~ 4.9 to 3.5 for low and high molecular mass PVA, respectively, this variation being produced at different log M_w values depending on PVA tacticity. At the sight of the values of q_{sat}, the possible structure of the complex was discussed. The correlations found along this work among several electrophoretic parameters obtained in NECEEM conditions with respect to both molecular mass and tacticity of PVA can be explained by assuming that the dye ions are stacked in a close proximity to each other within the structure of the complex. Correction of the stoichiometry taking into account the percentage of unbonding acetylated monomers ($q_{sat,c}$) confirmed the differences between tacticity groups. The shape of the PVA-CR complex band, the relative areas of the complex band and free dye peak, and the electrophoretic mobility and dissociation pseudo-first-order rate constant of the complex, were also related to both molecular mass and tacticity of PVA. Thus, the H samples gave complexes with lower absolute mobilities than the M+L samples. In comparison to M+L samples, these differences could be due to the larger distances between adjacent OH groups in H samples, which have a higher *rr*/ *mm* ratio than the M+L samples. Product $\mu \cdot [q_{sat} + (V_D / V_m)]$ decreased at all molecular masses, thus indicating that a free draining regime was not reached. The variation of this product also confirmed

the dependence of the mobility per complexed dye ion on tacticity. Therefore, useful information about both molecular mass and tacticity of PVA can be gained by CZE of PVA-CR mixtures. However, multivariate calibration, including the orthogonal variation of the molecular mass and *rr*/ *mm* ratio values along the set of standards, would be necessary to construct multivariate models capable of making predictions of these two responses with reasonable precision. The set of commercial PVA samples we collected and used in this work was adequate to demonstrate the dependence of CZE parameters obtained in NECEEM conditions on molecular mass and tacticity, but it was deficient to support multivariate calibration. Finally, although this should be also investigated, NECEEM could be useful to evaluate molecular mass and tacticity of other soluble non-charged polymers.

Acknowledgements

Work supported by Project CTQ2010-15335 (MEC of Spain and FEDER funds). M.B.-C. thanks the Universitat de València and Químicas Oro (San Antonio de Benagéber, Spain) for a Cinc Segles-Empresa grant for PhD studies.

References

[1] H.P. Clos, H. Engelhardt, J. Chromatogr. A, 802 (1998) 149.

[2] O. Grosche, J. Bohrisch, U. Wendler, W. Jaeger, H. Engelhardt, J. Chromatogr. A, 894 (2000) 105.

[3] J. Borisch, O. Grosche, U. Wendler, W. Jaeger, H. Engelhardt, Macromol. Chem. Phys., 201 (2000) 447.

[4] H. Engelhardt, M. Martin, Adv. Polym. Sci., 165 (2004) 211.

[5] H. Cottet, C. Simó, W. Vayaboury, A. Cifuentes, J. Chromatogr. A, 1068 (2005) 59.

[6] C.F. Welch, D.A. Hoagland, Polymer, 42 (2001) 5915.

[7] M. E. Starkweather, D. A. Hoagland, M. Muthukumar, Macromolecules, 33 (2000) 1245.

[8] H. Cottet, P. Gareil, J. Chromatogr. A, 772 (1997) 369.

[9] D. Long, A. V. Dobrynin, M. Rubinstein, J. Chem. Phys., 108 (1998) 1234.

[10] H. Cottet, P. Gareil, O. Theodoly, C. E. Williams, Electrophoresis, 21 (2000) 3529.

[11] M. Stefansson, M. Novotny, Anal. Chem., 66 (1994) 3466.

[12] J. Collet, C. Tribet, P. Gareil, Electrophoresis, 17 (1996) 1202.

[13] M. R. Aguilar, A. Gallardo, J. San Roman, A. Cifuentes, Macromolecules, 35 (2002) 8315.

[14] R.A. Wallingford, Anal. Chem., 68 (1996) 2541.

[15] J.P. Barry, D.R. Radtke, W.J. Carton, R.T. Anselmo, J.V. Evans, J. Chromatogr. A, 800 (1998) 13.

[16] M. Beneito-Cambra, J.M. Herrero-Martínez, G. Ramis-Ramos, J. Chromatogr. A, 1216 (2009) 9014.

[17] M. Berezovski, S.N. Krylov, J. Am. Chem. Soc., 124 (2002) 13674.

[18] S.N. Krylov, M. Berezovski, Analyst, 128 (2003) 571.

[19] A.P. Drabovich, M. Berezovski, V. Okhoninm, S.N. Krylov, Anal. Chem., 78 (2006) 3171.

[20] X. Lin, C.L. Coyler, J. Liq. Chromatogr. Relat. Technol. 31 (2008) 1620.

[21] S.N. Krylov, J. Biomol. Screening, 11 (2006) 115.

[22] S.N. Krylov, Electrophoresis, 28 (2007) 69.

[23] C. Sánchez, A. Horta, Laboratorio de Macromoléculas y Técnicas de Caracterización de Polímeros, Colección Aula Abierta, UNED, Madrid, 2000.

[24] T. Moritani, I. Kuruma, K. Shibatabi, Y. Fujiwara, Macromolecules, 5 (1972) 577.

[25] T.K. Wu, M.L. Sheer, Macromolecules, 10 (1977) 529.

[26] R. Fukae, K. Nakata, M. Takeo, T. Yamamoto, O. Sangen, Sen'i Gakkaishi, 56 (2000) 254.

[27] T. K. Wu, D. W. Ovenall, Macromolecules, 6 (1973) 582.

[28] L.J. Fraunenfelder, J. Assoc. Off. Anal. Chem., 57 (1974) 796.

[29] F. Ikkai, M. Shibayama, S. Nomura, C.C Han, Polym. Sci., 34 (1996) 939.

[30] N.J. Atkin, R.M. Abeysekera, D.H. Chenery, A.W. Robards, Polym. Sci., 39 (2001) 1471.

[31] F. Ikkai, M. Shibayama, S. Nomura, Macromolecules, 27 (1994) 6383.

[32] M. Tsujimoto, M. Shibayama, Macromolecules, 35 (2002) 1342.

[33] E. D. Olsen, Modern Optical Methods of Analysis, McGraw-Hill, New York, 1st ed., 1975.

[34] G.A. Ellestad, Chirality, 18 (2006) 134.

Chapter 14. A thermal desorption – gas chromatography – mass spectrometry study of outgassing from polymethacrylimide foam (Rohacell®)

JOURNAL OF SEPARATION SCIENCE

Enrique Javier Carrasco-Correa[a]
José Manuel Herrero-Martínez[a]
Lina Consuegra[a]
Guillermo Ramis-Ramos[a*]
Rafael Mata Sanz[b]
Benito Gimeno Martínez[b]
Vicente E. Boria Esbert[c]
David Raboso García-Baquero[d]

[a]*Department of Analytical Chemistry, University of Valencia, Dr. Moliner 50, 46100 Burjassot, Valencia, Spain*
[b]*Department of Applied Physics-ICMUV, Faculty of Physics, University of Valencia, 46100 Burjassot, Valencia, Spain.*
[c]*Department of Communications-iTEAM, Polytechnic University of Valencia, 46022 Valencia, Spain*
[d]*European Space Agency, ESA/ESTEC, Noordwijk, The Netherlands*

[1] Accepted

J. Sep. Sci. 2015, XX, XXXX-XXXX

Research Article [1]

A thermal desorption - gas chromatography – mass spectrometry study of outgassing from polymethacrylimide foam (Rohacell®)

Polymethacrylimide foams are often used as light structural materials in outer-space devices; however, the closed cells of polymethacrylimide foams contain many volatile compounds which are outgassed even at low temperatures. These compounds ignite as plasmas under the intense radio-frequency fields used in outer-space communications. Since plasmas may cause spacecraft fatal events, the conditions in which they are ignited should be investigated. Therefore, qualitative and quantitative knowledge about polymethacrylimide foam outgassing should be established. Using thermogravimetric analysis, weight losses amounted to 2% and 3% at ca. 100 ºC and 200 ºC, respectively. Thermal desorption coupled to gas chromatography with mass spectrometry detection was used to study the offgassed compounds. Using successive 4-min heating cycles at 125 ºC, each one corresponding to an injection, significant amounts of nitrogen (25.3%), water (2.6%), isobutylene (11.3%), tert-butanol (2.9%), 1-propanol (11.9%), hexane (25.3%), propyl methacrylate (1.4%), higher hydrocarbons (11.3%), fatty acids (2.2%) and their esters (1.3%), and other compounds were outgassed. Other compounds were observed during the main stage of polymethacrylimide foam thermal destruction (220-280 ºC). A similar study at 175 ºC revealed the extreme difficulty in fully outgassing polar compounds from polymethacrylimide foams by baking, also showing the different

composition of the offgassed atmosphere which can be expected in the long term.

Keywords: outgassing; outer-space materials; thermal desorption; polymethacrylimide foam; Rohacell®

14.1. Introduction

Polymethacrylimide foams (PMIs), marketed as Rohacell® (Evonik Degussa, Germany), are manufactured by free radical polymerization of methacrylonitrile and methacrylic acid using light alcohols as blowing agents [1]. The rigid closed-cell structure of PMIs provides outstanding performance concerning to fatigue and creep resistance, low density, rigidity and easy of machining. Further, PMIs are excellent dielectrics, the heat conductivity and thermal expansion coefficient are very low, and rigidity is maintained up to at least 170 ºC, press shaping without decomposition being possible within the 170-190 ºC range. These properties made PMIs to be an excellent choice for a number of technological applications including sandwich material for antennas and radomes, filling for rotor blades in the wind energy industry, and core parts in the automotive, watercraft and space industries. PMIs are also resistant to degradation by radiation (e.g., x-ray, UV) and atomic oxygen exposure which is important for use as external outer-space spacecraft materials [1]. However, the closed-cell structure provides extremely large internal surfaces and available internal volumes which make PMIs prone to retain water and other compounds from external sources. In addition, PMIs contain volatile organic compounds (VOCs) which were trapped in the closed-cell structure during polymerization. Further, PMIs have polar retention sites, i.e. ester and secondary amide groups, where polar compounds are strongly retained. Thus, both entrapment and adsorption of volatile compounds makes PMIs to be unadvisable for some applications.

The emission of volatile substances from materials, the so-called outgassing [2-4], is a serious concern in outer-space applications. In a microgravity environment, outgassing gives rise to a thin but complex and permanent atmosphere of the offgassed products around the spacecraft [1, 5]. Nitrogen, water, carbon dioxide and a variety of VOCs including monomers, plasticizers and solvents, can be expected [2]. The on-board instruments of the Rosetta Mission (European Space Agency, ESA) were used to monitor the

spacecraft outgassing for 6 years during the cruise phase; water and VOCs, including polycyclic aromatic hydrocarbons, solvents (toluene, xylene) and residues of the propellant, were found [6]. In outer-space applications, outgassing is undesirable for several reasons. First, the released compounds can be re-deposited on optical components, thus degrading their performance [4, 6]. Degradation of components has been shown to be also due to back-scattering of pollutants produced by intermolecular collisions involving only outgassed molecules (self-scattering) and collisions between outgassed molecules and molecules in the ambient atmosphere (ambient scattering) [7]. Second, UV irradiation coming from the Sun and planetary coronas may result in the decomposition of the organic compounds which are always present around the spacecraft, with the subsequent build-up of a carbonaceous layer on optical components and surfaces of charge-coupled devices thus degrading their performance [8]. Further, trace amounts of contamination have been shown to greatly reduce the performance of space based laser systems [9]. Third, pollution interferes with sensing devices and analytical instruments by increasing the background of chemical measurements. Further, the interpretation of organic analysis of extraterrestrial samples is hindered in the presence of the organic contaminants, particularly if they are not well known [10]. Finally, the offgassed products can be ionized, high energy ions being capable of causing irreversible damage to spacecraft components and instruments [1, 2]. Ionization can be produced by outer-space radiation [2], but also by high-voltage components and radio-frequency sources of the spacecraft itself, such as antennas, which may give rise to the ignition of highly destructive local plasmas [11, 12].

The early recognition of the importance of organic contamination allowed the evolution of a control program encompassing spacecraft design, mission operations, flight operations, and the design of the instrumentation for chemical analysis [10]. Accordingly, all organic materials for use in space systems shall be evaluated to determine their outgassing characteristics [13]. Spacecraft

outgassing is minimized by careful selection of the materials and by hermetic sealing whenever possible. A bakeout, that is, to treat the material in vacuum or in a controlled atmosphere at temperatures as high as possible, is recommended to accelerate outgassing from materials, thus reducing the content of contaminants before use [2, 3, 14].

To evaluate outgassing from polymers, gas chromatography coupled to mass spectrometry (GC-MS) is most usually preferred [14-17]. In addition, when dealing with solid samples, all the GC injection requirements are superbly managed using a thermal desorption/sorption system (TD). In particular, with TD injection both resolution and limits of detection are largely improved, which is particularly useful when the analytes should be preconcentrated from large volumes, as occurs in the investigation of air pollutants, when the sample contains components largely differing in volatility, or when slowly outgassing from a solid sample should be monitored [18-20]. Jansen et al. [21] used TD-GC coupled to Fourier-transform infrared spectroscopy detection to study outgassing from dimethylpolysiloxane (silicone), polyoxymethylene and poly(methyl-methacrylate). In a TD-GC-MS study of outgassing of polyimides, adhesives and other chemicals used in the manufacturing of radiation detectors, styrene and aromatic solvents were confirmed to cause gain losses [16]. TD-GC-MS has been also used to study the outgassing characteristics of cross-linked epoxy-based SU-8 resin; carbon dioxide and a series of VOCs were found [14]. Also using TD-GC-MS, flame retardants (organophosphorus triesters) and plasticizers (phthalate esters) were found to be the main contaminants of silicon wafer surfaces [17].

Outgassing studies should be performed within the range of temperatures which are expected to be reached for the addressed material. Thus, the ESA recommends testing outgassing of space materials at temperatures up to 125 ºC [3, 4]. Most spacecraft components are designed to operate below 70 ºC; however, 125 ºC can be reached for radiation absorbent materials such as solar panels [22], and a peak value as high as 200 ºC was reported for a piece of

insulation of the Hubble Space Telescope [23]. Using thermogravimetric analysis (TA) and a quadrupole mass spectrometer, Hogue et al. [1] studied outgassing of water from PMIs at different temperatures up to 160 ºC. Water was found to be very slowly released, which was attributed to chemical affinity for the PMI polar retention sites. Drying of the material for several hours at 125 °C was recommended. However, as far as we know, studies about outgassing from PMIs focusing on VOCs have not been published. In this work, outgassing of Rohacell® 31HF, which is the lightest and consequently the PMI type most frequently used in aeronautical and space applications, was studied. Using TA, the stages of outgassing and thermal destruction of the polymer, and the associated weight losses, were first established. Then, TD-GC-MS was used to know the nature, relative amounts and outgassing rates of the offgassed products at increasing temperatures. Duplicated series of injections were performed with a TD system provided with a cold trap. The offgassed products were first monitored by using successive 4-min heating cycles at 125 ºC. After 10 heating cycles at this temperature, outgassing during the PMI thermal destruction stages was studied by performing additional heating cycles at progressively higher temperatures up to 320 ºC. To reach high temperatures was of interest both to estimate the compounds which could be still present inside the samples after long heating periods at moderate temperatures, and to identify which new compounds could be further offgassed during episodes of local overheating, as those provoked by plasmas. Finally, fresh samples were used to also study outgassing at 175 ºC, which is higher than expected for normal use of PMI, but still safe to avoid irreversible destruction of the polymer. Thus, using successive short heating cycles at two different temperatures, namely 125 and 175 ºC, the differences between the outgassing rates of non-polar and polar compounds were studied.

14.2. Materials and methods

A Pyris Diamond Thermogravimetric Analyzer (TA, Perkin Elmer, Waltham, MA, USA) was used. The GC-MS chromatograms were obtained with a Focus DSQ II gas chromatograph provided with a single quadrupole MS detector (Thermo Fisher Sci., Waltham, MA, USA). The fused-silica capillary column was a TR-5MS (30 m, 0.25 mm i.d., 0.25 µm film, Thermo Fisher Sci.). Injection was performed with a Series 2 UNITY Thermal Desorption System (Markes Int., Pontyclun, UK), on-line coupled to the GC-MS instrument, and controlled by a Maverick software (version 4.1.29, Markes Int.).

The Rohacell® 31HF samples for TD-GC-MS were cut into 1-2 mm thick strips from a 5 mm thick sheet. Samples with a ca. 10 mg total weight were introduced into the TD quartz liner. Both pre-purge and sample desorption were performed with a 20 mL min^{-1} He stream, with the trap in line and the split opened also at 20 mL min^{-1}. Pre-purge time was 2 min. Sample desorption was performed at the selected temperature during 4-min, with the trap set at 10 ºC and in the presence of the same He gentle stream, which is necessary to convey the released compounds to the adsorption/desorption tube. After sample desorption, the trap was purged with He for 2 more min. Injection was carried out by heating the trap at the maximum rate up to 250 ºC. The trap was maintained at this temperature for 3 min with the split at 20 mL min^{-1}. During injection, the inlet and outlet split ratios were 1.2:1 and 11:1, respectively. The path between the TD system and the GC column was maintained at 140 ºC. Series of successive injections of the same sample were performed. Each series was performed in duplicate. Accordingly, all quantitative data given below in Tables 14.1-14.3 are average values calculated over the two data obtained from the duplicates. The differences between all the paired values amounted to an average of ca. 4.8% over the corresponding averages.

The GC carrier was He at 1 mL min^{-1}. The GC oven was initially maintained at 40 ºC for 10 min. This was necessary to manually match the starting of the chromatogram with the TD injection. Injection was triggered

during this isothermal period, about 2 min before starting the GC temperature ramp. This later was set at 8 ºC min^{-1} until reaching 260 ºC. The final hold at 260 ºC was 2 min. The GC-MS transfer line and ion source were both set at 280 °C. Ionization was done by electron impact at 70 eV. The spectrometer was used in the ion-positive mode, the scan rate was 500 a.m.u. s^{-1} and the *m/z* 10-500 range was scanned. Blanks (an empty liner) were run at the beginning of each series of experiments; however, no significant peaks were observed on the chromatograms of the blanks.

First, tentative compound identifications were made by means of MS automatic searches using the NIST Standard Reference Database (Gaithersburg, MD, USA). Analysis and comparison of the chromatograms was also conveniently performed using OpenChrom, an open source software for the MS analysis of chromatographic data [24]. Only those candidates exceeding or approaching 90% match were accepted. Further, the presence of essentially the same compounds in several chromatograms of the same series largely increased the reliability of the identifications. Confirmation of peak identification was performed by co-chromatographing Rohacell® 31HF with as many standards as could be gathered. For this purpose, ca. 5 mg Rohacell® 31HF samples were introduced in the quartz liner. A small plug of glass wool was also introduced. Besides, a mixture of the following standards was prepared by weighing: *tert*-butanol (quality, 99%), methacrylic acid (99%), propyl methacrylate, methacrylamide (97%), butylated hydroxytoluene (99%), oleic acid (99%) and diisooctylphthalate (96%) from Sigma Aldrich (Milwakee, WI, USA), and butyl octyl phthalate (98%) from LGC standards (Teddington Middlesex, UK). Since *ca.* 50 mg of each standard was weighted, the mixture contained *ca.* 125 mg of each standard per gram of mixture. A 1 µL syringe was used to deposit 0.1 µL of this mixture on the glass wool plug, the tube was put in its place for injection and the injection protocol was started. The retention times of both the standards and other tentatively identified compounds were also reported as retention indexes (Kováts indexes, RI) to be

hereafter used for reference. For this purpose, alkane standard solutions C8-C20 and C21-C40 from Fluka (Buchs, Switzerland) were injected.

14.3. Results and discussion

14.3.1. Thermogravimetric analysis

The TGA traces obtained at 2 and 10 ºC min^{-1} are shown in Fig. 14.1. A quick 2% weight loss was observed up to 65 ºC. This was followed by a slower and steady loss up to ca. 220 ºC. The accumulated loss reached 3% at ca. 220 ºC. No differences between the two heating rates, 2 and 10 ºC min^{-1}, were observed up to 220 ºC. At higher temperatures, PMI underwent an irreversible and quick two-step decomposition, with some delay of the 250-270 ºC transition point between the two steps at the faster heating rate.

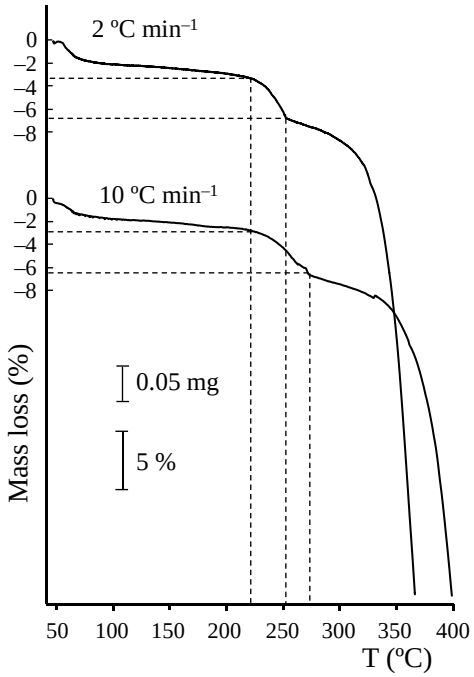

Fig. 14.1. TGA of Rohacell® 31HF at 2 and 10 ºC min^{-1}.

14.3.2. Offgassed compounds and outgassing rates at 125 ºC

The 1st and 10th (last) chromatograms obtained during the successive 4-min heating cycles at 125 ºC are shown in Fig. 14.2. The chromatograms contain a series of large and medium intensity peaks, as well as many small peaks. Only those peaks reaching a signal-to-noise ratio (S/N) larger than 10, were considered. These compounds, ordered by increasing GC retention time, and including CAS and abundance (as S/N along the successive heating cycles), are given on Table 14.1. The first significant peak was nitrogen, followed by a small peak of water and several light VOCs. Among these, the most abundant were two hydrocarbons, namely isobutylene (2-methyl-1-propene, or its isobaric trans-butene) and hexane, and two alcohols, tert-butanol and 1-propanol. These are solvents of the monomers and blowing agents, necessary to generate the closed-cell structure during PMI copolymerization [1]. The double peak of hexane that appears in the chromatogram of Fig. 14.2, upper part, should be attributed to column overloading. From the two hexane peaks, the first one was only present in the chromatogram of the first heating cycle. On the other hand, the small baseline shifts of Fig. 14.2, lower part, were occasionally observed when the vertical axis was largely expanded, and should be attributed to weak carrier leaks at the column / MS source connection.

The decrease of the peak areas of hexane and the other compounds along the series of successive 4-min heating cycles is illustrated in Fig. 14.3A, and the relative areas (all them starting from 1) are compared in Fig. 14.3B. The amounts of released nitrogen decreased to negligible values after the 3rd cycle (12 min of accumulated heating time). The VOCs were very slowly outgassed, significant amounts being still released after 10 cycles (40 min of accumulated heating time). As shown below in Sections 14.3.3 and 14.3.4, only small portions of the total contents of nitrogen and the VOCs were outgassed during the 10 cycles at 125 ºC, by far most of them remaining inside the closed-cell structure of PMI. Therefore, outgassing at 125 ºC was much slower than it might seem by solely looking at the traces in Figs. 14.3A and 14.3B. On the

other hand, the differences among the releasing rates of the compounds were small (see Fig. 14.3B). Only 1-propanol was outgassed at a slightly lower rate than the other compounds, which should be attributed to a stronger adsorption of this polar compound on the PMI polar sites.

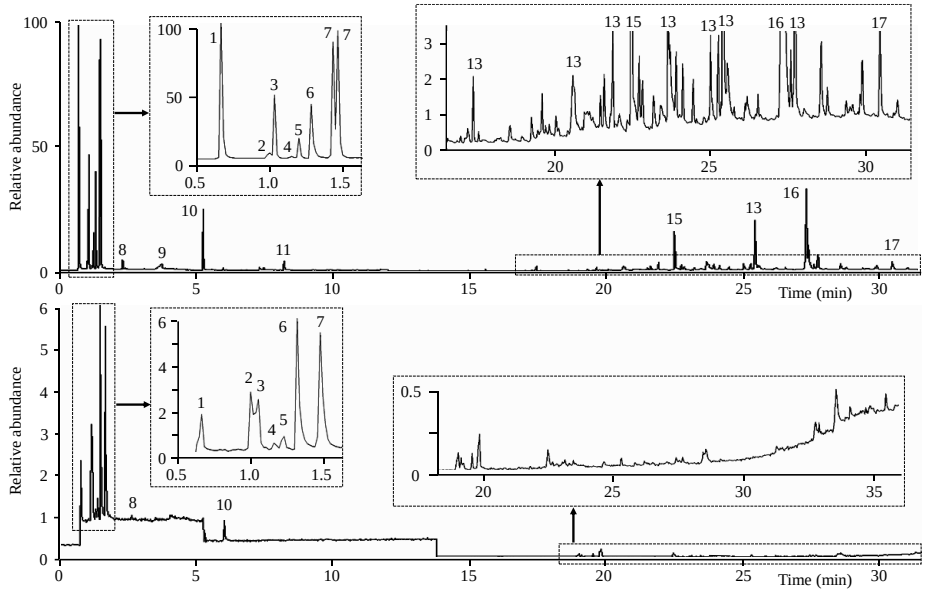

Fig. 14.2. TICs obtained by successive 4-min periods of thermal desorption at 125 ºC. Two chromatograms corresponding to the 1st (A) and 10th (B) cycles are shown. Peak identification as indicated on Table 14.1. The double peak of hexane in the chromatogram of the upper part was due to column overloading.

In addition, methacrylic acid, one of the two monomers used in PMI copolymerization, and its 1-propanol ester, namely 1-propyl methacrylate, were also outgassed. Along the series of chromatograms, the areas of the propyl ester peak were more than 10 times larger than those of the free monomer, which agrees with the large amounts of 1-propanol. N-t-butylmethacrylamide was also outgassed; however, free methacrylonitrile (2-methyl-2-propenenitrile, the other monomer used in PMI copolymerization) did not outgas at 125 ºC. As commented below in Section 14.3.3, after outgassing the sample at 125 ºC, methacrylonitrile was indeed outgassed by increasing the sample temperature at 160 ºC and higher. Methacrylonitrile is a fairly volatile compound (boiling

point, 90 ºC), then, lack of outgassing of this compound at 125 ºC could also be due to strong adsorption on the PMI polar sites.

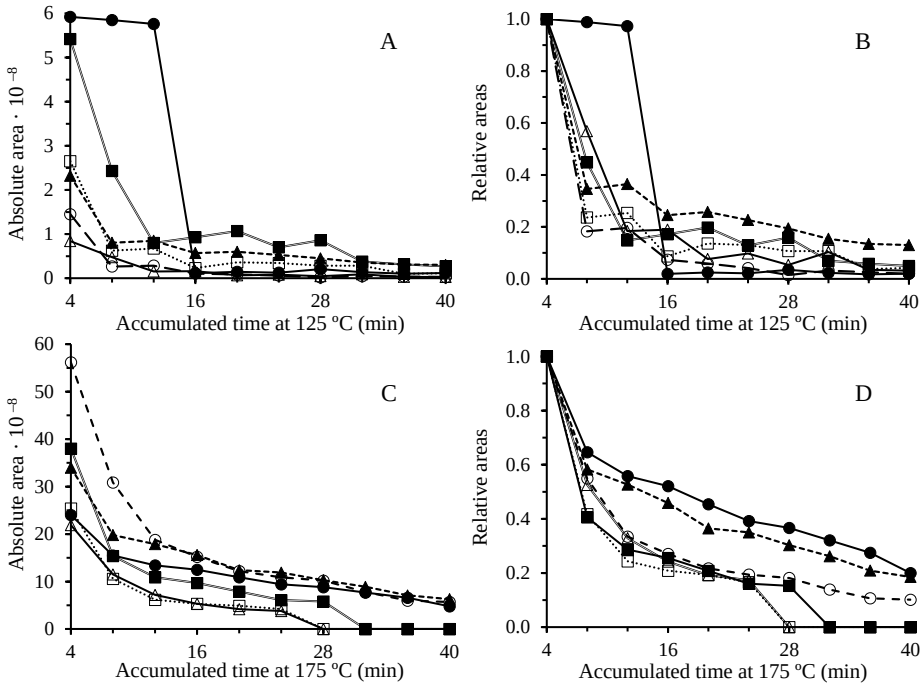

Fig. 14.3. Decrease of the absolute (left: A, C) and relative (right: B, D) peak areas of the largest peaks along the series of successive 4-min heating cycles at 125 ºC (up: A, B) and 175 ºC (down: C, D). Peak identification: nitrogen (●), isobutylene (□), tert-butanol (Δ), 1-propanol (▲), hexane (■), propyl methacrylate (○).

At long retention times, several higher alkanes (high molecular mass hydrocarbons) were observed; however, excessive fragmentation in the mass spectrometer hindered individual identification. Within the same retention time region, several saturated and mono-unsaturated free fatty acids with 16 and 18 carbon atoms in the alkyl chain, and their esters with both 1-propanol and glycerol, were also outgassed.

Table 14.1. Compounds released during 10 successive 4-min heating cycles at 125 ºC

ID [a]	RI [a]	Compound and CAS	Abundance as signal-to-noise (S/N) ratio [b]
1	563	Nitrogen, 7727-37-9	2675; 2722; 2866; 64; 101; 72; 148; 69; 67; 82
2	578	Water, 7732-18-5	105; 80; 82; 71; 64; 57; 65; 49; 77; 84
3	579	Isobutylene (2-methyl-1-propene), 115-11-7, or trans-butene, 624-64-6	1187; 362; 342; 133; 207; 175; 171; 152; 71; 81
4	584	2,3-Epoxy-2-methyl-butane, 5076-19-7, or 3-amino-2-oxazolidinone, 80-65-9, or trimethyl oxirane, 5076-19-7	23: 33; 9; 17; 9; 7; 9; 7; 10; 10
5	587	tert-Butanol, 75-65-0	403; 247; 79; 97; 44; 43; 28; 45; 19; 18
6	590	1-Propanol, 71-23-8	1127; 461; 468; 322; 386; 288; 274; 193; 197; 208
7	599	Hexane, 110-54-3	2612; 1411; 512; 742; 757; 375; 527; 192; 198; 183
8	702	3-Hydroxy-3,5-dimethyl-2-hexanone, 6321-14-8, or tert-butyl isopropyl ether, 17348-59-3	87; 42; 20; 8; 8; ND
9	804	Methacrylic acid, 79-41-4	51; 33; 29; 21; 18; 9; 13; 6; ND
10	881	Propyl methacrylate, 2210-28-8	722; 152; 136; 58; 54; 31; 36; 24; 24; 20
11	1023	N-t-Butylmethacrylamide, 6554-73-0	103; 11; 9; ND
12	-	Higher hydrocarbons (at least 5 different compounds) [c]	47; 358; 792; 257; 167; 36; 30; ND
13	-	Oleic acid, 112-80-1, and other fatty acids (saturated and unsaturated, 16–18 carbon atoms) [c]	247; 340; 79; 66; 9; 12; 6; ND
14	1514	Butylated hydroxytoluene, 128-37-0	ND; 8; 7; 8; 7; 7; 7; 6; 8; ND
15	1872	Butyl-octyl phthalate, 84-78-6	457; 12; ND
16	2131	2,3-Dihydroxypropyl elaidate, 2716-53-2, and other esters of fatty acids [c]	1001; 19; 5; 5; 5; 9; ND
17	2310	Diisooctyl phthalate, 27554-26-3	87; 63; 63; 34; ND

[a] ID, peak identification according to the chromatograms of Fig. 14.2; RI, retention index (Kováts index).

[b] Abundance shown along the 10 successive chromatograms (average values of two series) expressed as S/N at the peak maximum; ND, not detected in the 1st chromatogram or in the chromatograms that followed after the last one.

[c] Compounds giving rise to several peaks of the same class at different retention times; on the abundance column, only the S/N of the highest peak of the class is given.

A compound identified as 2,3-dihydroxypropyl elaidate, the monoester of elaidic acid (the trans-isomer of oleic acid) and glycerol, was released along the first four cycles (16 min). The presence of fatty acids and their glycerol monoesters suggests the use of partially saponified oils of vegetal origin (soaps), probably introduced in the PMI polymerization mixture as emulsifiers and foaming agents. Butylated hydroxytoluene, a common hydrophobic antioxidant, was also observed along 8 heating cycles. Finally, at least two esters of phthalic acid, which are common plasticizers, were also released along the first 4 cycles.

14.3.3. Offgassed compounds at temperatures higher than 125 ºC

The samples already outgassed at 125 ºC during 10 successive 4-min heating cycles were further heated during additional 4-min cycles, starting at 160 ºC and successively increasing the temperature at 200, 240, 280 and 320 ºC during the cycles that follow. In this way, the study at 160 ºC and higher temperatures was performed over a simplified background, where most of the light compounds were already outgassed. This made easier to distinguish between the compounds outgassed before and after PMI thermal degradation. Since thermal destruction of the polymer starts above 220 ºC (Fig. 14.1), only compounds initially present inside the PMI should be outgassed during the cycles at 160 ºC and 200 ºC. Accordingly, the compounds outgassed at these two temperatures were those already observed at 125 ºC (see Table 14.2); however, as next commented, a few compounds not observed at 125 ºC showed up at 160 ºC. Another difference with respect to that observed in the chromatograms obtained at 125 ºC was the large increase of the abundances of a series of compounds including isobutylene, tert-butanol, 1-propanol, methacrylic acid, n-propyl methacrylate and N-t-butylmethacrylamide. It should be noted that all these compounds were either moderately or strongly

polar. This further underlined the strong retention and therefore the slow outgassing rates of polar compounds from PMI at any temperature.

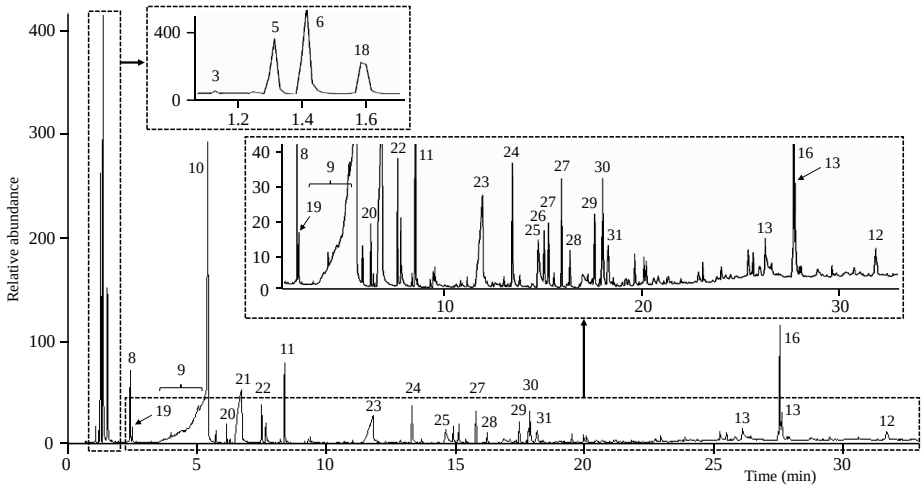

Fig. 14.4. Chromatogram corresponding to the 4-min heating cycle at 240 ºC. The sample was previously outgassed during 10 cycles at 125 ºC, followed by 2 more cycles at 160 and 200 ºC. Peak identification as indicated on Tables 14.1 and 14.2.

Concerning to the compounds not observed before at 125 ºC, an intense peak of methacrylonitrile and small peaks of alpha-methylstyrene and n-propyl benzoate showed up at 160 ºC and higher temperatures. The outgassing of methacrylonitrile agreed with the presence in PMI of all the unreacted monomers of the copolymer, and not only methacrylic acid and its propyl ester. As indicated above, lack of outgassing of methacrylonitrile at 125 ºC can be explained by a rather strong retention of this polar compound. Other newly offgassed compounds including n-propyl acetate, 2,6-octadiene, methacrylamide and benzoic acid were observed at 200 ºC. However, the most complex chromatograms, showing many compounds not observed at lower temperatures, were obtained at 240 and 280 ºC, when the main stage of PMI thermal destruction took place. The chromatogram obtained at 240 ºC is shown in Fig. 14.4. The number of offgassed compounds largely decreased at 320 ºC. However, the chromatograms obtained at 320 ºC still showed an intense peak of methacrylonitrile, as well as peaks of all the compounds already outgassed

at 125 ºC. Therefore, the contents of VOCs in PMIs can be reduced by baking, but significant amounts of them will always remain within the foam. Most likely, to reduce their contents to negligible amounts without PMI thermal destruction is not possible.

14.3.4. Offgassed compounds and outgassing rates at 175 ºC

A bakeout has been defined as the activity of increasing the temperature of hardware to accelerate its outgassing rates with the intent of reducing the content of molecular contaminants within the hardware [3]. A bakeout should improve the outgassing characteristics of materials thus widening the scope for safe applications [2]. As discussed above, polar compounds will be always trapped or retained within PMI, but after a bakeout at a temperature as higher as possible, further outgassing at the much lower operation temperatures of PMI components could be negligible. Then, to estimate how much the outgassing behavior of PMI could be improved by baking, series of 4-min heating cycles at 175 ºC were performed by duplicate. This temperature is high regarding the normal operation use of this material, and at the same time it is safe enough to avoid thermal degradation or softening during bakeout.

From a qualitative point of view, the compounds released by heating PMI at 175 ºC were essentially the same as those outgassed at 125 ºC. The chromatograms (not shown) also resembled closely those obtained by heating at 160 ºC after persistently outgassing the samples at 125 ºC. The only noteworthy difference was that methacrylonitrile was not outgassed by heating the fresh PMI samples at 175 ºC. This difference could be due to the presence of an excess of methacrylic acid and propyl methacrylate in these samples. At 175 ºC, copolymerization was probably resumed, thus methacrylonitrile reacting with the excess of methacrylic acid and its propyl ester. Instead of this, an excess of methacrylonitrile inside PMI may result by persistently outgas the

other monomers at 125 ºC. This methacrylonitrile excess was then outgassed when the same samples were heated at higher temperatures.

The decrease of the abundances of the main offgassed compounds along the successive 4-min heating cycles at 175 ºC is shown in Fig. 14.3C, and the relative areas (all them starting from 1) are compared in Fig. 14.3D. By comparing plots A and C of Fig. 14.3, the peak abundances were about 10 times higher at 175 ºC than at 125 ºC. Therefore, the VOCs were very slowly outgassed at 125 ºC, by far most of them remaining within the PMI after 10 heating cycles. This further underlined the difficulty in removing most of the VOCs from PMI. Also, it should be noted that the compounds released in higher amounts were not the same at 125 ºC and 175 ºC. At 175 ºC the compound most abundantly released was propyl methacrylate, whereas nitrogen and hexane where the most abundant using 125 ºC, at least during the first heating cycles. Therefore, outgassing of the polar compounds was much slower than that of the non-polar compounds at low temperatures.

On the other hand, the differences between the outgassing rates of non-polar and polar compounds were enhanced by outgassing at 175 ºC when compared to 125 ºC. Thus, at 125 ºC, all compounds were very slowly released after the 3rd or 4th cycles. Instead of this, hexane, isobutylene and tert-butanol seemed to be exhausted after 7-8 cycles at 175 ºC, whereas outgassing of the more polar 1-propanol and propyl methacrylate was still under way after 10 cycles. Also at 175 ºC, the continuous outgassing of nitrogen was remarkable, and should be explained by trapping within the PMI closed cells. Thus, a bakeout at 175 ºC can be recommended to improve the outgassing behavior of PMIs. This will largely reduce or virtually eliminate non-polar and weakly polar compounds; however, the most polar compounds will be only partially outgassed. Significant amounts of these later will remain inside the PMI for long.

Table 14.2. Compounds released at increasing temperatures after outgassing at 125 ºC for 40 min (10 accumulated 4-min cycles)

ID [a]	RI [a]	Compound and CAS	Abundance as signal-to-noise ratio [b]				
			160 ºC	200 ºC	240 ºC	280 ºC	320 ºC
1	563	1 Nitrogen, 7727-37-9	50	711	ND	619	ND
3	579	Isobutylene (2-methyl-1-propene), 115-11-7, or trans-butene, 624-64-6	513	412	378	353	712
5	587	tert-Butanol, 75-65-0	1094	2585	6466	11302	1420
6	590	1-Propanol, 71-23-8	5328	6494	10345	12210	9102
18	702	Methacrylonitrile, 126-98-7	2431	4205	3722	11868	2139
8	719	3-Hydroxy-3,5-dimethyl-2-hexanone, 6321-14-8, or tert-butyl isopropyl ether, 17348-59-3	183	518	1719	12140	749
19	722	n-Propyl acetate, 109-60-4	ND	390	343	1849	ND
9	804	Methacrylic acid, 79-41-4	290	784	1044	2095	799
10	881	Propyl methacrylate, 2210-28-8	2085	4317	6738	11541	4824
20	910	2,6-Octadiene, 4974-27-0	ND	143	450	1932	ND
21	1019	Methacrylamide, 79-39-0	ND	506	1280	1804	1133
22	1021	alpha-Methylstyrene, 98-83-9	141	399	908	4072	ND
11	1023	N-t-Butyl methacrylamide, 6554-73-0	208	716	1928	6046	2113
23	1187	Benzoic acid, 65-85-0	ND	120	654	868	47
24	1287	n-Propyl benzoate, 2315-68-6	32	193	887	3645	ND
25	1288	Benzamide, 55-21-0	ND	ND	334	504	ND
26	1380	2-Methyl-2-pentyl-1,1-cyclopropanedicarbonitrile, 16738-90-2	ND	ND	366	1433	ND
27	-	2-Methyl-2-pentyl-1,1-cyclopropanedicarbonitrile, 16738-90-2, and at least 4 isomers	ND	ND	776	2835	ND
28	1455	N-(1,1-Dimethylethyl)-benzamide, 5894-65-5	ND	ND	258	867	ND
29	1534	6,10-Dimethyl-3-(1-methylethyl)-6-cyclodecene-1,4-dione, 13657-68-6	ND	ND	503	2800	ND
30	1560	Probably N-cyclopentylcarbonyl glycine methyl ester, 0-00-0	ND	ND	754	3098	ND
31	1582	Probably 4-hexenoic acid, 2-acetyl-2-methyl-, ethyl ester, (E)- 125163-78-2	ND	ND	280	1133	ND
13	-	Oleic acid, 112-80-1, and other fatty acids (saturated and unsaturated, 16–18 carbon atoms) [c]	ND	386	260	537	ND
16	2131	2,3-Dihydroxypropyl elaidate, 2716-53-2, and other esters of fatty acids [c]	ND	600	2742	9410	722

[a] Peak identification (ID) according to the chromatograms of Figs. 14.2 and 14.4; RI, retention index (Kováts index).

[b] Abundance expressed as signal-to-noise ratio (S/N) at the peak maximum; ND, not detected.

[c] On the abundance columns, the S/N of the homolog or isomer showing the highest peak of the class is given.

14.3.5. Composition of the atmosphere outgassed by PMI components

An estimation of the composition of the gases released at both 125 ºC and 175 ºC is given in Table 14.3. The composition of the outgassed atmosphere is given first in percentages calculated by adding the areas of the addressed peak along the series of 10 successive heating cycles, divided by the sum of the accumulated areas of all the peaks along all the series. Also in Table 14.3, the values in italics are corrected percentages, calculated by taking into account the relative sensitivities of the compounds with respect to hexane. The relative sensitivities were first used to correct the peak areas, and the corrected percentages of the compounds were calculated from these later. Other details are given in Table 14.3. As observed, the main offgassed products at 125 ºC and 175 ºC were not the same. By considering only the most abundant compounds, when the temperature was increased from 125 ºC to 175 ºC, large reductions of the percentages of nitrogen and hexane were observed, whereas the percentages of isobutylene and propyl methacrylate largely increased. Thus, the atmosphere generated at the higher temperature was richer in the more polar compounds than that obtained after persistently heating PMI at 125 ºC for an accumulated time of 40 min. Therefore, it can be expected that the atmosphere generated at any low temperature around a PMI component in a microgravity environment will be initially richer in the non-polar compounds, thus resembling the composition indicated in Table 14.3 for 125 ºC. However, with time, the atmosphere will slowly become richer in the polar compounds, thus slowly approaching that described in Table 14.3 for 175 ºC. This is important, since fatal events due to plasma ignition produced long time after launching can be due to the slowly increase of pressure of the thin atmosphere surrounding the spacecraft, but also to changes in its composition.

Table 14.3. Relative values (%) of the accumulated peak areas along 10 successive heating cycles at either 125 or 175 ºC, and absolute weight losses in mg per 100 gram of PMI foam, by assuming a total loss of 3%.

ID	Compound and relative sensitivity respecting hexane [a]	At 125 ºC [b]	At 175 ºC [b]	At 175 ºC [c]
1	Nitrogen	21.2; *25.3*	8.7; *11.5*	350
2	Water	2.2; *2.6*	0.5; *0.7*	20
3	Isobutylene or trans-butene	9.5: *11.3*	20.1: *26.6*	800
4	2,3-Epoxy-2-methyl-butane or similar	0.4; *0.5*	0.1; *0.1*	3
5	tert-Butanol (1.4)	3.4; *2.9*	3.4; *3.2*	100
6	1-Propanol (1.2)	12.0; *11.9*	10.1; *11.1*	330
7	Hexane (1.0)	21.2; *25.3*	9.7; *12.8*	380
8	3-Hydroxy-3,5-dimethyl-2-hexanone or similar	0.6; *0.7*	3.8; *5.0*	150
9	Methacrylic acid (3.1)	0.6; *0.2*	0.5; *0.2*	10
10	Propyl methacrylate (3.5)	4.1; *1.4*	13.1; *4.9*	150
11	N-t-Butyl methacrylamide	0.4; *0.2*	0.4; *0.2*	10
21	Methacrylamide (2.7)	0; *0*	1.5; *0.7*	20
12	Higher hydrocarbons (1.3)	12.3; *11.3*	13.2; *13.4*	400
13	Oleic acid and other fatty acids (2.6)	4.7; *2.2*	5.1; *2.6*	80
14	Butylated hydroxytoluene (1.8)	0.1; *0.1*	0.1; *0.1*	3
15	Butyl-octyl phthalate (2.1)	1.6; *0.9*	1.7; *1.1*	30
16	2,3-Dihydroxypropyl elaidate and other fatty acid esters	3.3; *1.3*	3.5; *1.5*	46
17	Diisooctyl phthalate (2.2)	0.8; *0.4*	0.9; *0.5*	20

[a] Relative sensitivity of the addressed compound for MS detection, calculated as (peak area / concentration) / (hexane peak area / hexane concentration); in order to calculate corrected areas, when the standard was not available the relative sensitivity was assumed to be 1; however, for N-t-butylmethacrylamide and fatty acid esters the value 3 was adopted. Peak identification and other details as in Tables 14.1 and 14.2.

[b] Released amounts of the compounds as percentages, calculated by adding the area of the addressed peak along the series of 10 cycles, divided by the sum of the areas of all the peaks also along all the series. In italics, the same calculation but performed using corrected peak areas (divided by the relative sensitivity of the addressed compound).

[c] Calculated absolute loss of the addressed compound in mg per 100 g of PMI foam (according to the corrected percentages of the accumulated losses at 175 ºC), by assuming a total weight loss of 3% (the sum of losses is 3 g).

On the other hand, the reduction of the percentages of total outgassed nitrogen and hexane at 175 ºC when compared to 125 ºC (see Table 14.3) provided further evidence that these non-polar compounds were effectively depleted from PMI after the 7-8 first 4-min cycles at 175 ºC. On the contrary, the total percentages of isobutylene, polar compounds as 1-propanol and propyl methacrylate, and large molecular mass compounds as higher hydrocarbons and fatty acids and their esters, increased or remain constant upon increasing the baking temperature. This further evidenced the difficulty in removing polar compounds from PMI. The last column of Table 14.3 provides the mass of each compound (in mg) which can be expected at the long term by outgassing 100 g of untreated Rohacell® 31HF. These values, which were obtained from the corrected percentages of the compounds released at 175 ºC by assuming a total

14.4. Concluding remarks

According to the TGA traces and TD-GC-MS studies, the contents of nitrogen, water and VOCs in Rohacell® 31HF amounts to more than 3% of its weight. At the temperatures expected for normal operation of outer-space devices, mainly nitrogen, hexane, isobutylene, tert-butanol, 1-propanol, methacrylic acid and its propyl ester, higher alkanes and surfactants are outgassed. Fatty acids and their esters with 1-propanol and glycerol are included in the latter, being probably present as residues of partially saponified vegetable oils (soaps). Under normal operation conditions (below 125 ºC), outgas of nitrogen and VOCs from PMI components is very slow, particularly for the most polar compounds as 1-propanol and propyl methacrylate. This is not good for devices that should operate in the outer-space for years, since the risks associated to outgassing will slowly but steadily increase with time.

Exhaustive knowledge about the compounds released at 125 ºC and 175 ºC from fresh PMI samples has been provided (Tables 14.1 and 14.3). These data show to what extent the PMI outgassing characteristics can be improved by baking at 175 ºC, which is safe enough to avoid thermal destruction of the material during the bakeout. Thus, hexane and isobutylene can be fully depleted

by baking at 175 ºC; however, at this temperature, nitrogen and strongly polar compounds are very slowly outgassed, most of them remaining within the PMI closed-cell structure for long. Therefore, the polar compounds of Tables 14.1 and 14.3 should be further investigated in relation to its ability to ignite plasmas in thin atmospheres when irradiated with different RF bands and powers. Within this concern, the compounds exclusively outgassed at temperatures over 220 ºC, during the main stage of PMI thermal destruction (Table 14.2), are also of interest. This is because these compounds are also released when a RF plasma ignites close to a PMI component, and because the compounds newly added to the plasma could reinforce its devastating effects. Among the compounds to be investigated, methacrylonitrile should be included, since this compound will be also outgassed from overheated PMI if methacrylic acid and its esters have been previously depleted.

Acknowledgements

Work supported by Project CTQ2014-52765-R (MEC of Spain and FEDER funds). E.J.C-C. thanks the MINECO of Spain for an FPI grant. The contribution of the European High Power Space Materials Laboratory - A laboratory funded by the European Regional Development Fund - A way of making Europe - is also acknowledged.

References

[1] Hogue, P., Rooney, M., Web, A., Huebert, D., Marinelli, B., Daugherty, A., Price, D. J. Proc. Int. SAMPE Symp. Exhibit., 2007, 52, 14-27.

[2] ESA-ESTEC, Requirements and Standards Division, ECSS-Q-ST-70-01C: Cleanliness and contamination control, Noordwijk 2008.

[3] ESA-ESTEC, Requirements and Standards Division, ECSS-Q-ST-70-02C: Thermal vacuum outgassing test for the screening of space materials, Noordwijk 2008.

[4] ESA-ESTEC, Requirements and Standards Division, ECSS-Q-TM-70-52A: Kinetic outgassing of materials for space, Noordwijk 2011.

[5] ESA-ESTEC, Requirements and Standards Division, ECSS-Q-ST-70-29C: Determination of offgassing products from materials and assembled articles to be used in a manned space vehicle crew compartment, Noordwijk 2008.

[6] Schläppi, B., Altwegg, K., Balsiger, H., Hässig, M., Jäckel, A., Wurz, P., Fiethe, B., Rubin, M., Fuselier, S. A., Berthelier, J. J., De Keyser, J., Rème, H., Mall, U.. J. Geophys. Res.: Space Phys., 2010, 115, A12, 14 pp.

[7] Robertson, S. J., 1976, Interim Rep. LMSC-HREC TR D496676.

[8] Riedo, A., Wahlström, P., Scheer, J. A., Wurz, P., Tulej, M., J. Appl. Phys. 2010, 108, 114915

[9] Chen, P., Hedgeland, R., Ramsey, L., Rivera, R., Houston, K., Proc. SPIE 6291, 2006, 629104; doi:10.1117/12.681175; http://dx.doi.org/10.1117/12.681175

[10] Flory, D. A., Oró, J., Fennessey, P. V. Origins of life 1974, 5, 443–455.

[11] Arenas, S., Monjas, F., Montesano, A., Montesano, C., Mangenot, C., Salghetti, L. Proc. 5th Eur. Conf. Antennas Propagation (EuCAP), 1018–1022. Rome 2011.

[12] Monjas, F., Montesano, A., Montesano, C., Llorente, J. J., Cuesta, L. E., Naranjo, M., Arenas, S., Madrazo, I., Martínez, L. Proc. 4th Eur. Conf. Antennas Propagation (EuCAP), 1–5. Barcelona 2010.

[13] ESA-ESTEC, Requirements and Standards Division, ECSS-Q-ST-70C, Rev.1, DIR1: Materials, mechanical parts and processes, Noordwijk 2013.

[14] Melai, J., Salm, C., Wolters, R., Schmitz, J. Microelectron. Eng. 2009, 86, 761–764.

[15] Keller, M., Gommel, U., Verl, A. Chem. Eng. Transac. 2012, 30, 301–306.

[16] Andersson, H., Andersson, T., Heino, J., Huovelin, J., Kurvinen, K., Lauhakangas, R., Nenonen, S., Numminen, A., Ojala, J., Orava, R., Schultz, J., Sipilä, H., Vilhu, O. IEEE Transac. Nucl. Sci. 2004, 51, 2110-2118.

[17] Hayeck, N., Gligorovski, S., Poulet, I., Wortham, H. Talanta 2014, 122, 63-69.

[18] Pal, R., Kim, K.-H., J. Sep. Sci. 2007, 30, 2708-2718.

[19] Stashenko, E. E., Martínez, J. R., J. Sep. Sci. 2008, 31, 2022-2031.

[20] Schröder, W., J. Sep. Sci. 2011, 34, 317-322.

[21] Jansen, J. A. J., Haas, W. E. Anal. Chim. Acta 1987, 196, 69–74.

[22] Wingate, C. A., in: Picasane, V. L., Moore, R. C. (eds), Fundamentals of Space Systems, Spacecraft Thermal Control, Oxford Univ. Press., Oxford 1994, pp. 433-468.

[23] Dever, J., Banks, B., de Groh, K., Miller, S., in: Myer, K. (ed), Handbook of Environmental Degradation of Materials, Degradation of spacecraft materials, William Andrew Publ., New York 2005, pp. 465-501.

[24] Wenig, Ph., Odermatt, J. BMC Bioinformatics 2010, 11, 405. https://www.openchrom.net. Accessed 7 Febr 2015.

Chapter 15. Determination of alcohols in essential oils by liquid chromatography with ultraviolet detection after chromogenic derivatization

Journal of Chromatography A, 1296 (2013) 157–163

Contents lists available at SciVerse ScienceDirect

Journal of Chromatography A

journal homepage: www.elsevier.com/locate/chroma

Determination of alcohols in essential oils by liquid chromatography with ultraviolet detection after chromogenic derivatization

Juan Ródenas-Montano, Enrique J. Carrasco-Correa, Miriam Beneito-Cambra, Guillermo Ramis-Ramos, José Manuel Herrero-Martínez*

Department of Analytical Chemistry, Faculty of Chemistry, University of Valencia, Dr. Moliner 50, 46100 Burjassot, Valencia, Spain

An HPLC-UV method to determine compounds having an hydroxyl functional group in plant essential oils is developed. The sample is diluted with 1,4-dioxane and the analytes are derivatized with phthalic anhydride. The derivatives (phthalates hemiesters) are separated on a C8 column using an ACN/water gradient. Separation conditions were optimized using the DryLab® method development software. For the alcohols and phenols present in mint and rose essential oils, optimization led to a *ca.* 40 min gradient time and a column temperature of 8 ºC. The alcohol and its derivatives were identified using HPLC-MS detection. A large sensitivity enhancement was obtained by derivatization protocol. The HPLC-UV method was compared to GC-FID and GC-MS. The limits of detection (LODs) obtained by the proposed method were better than those obtained by GC-FID and of the same order as those achieved by GC-MS. The three methods were satisfactorily applied to the determination of alcohols in essential oils. Therefore, the recommended method is of interest as an alternative to GC methods, to investigate the presence of compounds having an alcohol group at low concentrations in essential oils.

Keywords: essential oils; alcohols; chromogenic derivatization; DryLab; HPLC-UV

15.1. Introduction

Essential oils, which are obtained from plant parts by steam distillation, are used in a variety of applications, mainly in cosmetics, personal care products and in natural medicine [1]. Biosynthesized by a considerable number of aromatic plants, these oils are constituted by complex mixtures of a large variety of volatile substances, most of them showing a strong sensorial impact. These oils are predominantly constituted by monoterpene and sesquiterpene hydrocarbons, their oxygenated derivatives, a variety of aliphatic oxygenated compounds, and a few aromatic compounds [2]. Apart from its wide use in the flavor and cosmetic industries, several pharmacological (antimicrobial, antifungal, insecticidal, anthelmintic, antioxidant) properties have been reported [3-5]. Owing to the widespread industrial applications, its influence on human health and the defense of the consumer rights, methods for the quick and reliable characterization of essential oils are required.

Essential oils are usually analyzed by GC-FID, MS detection [6, 7] and recently GC-olfactometry [8]. However, difficulties in the GC-MS peak identification of these complex samples due to the fact that many terpenes have identical mass spectra occur with some frequency [9]. This is a consequence of the close similarities, both in the initial molecule or in the fragmentation patterns and rearrangements after ionization. Therefore, GC-MS identification of these compounds is frequently confirmed by using the retention indexes [10]. In addition, structural alterations of thermally labile compounds may occur during GC due to the high injector temperatures or contact with the catalytically active surfaces of columns or liners [11]. For these reasons, alternative methods to GC, which avoid the use of high temperatures, and which could be used for reference, are of interest.

Owing to the volatility and low UV absorptivity of most of their components, essential oils have been scarcely analyzed by HPLC [6, 12-20]. In fact, most HPLC reports dealing with essential oils have focused on the

detection of the non-volatile fraction of citrus oils [6, 14-16], sample cleaning or fractionation previous to GC [17]. However, HPLC has been used to detect specific terpenoids [18, 19]. Recently, Turek and Stintzing [20] have reported an HPLC-UV-MS^2 method to characterize fingerprint of essential oils. The essential oils were characterized by their respective UV peak patterns, which were mainly due to the absorbent components.

Alcohols and a variety of multifunctional compounds also containing hydroxyl functional groups constitute an important part of essential oils [2]. Thus, among the 100 compounds most frequently reported in essential oils, 25 of them are aliphatic alcohols and 4 of them are esters of aliphatic alcohol residues with more than 4 carbon atoms [21]. Among the 49 components studied by Turek and Stintzing [20] in seven essential oils, 13 were aliphatic alcohols (a *ca.* 27%), any of them showing an absorbance maximum over 200 nm, and 3 of them were phenols.

To enable or to enhance the absorptiometry, fluorimetric or mass spectrometric response of aliphatic alcohols in the UV, pre-column derivatization with either a symmetric cyclic anhydride [22-25], an acyl chloride [26], an isocyanate [27] or another reagent [28, 29], is frequently used. With pre-column derivatization, the determination of non-absorbing alcohols with low LODs in complex matrices is possible.

As far as we know, methods for essential oils based on the derivatization of alcohols and other active hydroxyl functional groups as phenols, followed by HPLC with UV or fluorometric detection of the derivatives have not been yet described. Nevertheless, this approach should provide sensitive methods, useful to characterize the alcoholic fraction of the essential oils, and an alternative to the predominant use of GC-MS methods. According to Babushok *et al.* [21], a *ca.* 25% of the most frequent components reported in essential oils are aliphatic alcohols. These compounds should give and enhanced response after derivatization of the alcohol group. In addition, phenols such as thymol,

carvacrol or eugenol are also derivatized. These compounds showed a remarkable molar absorptivity in the UV; however, their LODs could be also improved after derivation. In this work, the aliphatic alcohols present in mint and rose essential oils were determined by HPLC-UV after esterification with phthalic anhydride. Samples of *Mentha Arvensis* and *M. Piperita*, and two commercial samples of *Mentha* and *Rose* essential oils, were studied. The advantages and limitations the proposed method are discussed. Figures of merit, including limits of detections, are evaluated and compared to those obtained by GC-FID and GC-MS.

On the other hand, traditional strategies for the development of robust HPLC methods to separate the components of complex samples require considerable skill and patience of the chromatographer. This labor intensive and time-consuming process is shortened and greatly facilitated by using a computer-assisted HPLC method development software [30]. Further, the chances of finding a true absolute optimum, rather than a secondary relative optimum, largely increase. In this work, DryLab® was used to optimize the HPLC separation conditions for the alcohol and phenol derivatives found in mint and rose essential oils. For this purpose, a small well-defined number of experiments were performed to predict the effect of variations of the mobile phase composition, gradient time and column temperature on the peak position and shape [31-33].

15.2. Experimental

15.2.1. Reagents and samples

Urea, phthalic anhydride and menthol from Fluka (Buchs, Switzerland), ammonium hydroxide from Panreac (Barcelona, Spain), 1,4-dioxane, HPLC grade MeOH and ACN from Scharlab (Barcelona), and camphor, geraniol, β-citronellol, terpinene-4-ol, thymol, isopulegol, carveol, linalool and phenyl ethyl alcohol from Sigma-Aldrich (St. Louis, MO, USA) were used. Deionized

water (Barnstead deionizer; Sybron, Boston, MA) was also used. Commercial essential oils of mint and rose from Al Fayed (Aswan, Egypt), and *Mentha arvensis* and *M. piperita* oils supplied by Guinama (Valencia, Spain) were also used.

15.2.2. GC procedures

The GC-FID analysis was performed with a Focus system equipped with an AI 3000 autosampler from Thermo Fisher Scientific (Austin, TX, USA). A TRB-5 capillary column (30 m, 0.32 mm i.d., 0.50 µm film thickness) from Teknokroma (Barcelona) was used. The GC oven temperature program was operated as follows: 50 ºC (2 min), followed by rising to 250 ºC at 20 ºC min^{-1} with a final 250 ºC plateau (5 min). The FID was set at 280 ºC. The GC injection port was set at 250 ºC; an injection volume of 10 µL was used under split mode (5:1). Nitrogen was used as a carrier gas at a constant flow rate of 1 mL min^{-1}.

The GC-MS analysis was performed on a Focus DSQ II gas chromatograph provided with an AI 3000 autosampler and single quadrupole MS detector from Thermo Fisher Scientific. The analytical fused-capillary column was a TR-5MS (30 m, 0.25 mm i.d., 0.25 µm film thickness) from Thermo Fisher Scientific. The GC oven temperature program was as indicated above. The injector, transfer line and ion source temperatures were set at 280 °C. The injection volume was 4 µL under splitless mode. Ionization was done by electron impact at 70 eV. Ions within the *m/z* 50-400 range were monitored. Helium was used as the carrier gas at a flow rate of 1 mL min^{-1}. For GC-FID and GC-MS analysis, both standards and samples were diluted in hexane and injected. For quantitation studies, camphor was used as internal standard. Calibration curves of several alcohols up to 200 µg mL^{-1} were constructed.

15.2.3. Derivatization procedure

The derivatization procedure was adapted from literature [23]. The esterification reaction is depicted in Fig. 15.1. The derivatized alcohol compounds showed absorption maxima at 230 nm, giving high molar absorptivities comprised in the range 8770-11720 L mol^{-1} cm^{-1}. These values were consistent with those reported in the literature [34]. The esterification protocol was carried out as follows. Briefly, 0.2 g of essential oil or an aliquot of a solution of 5000 µg mL^{-1} of an alcohol standard was weighed. Then, 0.75 g of phthalic anhydride, 0.25 g of finely ground urea and 2 mL of 1,4-dioxane were added. The mixture was shaken in vortex and heated at 105 ºC in a silicone oil thermostatic bath for 90 min. After cooling, the final volume was completed to 12 mL with a 2:1 MeOH/water containing 0.1 M NH_3. The solutions were properly diluted in ACN/water and injected immediately into the HPLC or kept at -20 ºC until use. In all cases, satisfactory reaction yields (*ca*. 97-99%) were achieved.

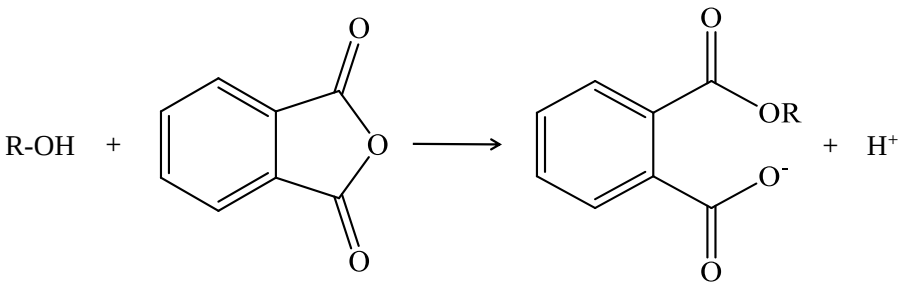

Fig. 15.1. Esterification of alcohols with phthalic anhydride.

15.2.4. HPLC separation of the alcohol derivatives

A 1100 series HPLC system equipped with a binary pump, a thermostatic column compartment, and a UV-Vis variable wavelength detector (Agilent Technologies, Waldbronn, Germany), was used. The separation was carried out with an Ascentis-Express C8 fused-core column (15 cm × 4.6 mm ID, 2.7 µm

particle size) from Supelco (Bellefonte, PA, USA). ACN/water mobile phases containing 0.1% acetic acid were used. Gradient elution was carried out from 30 to 80% ACN. In all cases, the flow rate was 1 mL min^{-1}, 20 µL was injected, and all injections were performed by triplicate. The detection wavelength was 230 nm. In order to optimize the separation conditions using DryLab® (Molnár Institute, Berlin, Germany), the following initial set of four chromatograms were obtained. For each sample, two linear gradients, with gradient times of 20 and 40 min, were used, and for each gradient time, two chromatograms at two column temperatures, 10 and 25 ºC, were obtained. The chromatograms were imported with the PeakMatch® software in AIA format (*.cdf) for "peak tracking", which refers to the matching of peaks of the same compound between runs where conditions have changed. After exporting, peaks areas were compared. Very small peak areas were not included in the studies that follow. The resulting retention times and peak areas of individual peaks were used as input data for method development with DryLab®

For HPLC-MS experiments, the liquid chromatograph was coupled (in series with the UV-Vis detector) to the ESI source of a high speed Triple TOF™ 5600 mass spectrometer (AB SCIEX, Concord, Canada). The Triple TOF working conditions were: ion spray voltage floating, 5500 and -4500 V for positive and negative-ion modes, respectively; curtain gas, 25 psi, interface heater temperature, 450 ºC; ion source gas 1 and 2, 50 psi. All data were acquired using the information-dependent acquisition (IDA) mode with Analyst TF 1.5 software (AB SCIEX). For IDA parameters, 0.25 s MS survey scan in the mass range of *m/z* 50-650 were followed by 30 MS^2 scans of 50 ms in the mass range of 50-650 (total cycle time, 1.75 s).

15.3. Results and discussion

15.3.1. Optimization of the HPLC separation of derivatized alcohols in mint and rose essential oils

A chromatogram of a derivatized sample of commercial (Al Fayed) essential mint oil is shown in Fig. 15.2A. This chromatogram, showing a complex peak pattern, was obtained after optimization of the separation conditions using DryLab®. Only the peaks with a significant signal-to-noise ratio were included in the optimization of the separation conditions. The chromatograms obtained before optimization (not given) showed a few well-resolved peaks and some groups of partially resolved peaks. Care was taken of recognizing all the peaks of these groups to be individually included in DryLab® for separation optimization. Additionally, the peaks of the reagent blank, which were located at the head of the chromatogram, were excluded. The selection process resulted in a set of 12 peaks. Then, DryLab® was used to optimize both the gradient time and the column temperature. To design the initial set of experiments, the following was taken into account: a) the initial and final ACN concentrations, 30% and 80%, respectively, were selected according to the literature related to the HPLC separation of phthalates of alcohols with $8 < n < 18$ carbon atoms [23, 25]; b) for convenience, the minimal and maximal gradient time was set at 20 and 40 min, respectively; c) the column temperature was allowed to vary from 5 to 25 ºC. From the initial set of four chromatograms, DryLab® predicted the peak locations in all intermediate working conditions, also calculating the resolution between the successive peak pairs. From these, a resolution map with red areas corresponding to the highest resolution of the most critical peak pair (R_C), was provided. The resolution map for the derivatized sample of Al Fayed mint essential oil is shown in Fig. 15.3. The best resolution was predicted for a 39 min gradient time at a column temperature of 8ºC. As shown in Fig. 15.2, the chromatogram obtained in these conditions (Fig. 15.2A) satisfactorily matched with the predicted

chromatogram (Fig. 15.2B). The experiments which follow were performed in these conditions.

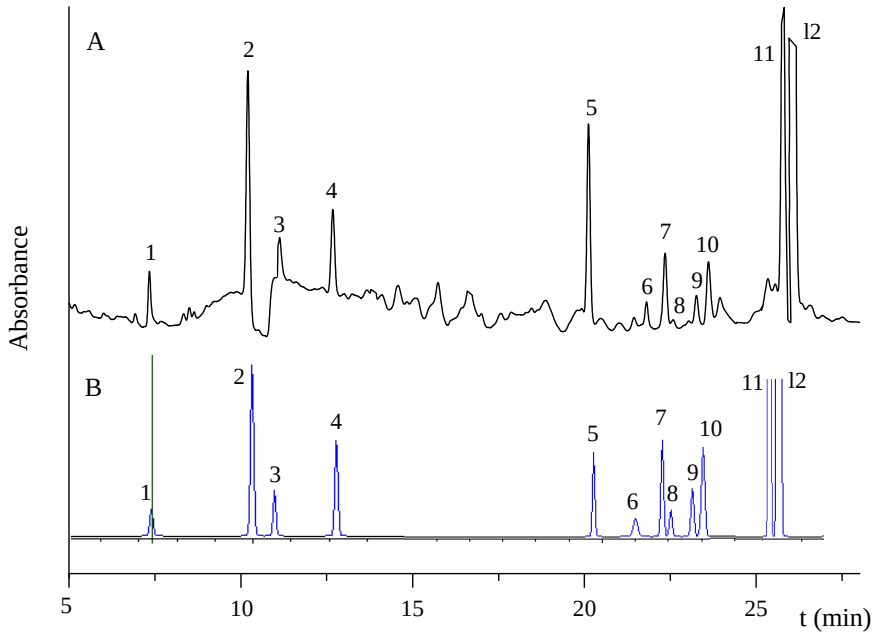

Fig. 15.2. Experimental (A) and predicted (B) chromatograms of the derivatized commercial (Al Fayed) mint essential oil obtained in the optimized separation conditions (from 30% to 80% ACN in 39 min at 8 ºC). The 12 peaks marked with numbers were those included in the optimization of the sepration by DryLab®.

The peak retention times and resolutions for the predicted and experimental chromatograms, obtained in the optimized conditions, are given and compared in Table 15.1. The average relative errors in the retention times and resolutions were 1.2% and 19.1%, respectively. Similar levels of accuracy for DryLab®, in terms of the predicted retention times, have been recently reported [35, 36]. The prediction errors were much larger for resolutions than for retention times, but this agrees with other reported values [36]. It should be noted that the errors of predicted resolutions depend on both the retention time errors and the uncertainties of peak width and symmetry [36].

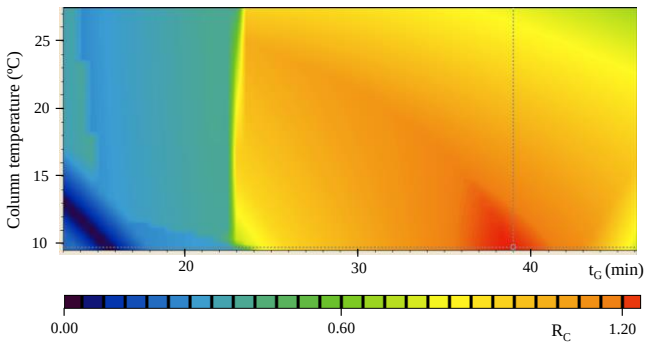

Fig. 15.3. Two-dimensional resolution map of gradient time *versus* column temperature for the derivatized Al Fayed mint essential oil. Blue and red areas correspond to low and high resolutions of the most critical peak pair, respectively.

Samples of *Mentha Arvensis* and *M. Piperita,* and the Al Fayed sample of rose essential oil, were also derivatized as indicated, and aliquots were injected. For each essential oil, the initial set of four chromatograms was obtained, and optimization of the separation conditions with Drylab® was performed. For a given set of HPLC conditions, the chromatograms of the derivatized *M. Arvensis* and *M. Piperita* oils were closely similar to those obtained with the Al Fayed mint essential oil. Therefore, the resolution maps for the three mint oils predicted the same set of optimal conditions, i.e. a 39 min gradient time and 8 ºC. Concerning to the rose essential oil, a total of eight peaks was selected for optimization. The best resolution of the most critical peak pair was predicted for a 37 min gradient time at 6 ºC (resolution map not shown); however, for simplicity, we decided to use the optimal conditions obtained for the mint essential oils (39 min gradient time and 8 ºC) also for the rose essential oil, since the resolution of the most critical peak pair (R_C = 1.34) was only slightly lower than that obtained in the optimal conditions (R_C = 1.51). Predicted and experimental chromatograms of a sample of derivatized rose essential oil, obtained in these conditions, are given in Figs. 15.4A and 15.4B, respectively. For the rose essential oil, in these conditions, retention times and resolutions were predicted with average errors of 1.3% and 29.1%, respectively.

Table 15.1

Predicted and experimental retention times and resolution data for the optimized separation of derivatized compounds present in a commercial mint essential oil.

Peak	Retention time				Resolution			
	Experimental	Predicted	Diff.[a]	% Error[b]	Experimental	Predicted	Diff.[a]	% Error[b]
1	7.26	7.38	-0.12	1.6	8.76	10.90	-2.13	19.5
2	10.13	10.30	-0.17	1.6	3.51	2.75	-0.76	27.7
3	11.07	10.95	0.12	1.1	5.21	8.57	-3.36	39.2
4	12.56	12.74	-0.18	1.4	26.04	28.50	-2.46	8.6
5	20.00	19.52	0.48	2.4	7.00	6.00	1.00	16.7
6	21.67	21.31	0.36	1.7	1.80	2.73	-0.93	34.0
7	22.20	22.20	0.00	0.0	0.90	0.75	0.14	18.5
8	22.44	22.38	0.06	0.3	3.14	2.86	0.29	10.0
9	23.10	22.98	0.12	0.5	1.33	1.00	0.33	33.3
10	23.45	23.27	0.18	0.8	6.55	6.40	0.15	2.3
11	25.60	25.18	0.42	1.7	1.20	1.20	0.00	0.0
12	25.95	26.54	0.42	1.6				
Average standard error				1.2				19.1

[a] Difference = Experimental - Predicted

[b] % Error: [(Experimental-Predicted)/Predicted] × 100

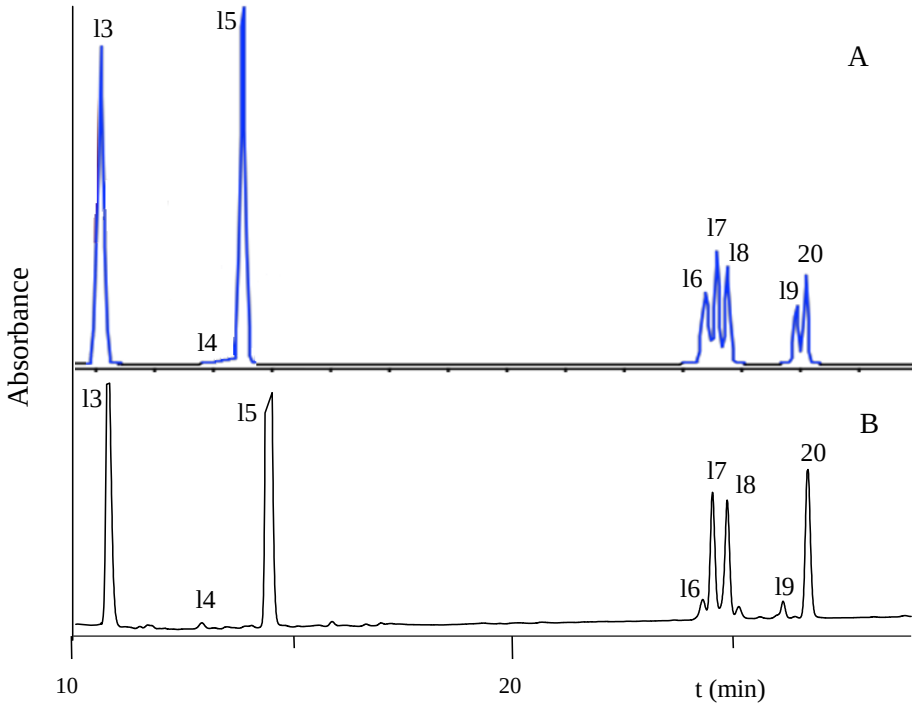

Fig. 15.4. Experimental (A) and predicted (B) chromatograms of the derivatized Al Fayed rose essential oil obtained in the optimized conditions of Fig. 15.2. The 8 peaks marked with numbers were those included in the optimization of the separation by DryLab®.

15.3.2. Identification of underivatized and derivatized alcohols in essential oils using HPLC-MS

In order to identify the chromatographic peaks (Figs. 15.2 and 15.4), MS detection was also coupled in series with the UV-Vis detection. Chromatograms of both alcohol standards and the Al Fayed mint and rose essential oils, without and with previous derivatization with phthalic anhydride, were obtained. All chromatograms were obtained in the optimal conditions for the derivatized mint essential oil. The TICs and several EICs of the same mint essential oil, without and with previous derivatization with phthalic anhydride,

are shown in Figs. 15.5A and 15.5B, respectively. A reagent blank, prepared by using the derivatization procedure in the absence of a sample, was also chromatographed. This chromatogram showed that the reagent peaks were eluted at the head of chromatogram, thus causing no interference (not shown). For the underivatized essential oils, satisfactory signals from positive quasimolecular ions $[M+H]^+$ [20, 37, 38] were obtained at the retention times of several sample components. As shown in Table 15.2, the *m/z* values agreed with the expected values for several compounds, which are common components of the mint and rose essential oils, and which also have an alcohol functional group. MS^2 data was also used to confirm peak identifications. In particular, the *m/z* differences between several MS^2 intense peaks corresponding to loss of water, and several easily recognizable fragments, were useful [37, 38]. For the mint essential oils, five from twelve peaks; which were selected for HPLC optimization (see Fig. 15.3), were identified. The identification was confirmed by injecting the alcohol standards. These gave the same MS and MS^2 spectra at the same retention times as the target compounds. Evidence of the presence of these alcohols in the mint essential oils was subsequently confirmed by GC-MS (Section 15.3.3).

For the derivatized essential oils, the ESI was operated in the ion-negative mode. As also shown in Table 15.2, the intense signals of the $[M-H]^-$ ions of the phthalate esters of the same alcohols observed with the underivatized oils were obtained. The MS^2 fragments of the hemiesters were also used to support peak identification [39, 40]. The predominant fragment ions were deprotonated phthalic acid (*m/z* 165), and the alcohol residues (as $[M-H]^-$), obtained by cleavage of the ester bond, as well as fragments of the alcohol residue (Table 15.2) [39, 40]. Using the information provided by MS detection, the peaks on the chromatograms obtained with UV detection were identified.

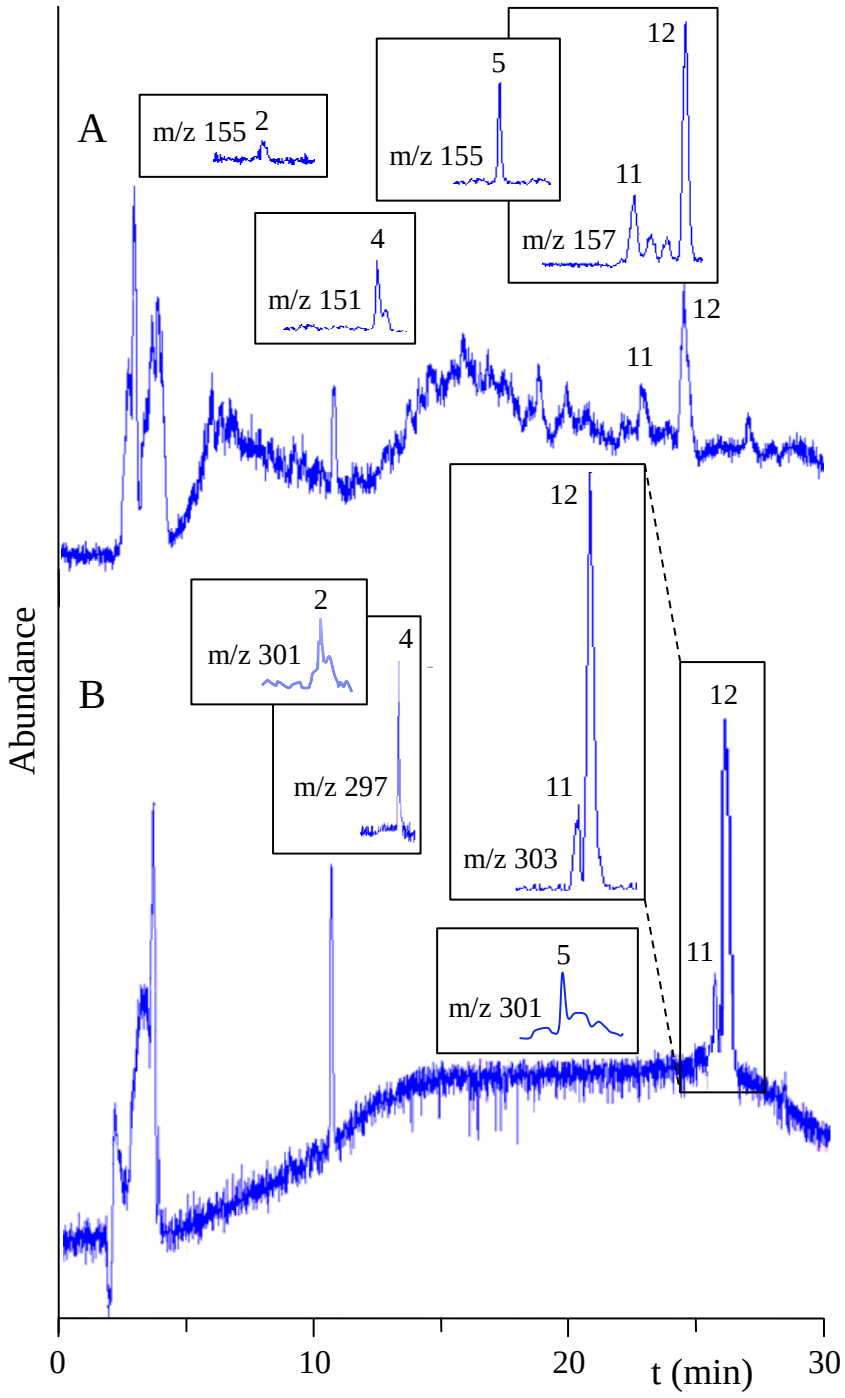

Fig. 15.5. TIC and EICs of a sample of underivatized (A) and derivatized (B) Al Fayed essential oil. Peak labeling and *m/z* for EICs are indicated in Table 15.2.

Table 15.2

Chemical formula, parent ion and fragments of underivatized and derivatized alcohols found in the mint and rose essential oils.

Peak label	Compound	Formula	ESI (+)-MS (m/z)[a]	MS^2 (+) (m/z)	Derivative formula	ESI (-)-MS (m/z)[b]	MS^2 (-) (m/z)
Mint oils							
2	Terpinene-4-ol	$C_{10}H_{18}O$	155	137, 107	$C_{10}H_{18}O$-$C_8H_4O_3$	301	257, 165, 153, 135
4	Thymol	$C_{10}H_{14}O$	151	135, 121	$C_{10}H_{14}O$-$C_8H_4O_3$	297	253, 165, 149, 133
5	Isopulegol	$C_{10}H_{18}O$	155	137, 83	$C_{10}H_{18}O$-$C_8H_4O_3$	301	257, 165, 154, 135
11	β-Citronellol	$C_{10}H_{20}O$	157	137, 83	$C_{10}H_{20}O$-$C_8H_4O_3$	303	259, 165, 155, 135
12	Menthol	$C_{10}H_{20}O$	157	137, 83	$C_{10}H_{20}O$-$C_8H_4O_3$	303	259, 165, 155, 135
Rose oil							
13	Terpinene-4-ol	$C_{10}H_{18}O$	155	137, 107	$C_{10}H_{18}O$-$C_8H_4O_3$	301	257, 165, 153, 135
14	Carveol	$C_{10}H_{16}O$	153	135, 107	$C_{10}H_{16}O$-$C_8H_4O_3$	299	255, 165, 151, 133
15	Phenylethyl alcohol	$C_8H_{10}O$	123	105, 95	$C_8H_{10}O$-$C_8H_4O_3$	269	225, 165, 121, 93
17	Linalool	$C_{10}H_{18}O$	155	137, 95	$C_{10}H_{18}O$-$C_8H_4O_3$	301	257, 165, 153, 135
18	Geraniol	$C_{10}H_{18}O$	155	137, 95	$C_{10}H_{18}O$-$C_8H_4O_3$	301	257, 165, 153, 135
20	β-Citronellol	$C_{10}H_{20}O$	157	137, 83	$C_{10}H_{20}O$-$C_8H_4O_3$	303	259, 165, 155, 135

In Fig. 15.6A, a UV chromatogram of an underivatized sample of mint essential oil is shown. The peak of the only component which absorbs at 230 nm, thymol, was observed on this chromatogram. The arrows on chromatogram indicate the retention times of the compounds of Table 2, which were identified by HPLC-MS/MS^2. In Fig. 15.6B, the UV chromatogram of the derivatized sample of the same mint essential oil is given. The predominant peak of menthol (peak no. 12), and the peaks of the other four compounds (given in Table 15.2) were identified. By comparing the chromatograms of Figs. 15.6A and 15.6B, it is deduced that the alcohol derivatives appeared in the same elution order than the corresponding underivatized alcohols, but with larger retention times, which could be explained by the presence of the phthalate moiety. The HPLC-UV-MS chromatograms of underivatized and derivatized rose essential oil were also obtained. Based on the MS data given in Table 15.2 (columns 4 and 7), up to six peaks corresponding to several alcohols (out of the eight peaks initially recognized for separation optimization) were identified.

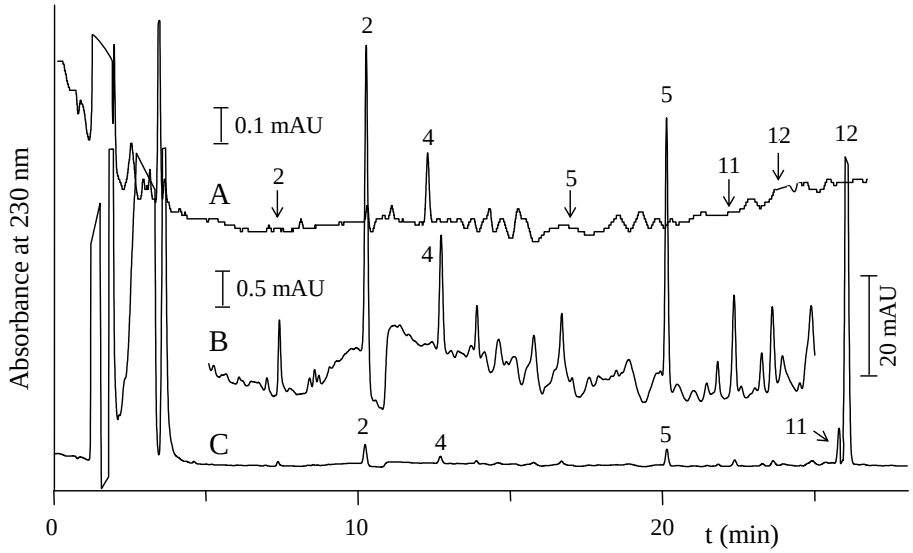

Fig. 15.6. HPLC-UV chromatograms of the underivatized (A) and derivatized (B and C) Al Fayed EO The trace B is an expanded view of trace C. The arrows shown in trace A indicate the retention time of the underivatized alchol compontents, as deduced from the TIC and EICs. Other details are indicated in Fig. 15.5.

15.3.3. Quantitation studies

The proposed HPLC-UV method was evaluated in terms of precision, linearity and sensitivity (limit of detection). Retention time and peak repeatabilities, and LODs at a signal-to-noise ratio of S/N = 3 were obtained (Table 15.3). Intra- and inter-day repeatabilities were obtained by injecting a standard mixture containing 1 μg mL^{-1} of each analyte three times per day over 3 days. External calibration curves were linear over the range 200 μg mL^{-1}, with correlation coefficients better than r = 0.998. Standard addition calibration curves were also obtained by adding to the essential oils three solutions with increasing alcohol concentrations up to 100 μg mL^{-1}. The curves were linear with r > 0.999, and in all cases the sensitivity was the same as with the external calibration method.

Table 15.3

Significant analytical parameters of the proposed HPLC-UV method and a comparison with the LODs obtained by GC methods.

Analyte	t_R (%)[a]	Area (%)[a]	LOD HPLC-UV (μg mL^{-1})	LOD GC-FID (μg mL^{-1})	LOD GC-MS (μg mL^{-1})
Terpinene-4-ol	0.11; 0.37	1.37; 2.91	0.08	1.1	0.07
Thymol	0.09; 0.33	2.12; 3.37	0.08	0.9	0.05
Isopulegol	0.05; 0.31	1.53; 3.14	0.021	1.1	0.06
β-Citronellol	0.03; 0.37	1.83; 2.92	0.08	1.2	0.06
Menthol	0.13; 0.34	1.50; 3.05	0.17	1.1	0.08
Carveol	0.17; 0.33	1.39; 3.22	0.19	1.0	0.10
Phenyl ethyl alcohol	0.08; 0.42	1.13; 2.97	0.20	1.1	0.09
Linalool	0.12; 0.31	1.46; 3.01	0.15	1.0	0.13
Geraniol	0.02; 0.34	1.87; 3.21	0.18	1.0	0.020

[a] As intra- and inter-day relative standard deviations.

Table 15.4

Alcohol concentrations (% w/w) found by HPLC-UV of the alcohol phthalates, GC-FID and GC-MS in the mint essential oils.

Analyte (%)	Al Fayed mint			*M. Arvensis*			*M. Piperita*		
	HPLC-UV	GC-FID	GC-MS	HPLC-UV	GC-FID	GC-MS	HPLC-UV	GC-FID	GC-MS
Terpinene-4-ol	0.20 ± 0.02	0.22 ± 0.01	0.26 ± 0.01	0.44 ± 0.07	0.47 ± 0.05	0.42 ± 0.03	0.21 ± 0.03	0.19 ± 0.02	0.22 ± 0.01
Thymol	0.08 ± 0.01	0.09 ± 0.02	0.11 ± 0.01	2.11 ± 0.31	2.07 ± 0.22	2.08 ± 0.17	0.17 ± 0.01	0.19 ± 0.01	0.19 ± 0.01
Isopulegol	0.06 ± 0.02	0.05 ± 0.01	0.07 ± 0.01	0.14 ± 0.06	0.13 ± 0.05	0.16 ± 0.02	-	-	-
β-Citronellol	0.33 ± 0.08	0.28 ± 0.05	0.29 ± 0.01	0.05 ± 0.01	0.06 ± 0.01	0.05 ± 0.01	0.31 ± 0.07	0.32 ± 0.04	0.29 ± 0.02
Menthol	17.81 ± 1.10	16.79 ± 0.87	17.55 ± 0.54	25.72 ± 0.85	24.97 ± 0.92	26.51 ± 0.73	15.87 ± 0.92	16.13 ± 0.67	15.72 ± 0.48

GC with FID and MS detection was also applied for qualitative and quantitative analyses of alcohols in the underivatized essential oils. The presence of alcohol peaks was confirmed by retention index and MS data, and by injecting alcohol standards. The calibration curves were linear over the range 1-200 µg mL^{-1} for GC-FID and GC-MS, with correlation coefficients better than $r = 0.999$. The LODs (S/N = 3) are shown in the last two columns of Table 15.3.

Next, alcohol components of the mint and rose essential oils were quantified by using the proposed HPLC-UV method, and the results were compared with those obtained with GC-FID and GC-MS (Tables 15.4 and 15.5). The HPLC-UV and GC procedures yielded similar values for all the analytes, with no significant differences at the 95% confidence level. As shown in Table 15.4, menthol was the major constituent of all the mint essential oils, which was in agreement with literature [41], whereas phenyl ethyl alcohol (Table 15.5) was the main alcohol present in rose essential oil [42, 43].

Table 15.5

Alcohol concentrations (%, w/w) found by HPLC-UV of the alcohol phthalates, GC-FID and GC-MS in the Al Fayed rose essential oil.

Analyte (%)	HPLC-UV	GC-FID	GC-MS
Terpinene-4-ol	0.75 ± 0.11	0.77 ± 0.08	0.77 ± 0.04
β-Citronellol	1.07 ± 0.23	1.11 ± 0.12	1.04 ± 0.06
Carveol	0.03 ± 0.02	0.04 ± 0.01	0.04 ± 0.01
Phenyl ethyl alcohol	4.53 ± 0.62	4.61 ± 0.54	4.57 ± 0.33
Linalool	0.59 ± 0.07	0.61 ± 0.10	0.61 ± 0.05
Geraniol	0.68 ± 0.17	0.65 ± 0.11	0.68 ± 0.05

The HPLC-UV method was compared to the GC procedures in terms of chromatographic performance. Sample preparation for GC is

straightforward, whereas derivatization is required for HPLC. There is also abundant literature describing the GC separation of essential oil components, whereas HPLC-UV literature related to the subject is scarce. Further, method development is more complex in HPLC than in GC; however, the use of modeling software like DryLab® reduced significantly the effort and time required for separation optimization. Regarding sensitivity, HPLC-UV of the alcohol phthalates has yielded LODs closely similar to those achieved by GC-MS, and better than those obtained by GC-FID (Table 15.3). In addition, alcohol derivatization followed by HPLC-UV is more selective than GC for the target analytes. Concerning analysis time, the drawback of derivatization is the time required to prepare the derivatives; however, in routine analysis much time can be saved by simultaneously derivatizing many samples. Also, methods for quick sample derivatization using off-line and on line [44, 45] microwave irradiation, have been described. Concerning the separation time, HPLC and GC are similar. Finally, a drawback of GC is the need for volatility of the analytes, which limits the range of compounds that can be analyzed. In addition, structural alterations of thermally labile compounds may occur during GC analysis. The proposed HPLC-UV method constitutes an alternative which can be useful to confirm or to extend GC studies. It is also complementary to the direct analysis of underivatized essential oils by HPLC-UV, since the alcohol components have low molar absorptivities [20]. Derivatization of alcohols is also useful in HPLC-ESI-MS, since aliphatic alcohols usually give low sensitivities [23]. Finally, phthalic anhydride has been used in this work, but substantial improvements of the LODs can be achieved using diphenic anhydride [23] or other reagents providing higher absorptivities or enabling fluorimetric detection.

15.4. Conclusions

An HPLC-UV method for the determination of alcoholic fraction of essential oils, based on their pre-column derivatization with an aromatic anhydride, has been developed. Quick and safe optimization of the chromatographic separation conditions for the alcohol fraction of mint and rose essential oils was achieved with the DryLab® method development software. The compounds found were identified using HPLC-MS of both derivatized and underivatized samples, and also by comparison to the GC-FID and GC-MS traces of the underivatized samples. The derivatized analytes provided a dramatic increase in UV absorption. Thus, the LODs obtained with the proposed method were similar to those obtained by GC-MS, and clearly better than those achieved by GC-FID. Then, the proposed method constitutes a good alternative to characterize and quantify components having an alcohol group in essential oils.

Acknowledgements

Project CTQ2010-15335 (MINECO of Spain and FEDER); E.J.C.-C. thanks the MINECO for an FPI grant for PhD studies. Many thanks are also due to K. Monks and I. Molnár (Molnár Institute for Applied Chromatography, Berlin, Germany) for their help in DryLab® software.

References

[1] M. Lis-Balchin, J. Royal Soc. Health, 117 (1997) 324.

[2] R.P.W. Scott, in: P. Worsfold, A. Townshend, C. Poole (Eds.), Encyclopedia of Analytical Science, Elsevier, Amsterdam, 2005.

[3] S. Burt, Int. J. Food Microbiol., 94 (2004) 223.

[4] F. Bakkali, S. Averbeck, D. Averbeck, M. Idaomar, Food Chem. Toxicol., 46 (2008) 446.

[5] H.M.A. Cavanagh, Nat. Prod. Commun., 2 (2007) 1297.

[6] G.B. Lockwood, J. Chromatogr. A., 936 (2001) 23.

[7] C.M. Franz, Flavour Fragr. J., 25 (2010) 112.

[8] M.C. Díaz-Maroto, N. Castillo, L. Castro-Vázques, M.A. González-Viñas, M.S. Pérez-Coello, Flavour Fragr. J., 22 (2007) 114.

[9] W.A. König, N. Bulow, Y. Saritas, Flavour Frag. J. 14 (1999) 367.

[10] R. Adams, Identification of essential oil components by gas chromatography/quadrupole mass spectrometry, Allured, Carol Stream, IL, USA, 2001.

[11] J.V. Hinshaw, LC-GC North Am., 20 (2002) 120.

[12] M.S.F. Ross, J. Chromatogr., 118 (1976) 273.

[13] J. Píry, A. Príbela, J. Chromatogr. A, 665 (1994) 105.

[14] P. Dugo, L. Mondello, L. Dugo, R. Stancanelli, G. Dugo, L. Pharm. Biomed. Anal., 24 (2000) 147.

[15] E. Frerot, E. Decorzant, J. Agric. Food Chem., 52 (2004) 6879.

[16] G. Dugo, P.Q. Tranchida, A. Cotroneo, P. Dugo, I. Bonaccorsi, P. Marriott, R. Shellie, L. Mondello, Flavour Fragr. J., 20 (2005) 249.

[17] L. Mondello, P. Dugo, G. Dugo, A.C. Lewis, K.D. Bartle, J. Chromatogr. A., 842 (1999) 373.

[18] V. Solinas, C. Gessa, J. Chromatogr., 219 (1981) 332.

[19] C. Villa, R. Gambaro, E. Mariani, S. Dorato, J. Pharm. Biomed. Anal., 44 (2007) 755.

[20] C. Turek, F.C. Stintzing, Anal. Bioanal. Chem., 400 (2011) 3109.

[21] V.I. Babushok, P.J. Linstrom, J.J. Reed, I.G. Zenkevich, R.L. Brown, W.G. Mallard, S.E. Stein, J. Chromatogr. A, 1157 (2007) 414.

[22] R.A. Wallingford, Anal. Chem., 68 (1996) 2541.

[23] A. Micó-Tormos, C. Collado-Soriano, J.R. Torres-Lapasió, E. Simó-Alfonso, G. Ramis-Ramos, J. Chromatogr. A, 1180 (2008) 32.

[24] A. Micó-Tormos, E. Simó-Alfonso, G. Ramis-Ramos, J. Chromatogr. A, 1203 (2008) 47.

[25] M.J. Lerma-García, G. Ramis-Ramos, J.M. Herrero-Martínez, J.V. Gimeno-Adelantado, E.F. Simó-Alfonso, J. Chromatogr. A, 1216 (2009) 230.

[26] J. Morvan, M. Saluden, V. Agasse, F. Barbot, P. Cardinael, J. Bouillon, G. Decock, Anal. Bioanal. Chem., 384 (2006) 1409.

[27] G. Chávez, B. Bravo, N. Piña, M. Arias, E. Vivas, F. Ysambertt, N. Márquez, A. Cáceres, Talanta, 64 (2004) 1323.

[28] C.R. Pratesi, L. Faccetti, N. Andriollo, G. Cassani, Riv. Ital. Sostanze Gr., 83 (2006) 18.

[29] M. Beneito-Cambra, V. Bernabé-Zafón, E.F. Simó-Alfonso, G. Ramis-Ramos, Rapid Commun. Mass Spectrom., 24 (2010) 2093.

[30] J.C. Berridge, Techniques for the Automated Optimization of HPLC Separation, Wiley, New York, 1985.

[31] L.R. Snyder, J.W. Dolan, D.C. Lommen, J. Chromatogr., 485 (1989) 65.

[32] J.A. Lewis, D.C. Lommen, W.D. Raddatz, J.W. Dolan, L.R. Snyder, I.J. Molnar, Chromatography, 592 (1992) 183.

[33] R.G. Wolcott, J.W. Dolan, L.R. Snyder, J. Chromatogr. A, 869 (2000) 3.

[34] E. Ayranci, E. Bayram, J. Haz. Mat. B,122 (2005) 147.

[35] R.M. Krisko, K. McLaughlin, M.J. Koenigbauer, C.E. Lunte, J. Chromatogr. A, 1122 (2006) 186.

[36] S. Fekete, J. Fekete, I. Molnar, K. Ganzler, J. Chromatogr. A, 1216 (2009) 7816.

[37] M. Glasius, M. Duane, B.R. Larsen, J. Chromatogr. A, 833(1999) 121.

[38] M. Holcapek, R. Jirásko, M. Lísa, J. Chromatogr. A, 1217 (2010) 3908.

[39] Z. Li, L. Xu, C. Peng, H. Kuang, C. Xu, L. Wang, F. Xue, T. Ding, C. Sheng, Y. Gong, J. Chromatogr. Sci., 49 (2011) 337.

[40] Z. Li, W. Xiong, H. Lin, L. Zhuo, S. Lv, X. Tang, M. Chen, Z. Zou, Z. Lin, B. Qiu, G. Chen, J. Sep. Sci., 36 (2013) 477.

[41] J.-M. D. Dimandja, S.B. Stanfill, J. Grainger, D.G. Patterson, Jr., J. High Resol. Chromatogr., 23 (2000) 208.

[42] M.Z. Özel, A.A. Clifford, Flavour Frag. J., 19 (2004) 354.

[43] K.G.D. Babu, B. Singh, V.P. Joshi, V. Singh, Flavour Frag. J., *17 (*2002) 136.

[44] G. Chávez, B. Bravo, N. Piña, M. Arias, E. Vivas, F. Ysambertt, N. Márquez, A. Cáceres, Talanta, 64 (2004) 1323.

[45] M. Arias, R. Bauza, J. Rodríguez, G. Castañeda, A. Ríos, Electrophoresis, 29 (2008) 3060.

SECTION IV. Summary of results, discussion and conclusions

This PhD Thesis reports mainly on the design, construction and characterization of novel monolithic materials and the investigation of their potential applications in separation science. The monoliths developed in this work constitute a contribution in the areas of CEC and reversed-phase, chiral and IAM chromatography liquid modes. Significant enhancements of surface area, retention, tunable selectivity, and other features, as those contributed in this work, should eventually place polymeric monolith technology in a competitive position in comparison to other chromatographic materials (silica monoliths and packed columns). Another challenge covered by this PhD Thesis was to develop methods for the characterization of certain raw materials (polyvinyl alcohol and Rohacell®) and for alcohols in essential oils.

In this section of the PhD Thesis, and as required by the aforementioned regulation of the University of Valencia a summary of the results and the most relevant conclusions is presented.

A) Development and application of novel monolithic materials

A.1. Synchronized gradient elution in capillary liquid chromatography

A method to optimize and keep control on gradient elution in capillary liquid chromatography (cHPLC) was studied. Focus was placed on the cHPLC systems which rely on the splitting of a primary flow, F_1, to provide the much smaller secondary flow, F_2, required at the injection device and analytical column. Owing to the tiny secondary flow rates, system synchronization is necessary both to achieve proper optimization of gradient elution methods, and to avoid the analytes to be totally or partially eluted in the initial isocratic conditions.

A relevant feature of the systems that rely on the splitting of a primary flow is the dependence of F_1 from the backpressure, P. When the backpressure increases, F_1 is automatically increased by the instrument control software, thus

to make possible for the EMPV to maintain the secondary flow rate, F_2, at a fixed selected value. The primary flow rate can only be programmed by ranges, and these are established by the instrument manufacturer. Within each range, F_1 increased linearly as P increases, until reaching the maximum value allowed for the flow rate range. Thus, operation over the maximum primary flow rate of the range does not guarantee the maintenance of the secondary flow rate at the specified value, controlling F_2 should be devised.

Measurement of the delay time, t_{de}, in the absence and presence of the column, showed that a correction of the delay time is necessary, and that a match time should be calculated to synchronize the system. Synchronization of the arrival of the end of the sample plug and the gradient front to the column inlet should be procured before the column, namely, immediately after the arrival of the sample and mobile phase flows to port 2 of the injection valve. This can only be achieved by switching back the injection valve to bypass immediately after the arrival of the end of the sample plug to port 2. At the same time, the gradient should have been started a time before or after the injection, just to allow the gradient front to arrive to port 1 simultaneously with the arrival of the end of the sample plug to port 2. A case to be considered is the optional inclusion in the method of an initial isocratic period. This should be also programmed under system synchronization, by delaying the arrival of the gradient front to port 1 of the valve within the required initial isocratic period.

The time required by the mobile phase to move from the mixing point T to port 1 should be supplemented by a match time, t_M, to be subtracted or added to the gradient starting time. Accordingly, the gradient will start either before or after the injection, respectively. A procedure to establish t_M was then devised and demonstrated.

Synchronization of the arrival of both the sample and the gradient front to the column can be achieved if the valve is switched to bypass at t_V, that is, immediately after the arrival of the end of the sample plug to the valve. Two

simple experiments addressed to measure both t_V and t_M have been described. The benefits obtained by switching the valve to bypass immediately after the injection, and by proper use of t_V and t_M to synchronize the system, were demonstrated.

The highlights of this work can be summarized as follows:

- *The relevance of synchronizing gradient elution in capillary HPLC was highlighted.*
- *The switching of the injection valve to bypass at a given time after the injection, and the gradient start at a match time before or after injection, were shown to be necessary for full system synchronization.*
- *Experiments to measure these two key parameters to achieve synchronization were described.*
- *The benefits of synchronization on efficiency and time saving were demonstrated.*

A.2. *Sensitive determination of parabens in human urine and serum using methacrylate monoliths and reversed phase capillary liquid chromatography mass spectrometry*

A method for the determination of parabens in human urine and serum by cLC in RP mode with UV-Vis and MS detection using BMA-based monolithic columns has been developed. The influence of the composition of the polymerization mixture was studied. Baseline resolution of the analytes was achieved through a mobile phase of acetonitrile/water using gradient elution. Additionally, DLLME was combined with both cLC-UV and cLC-MS to achieve a highly sensitive determination of parabens in human urine and serum samples.

First, a series of BMA-based monolithic stationary phases were systematically prepared by variation of several parameters (percentages of 1,4-BuOH and 1-PrOH in the porogenic solvent, monomers/porogens and BMA/EDMA ratios) in the polymerization mixture. Next, the elution of parabens using the selected column (A6) with different flow rates and elution gradients was studied. The influence of flow rate on the chromatographic performance was examined. The performance of the selected column for parabens was also compared to that of previously reported for packed columns and other monolithic columns. The efficiencies obtained in this work (P_C = 20-24) can be favorably compared to those reported for conventional microparticulate columns packed with 5-µm silica particles (P_C = 21 for 12.5-min gradient and 23 for 10 min-gradient time). An advantage of the proposed method over other reported HPLC methods is the reduced solvent consumption. Additionally, the cost of a polymeric monolithic column is less than that of conventional C18 column, and the need of specialized ultra-high pressure systems for sub-2 µm particles is not required.

Next, the monolithic capillary column was connected to a cLC system coupled to an ESI-MS nanospray in order to use a more sensitive and specific detector to analyze biological samples. The MS and MS/MS behavior of parabens under negative ion ESI was investigated using direct infusion of standard solutions into the mass spectrometer. Thus, the MS response of parabens increased after replacing acetic acid by ammonium acetate in the mobile phase; however, at contents higher than 0.04% NH_4AcO, a weak inhibition of the MS response was observed.

The repeatibility of preparation monolithic columns, column-to-column (three columns made from the same polymerization mixture) and batch-to-batch (three batches of three columns each) was established. Acceptable values were achieved for both retention times and peak areas, with RSD values ranging from 4.7 to 5.6% for column-to-column, and from 6.2 to 7.8% for batch-to-

batch. More than 100 injections of the standard mixture and 200 injections of real samples were performed without the need of replacing the column; therefore, the stability of the column was satisfactory.

The optimized method was applied to the analysis of target analytes in urine and serum samples collected from different volunteers. Peak identification in UV detection was performed by comparing the retention times and absorption spectra with those of the standards, and when necessary, by spiking the sample extracts with the standards. The data obtained using both detection modes were compared, and no significant differences were found after application of the statistical test for paired data at 95% confidence level. However, the paraben levels could not be measured by cLC-UV in certain biological samples. Consequently, cLC-MS should be preferred due to the possibility of reaching much lower LODs.

The highlights of this work can be summarized as follows:

- *Polymeric monoliths were applied to the analysis of parabens in biological samples.*
- *DLLME sample preconcentration, followed by cLC-MS using monolithic columns at the chromatographic separation step, were successfully combined.*
- *A method for the rapid and very sensitive determination of parabens in urine and serum was described.*

A.3. Evaluation of 2,3-epoxypropyl groups and functionalization yield in glycidyl methacrylate monoliths using gas chromatography

Poly(GMA-*co*-EDMA) is most frequently used as parent monolith to obtain stationary phases with a variety of surface chemistries for HPLC and CEC. Functionalization is performed by opening the accessible 2,3-epoxypropyl groups of the monolith with a suitable reagent. The number of 2,3-

epoxypropyl groups which are accessible before and after the functionalization reaction, and the grafting yield, are important parameters, required both to optimize functionalization and to interpret the chromatographic performance of functionalized monoliths. In this work, a method capable of providing this information for parent and functionalized poly(GMA-*co*-EDMA) monoliths, prepared in silica capillaries and other supports, was proposed.

For this purpose, H_2SO_4 was used to open the epoxy rings of the 2,3-epoxypropyl groups to yield 2,3-dihydroxypropyl groups. Second, glycerol was liberated by reducing the ester bonds with $LiAlH_4$. With the proposed two-step reaction procedure, the initially available epoxy groups and the sum of the unreacted 2,3-epoxypropyl and 2,3-dihydroxypropyl groups of functionalized monoliths, were both established by measuring the single peak of glycerol. On the other hand, for functionalized monoliths, and either with or without previous opening of the residual epoxy groups with H_2SO_4, reduction with $LiAlH_4$ was used to liberate the functionalization ligand with an attached 2,3-propyldiol chain. Thus, the chromatograms obtained with functionalized monoliths showed an additional peak when the resulting molecule had enough volatility. This also provided direct information about the functionalization yield. In this work, this was the case for NH_3 and DEA, but not for epinephrine.

The flushing time for the reactions of parent monoliths with both H_2SO_4 and $LiAlH_4$ was optimized. It was necessary to flush the capillary with H_2SO_4 for at least 1 h to achieve total hydrolysis of the 2,3-epoxypropyl groups. The conditions selected for the $LiAlH_4$ ester bond reduction were flushing the column at room temperature with a 100 mM $LiAlH_4$ solution in hexane at 100 µL h^{-1} for 2 h. The proposed procedure was next applied to the joint determination of the accessible 2,3-epoxypropyl and 2,3-dihydroxypropyl groups in the capillary monoliths (before and after functionalization of the monoliths). All these chromatograms showed the peak of glycerol, as well as a small peak of ethylene glycol due to the reduction of the two ester bonds of

EDMA bridges of the polymer structure. From these values, the corresponding functionalization yields were calculated. The parent monoliths showed a quite satisfactory 1.7 % repeatibility. The derivatized monoliths gave values close to 3 %, which can be attributed to both the variability of the monolith functionalization reactions and the smaller amounts of glycerol which were released.

On the other hand, evidence on the different properties of monoliths prepared in rather different formats was provided by comparing the contents of the accessible 2,3-epoxypropyl and 2,3-dihydroxypropyl groups. Thus, the method provided evidence that the monoliths polymerized inside 100 µm I.D. capillaries have an excess of reactive sites with respect to the equivalent monoliths obtained in glass vials, probably due to self-screening of the UV-radiation in these later. Thus, the method could be also useful to reveal differences in monoliths prepared in different supports using different initiating systems (photo, thermal, and chemical initiation).

The highlights of this work can be summarized as follows:

- *The proposed method provides simple and reliable evaluation of the functionalization yield of GMA-based monoliths prepared in different supports.*
- *The content of the epoxide moieties on the monolith surface can be measured from the released glycerol by GC-FID.*
- *Comparison of parent and functionalized GMA-based monoliths in different supports revealed differences in structure.*

A.4. Methacrylate monolithic columns functionalized with epinephrine and epinephrine-quinone for capillary electrochromatography applications

Epinephrine-bonded polymeric monoliths for CEC were developed by nucleophilic substitution reaction of epoxide groups of poly(GMA-*co*-EDMA) monoliths using epinephrine as nucleophilic reagent. Monolith

functionalization was achieved in dynamic conditions. Successful chemical modification of the monolith surface was ascertained by *in situ* Raman spectroscopy characterization. In addition, the amount of epinephrine groups that was bound to the monolith surface was evaluated by oxidation of the catechol groups with Ce(IV), followed by spectrophotometric measurement of unreacted Ce(IV). The chromatographic behavior of the epinephrine-bonded monolith in CEC conditions was assessed with test mixtures of alkyl benzenes, aniline derivatives and substituted phenols. The epinephrine-bonded monolith was further modified by oxidation with a Ce(IV) solution.

Afterwards, the opening of the epoxide groups of the monolith surface with epinephrine was investigated. For this purpose, the reaction conditions that favored the bimolecular nucleophilic substitution (SN_2) reaction of the epoxide ring opening with the secondary amine group of epinephrine, and concomitantly minimize the competitive hydrolysis (ring opening of epoxide with hydroxyl ions), were optimized. For this purpose, the concentration of epinephrine and the flow rate were kept constant, at 10 mM and 4 µL min^{-1}, respectively, and both temperature and reaction time were optimized. The separation of a mixture of alkyl benzenes on a series of derivatized monolithic columns was used to assess the bonding of epinephrine at increasing reaction temperatures. These columns were obtained by flushing the epinephrine solution for 2 h. In the case of the temperature, the retention of the alkyl benzenes increased from 25 ºC to 60 ºC, higher temperatures leading to a retention decrease. The retention times of alkyl benzenes obtained with monolithic columns which were derivatized at 60 ºC using increasing reaction times showed a plateau after 2 h. This suggested the saturation of all accessible epoxide groups with epinephrine.

To characterize the epinephrine functionalized GMA-based monoliths, SEM images were first taken. However, no significant differences in monolith structures, i.e. the macropore and globule size morphology, between the

functionalized and unfunctionalized monoliths were observed. Then, Raman spectroscopy was employed to probe the surface of the monoliths. Raman spectra were recorded directly on the monolith within the confines of the fused-silica capillaries. Two bands in the epinephrine-bonded monoliths which were absent in the unfunctionalized monoliths were observed. The control of the yield of the surface functionalization reaction was established by redox reaction of the phenolic groups of bonded epinephrine with Ce(IV). This reaction is specific to catechols which are quantitatively oxidized to quinones. Thus, the surface coverage with epinephrine groups in the 8.5 cm long monolithic capillary columns of 100 µm i.d was *ca.* 0.08 ± 0.01 µmol (n = 3), which corresponds to about 0.5 mmol of bonded groups per gram of monolithic polymer.

In order to test the chromatographic properties of the poly(GMA-*co*-EDMA) monolith before and after functionalization with epinephrine, the separation of mixtures of uncharged and ionizable solutes was investigated. In both monoliths, alkyl benzenes were eluted in the order of increasing hydrophobicity; however, an enhanced retention was evidenced in the epinephrine-bonded monolithic column. Also, the efficiencies of both columns were evaluated by obtaining van Deemter curves for all the alkyl benzenes. Minimum plate heights comprised between 4.0–5.1 µm and 3.1–5.5 µm were obtained for the unfunctionalized and epinephrine-bonded monoliths, respectively. The separation of basic analytes (anilines) by CEC using both the unfunctionalized and epinephrine functionalized monoliths under the same conditions were also compared. For the epinephrine-bonded monolith, a higher retention of the aniline derivatives was observed. A separation of phenol derivatives was also studied. The phenol derivatives showed also a much higher retention on the epinephrine-bonded monolith than on the unfunctionalized monolith, whereas the elution order was the same.

The highlights of this work can be summarized as follows:

- *A novel monolithic column functionalized with epinephrine for CEC was described.*
- *A redox method with spectrophotometric monitoring to evaluate the amount of bonded-epinephrine was described.*
- *Easy and reversible column modification by redox reactions was demonstrated.*
- *Enhancement of separation by several interaction mechanisms was observed.*
- *Good reproducibility in column preparation and separation of the test analytes was found.*

A.5. Phosphatidylcholine covalently linked to a methacrylate-based monolith as biomimetic stationary phase for capillary liquid chromatography

A strategy to immobilize phospholipids onto polymer-based stationary phases was introduced. Methacrylate-based monoliths in capillary format were modified by PC through EDC coupling to obtain stationary phases suitable to mimic cell surface membranes. The covalent coupling reaction involves the phosphate group in phospholipids; therefore, the described methodology is suitable for all types of phospholipids. Immobilization of PC on the monolith was confirmed by ATR-FTIR spectroscopy and GC-MS analysis of the fatty alcohol profile generated upon reductive cleavage of the fatty acyl side chains of the phospholipid on the monolith surface with $LiAlH_4$. The prepared stationary phases were evaluated through studies on the retention of low-molar mass model analytes including neutral, acidic, and basic compounds.

Four strategies to introduce the phospholipid ligand onto poly(GMA-*co*-EDMA) monolith were tested. However, only the multistep monolithic surface modification strategy gave a stationary phase with a high amount of

immobilized phospholipids. First, the oxirane ring from GMA was opened through reaction with HMD to create an amino stationary phase. After that, the amino monolith was modified by GA and HMD, and PC was covalently bound to it via an EDC coupling reaction. Finally, the formed imino groups were reduced by SCBH to stabilize the bonding. This approach has several advantages over preparation procedures used earlier for column synthesis. First of all, PC is permanently immobilized to the functionalized poly(GMA-*co*-EDMA) monolith by covalent coupling. This provides improved stability of the stationary phase as compared to stationary phases prepared only by adsorption, especially when organic solvents are used as components of the mobile phase.

The presence of PC groups attached onto the surface of the poly(GMA-*co*-EDMA) monolith was demonstrated by ATR-FTIR of the bulk material and of the monolith prepared inside the capillary. Several bands were used to confirm each functionalization step. Furthermore, GC-MS was used to confirm the immobilization of PC. The fatty acyl chains were cleaved from the monolith surface by reduction of the ester to the corresponding alcohol using $LiAlH_4$ and the released alcohols were analyzed by GC-MS.

All synthesized monolithic columns were evaluated in capillary LC under RP separation conditions as first utilizing alkylbenzenes as test analytes and ACN–water as mobile phase. Since a multistep preparation procedure was used for the synthesis of the capillary columns, we investigated the influence of all individual modification steps on the separation of analytes employing an alkylbenzene mixture. Poor separation of the sample mixture was observed for all the steps previous to the PC bonding. PC, when covalently bonded to the modified monolithic support, significantly improved the separation selectivity of the stationary phase. The retention factor for hexylbenzene was 4.5 times higher than for the original poly(GMA-*co*-EDMA) monolith; the retention factor of hexylbenzene was 2.8 on the poly(GMA-*co*-EDMA) monolith, whereas a value as high as 12.7 was achieved on the PC-modified monolith.

The interactions between analytes and the phospholipid stationary phase were observed utilizing test analytes like organic acids and a diverse set of well-described UV-detectable compounds. The variation of the retention of neutral, acidic and basic compounds on the synthesized PC column was investigated by changing the ACN concentration in the mobile phase. On the other hand, the synthesized columns can operate under fully aqueous phase conditions and the resultant data do not need extrapolation to 100% aqueous conditions, as typically done in IAM chromatography whereas it is problematic in RP chromatography. The effect of increasing ionic strength of the mobile phase on the retention of the tested compounds was also examined. The retention of tested compounds gradually decreased with increasing ionic strength of the mobile phase. Drug partitioning into the synthesized stationary phases was evaluated under cLC conditions employing a set of unrelated drugs and Dulbecco's phosphate-buffered saline solution as a mobile phase. The poly(GMA-*co*-EDMA) monolith strongly retained compounds containing amino groups (aniline, *p*-toluidine, *p*-, *m*-nitroaniline) under the separation conditions. Immobilization of PC to this monolith lowered retention of these compounds, and slightly improved retention of acidic ones. When parameters such as rat intestinal drug absorption was applied to investigate interactions among tested drugs and the PC monolith, the coefficient of variation, r^2, increased from 0.55 to 0.73. The synthesized columns were stable for more than six months.

Therefore, this work described a novel methodology for preparing biomembrane mimicking monolithic columns for capillary LC. Our data showed that the synthesized stationary phase, consisting of zwitterionic PC covalently bonded to a poly(GMA-*co*-EDMA) monolith through EDC coupling, possesses improved stability in contrast to physically adsorbed phospholipid stationary phases. The suggested technique of column preparation through EDC coupling involves the phosphate group in the phospholipid in order to form a phosphoramidate linkage. Thus, this coating procedure enables

to covalently immobilize all kinds of phospholipids, not only those containing (primary) amino groups. In addition, this means that the phospholipid polar head groups will be free for additional electrostatic interactions. This methodology will strongly broaden the field of immobilized phospholipid stationary phases for chromatography, which is of importance for elucidation of binding interactions between biologically relevant compounds and biomembranes.

The highlights of this work can be summarized as follows:

- *Poly(GMA-co-EDMA) monolithic stationary phases with covalently bonded soybean PC were prepared.*
- *The synthetized columns were characterized by ATR-FTIR and cLC.*
- *The developed columns could be used in the IAM chromatography mode.*
- *The synthetized monolith showed high stability even with fully aqueous mobile phases.*

A.6. Polymethacrylate monoliths with immobilized poly-3-mercaptopropyl methylsiloxane film for high-coverage surface functionalization by thiol-ene click reaction

New polythiol-functionalized macroporous monolithic polymethacrylate-polysiloxane composite materials were presented. These new materials can be useful substrates for highly efficient immobilization of (chiral) catalysts, chromatographic ligands, and other functional moieties by thiol-ene click reaction. A 3-step functionalization by amination of the epoxy monolith, followed by its vinylation with AGE and subsequent thiolation by coating of a PMPMS thin film, followed by crosslinking by click reaction, furnished a monolith with more than 2-fold enhanced thiol coverage with respect to the parent monolith. The further functionalization of this PMPMS modified monolith with a clickable chiral quinine carbamate selector clearly documented

the benefit with highly dense thiol surfaces for such reactions and synthesis of functional materials with proper ligand loadings.

To modify epoxy groups of the monolith with the polythiol, a 10% PMPMS (v/v) solution in acetone was used monolith derivatization via SN_2 reaction (SN_2-type thiolation). This solution gave a backpressure compatible with syringe pump operation, and it was employed to perform functionalization studies at several temperatures and distinct reaction times. Presumably, a part of the thiol groups of PMPMS were bound to the surface, and the unreacted thiol groups remain available for either solute interaction or further derivatization. After reaction of PMPMS with the monolith surface, the still available unreacted thiol groups on the modified monolith surface were determined by the DPDS assay. However, the concentrations obtained at different times and temperatures were lower than those achieved using sodium hydrogen sulfide as reagent for monolith modification. Possible reasons for this unexpected finding were low reactivity of the thiols at neutral conditions, hindered access of the large and bulky polymeric PMPMS molecules to the reactive epoxy groups on the polymethacrylate surface, excessive reaction of a large portion of the thiol groups of PMPMS with the polymer surface, or disulfide bridge formation between thiols of adjacent pendent groups. To overcome the problem of limited thiol coverage, a different approach with a spacer arm in-between the monolith surface and the coated PMPMS layer was tried. For this purpose, a surface functionalization procedure comprising the following three steps was developed: (i) conversion of the epoxy functionalities into amino moieties using ammonia (amination); (ii) attachment of AGE to the ammonia groups (vinylation); and (iii) bonding of PMPMS thiol groups by means of a click reaction to the double bonds of AGE (click-type thiolation). The key difference with respect to direct functionalization was the introduction of a spacing arm prior to bonding PMPMS, which led to higher reaction yields. For evaluation of these factors, the whole three-step derivatization procedure was carried out and the effect of the investigated factor was assessed by finally

evaluating the available thiol groups of the resulting monolith. These columns showed at least a 2-fold increase in the concentration of available thiol groups respect to other columns described both in this work and in literature. To document that elevated levels of reactive thiols can be beneficially translated into higher surface coverage of other ligands accompanied with improved selectivity, a clickable chiral selector was bonded onto the thiol-monoliths. For this purpose, a quinine carbamate derivative, *t*-BuCQN, was selected. Finally, performic acid oxidation was used to tune the surface characteristics thus to enhance enantioselective interactions by inhibiting non-specific ones.

The various quinine carbamate-bonded monolithic columns developed in this work were chromatographically evaluated with DNB-(*R*,*S*)-Leu in CEC mode. Test results for other probes (alkyl benzenes, benzoic acids and amines) were also provided. As demonstrated, the non-oxidized column obtained from multi-step functionalization provided enhanced resolution of *ca.* 109 % and the efficiency was also improved in *ca.* 260 %. On the other hand, the oxidized columns showed improvements in resolution and efficiency of 300 %. Column reproducibility could be a critical factor. However, for all tested parameters, satisfactory RSD values (below 9%) were obtained for all columns.

In summary, a novel surface chemistry of monoliths was described by coating them with PMPMS, a polymer with many reactive thiol groups. The high densitity of thiol groups on the surface was due to both the introduction of an spacer arm prior to the PMPMS bonding, and the use of only part of the thiol groups for bonding, most of them remaining free for interaction with the analytes or for further surface modification. Thus, a clickable chiral selector, viz. *t*-BuCQN, was bonded on the modified surface giving rise to an elevated ligand density. Finally, retention mechanisms other than those due to the chiral selector were minimized by selective oxidation of the thiol-eter and remaining thiol groups. This strategy made possible the preparation of a zwitterionic chiral column showing increased analyte retention, excellent selectivity (minimized

non-specific interactions with the underlying monolith skeleton), superior sample loading capacity and very large separation factors for the chiral probe.

The highlights of this work can be summarized as follows:

- *Methacrylate monolith surfaces were coated with a covalently bonded film of poly-3-mercaptopropyl-methylsiloxane film.*
- *A functional polysiloxane film was then chemically crosslinked to the surface.*
- *The resultant composite materials allowed clickable high-density surface functionalization.*
- *This concept was demonstrated by thiol-ene click reaction with quinine carbamate.*
- *The resultant chiral monoliths were tested for enantiomer separation by CEC.*

A.7. Zwitterionic codeine-derived methacrylate monoliths for enantioselective capillary electrochromatography of chiral acids and chiral bases

The preparation of a *de novo* designed low molecular mass chiral selector based on the thiol-ene click addition of NACME ester to codeine, followed by reaction with AIC and hydrolysis to yield the corresponding zwitterionic chiral selector, was described. This zwitterionic codeine-derived chiral selector was bonded to the surface of a methacrylate monolith by means of four successive reactions. First, the epoxy groups were converted into amine residues, followed by reaction with AGE. In this way, a spacer arm was bonded to the surface before coating and cross-linking PMPMS via radical addition (thiol-ene click reaction) to the surface. In order to improve the performance of the monolithic chiral stationary phase, thio ether and residual thiol groups were oxidized to sulfonyl and sulphonate groups, respectively. This novel CSP was evaluated by CEC using two chiral model compounds, namely *N*-3,5-dinitrobenzoyl-R,S-

leucine (retained by an anion-exchange mechanism) and mefloquine (by retained cation-exchange). A series of chiral β-blockers and amino acid derivatives was used to further check the performance of the modified monolith under the optimal conditions.

The zwitterionic CSP was prepared using established methodologies. Thus, COD was firstly reacted with NACME in the presence of AIBN via thiol-ene click chemistry. The chemical shifts of the ^{1}H NMR spectrum demonstrated that the attack of NACME on the double bond occurred exclusively on the carbon atom C7. Subsequently, the secondary hydroxyl group of ring C of COD was derivatized with AIC furnishing a urethane functionality. This introduced a hydrogen-donor/acceptor system for interaction with solutes and a linker for immobilization of the chiral selector by thiol-ene click reaction. For this purpose, the product was dissolved in anhydrous THF, and AIC in presence of TEA as catalyst was added. The reaction product, COD-NACME-AIC, gave a single peak in RP-HPLC. In the last step, the methylester of cysteine was hydrolyzed to obtain the zwitterionic codeine-derived chiral selector (COD-NAC-AIC). A single peak in RP-HPLC and stereoselective HPLC with a chiral anion-exchanger (Chiralpak QN-AX) which has proven broad stereoselectivity for chiral *N*-derivatized amino acid derivatives confirmed, along with the corresponding NMR spectra, the presence of a single stereoisomer.

The resultant zwitterionic codeine-derived selector had 6 centers of chirality embedded in a rigid backbone (*5R,6R,7R,9R,13S,14R*) with a conformationally flexible chiral NAC side chain harboring another stereogenic center (*2R*) and a further achiral allylcarbamoyl substituent acting as linker for immobilization. The tert-amine of the COD backbone represents a weak anion-exchange (WAX) site, and the carboxylic group of cysteine constitutes the weak cation-exchange (WCX) site. In addition to these primary ion-exchange sites, this chiral selector possesses a π-π-interaction site (π-base in the A-ring of the morphinene backbone) as well as two hydrogen donor/acceptor systems

(carbamate at C6 and amide of NAC) as supportive interaction sites. The A and C-rings are arranged perpendicular to each other and form a cleft for analyte insertion driven by ion-pairing at a counterionic ion-exchange site, whereas complex stabilization is supported by directed π-π-interactions and hydrogen bonds of adjacent binding sites.

Since enantioselective chromatography requires a substantial amount of chiral moieties on the surface, a new approach of thiolation of the monolith surface for subsequent bonding of the chiral selector by thiol-ene click reaction was pursued. In the first step, the epoxy groups were converted into primary amino groups using ammonia. The amino groups were then derivatized with AGE. Onto the surface of this allyl-modified monolith, a thin film of PMPMS was obtained by binding to the allyl groups from the prior bonded AGE linker through thiol-ene click reaction. To evaluate the coverage of the monolith with PMPMS as well as the CS, the DPDS assay was used. First, the thiol concentration of the monoliths modified with PMPMS was determined. The amount of free thiol groups on the monolith surface was 2.21 mmol SH g^{-1} of monolith. After reaction with COD-NAC-AIC, the total free thiol groups amounted to 0.38 mmol SH g^{-1} of monolith. Hence, the yield of the thiol derivatization, calculated from the difference between the free thiol groups before and after the reaction, was 83%. This corresponded to 1.83 mmol COD-NAC-AIC g^{-1} monolith.

Retention of acidic and basic analytes on zwitterionic CSPs in non-aqueous media was evaluated by CEC. The CEC experiments were made using protonated DEA and acetate as counterions with respect to the carboxylate and amino groups of the CSP, respectively. As observed, retention decreased with increase of counterion concentration. Further, plots of log k versus the logarithm of the counterion concentration (log c) revealed linear dependencies of the two pairs of enantiomers for each type of chiral solute in accordance with a stoichiometric displacement model. This is a clear indication that retention

takes place by ion-exchange processes, i.e. anion-exchange for DNB-Leu and cation-exchange for mefloquine. In order to explore suitable CEC operation conditions, the dependence of the overall performance of the CSP on different acid-to-base ratios, as a way of controlling the proton activity in the nonaqueous medium, was investigated. As observed, enantioselectivity and enantiomeric resolution were only slightly modified when the acid-to-base ratio increased. Thus, there was some minor effect of the proton activity in the eluent on efficiency of DNB-Leu, and a somewhat larger effect for mefloquine. The influence of counterions on the elution of mefloquine was studied by using NH_3, DEA and TEA. The co-ion (AcO^-) was kept constant in this series of experiments. The retention of mefloquine displayed a strong dependence on the nature of the counterion, whereby the elution strength increased in the order: TEA < DEA < NH_3. The elution of DNB-*R,S*-Leu was studied in the presence of the following counterions: FA, HAcO and TFA. The co-ion was DEA in all the experiments. Elution strength for DNB-*R,S*-Leu increased in the following order: FA < HAcO < TFA. Although, protic solvents such as MeOH are required to mediate acid-base equilibria and hence to also sustain ion-exchange processes, polar aprotic solvents like ACN should be also present to improve the CSP performance. Several chiral solutes were additionally tested to explore the CEC performance of the CSP with optimized conditions for a structurally broader solute set. β-Blockers and amino acid derivatives carrying a variety of functional groups were examined.

The highlights of this work can be summarized as follows:

- *A new chiral selector based on a codeine derivative has been synthetized.*
- *A high-coverage of monolithic columns with a polythiol has made possible a high density of the bonded chiral codeine derivative.*
- *Chiral CEC separations for acid and basic compounds have been demonstrated and optimized.*

A.8. Polymeric monolithic columns with a high coverage of silver nanoparticles for chromatographic separations

A methodology to prepare polymeric monoliths with enhanced surface coverage with SNPs has been described. For this purpose, the pore surface of the parent monolith, poly(glycidyl methacrylate-co-ethylene dimethacrylate), was functionalized with poly-3-mercaptopropyl methyl siloxane, a polythiol, using a three-step procedure. Subsequently, the monolith was successively coated with two SNP layers. The second SNP layer was attached to the first one through a self-assembly process driven by a dithiol. The synthetized hybrid materials were characterized using thermogravimetric analysis and energy dispersive x-ray spectroscopy. Aromatic hydrocarbons and proteins were used to evaluate the chromatographic performance of these novel materials.

First, the monoliths modified with PMPMS provided dense coverages with reactive thiol groups (2.32 mmol thiol g–1 monolith). Aftewards, a SNP dispersion was pumped through the monolithic column. As the 20 nm SNPs were attached to the monolith, its color changed from white to dark red. When SEM micrographs of this monolith were taken with a BSE detector, an excellent surface coverage with SNPs was observed. Elemental analysis using EDAX indicated the presence of 59.8 wt% silver, and the TGA result was consistent with this value (Eq. 1, 62.9 wt% silver). The accessible surface of the SNPs was then functionalized by flushing the column with pure liquid HDT at 120 µL h^{-1}. A plateau was reached after flushing 5 mL. As observed, SNPs were not detected on the monolith surface, probably because they were covered by a layer of bonded alkanedithiol. The SNPs were also probably crosslinked each other though alkyldithiol bridges. Then, this column was flushed again with a SNP dispersion by following the procedure described above. The SEM/BSE image also showed an excellent and remarkably regular coverage of the polymer surface with the SNPs. The contents of silver in this monolith was estimated by both EDAX and TGA as 90.2 wt% and 95.7 wt%, respectively.

The surface of the monolithic column with the SNP multilayer film was finally modified with an alkanethiol (HMT). In order to achieve a complete coverage of this second SNPs layer, the volume of this ligand to be forced through the column at 120 µL h^{-1} was also optimized. A plateau was reached after flushing the column with 3 mL.

The chromatographic performance of the different monolithic columns described in this work was tested using small molecules (aromatic hydrocarbons) and proteins. The separation of aromatic hydrocarbons improved dramatically after the attachment of the first SNP layer. In fact, retention increased according to the degree of unsaturation of the test solute. When this monolithic column was functionalized with HDT, a decrease in retention, particularly remarkable for the late eluting compounds, was evidenced. Also, a slight improvement in efficiency was observed. The strong interaction between unsaturated compounds and SNPs was again evidenced after attachment of the second SNPs layer, giving rise to an increase of retention and peak broadening. When this column was treated with HMT, efficiency increased and an improvement in peak shape was again observed giving higher efficiencies than those modified with HDT. Separation of proteins with the parent and modified columns was also tested. For the column with two SNP layers and finished with HMT, resolution between three proteins was successfully achieved. It's worth to note that this separation was achieved with a ligand having an alkyl chain length much shorter than those used in other reported studies.

The highlights of this work can be summarized as follows:

- *A multi-step preparation of methacrylate monoliths modified with polythiol and two layers of silver nanoparticles was described.*
- *High-coverage of silver nanoparticles was achieved.*
- *The monoliths exhibited improved chromatographic performance for small and large molecules.*
- *Separation of proteins in isocratic elution conditions was achieved.*

A.9. Hybrid methacrylate monolithic columns containing magnetic nanoparticles for capillary electrochromatography

VMNPs were incorporated into polymethacrylate monolithic columns to develop novel stationary phases with enhanced separation performance. The VMNPs were dispersed in a polymerization mixture containing GMA and EDMA as monomers, CYC and DOD as porogens and AIBN as initiator. The stability of the VMNPs in the polymerization mixture was investigated at several VMNP contents. Using short UV-polymerization times, polymeric beds with homogenously dispersed VMNPs were obtained. The novel stationary phases were characterized by scanning electron microscopy. The chromatographic performance of these hybrid monoliths was evaluated by CEC using alkyl benzenes and OPs as test solutes.

The stability of the VMNP suspensions in the polymerization mixture was studied. For this purpose, light scattering was used to monitor suspensions containing between 0 and 5 wt% VMNPs. Polymerization mixtures showed that with suspensions containing between 0.5 and 2 wt% VMNPs were quite stable, showing negligible sedimentation for at least 20 min (up to 45 min for the 2 wt% mixture). On the contrary, for the mixture having 5 wt% VMNPs, sedimentation was perceptible after ca. 6 min. The results obtained by monitoring scattered light agreed with that visually observed

SEM images of all the monoliths were obtained at different magnification powers. At high magnifications, SEM images provided further evidence about the higher surface area of the VMNP modified monoliths. The globules containing the VMNPs exhibited more protuberances than that observed in the absence of VMNPs. This was also deduced from the more wavy edges of the globules. On the other hand, SEM/EDAX analysis confirmed the presence of VMNPs in the monoliths. As an example, the hybrid monoliths prepared with 2 wt% VMNPs showed 2.1 iron atom%. Thus, SEM/EDAX provided evidence of the incorporation of the VMNPs to the monoliths. Further evidence about the higher surface roughness of the resulting modified monoliths was achieved by measuring the BET surface area. In fact, the BET analysis of hybrid monoliths containing VMNPs showed significantly larger values (up to 17.8 m^2 g^{-1}) in comparison to that of the control monolith (5.1 m^2 g^{-1}).

The CEC performance of the hybrid monolithic columns containing incorporated VMNPs was evaluated using different mixtures of test analytes. For all the monoliths, the retention on the monoliths copolymerized with VMNPs was significantly higher than that obtained on the control monolith. An increase of retention can be due to a higher affinity of the analytes for the stationary phase as well as to an increase of the stationary to mobile phase ratio. Since the VMNPs were vinylized, they were probably covered by poly(GMA-*co*-EDMA). Covering of the VMNPs by the polymer would also explain why, in spite of the well-known affinity between iron and many phosphorus compounds, the selectivity was not modified when VMNPs were introduced in the monolith In addition, a non-linear decrease in the EOF mobility was observed at increasing VMNP contents This should be attributed to a decrease of the density of the quaternary ammonium functionalities of META (ionizable monomer) on the monolith surface.

Then, a series of experiments were performed in order to study the retention mechanisms in the hybrid monoliths. The mixture of alkyl benzenes

was first injected. Plots of log *k* versus log $P_{o/w}$ showed positive correlations. Therefore, the main retention mechanism was hydrophobic attraction (van der Waals interactions). Then, the test mixture of organophosphorous compounds was injected. These compounds also showed a decrease of retention as the ACN concentration increased, thus also indicating a predominant RP mechanism.

In the monoliths containing 1 wt% VMNPs, the H_{min} values were within the 6.6-9.4 µm range, whereas for the control monolith obtained in absence of VMNPs, the H_{min} values ranged between 14.8 and 21.0 µm. Additionally, the hybrid monoliths also showed lower mass transfer contributions (*C*-term) (0.003 ms) than that obtained with the control monolith (0.089 ms). The best separation of organophosphorous pesticides was achieved by using the hybrid monolith containing 2 wt% VMNPs.

The highlights of this work can be summarized as follows:

- *A one-step preparation of hybrid methacrylate monoliths copolymerized with vinylized magnetic nanoparticles was described.*
- *The method is easy, quick and reproducible.*
- *The new monoliths exhibited enlarged surface area and enhanced retention while efficiency was preserved.*

B) Characterization of raw materials

B.1. Evaluation of molecular mass and tacticity of polyvinyl alcohol by non-equilibrium capillary electrophoresis of equilibrium mitures of a polymer and a dye

NECEEM has been used to characterize PVA. Commercial PVA samples with different molecular masses, from M_w = 15 up to 205 kDa, were used. According to the ^{13}C NMR spectra, the samples also differed in tacticity (stereoregularity). Mixtures of PVA and the anionic azo-dye CR were injected in the presence of a borate buffer. The electropherograms gave a band and a peak due to the residual PVA-CR complex and the excess dye, respectively, plus a superimposed exponential decay due to the partial dissociation of the complex during migration. The stoichiometry of the PVA-CR complex q = [monomer]/ [dye], reached a maximum, q_{sat}, which depended on both M_w and tacticity of PVA. Thus, q_{sat} decreased from a molar ratio of ca. 4.9 to 3.6 at increasing M_w values, this variation also being largely dependent on tacticity. A similar dependence of the electrophoretic mobility of the complex on both M_w and tacticity was also observed. A possible explanation, based on the formation of a stack of CR ions inside the PVA-CR complex, was proposed and discussed. Finally, at increasing M_w values, the stability constant of the complex increased slightly (from log $K_s \approx$ 2.5 to 4.0), and the pseudo-first order dissociation rate of the complex decreased (from ca. 0.06 to 0.02 s^{-1}), this later parameter also showing a dependence on both M_w and tacticity.

The formation of PVA-CR complexes was first studied by filling the capillary with PVA-CR mixtures containing 20 mM borax. For the 49 kDa PVA sample, the UV-vis spectrum of a 4 mM CR solution was largely modified when the mixture also contained increasing PVA concentrations. Thus, from q = [monomer]/ [dye] = 0 to 6, the molar absorptivity at the maximum of the main absorption band increased in a ca. 30%, and a large bathochromic shift of about 40 nm was also observed. Similarly, an intensity increase of ca. 55% and a

batochromic shift of ca. 50 nm were observed with a conventional spectrophotometer when 0.4 mM PVA was added to a 0.1 mM CR solution. This implies a major change in the physico-chemical environment of the CR probe.

The time required to equilibrate the mixtures before injection was studied. For this purpose, aliquots of a solution containing 20 mM borax, 4 mM CR and 16 mM PVA monomers were injected at regular time intervals after mixing the reagents. The area due to the remaining complex, $A_{PVA\text{-}D}$, was estimated by doubling the area of the left half of the complex band. The rest of the area, due to both the initial free dye and the dye released by the complex during migration, was measured as $A_{Total} - A_{PVA\text{-}D}$. A small increase of the electrophoretic mobility of the complex (ca. 4%), was observed during the first two hours after mixing the reagents.

Series of electropherograms also obtained with 4 mM CR and increasing PVA concentrations (increasing q values) were used to estimate the saturation point or maximal stoichiometry of the PVA-CR complexes, q_{sat}, for all the PVA samples. When q was increased, the area of the PVA-CR complex, $A_{PVA\text{-}D}$, increased linearly up to $q \approx 4$, and the rest of the total area decreased proportionally. When $q \geq 5$, that is, above the saturation point, the peak due to the excess dye was not observed any longer, and $A_{PVA\text{-}D}$ decreased steadily.

Electropherograms obtained with PVA samples of increasing molecular mass, also corresponding to different tacticities were used to study the relationship with the M_w and the tacticity. As observed in the electropherograms, M+L samples showed a sharper complex band than that of the H samples. In addition, within each tacticity group, the electrophoretic mobility of the complex was reduced at increasing molecular mass. The relationships among electrophoretic mobility of the complex formed in the presence of an excess dye, molecular mass and tacticity are better recognized. Within each tacticity group, the absolute electrophoretic mobility decreased

slightly at increasing log M_w values. Therefore, electrophoretic mobilities indicated that charge density of the complexes decreased at increasing molecular masses.

The highlights of this work can be summarized as follows:

- *The NECEEM theory can be applied to the characterization of synthetic polymers as PVA.*
- *It was shown that both the Mw and the tacticity of polymers depended on the electrophoretic mobility and peak shape.*
- *A method to estimate the tacticity of synthetic polymers was described.*

B.2. A thermal desorption - gas chromatography - mass spectrometry study of outgassing from polymethacrylimide foam (Rohacell®)

PMI foam, marketed as Rohacell®, is often used as light structural material in spacecraft devices; however, the closed cells of the foam contain many volatile compounds which are outgassed even at low temperatures. Offgassed compounds easily ignite plasmas under the intense radio-frequency fields used in outer-space communications. Therefore, the outgassing properties of these materials should be known, and the nature of the compounds released in significant amounts should be established, to reduce the risks of spacecraft fatal events. In this work, the outgassing of PMI foams was studied using both TGA and TD coupled to gas chromatography with mass spectrometry detection (TD-GC-MS). Weight losses amounted reached 3% at ca. 210 ºC, when the destruction of the PMI foam polymer scaffold began. Outgassing at 125 ºC was first studied by using successive 4-min heating cycles, each one corresponding to a TD-GC-MS injection. Finally, the sequence of 4-min heating cycles was repeated by using 175 ºC instead of 125 ºC. The

comparison of outgassing at these two temperatures revealed the extreme difficulty in fully outgassing PMI foams.

TGA was performed at two heating rates, namely 2 and 10 ºC per minute. At low temperatures, up to 65 ºC, Rohacell® 31HF (the PMI foam most frequently used in spacecraft devices) showed a quick 1.5% weight loss. The TGA curve showed a lower and fairly constant slope between 65 ºC and approximately 210 ºC. The total weight loss amounted to ca. 2% at 100 ºC, reaching 3% at ca. 220 ºC. Mainly nitrogen and a series of light organic solvents were released below 220 ºC. Other compounds, such as monomers (methacrylic acid), plasticizers and foaming agents (surfactants), were released in lesser amounts. As observed, no differences between the two heating rates, 2 and 10 ºC min^{-1}, were observed up to 230 ºC. At higher temperatures, the material underwent irreversible decomposition which was produced with some delay at the faster heating rate.

The chromatograms of outgassing cycles contained a series of large and medium intensity peaks, as well as many small peaks. Only those peaks which were observed at least in three chromatograms, also reaching a S/N larger than 10, were considered. Several light compounds were eluted within the first 2 min after TD injection. The first peak was nitrogen. Water and a series of light VOCs followed. Among these, the most abundant were two hydrocarbons, namely isobutylene (2-methyl-1-propene) and hexane, and two alcohols, tert-butanol and 1-PrOH. Isobutylene could be mixed up with its isomer, trans-butene, since these two isomers give isobaric ions also having closely similar mass spectra. The hydrocarbons were probably present as solvents in the polymerization mixture, and the light alcohols were used as blowing agents, to promote the closed-cell structure of PMI foams during polymerization. Water and a few other VOCs were released in lesser amounts.

As in other polymers, free monomers were present in Rohacell® 31HF as the remaining of incomplete polymerization. Thus, immediately after the

lightest VOCs, methacrylic acid was eluted. This is one of the two monomers which are claimed to be the two main building blocks of PMI foams. Several higher alkanes (high molecular mass hydrocarbons), with a minimum of 15 carbon atoms in the alkyl chain, were also observed. The mass spectrometer reveals the presence of these compounds, but excessive fragmentation hindered individual identification. These hydrocarbons could be produced during synthesis by radical polymerization of 2-methyl-1-propene (or trans-butene). Degradation of the PMI polymer (chain scission) to yield long chain hydrocarbons is unlikely at 125 ºC. Several saturated and mono-unsaturated free fatty acids with 16 and 18 carbon atoms in the alkyl chain, and their esters with both 1-propanol and glycerol, were also released. Fatty acids are surfactant compounds (soaps) most likely used during PMI foam synthesis as emulsifiers and foaming agents.

From a qualitative viewpoint, the chromatograms obtained by heating at 175 ºC were closely similar to those obtained by using 125 ºC, thus, the compounds released were essentially the same. The chromatograms also resembled those obtained by heating at 160 ºC. Concerning to the relative peak areas, the differences between strongly and weekly retained compounds were enhanced at 175 ºC compared to 125 ºC. Thus, a strongly polar compound as 1-propanol was less rapidly released than apolar compounds as hexane or weekly polar compounds as isobutylene. The slow outgassing of nitrogen was remarkable, and could be explained by trapping within the closed cells of the foam. Thus, a bakeout at 175 ºC can be recommended to improve the outgassing behavior of Rohacell® 31HF; however, this treatment will only reduce rather than fully eliminate the risks derived from outgassing.

The highlights of this work can be summarized as follows:

- *The application of successive short heating cycles at different temperatures for TD inejection is an excellent tool to investigate outgassing.*
- *The outgassing characteristics of PMI foam, including the identification and quantitation of the compounds released in significant amounts, were described.*
- *The atmosphere generated by PMI outgassing varies with time, polar components showing increasing concentrations.*

B.3. Determination of alcohols in essential oils by liquid chromatography with ultraviolet detection after chromogenic derivatization

An HPLC-UV method to determine compounds having an hydroxyl functional group in plant essential oils was developed. The sample was diluted with 1,4-dioxane and the analytes were derivatized with phthalic anhydride. The derivatives (phthalate hemiesters) were separated on a C8 column using an ACN/water gradient. Separation conditions were optimized using the DryLab® method development software. For the alcohols and phenols present in mint and rose essential oils, optimization led to a *ca.* 40 min gradient time and a column temperature of 8 ºC. The alcohols and its derivatives were identified using HPLC with MS detection. A large sensitivity enhancement was obtained after derivatization. The HPLC-UV method was compared to GC-FID and GC-MS. The LODs obtained by the proposed method were better than those obtained by GC-FID and of the same order as those achieved by GC-MS. The three methods were satisfactorily applied to the determination of alcohols in essential oils. Therefore, the recommended method is of interest as an

alternative to GC methods, to investigate the presence of compounds having an alcohol group at low concentrations in essential oils.

DryLab® was used to optimize both the gradient time and the column temperature. To design the initial set of experiments, the following was taken into account: a) the initial and final ACN concentrations, 30% and 80%, respectively, which were selected according to the literature; b) for convenience, the minimal and maximal gradient time was set at 20 and 40 min, respectively; c) the column temperature was allowed to vary from 5 to 25 ºC. From the initial set of four chromatograms, DryLab® predicted the peak locations in all intermediate working conditions, also calculating the resolution between the successive peak pairs. From these, a resolution map with red areas corresponding to the highest resolution of the most critical peak pair (R_C), was provided. The best resolution was predicted for a 39 min gradient time at a column temperature of 8 ºC.

Samples of *Mentha Arvensis* and *M. Piperita,* and Al Fayed (Egypt) samples of mint and rose essential oils, were also derivatized as indicated, and aliquots were injected. For each essential oil, the initial set of four chromatograms was obtained, and optimization of the separation conditions with Drylab® was performed. For a given set of HPLC conditions, the chromatograms of the derivatized *M. Arvensis* and *M. Piperita* oils were closely similar to those obtained with the Al Fayed mint essential oil. Therefore, the resolution maps for the three mint oils predicted the same set of optimal conditions, i.e. a 39 min gradient time and 8 ºC.

In order to identify the chromatographic peaks, MS detection was also coupled in series with the UV-Vis detection. Chromatograms of both alcohol standards and the Al Fayed mint and rose essential oils, without and with previous derivatization with phthalic anhydride, were obtained. All chromatograms were obtained in the optimal conditions for the derivatized mint essential oil. A reagent blank, prepared by using the derivatization procedure in

the absence of a sample, was also chromatographed. This chromatogram showed that the reagent peaks were eluted at the head of chromatogram, thus causing no interference. For the underivatized essential oils, satisfactory signals from positive quasimolecular ions $[M+H]^+$ were obtained at the retention times of several sample components. In particular, the *m/z* differences between several MS^2 intense peaks corresponding to loss of water, and several easily recognizable fragments, were most useful. Next, alcohol components of the mint and rose essential oils were quantified by using the proposed HPLC-UV method, and the results were compared with those obtained with GC-FID and GC-MS. The HPLC-UV and GC procedures yielded similar values for all the analytes, with no significant differences at the 95% confidence level.

The highlights of this work can be summarized as follows:

- *A robust HPLC-UV method to determine alcohols in essential oils was described.*
- *A reliable derivatization protocol of alcohols with phthalic anhydride wass proposed.*
- *Quick and safe optimization of the HPLC-UV separation was achieved with DryLab®.*
- *After optimization, the proposed method was favorably compared to GC methods.*